HYDROXYPROPYLMETHYLCELLULOSE: A NEW MATRIX FOR SOLID-SURFACE ROOM-TEMPERATURE PHOSPHORIMETRY

Vincent N. Hamner

Dissertation submitted to the Faculty of the
Virginia Polytechnic Institute and State University
in partial fulfillment of the requirements for the degree of

DOCTOR OF PHILOSOPHY
in
Chemistry

R.E. Dessy, Chairman

Advisory Committee:
M.R. Anderson
J.O. Glanville
J.S. Merola
B.M. Tissue

January 21, 1999

Blacksburg, Virginia

Keywords: Phosphorescence Spectroscopy, Hydroxypropylmethylcellulose (HPMC), Cellulose, Robust Statistics, Outliers, Cohesion (or Solubility) Parameters

HYDROXYPROPYLMETHYLCELLULOSE: A NEW MATRIX FOR SOLID-SURFACE ROOM-TEMPERATURE PHOSPHORIMETRY

by

Vincent N. Hamner

R.E. Dessy, Chairman

Chemistry

(Abstract)

This thesis reports an investigation of hydroxypropylmethylcellulose (HPMC) as a new solid-surface room-temperature phosphorescence (SSRTP) sample matrix. The high background phosphorescence originating from filter paper substrates can interfere with the detection and quantitation of trace-level analytes. High-purity grades of HPMC were investigated as SSRTP substrates in an attempt to overcome this limitation. When compared directly to filter paper, HPMC allows the spectroscopist to achieve greater sensitivity, lower limits of detection (LOD), and lower limits of quantitation (LOQ) for certain phosphor/heavy-atom combinations since SSRTP signal intensities are stronger. For example, the determination of the analytical figures of merit for a naphthalene/sodium iodide/HPMC system resulted in a calibration sensitivity of 2.79, LOD of 4 ppm (3 ng), and LOQ of 14 ppm (11 ng). Corresponding investigations of a naphthalene/sodium iodide/filter paper system produced a calibration sensitivity of 0.326, LOD of 33 ppm (26 ng), and LOQ of 109 ppm (86 ng). Extended purging with dry-nitrogen gas yields improved sensitivities, lower LOD's, and lower LOQ's in HPMC matrices when LOD and LOQ are calculated according to the IUPAC guidelines.

To test the universality of HPMC, qualitative SSRTP spectra were obtained for a wide variety of probe phosphors offering different molecular sizes, shapes, and chemical functionalities. Suitable spectra were obtained for the following model polycyclic aromatic hydrocarbons (PAHs): naphthalene, p-aminobenzoic acid, acenaphthene, phenanthrene, 2-naphthoic acid, 2-naphthol, salicylic acid, and triphenylene.

Filter paper and HPMC substrates are inherently anisotropic, non-heterogeneous media. Since this deficiency cannot be addressed experimentally, a robust statistical method is examined for the detection of questionable SSRTP data points and the deletion of outlying observations. If discordant observations are discarded, relative standard deviations are typically reduced to less than 10% for most SSRTP data sets. Robust techniques for outlier identification are superior to traditional methods since they operate at a high level of efficiency and are immune to masking effects.

The process of selecting a suitable sample support material often involves considerable trial-and-error on the part of the analyst. A mathematical model based on Hansen's cohesion parameter theory is developed to predict favorable phosphor-substrate attraction and interactions. The results of investigations using naphthalene as a probe phosphor and sodium iodide as an external heavy-atom enhancer support the cohesion parameter model.

This document includes a thorough description of the fundamental principles of phosphorimetry and provides a detailed analysis of the theoretical and practical concerns associated with performing SSRTP. In order to better understand the properties of both filter paper and HPMC, a chapter is devoted to the discussion of the cellulose biopolymer. Experimental results and interpretations are presented and suggestions for future investigations are provided. Together, these results provide a framework that will support additional advancements in the field of solid-surface room-temperature phosphorescence spectroscopy.

Dedication

During my stay in Blacksburg,
Mr. Buddy Alls treated me as if I were a member of his own family.
We climbed a lot of mountains together, dug a few `seng roots,
and even caught a fish or two.
I initially thought that those distractions would make my quest for the Ph.D. more difficult, but instead they made the journey easier.

This work is dedicated to my friend
Mr. Buddy (*Blue*) Alls
March 19, 1938 - January 14, 1995

Acknowledgments

I owe my thanks to Dr. Ray Dessy and Lee Dessy. The guidance and encouragement provided by both have helped me to reach my destination. From the beginning, I've had the freedom to select my own projects and pursue my own research interests. This has allowed me to choose the road less traveled… and it has made all the difference. Few other graduate students are permitted such autonomy.

During my graduate career, the members of the Dessy Group have been more than just colleagues -- they have been my friends and family. Whether it be the sharing of advice, laboratory techniques, or other expertise, each has made a contribution to my development as a professional scientist in one way or another. I offer my sincere thanks to each.

I appreciate the help provided by Mr. C.W. Yip. Since the day my computer first arrived in the laboratory, Yip helped me to maintain my system and insure that it was continually outfitted with the best software tools possible. In addition to this *Yipsterization* process, he also provided me with much of the training necessary to use those tools. As "payment" for his many consultations, I owe him a truckload of Pepsi®. Hopefully he's be too busy with his job as computer wizard at Wake Forest U. to recall the debt.

I am indebted to my friend, colleague, and wife, Josette. Josette volunteered a significant amount of time and assistance during the final stages of this research. Her keen observations and insight allowed me to improve both the reproducibility and sensitivity of the RTP technique. Her contributions to the success of this project and the quality of this dissertation are appreciated very much.

I am indebted to Dr. Elizabeth Creamer, director of the Liberal Arts and Sciences (LASc) Advising Center and to Dr. Michael Ogliaruso, Dean of the College of Arts and Sciences. Dr. Creamer and Dean Ogliaruso provided me with continued financial support in the form of a graduate assistantship at a time when my own department would not. It has been my pleasure to work for Dr. Creamer and to assist literally hundreds of students during their quest for the LASc degree.

On the campus of Virginia Tech, I am thankful for the assistance, advice, and instruction given by the Chemistry Department electronics shop, the Chemistry Department surface analytical lab, the Physics Department machine shop, and the Statistics Department consulting center. Dr. Jeffrey Birch (statistics) provided the robust statistical algorithms and tutelage that allowed me to detect potential outliers in my data via the use of Tukey Biweight m-estimators. Mr. Fred Blair machined the components that were used to modify the Perkin-Elmer front-surface accessory for this project.

Thankfully, Dr. Gary Long permitted me access to the Perkin-Elmer LS-50 luminescence spectrophotometer in the physical chemistry teaching laboratory. Although the LS-50 instrument was originally purchased for teaching purposes, I was able to use it freely for my research investigations during the evenings, late at night, and on weekends. Without access to the LS-50, this project would not have been completed.

I'm grateful to Dr. Brian Tissue for providing me with unrestricted access to his sample preparation lab. The hydraulic laboratory press and pellet die found therein were also essential to the completion of this project.

My friend and colleague, Dr. Bill Bender, was most helpful in providing samples of Dow's Methocel products and related technical literature. His contribution to the success of this research project will always be much appreciated.

The Perkin-Elmer Corporation has supported this research in many ways. For two years of my graduate career, Perkin-Elmer provided financial assistance in the form of tuition fellowships. These funds were especially appreciated since they were awarded at a time when the University continued to bill its graduate students for tuition (the old days!). During the final stages of this project, Dr. Pam Perrone loaned a $2,120.\underline{00}$ Perkin-Elmer front-surface sample accessory for use with the LS-50 instrument. I'm sincerely grateful to both Dr. Perrone and P-E.

My parents, Tom and Janet Hamner, have given me much encouragement during the past 8 years. Their contributions to the success of this project are perhaps most important of all. Financial assistance was necessary during the final 8 months of active research and they were there to provide it. This dissertation would not have been finished otherwise. I'm grateful to both for their help.

It is ironic that I have completed my formal training in chemistry while in residence at the same college where I began my studies nearly twelve years ago. I'm grateful to West Virginia Wesleyan College for providing unlimited internet access, free on-line Chemical Abstracts literature searching, free inter-library loan services, and the use of a new Pentium ThinkPad computer. Dr. Allen Hamner graciously loaned his office so that I might continue writing the dissertation on-campus during the Summer of 1998.

Mr. Aaron Karr provided an especially helpful search of Chemical Abstracts Online during the Summer of 1996. The libraries at Virginia Tech, Ohio State University, and the University of North Carolina at Wilmington have each been helpful during my literature investigations. Communications with Dr. Yue-Ling Wong (Wake Forest University), Dr. Colin Keary (Dow Chemical Company), Dr. Raymond Rowe (Zeneca Pharmaceuticals UK), Dr. Robert Hurtubise (University of Wyoming), Dr. Tuan Vo-Dinh (Oak Ridge National Laboratories), and Dr. Jim Winefordner (University of Florida) have all proven productive at various stages of the project. Mr. Ned Hill, of AAI's Physical Pharmacy Group (Wilmington, NC), provided the facilities and helpful tutelage that allowed for the determination of sample penetration depths in HPMC and filter paper pellets by optical microscopy.

The following companies provided gratis samples of potential SSRTP matrices: Micron Separations Inc., Poretics Inc., Filtron Technology Corporation, Schleicher & Schuell, Gelman Sciences, Ahlstrom Filtration Inc., Mark V Laboratory Inc., Millipore Corporation, the Dow Chemical Company, Aqualon, FMC, The National Starch and Chemical Company, and the A.E. Staley Company. Their generosity is much appreciated.

This dissertation was mostly produced on a 33MHz 80486 computer (16 Mb RAM; 2.4 Gb HD, 100 Mb Zip Drive). Operating systems: MS-DOS, Win 3.1, Win 95. Software: Word, Excel, PowerPoint, Chemdraw, Acrobat, and a variety of graphics/paint packages.

Table of Contents

List of Figures

List of Tables

"The job of a scientist is to do science,
maybe to apply it,
and then, if he is capable of doing so,
to explain what he has found."[1]

Edward Teller

[1] G. Barry Golson, Ed., *Edward Teller (August 1979)* in **The Playboy Interview**, New York: Playboy Press, 1981.

1.0 Introduction

Luminescence is generally defined as radiation emitted by atoms or molecules as they undergo a radiative transition from an excited energy level to a lower energy level.[2] Applications of luminescence methods to measure the properties of chemical and biochemical systems are plentiful in the literature. In the 1994 *Fundamental Reviews* issue of *Analytical Chemistry*, McGown, Warner, and Soper list more than 450 literature citations in their review titled "Molecular Fluorescence, Phosphorescence, and Chemiluminescence Spectrometry".[3] This review, encompassing the pertinent literature published from September 1991 to October 1993, was intentionally limited by the editors to incorporate only those topics considered to be of general interest to all scientists working within those fields of research. An earlier, more detailed, fundamental review in the same journal yielded 639 citations.[4]

Luminescence spectroscopy has been a useful analytical tool in a variety of disciplines. Applications are found in clinical, pharmaceutical, environmental, biological, medical, chromatographic, agricultural, industrial, and forensic laboratories. Luminescence techniques are widely used primarily because of the sensitivity and selectivity that can be achieved in trace analysis. Luminescence spectroscopy is inherently more selective than absorption spectroscopy due to at least five independently measurable variables which are characteristic of a given sample component:

1). emission intensity (as a function of predetermined excitation wavelength);
2). excitation efficiency (as a function of predetermined emission wavelength)
3). excited state lifetime;
4). emission polarization; and
5). quantum yield.

Molecular luminescence is typically divided into two broad classes: photoluminescence and chemiluminescence. For photoluminescence to occur, a molecule must become electronically excited as a result of an absorption of incident light energy. Soon thereafter, the molecule will re-emit a portion of that energy in the form of light. Fluorescence and phosphorescence are both photoluminescent processes. For chemiluminescence and bioluminescence, light is emitted as a result of thermal reactions in which the products (or intermediates) of the reaction are so energetic that they are electronically excited. Bioluminescence refers to those light-producing reactions that either occur within a biological system or are derived from one.[5]

The term *fluorescence* was originated by G.G. Stokes during his thorough investigation of photoluminescence in 1852. Stokes was the first investigator to clearly state that fluorescence

---

[2] R.J. Hurtubise, **Phosphorimetry: theory, instrumentation, and applications** New York: VCH Publishers, Inc., 1990.
[3] S.A. Soper, L.B. McGown, and I.M. Warner,*Anal. Chem.*, 1994, V. 66, p. 428R.
[4] E.L. Wehry, *Anal. Chem.*, 1986, V. 58, p. 13R.
[5] M.L. Grayeski, *Anal. Chem.*, V. 59, #21, p. 1243A.

was an emission process. He showed that emission intensity depends on sample concentration and proposed the principle that fluorescent emission is always of longer wavelength than the excitation (now known as Stokes' Law).[6] Stokes commented on the high sensitivity of fluorescent emission and predicted that fluorescence analysis was "...likely to prove a great value in the separation of organic compounds".[7]

Fluorescence is caused by the emission of light due to an "allowed" electronic transition between excited and ground states having the same spin multiplicity, usually singlet. The lifetimes for such transitions are typically from 10^{-7} to 10^{-9} s. According to the spectroscopic selection rules, the transition from an excited singlet state to a singlet ground state is spin-allowed and thus can occur with a high degree of probability.

There are processes which can compete with fluorescence. The excited molecule might lose energy by internal conversion or intersystem crossing. *Internal conversion* is a radiationless process whereby a molecule passes from a higher to a lower electronic state without the emission of light. After internal conversion occurs, rapid vibrational relaxation leaves the molecule in the lowest level of the lower electronic state. Alternatively, if there is a radiationless transition between the first excited singlet state to the lowest excited triplet state then this process is called *intersystem crossing*.[8] Because of the change of electronic spin which occurs with intersystem crossing, the spin selection rules are not obeyed rigorously. The slow, radiative transition back to the ground state is called phosphorescence.

Edmund Becquerel was the first to measure the excitation and emission spectra of several phosphors. Among the features that he measured was the duration of the photoluminescence after excitation ceased. He is credited with building the first phosphoroscope in 1858, with which he could measure emission lifetimes as short as 10^{-4} seconds.[9] *Phosphorescence* is defined as the emission of light due to a "forbidden" electronic transition between excited and ground states having different spin multiplicities, usually triplet to singlet. Lewis and Kasha first proposed this definition in 1944 and suggested that phosphorimetry might be a useful technique to identify certain organic molecules.[10] The analytical usefulness of phosphorimetry was firmly established in 1957 by Keirs, Britt, and Wentworth.[11] Since that time, phosphorimetry has developed into a popular method of analysis that can often provide complimentary information to fluorimetry regarding structure, reactivity, and environmental conditions.

Because phosphorescence is a spin-forbidden process, the rate of phosphorescence is relatively slow compared to other processes associated with excited molecules. This feature gives the electronic triplet state its long lifetime. Representative phosphorescence lifetimes will range from milliseconds to seconds. For phosphors in solution at room temperature, the long

---

[6] M.C. Goldberg and E.R. Weiner, *The Science of Luminescence*, **Luminescence Applications in Biological, Chemical, Environmental, and Hydrological Sciences** A.C.S. Symposium Series Vol. 383, American Chemical Society: Washington D.C., 1989.

[7] Sir G.G. Stokes, *Philos. Trans. R. Soc. London A*, 1852, V. 142, p. 463.

[8] D.M. Hercules, **Fluorescence and Phosphorescence Analysis: Principles and Applications**, New York: John Wiley & Sons, 1966.

[9] E. Bequerel, *Com. Rend. Acad. Sci.*, 1858, V. 46, p. 969.

[10] G.N. Lewis and M.J. Kasha, *J. Am. Chem. Soc.*, 1944, V. 66, p. 2100.

[11] R.J. Keirs, R.O. Britt and W.E. Wentworth, *Anal. Chem.*, 1957, V. 29, p. 202.

lifetime of the triplet state increases the probability of intermolecular collisions between analyte and solvent molecules (or solvent impurities). If collisional deactivation does occur, then a nonradiative energy transfer takes place and phosphorescence is quenched. Regular solution phosphorescence has been found to rarely occur at room temperature unless special measures are taken to lower the rates of competing processes. Until recent years, researchers assumed that the use of low-temperature solvents and cryogenic equipment were required in order to obtain analytically useful phosphorescence information. Useful phosphorescence measurements were made possible at liquid nitrogen temperatures (77K) by dissolving the analyte of interest in a solvent that would freeze to form a glass-like matrix. Solid-Surface Room-Temperature Phosphorimetry (SSRTP) is an alternative approach that yields suitable results while minimizing the extensive sample preparation steps typically required for low temperature phosphorescence measurements.

Although a variety of substrates have been investigated for SSRTP use, no single matrix material has proven to be acceptable for all applications. Furthermore, no detailed guidelines have been developed for selecting suitable sample matrices for room-temperature phosphorescence (RTP) primarily because the physical and chemical interactions responsible for RTP are not yet fully understood. Traditionally, filter paper has been the most widely used SSRTP support material since it is considered to be a universal matrix for most phosphors. Filter paper is manufactured from cellulose, a biopolymeric material that exhibits extensive inter- and intra-chain hydrogen bonding. As a result of these strong intermolecular interactions, a rigid network of cellulose chains is formed. SSRTP investigators have theorized that phosphors immobilized on filter paper become trapped between the cellulose macromolecules in a cage-like environment. However, filter paper is unacceptable for many RTP determinations since most types contain impurities that produce strong background phosphorescence emissions within the 400-600 nm range.[12] Numerous researchers have attempted to reduce these background emissions by washing, heating, and UV-bleaching the filter paper substrates. Unfortunately, these efforts have met with limited success.[12]

Since filter paper offers many strengths as an SSRTP support material, the author chose to study high-purity cellulose derivatives in an attempt to identify new matrix materials that do not yield strong phosphorescence background intensities. The most promising SSRTP substrate was *K4M PREM* hydroxypropylmethylcellulose (HPMC). The premium grades of HPMC are those cellulose ethers that are manufactured in a variety of highly-purified forms so that they may serve as modifiers in food products and as excipient materials for use in pharmaceutical preparations. Although of limited use as an RTP substrate in the powdered form, HPMC is one of those rare materials that can be easily formed into a pellet via direct compression methods. During these investigations, hundreds of HPMC pellets were manufactured for subsequent use as RTP substrates. In this manner, it was possible to determine analytical figures of merit and benchmark the performance of HPMC as an RTP support material. In direct comparison to filter paper, *K4M PREM* HPMC offers the SSRTP spectroscopist greater sensitivity, lower limits of detection, and lower limits of quantitation. Since RTP emission intensities are significantly

---

[12] T. Vo-Dinh, **Room Temperature Phosphorimetry for Chemical Analysis**, New York: John Wiley & Sons, 1984.

improved for HPMC-phosphor systems, background HPMC phosphorescence emissions are of less concern than those derived from filter paper supports. For the first time, experimental RTP results are supported by a model based on solubility (or cohesion) parameter theory. This work also provides a foundation for the use of robust statistical methods within the SSRTP community. Together, these results provide a logical framework that will support new advancements in the field of phosphorescence spectroscopy.

In order to provide a coherent and complete body of information, four major areas will be detailed within the dissertation. The following chapter gives an overview of the photophysical principles associated with the phosphorescence process and discusses the basic elements of *phosphorimetry*. The subsequent chapter provides a review of the chemical and physical properties of *cellulose and HPMC*. The *instrumentation* chapter opens with a basic discussion of the components that comprise a luminescence spectrometer. It concludes with a discussion of the Perkin-Elmer LS-50 spectrometer that was used during this project. The *experimental* chapter is concerned with the laboratory reagents, apparatus, and techniques that were employed in the investigation of the SSRTP matrices. The results of the investigations are found in this chapter as well. The final section provides a summary of the experimental results and an evaluation of the performance of HPMC as a new SSRTP matrix material.

2.0 Principles

This chapter will first provide a description of the photophysical principles associated with phosphorescence. A basic review of the elements of phosphorimetry will include such topics as heavy-atom phosphorescence enhancers, potential quenching agents, and temperature effects. The discussion of solid-surface room-temperature phosphorescence will incorporate a number of considerations such as matrix selection, solvent selection criteria, sample delivery, and sample drying. The chapter concludes with a short survey of the conventional SSRTP support materials.

2.1 Photophysical Principles of Phosphorescence

As mentioned earlier, fluorimetry and phosphorimetry are two complementary techniques that have been widely used for luminescence spectroscopy. Both methods of analysis deal with electronic state transitions in a molecule as opposed to changes associated with its vibrational, rotational, or other energy states. These photoluminescent techniques require that one measure and analyze the light emitted by an analyte as it returns from an excited electronic state to its lower energy ground state.

Figure 1 shows the electromagnetic spectrum that illustrates the various regions in which the basic spectroscopies operate. Phosphorescence spectroscopy has been commonly practiced within the UV and visible portions of the spectrum.

The remainder of the dissertation will be concerned with the photoluminescence produced by organic compounds; therefore, the term *phosphorescence* will henceforth refer exclusively to organic analytes. Organic molecules generally contain an even number of electrons. In the ground state, the lowest energy atomic orbitals are filled by electron pairs. The term *singlet state* refers to the electronic ground state of a molecule that has no net electron spin. This is in accordance with the Pauli exclusion principle which states that two electrons in an orbital
must have opposing spins and the total spin (S) must equal 0. A molecule becomes *excited* following the transition of an electron from an occupied orbital to an empty orbital. The excited state can either be a singlet or a triplet depending on the final orientation of the excited electron's spin. If the excited electron assumes a spin direction opposite of it's ground state counterpart (antiparallel; S=0) then a *singlet* excited state results. Alternatively, if the spin directions are the same (parallel; S=1) then the resulting excited state is referred to as a *triplet*. In this instance, the spin orientations of the excited electrons are no longer governed by the Pauli exclusion principle. Figure 2 provides a graphical illustration of the electron arrangements in a variety of representative singlet, doublet, and triplet states. Although rare, a number of molecules exist naturally as triplets in the ground state.

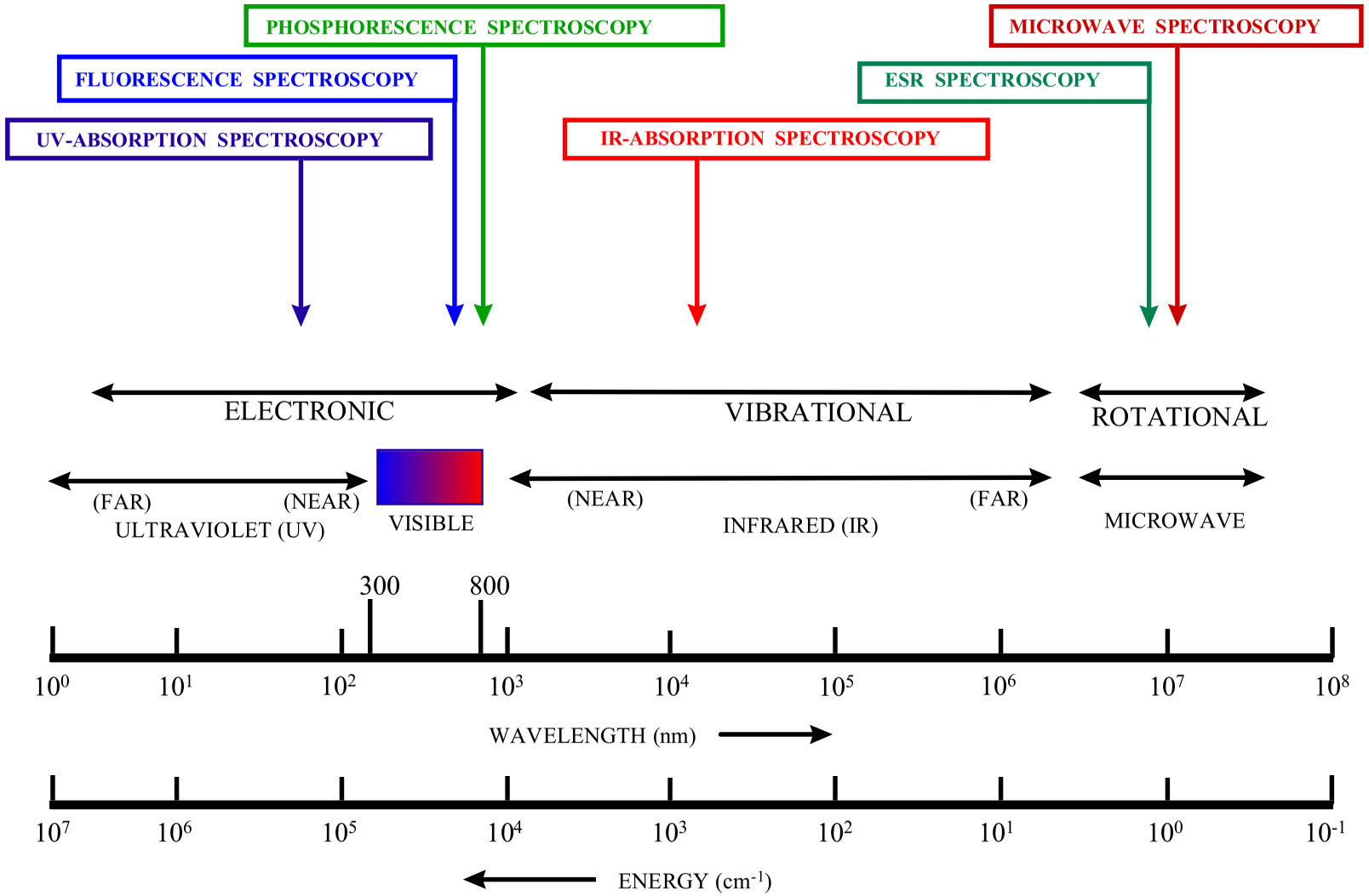

Figure 1. The Electromagnetic Spectrum (adapted from Vo-Dinh, 1984).

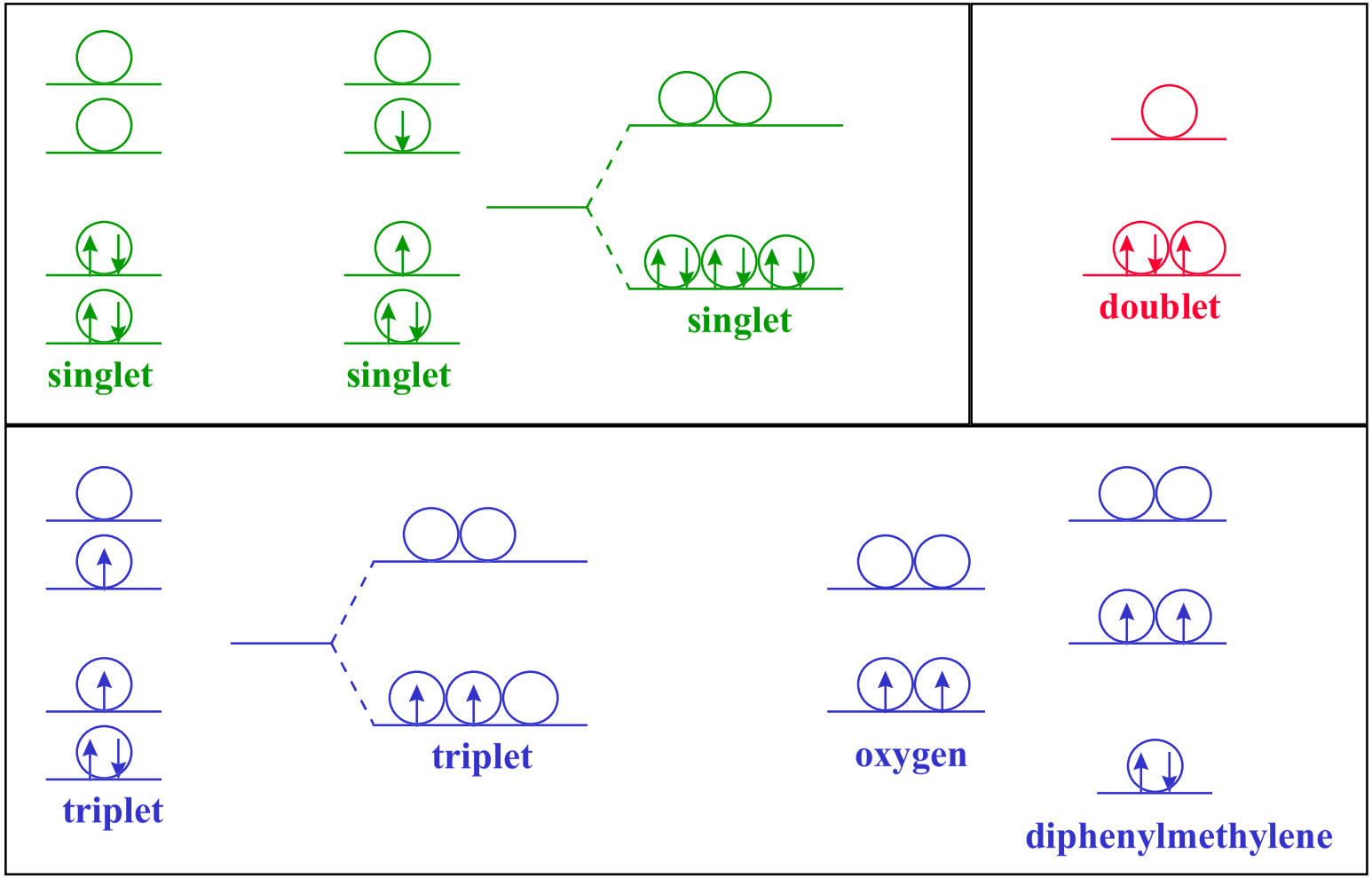

Figure 2. Representative Orbital Populations: Singlet, Doublet, and Triplet States.
(adapted from: G.H. Schenk, **Absorption of Light and Ultraviolet Radiation: fluorescence and phosphorescence emission**, Boston: Allyn and Bacon, Inc., 1973.)

The fundamental properties of the singlet and triplet states are significantly different. The singlet state is diamagnetic. The triplet state is paramagnetic. In fact, the terms "singlet" and "triplet" were adopted following the exposure of certain molecules to an external magnetic field. The triplet state, having a spin magnetic moment, will yield three distinct lines in a spectrum when placed in a magnetic field (the *Zeeman effect*) and the three Zeeman energy levels may be distinguished by their resulting polarizations (left-circular, right-circular, and linearly polarized). The singlet state, having no magnetic moment, will remain unchanged when placed in a strong magnetic field.

The organic molecules that provide the best phosphorescence are those that have extensive π electron systems (e.g. the aromatics and a few unsaturated aliphatics). For conjugated systems that contain N, O, or S, or having substituents with these *heteroatoms*, a new electronic state can result if an electron is promoted from a nonbonding *n* orbital to an antibonding π^* orbital. The resulting state is referred to as a $n\pi^*$ excited state. If the molecule has no hetero-atom, the new electronic state is likely to involve the promotion of an electron from a bonding π orbital to an antibonding π^* orbital -- a π-π^* transition.

Figure 3 shows the energy levels of an arbitrary organic molecule. Commonly referred to as a *Jablonskii diagram*, the individual clusters of horizontal lines illustrate the discrete **electronic energy levels** of the molecule. The lowest energy electronic state is referred to as the *singlet ground state* (S_0). All higher levels are excited singlet (S_n) and excited triplet (T_n) electronic states. Within each electronic state, there exist a number of **vibrational energy levels**. The corresponding **rotational energy levels** are typically not shown.

Following the absorption (A) of ultraviolet or visible light, a number of radiative and nonradiative transitions can occur within a molecule that has been promoted to a vibrational level in an excited electronic singlet state. These include:

1). Vibrational Relaxation (VR),
2). Internal Conversion (IC),
3). Fluorescence (F),
4). External Conversion (EC),
5). Intersystem Crossing (ISC), and
6). Phosphorescence (P).

Vibrational relaxation describes the loss of excess energy by a molecule as it experiences a decay to lower vibronic energy levels within a particular excited electronic state. The VR process is faster than an electronic excited state lifetime and it manifests itself as a release of thermal energy into the molecule's surroundings. *Internal conversion* is a nonradiative transition between electronic states of the same multiplicity. An example of IC would be the transition of a molecule from an electronic S_n state to an S_{n-1} vibrational level of the same energy. The probability of IC is enhanced when the potential energy curves for two electronic states cross such that the lower vibrational levels of the higher electronic state are approximately the same energy as higher vibrational levels of the lower electronic single state.

For the molecule in the S_1 state, there are a number of pathways that will allow it to return to the S_0 ground state. One pathway would involve a radiationless decay to the singlet ground state via IC and VR. Another pathway might involve the emission of a photon with no change in

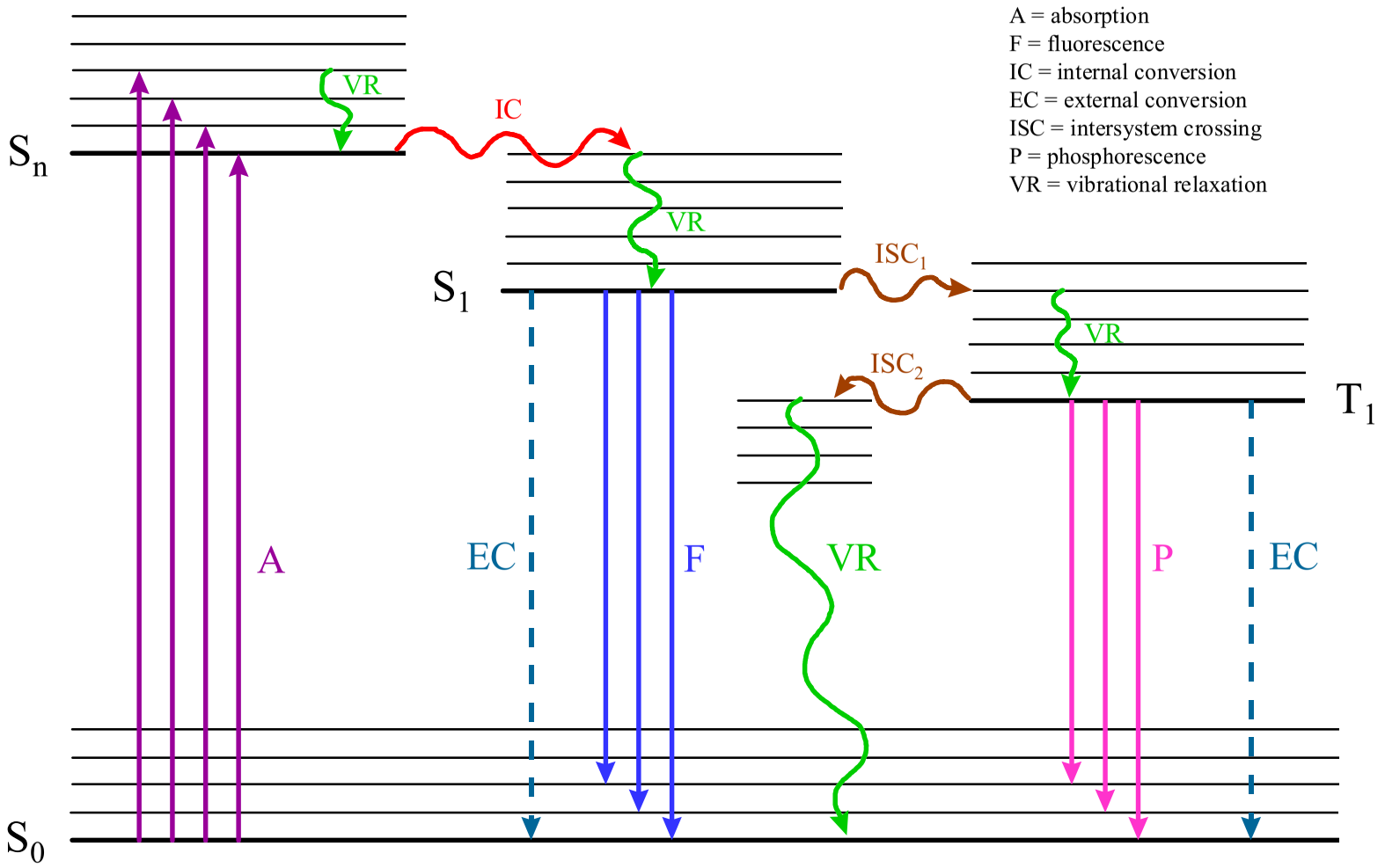

Figure 3. Jablonskii diagram.

spin multiplicity. Better known as *fluorescence*, this event provides a photon that corresponds to the difference in energy of the lowest vibrational level of the S_1 state and a vibrational level within the S_0 state. A fluorescence spectrum gives information about the vibrational structure of the ground state.

A molecule in the S_0 state possesses a given geometry and solvation. When radiation is first absorbed, the excited S_1 molecule will still possess the same geometry and solvation. Soon after the excitation step, the geometry and solvation of the molecule are converted to favorable arrangements associated with the S_1 state. This involves a lowering of the energy of the excited molecule. When a molecule in the S_1 state fluoresces, it returns to the S_0 state, but retains the S_1 geometry and solvation. The net effect is that the emission energy returned is less than the original excitation energy. Because electronic transitions occur so quickly, each atom will have nearly the same position and momentum before and after a transition. This is the basis of the *Franck-Condon principle*.[13]

External conversion refers to nonradiative processes in which excited states transfer their excess energy to other species within their surroundings (i.e. solvent or solute molecules). Dynamic quenching is one mechanism of external conversion that involves the nonradiative transfer of energy from an excited state species to other molecules during intermolecular collisions. One way to reduce the rate and hence, the probability, of dynamic quenching is to cool the sample.

Another pathway involves a process known as *intersystem crossing*. An example of an ISC event would involve the transition of a molecule from a vibrational energy level of the S_1 state to an vibrational level in the T_1 state having the same energy. Following this change in spin multiplicity, the molecule may then relax to the lowest vibrational energy level by VR. From the lowest energy T_1 level, the molecule may return to the S_0 ground state via three additional pathways. The first of these is another radiationless ISC process followed by VR (see ISC_2 in figure 3). EC is an alternate pathway that results in a nonradiative deactivation. The final possibility is a radiative transition to the S_0 ground state that results in the emission of a photon and spin flip. Better known as *phosphorescence*, this process yields information about the lowest triplet state T_1. Phosphorescence is favored for molecules and environmental conditions in which intersystem crossing is favorable ($k_{isc} > k_F + k_{ec} + k_{ic}$; where k represents a rate constant). Therefore, if $k_{isc} > k_F$, phosphorescence is favored over fluorescence. Furthermore, phosphorescence is usually only observed if the probability of external conversion is reduced by cooling or other techniques.[14]

Delayed fluorescence is sometimes mistaken for phosphorescence. Except for its unusually long lifetime, a delayed fluorescence spectrum is identical to a regular fluorescence spectrum. Although delayed fluorescence typically occurs in solution, compounds absorbed on solid-surfaces will sometimes yield this type of fluorescence as well.[15] Different mechanisms can produce delayed fluorescence. One type, referred to as *α-phosphorescence* (or *delayed thermal fluorescence* or *E-type delayed fluorescence* or *slow fluorescence*) results from the

---

[13] F. Ahmed, *J. Chem. Ed.*, 1987, V. 64, #5, p. 427.
[14] J.D. Ingle, Jr. and S.R. Crouch, **Spectrochemical Analysis**, New Jersey: Prentice Hall, 1988.
[15] C.A. Parker, **Advances in Photochemistry -- Vol. 2**, New York: Wiley Interscience, 1964.

thermal excitation of the triplet and reoccupation of the first excited singlet followed by fluorescence. For most molecules, delayed fluorescence is the result of what is termed a *biphotonic* process. The mechanism involves excitation to S_1, intersystem crossing to T_1, followed by triplet-triplet annihilation with one molecule being formed in S_0 and the other in S_1. The delayed fluorescence emission then arises from the decay of the S_1 molecule.

The triplet states of a molecule will always be of a lower electronic energy level than the corresponding singlet states. This is in agreement with Hund's rule which states that the energy of a level having parallel spins is always lower than that of a corresponding level with antiparallel spins. Hund's rule is explained qualitatively by considering the tendency for electrons with parallel spins to avoid one another. As a result, each experiences less coulombic interaction. This energy difference accounts for the occurrence of phosphorescence at longer wavelengths than fluorescence. By measuring the wavelength interval between the fluorescence λ_{max} and phosphorescence λ_{max}, it is possible to experimentally determine a $\Delta(S_1\text{-}T_1)$ value for the lowest excited states.

2.1.1 Characterization of Phosphorescence

A number of various types of phosphorescence data may be collected. Included are excitation and emission spectra, phosphorescence polarization, phosphorescence lifetimes, and luminescence quantum yield.

Most modern luminescence spectrometers allow the user to obtain both excitation and emission spectra. An emission spectrum is acquired by measuring the luminescence intensity of an analyte as a function of wavelength at a fixed excitation wavelength. Similarly, an excitation spectrum may be acquired by measuring the luminescence intensity at a fixed emission wavelength while varying the excitation wavelength. Emission spectra always occur at longer wavelengths than the wavelengths of the excitation spectrum. Figure 4 illustrates this feature for solid surface room-temperature phosphorescence excitation and emission scans. Because the lowest triplet is below the lowest excited singlet state, phosphorescence occurs at longer wavelength than does fluorescence. For phosphorescence, the emission spectrum is due to radiative decay from T_1 to different vibrational levels of S_0.

The shape of fluorescence and phosphorescence spectra often resemble that of the absorption band of longest wavelength. Usually there is an approximate mirror-image relationship between the luminescence emission and lowest energy absorption band. Figure 5 indicates the source of structure in a luminescence spectrum and illustrates why the emission spectrum is approximately the mirror image of the absorption spectrum. In the absorption spectrum, wavelength λ_0 corresponds to a transition from the lowest vibrational level of S_0 to the lowest vibrational energy level of S_1. Absorption maxima at higher energy (shorter wavelength) correspond to the S_0 to S_1 transition accompanied by absorption of one or more quanta of vibrational energy. Following absorption, the vibrationally excited S_1 molecule relaxes back to the lowest vibrational level of S_1 prior to emitting any radiation. As portrayed in the figure, emission from S_1 can go to any of the vibrational levels of S_0. The highest-energy transition is

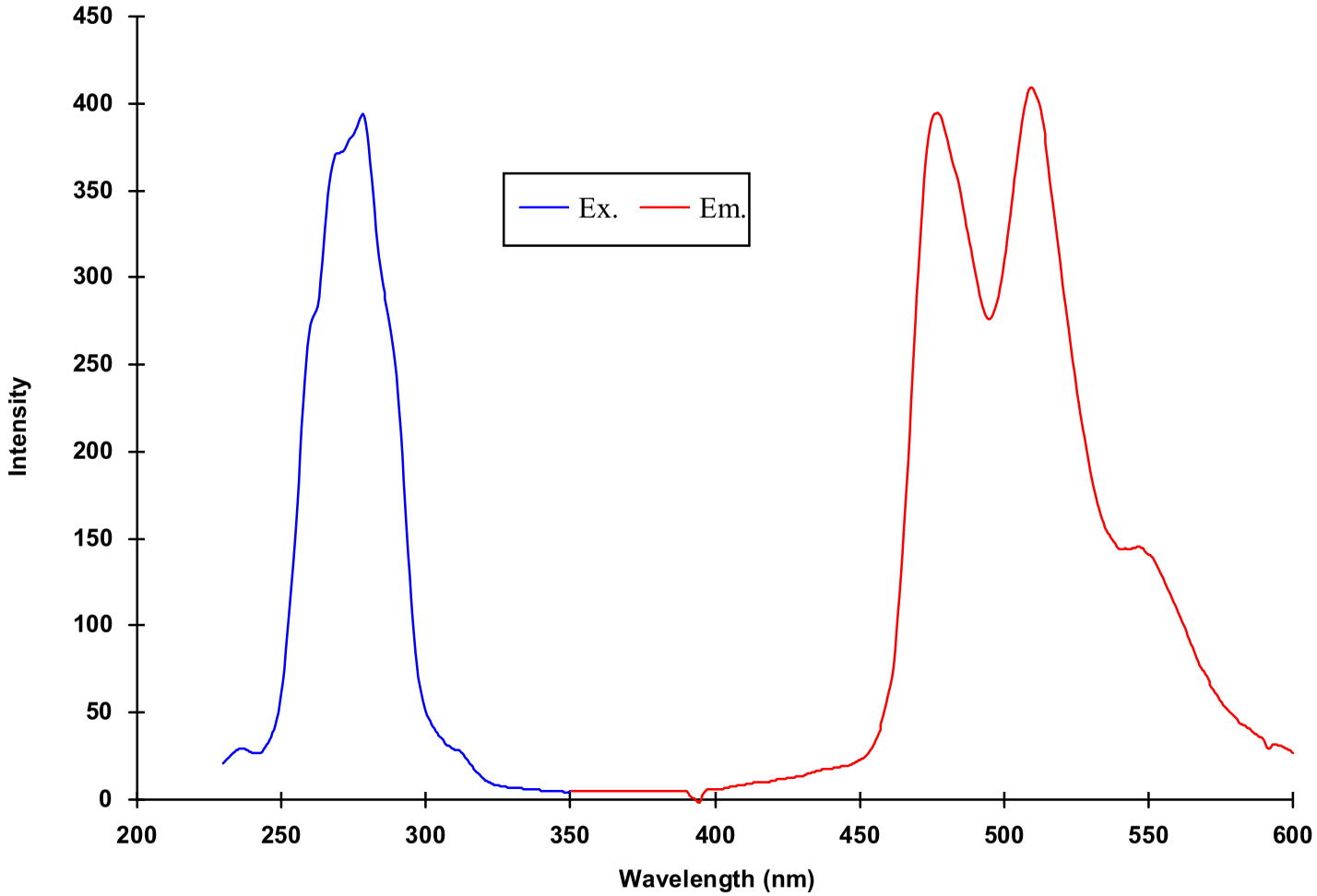

Figure 4: Representative SSRTP Excitation And Emission Spectra. Naphthalene on HPMC [K4M PREM].

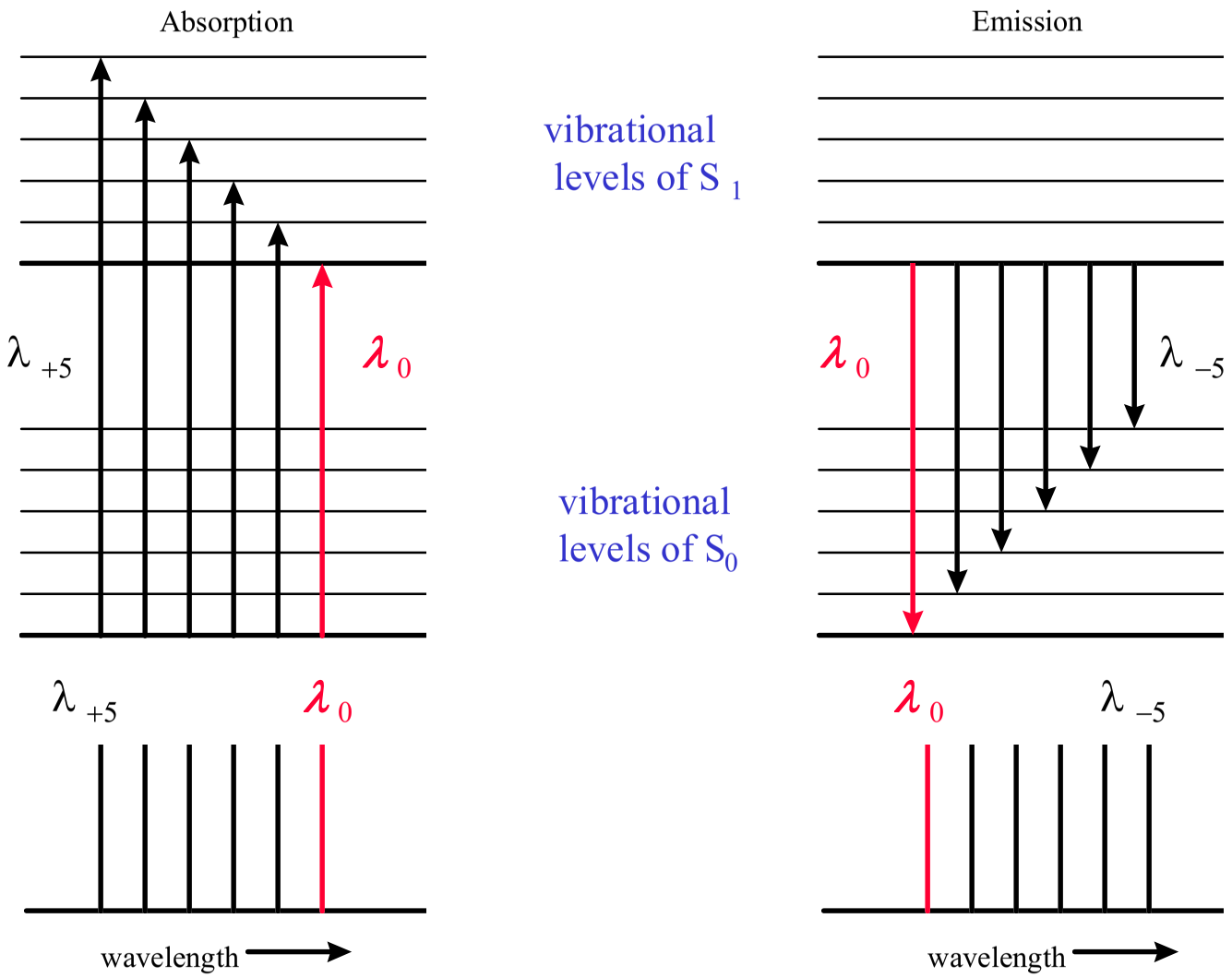

Figure 5. Explanation of approximate mirror-image relationship. (adapted from Harris, 1995)

found at wavelength λ_0, with a series of peaks following at longer wavelengths. The absorption and emission spectra will have an approximate mirror-image relationship if the spacings between vibrational levels are roughly equal and if the transition probabilities are similar.[16]

Electronic transitions are characterized by transition moments that can have unique orientations with respect to the molecular structure of the analyte. One way of determining the orientation of the emission transition dipole is to apply *phosphorescence polarization* measurement techniques. In practice, the polarization of the electronic transition is studied by using polarized light during the excitation of the analyte and polarized optics to characterize the polarization state of the emission phosphorescence. For aromatic hydrocarbons, the allowed transitions are in-plane polarized. Bearing this in mind, it is possible to determine something about the direction of the phosphorescence emission. For many hydrocarbons, the emitted phosphorescence is polarized perpendicular to the plane of the rings.[17]

Low temperature phosphorescence polarization measurements have been useful for differentiating between the $\pi\pi^*$ and $n\pi^*$ characters of the emitting triplet state. The $n \rightarrow \pi^*$ singlet transition is out-of-plane polarized whereas the $\pi \rightarrow \pi^*$ singlet transitions are in-plane polarized. Furthermore, phosphorescence arising from $n\pi^*$ triplet states is in-plane polarized whereas that from $\pi\pi^*$ triplets is out-of-plane polarized. Hurtubise has reported that very little work has been done in measuring phosphorescence polarization from compounds adsorbed on solid surfaces because of problems arising from scattered light.[2] Dalterio and Hurtubise have attempted to measure the extent of polarization of phosphors in this fashion at room temperature.[18] A value of zero polarization was measured and it was reported that depolarization had resulted from the scattering of the excitation radiation and the emitted phosphorescence. A more recent study by the same investigators discussed phosphorescence polarization measurements at lower temperatures.[19] Nevertheless, further experimental work will be required in order to optimize the measurement of phosphorescence polarization from scattering surfaces.

Phosphorescence lifetime, τ_P, is defined as the time required for an emission to decrease to 1/e of its original intensity following an excitation pulse. If $I_{P(t)}$ is the phosphorescence intensity at time t and $I_{P(0)}$ is the intensity at $t = 0$, then τ_P is given by:

$$I_{P(t)} = I_{P(0)} \exp.\left(\frac{-t}{\tau_P}\right)$$

Experimentally, phosphorescence is usually easily differentiated from fluorescence by its longer lifetime. The lifetimes for the *allowed* electronic transitions that yield fluorescence are typically from 10^{-7} to 10^{-9} s. The lifetimes of the *spin-forbidden* phosphorescence transitions typically range from milliseconds to seconds. The difference in phosphorescence lifetimes can allow one to resolve mixtures of compounds that exhibit similar spectra. The lifetime of phosphorescence

---

[16] D.C. Harris, **Quantitative Chemical Analysis**, New York: W.H. Freeman and Company, 1995.

[17] R.S. Becker, **Theory and Interpretation of Fluorescence and Phosphorescence**, New York: Wiley Interscience, 1969.

[18] R.A. Dalterio and R.J. Hurtubise, *Anal. Chem.*, 1983, V. 55, p. 1084.

[19] S.M. Ramasamy and R.J. Hurtubise, *Appl. Spectr.*, 1992, V. 46, p. 472.

is related to the rate constants for phosphorescence and nonradiative deactivation by the following equation:

$$\tau_P = \left(k_P + k'_{nr}\right)^{-1}$$

where $k'_{nr} = k'_{ec} + k'_{isc}$.

In the mid-1920's, the concept of quantum yield was defined and values were determined for many compounds. *Phosphorescence quantum yield* (also commonly referred to as *quantum efficiency*), ϕ_p, is the number of phosphorescence photons emitted divided by the number of photons absorbed by the sample. The maximum quantum yield would be achieved if each absorbed photon were able to produce one phosphorescence photon ($\phi_p = 1$). However, many competing processes (VR, IC, EC, ISC, and F) significantly reduce the quantum yield. In general, for polyaromatic hydrocarbons, an increase in the number of rings associated with the molecule will result in an increased quantum yield. Although there is some disagreement in the literature, $\phi_p = 0.1$ for naphthalene ($C_{10}H_8$), $\phi_p = 0.2$ for phenanthrene ($C_{14}H_{10}$), and $\phi_p = 0.42$ for triphenylene ($C_{18}H_{12}$).[17]

Phosphorescence quantum yield can be determined from the following equation:

$$\phi_P = \left(\frac{k_{isc}}{k_F + k_{nr}}\right)\left(\frac{k_P}{k_P + k'_{nr}}\right)$$

Therefore, ϕ_p corresponds to two factors: i). the fraction of the absorbed photons that produce triplet states and ii). the fraction of the triplet molecules that undergo phosphorescence. Even if intersystem crossing is efficient, phosphorescence may not occur if $k'_{nr} > k_P$. Nonradiative decay of T_1 is due to EC and ISC from T_1 to S_0. These processes can be combined mathematically as follows: $k'_{nr} = k'_{ec} + k'_{isc}$. Generally, $k'_{ec} >> k'_{isc}$. Thus, phosphorescence at room temperature is usually observed only if the probability of external conversion is significantly reduced by sufficiently trapping or immobilizing the phosphor.

Phosphorescence is sensitive to environmental effects such as matrix lattice vibrations, halogen substitutions, and solvent effects. For instance, a change from nonpolar to polar solvent will result in a spectral shift to either a higher or lower wavelength depending upon the nature of the electronic state. This solvent effect has been used to confirm the $\pi\pi^*$ and $n\pi^*$ natures of the various electronic transitions. For $n\pi^*$ transitions, an increase in solvent polarity will yield shifts to shorter wavelengths (blue shift); whereas, for the $\pi\pi^*$ transition, a shift to longer wavelengths (red shift) is observed with increasing solvent polarity.

For polyaromatic hydrocarbons, an increase in ring size will typically yield a phosphorescence shift toward longer wavelengths (e.g. anthracene > naphthalene > benzene). Linear polyaromatics will generally exhibit phosphorescence at longer wavelengths than nonlinear polyaromatics.[20]

---

[20] S.P. McGlynn, T. Azumi, M. Kinoshita, **Molecular Spectroscopy of the Triplet State**, New Jersey: Prentice-Hall, Inc., 1969.

El-Sayed has established a number of important properties associated with the intersystem crossing (ISC) process.[21,22] *El-Sayed's selection rules* observe that the rate of ISC between different electronic states is much faster than between electronic states of the same type. These rules are summarized by the following:

a). slow ISC: $S(\pi\pi^*) \Leftrightarrow T(\pi\pi^*)$ and $S(n\pi^*) \Leftrightarrow T(n\pi^*)$

b). fast ISC: $S(n\pi^*) \Leftrightarrow T(\pi\pi^*)$ and $S(\pi\pi^*) \Leftrightarrow T(n\pi^*)$

The rate of ISC for a given molecule can be enhanced by adding atoms of high atomic number. Phosphorescence quantum yield will increase for halogen-substituted aromatics as the atomic number of the halogen is increased. Referred to as the *internal heavy-atom effect*, this effect will also quench fluorescence emission and decrease the phosphorescence lifetime. The presence of heavy-atoms in the environment of the analyte also effects the nonradiative and radiative processes. This *external heavy-atom effect* will be discussed later in this document.

Vo-Dinh has noted that "...phosphorescence is a complex phenomenon involving multiple simultaneous molecular processes. A slight modification of the structure of the molecule of interest or a small variation in the chemical nature of the surrounding medium can produce drastic changes in the phosphorescence properties of the emitting compound. Fundamental studies of the triplet state are currently of great interest in photophysics, photochemistry, molecular biology, and quantum chemistry.".[12]

2.2 Basic Elements of Phosphorimetry

Ideally, one should be able to observe phosphorescence in gases, liquids, and solids at any temperature; however, as mentioned earlier, the probability of non-radiative decay is much greater than that of radiative emission due to the many competing processes that can occur during a lengthy phosphorescence lifetime. A few important considerations that can either enhance or interfere with phosphorescence measurement include the effects of heavy-atom, quenching agents, and temperature. In addition to addressing the two most common types of phosphorimetry (low temperature vs. room temperature), the following discussion will elaborate on the basic elements that are common to each technique.

2.2.1 General Considerations: The Heavy-Atom Effect

The heavy-atom effect has been found to be useful for low temperature phosphorescence (LTP) studies, room-temperature phosphorescence measurements in liquid solutions (RTPL), micelle-stabilized room-temperature phosphorescence (MSRTP) investigations, and solid-surface room-temperature phosphorescence (SSRTP) measurements. A heavy-atom in the presence of a molecule can increase its spin-orbit (S-O) coupling interaction. Schenk has cited a simple description of S-O coupling that is originally attributed to Turro.[23]

---

[21] M.A. El-Sayed, *J. Chem. Phys.* 1962, V. 36, p. 573.
[22] M.A. El-Sayed, *J. Chem. Phys.* 1963, V. 38, p. 2834.
[23] N.J. Turro, *J. Chem. Educ.*, 1969, V. 46, p. 2.

> "Turro represents the magnetic moment of the orbital motion of the electron in terms of a magnetic field at the center of the orbit; that is, at the nucleus. He then invokes the analogy of an external magnetic field which can flip a magnetic dipole from one orientation to another. The electron, by virtue of its spin and charge, is also a magnetic dipole. Although the electron is in orbit about the nucleus, the nucleus may be considered, by the laws of relativity, to be in orbit about the electron. The overall result is that the magnetic field of the nucleus can, and does, interact with the magnetic dipole of the electron, so that the resultant force causes the electron to flip its spin direction."[24]

Obviously, S-O coupling will depend on both the nuclear charge and the particular orbital of the electron. An electron with more "*s* character" will increase S-O coupling. Since the magnitude of the nuclear magnetic field is directly proportional to the nuclear charge of the heavy-atom, S-O coupling increases with increasing atomic number. Suitable functional groups that can increase the probability of spin-flip include: Cl, Br, I, NO_2, CO_2H, and others.[24]

The *internal heavy-atom effect*, which comes about when the heavy-atom is chemically bound to the compound of interest, was discovered in 1949 by McClure.[25] The improved S-O coupling provided by this effect can significantly enhance a molecule's phosphorescence emission. Because the spin-orbit coupling is large and electrons can readily become unpaired, the probability of intersystem crossing is substantially increased when a molecule contains a heavy-atom.

In addition to the internal heavy-atom effect, it is also possible to improve S-O coupling via the addition of an external heavy-atom. In 1952, this *external heavy-atom effect* was discovered by Kasha following studies of the effects of ethyl iodide on the singlet-triplet transitions of 1-chloronaphthalene.[26] It was observed in the laboratory that a binary solution of these two colorless components was of a yellow color. The effect was attributed to an increase of S-O coupling in the halonaphthalene. The external heavy-atom effect generally results in the following:

1). an increase in the $S_0 \rightarrow T_1$ absorption,
2). a decrease in the phosphorescence lifetime (τ_P),
3). a decrease in the fluorescence quantum yield (ϕ_f), and
4). a general increase in phosphorescence quantum yield (ϕ_p).[12]

Although it has been nearly fifty years since Kasha first reported that heavy-atoms can alter the rates of molecular spin-forbidden transitions, there is still not a universally accepted explanation of the fundamental interactions that occur between the phosphor and the heavy-atom. From a molecular point of view, S-O coupling causes a *mixing* of singlet and triplet states. Each singlet state is contaminated by a measure of triplet character and triplets become more *singlet-like*. White and Seybold have noted the following: "Despite the scrutiny that it has received,

---

[24] G.H. Schenk, **Absorption of Light and Ultraviolet Radiation: fluorescence and phosphorescence emission** Boston: Allyn and Bacon, Inc., 1973.
[25] D.S. McClure, *J.Chem. Phys.*, 1949, V. 17, p. 905.
[26] M. Kasha, *J. Chem. Phys.*, 1952, V. 20, p. 71.

many important features of the external heavy-atom effect remain obscure or confusing. Regarding the fundamental interactions between the aromatic compounds and the heavy-atom perturbing species, some authors claim that charge-transfer complexes are present, whereas others favor exchange interactions. Exciplexes have also sometimes been specifically mentioned.".[27]

Low Temperature Studies

Although the number of possible combinations of analyte vs. heavy-atom vs. analytical method are staggering, a few laboratories have investigated the heavy-atom S-O coupling effect on phosphorescence measurements by selecting well-defined systems. In 1962, the external heavy-atom effect on the LTP spectra and lifetimes of naphthalene and its 1-monohalogenated derivatives was measured by McGlynn, et al.[28] Propyl halides were added in order to achieve a heavy-atom enhancement. Since that time, Winefordner and colleagues have extensively studied the influence of the external heavy-atom effect on the sensitivity of LTP measurements.[29,30,31,32]

Room Temperature Investigations

Although the external heavy-atom effect is generally useful for enhancing all phosphorescence measurements, the technique is especially beneficial for SSRTP analyses. In most cases, the heavy-atoms are randomly dispersed in the entire sample volumes being analyzed. However, for SSRTP, the heavy-atoms can be concentrated on a small sample spot following the evaporation of the solvent(s). Therefore, the effective concentration of the heavy-atoms will be much greater for a dried spot compared to a solution. For a solid substrate such as paper, the heavy-atoms and the analyte molecules will be held in close proximity in the interstices between the cellulose fibers. This spatial constraint results in a more efficient heavy-atom effect.

The use of the external heavy-atom effect for the increase of SSRTP intensity was first reported in 1975 by Seybold and White.[33] Sodium iodide was reported to strongly decrease the fluorescence signal and increase the phosphorescence intensity of 2-naphthalene sulfonate (sodium salt). T. Vo-Dinh and others used sodium iodide once again in 1976 to enhance the SSRTP of a wide variety of compounds of biological and pharmaceutical interest.[34] In most cases, it was found to be very efficient in increasing phosphorescence quantum yield; thereby improving the limits of detection of the method.

Other investigators have likewise attempted to improve the phosphorescence quantum yields of model phosphors using heavy-atom salts. Table 1 provides a summary of potentially

---

[27] W. White and P.G. Seybold, *J. Phys. Chem.*, 1977, V. 81, p. 2035.
[28] S.P. McGlynn, M.J. Reynolds, G.W. Daigre, and N.D. Christodoyleas, *J. Phys. Chem.*, 1962, V. 66, p. 2499.
[29] L.V.S. Hood and J.D. Winefordner, *Anal. Chem.*, 1966, V. 38, p. 1922.
[30] R.J. Lukasiewicz, J.J. Mousa, and J.D. Winefordner, *Anal. Chem.*, 1972, V. 44, p. 963.
[31] J.J. Aaron, J.J. Mousa, and J.D. Winefordner, *Talanta*, 1973, V. 20, p. 279.
[32] R.J. Lukasiewicz, J.J. Mousa, and J.D. Winefordner, *Anal. Chem.*, 1972, V. 44, p. 1339.
[33] P.G. Seybold and W. White, *Anal. Chem.*, 1975, V. 47, p. 1199.
[34] T. Vo-Dinh, E. Lue Yen, and J.D. Winefordner, *Anal. Chem.*, 1976, V. 48, p. 1186.

Table 1. Salts that have been investigated as potential external heavy-atom phosphorescence enhancers.

Heavy-Atom Salt	Year	Reference
sodium iodide (NaI)	1975 1976 1979 1992 1993	Seybold & White, *Anal. Chem*. V. 47, p. 1199. Vo-Dinh, et al., *Anal. Chem*., V. 48, p. 1186. Vo-Dinh, et al., *Anal. Chem*., V. 51, p. 1915. Purdy & Hurtubise, *Appl. Spectr*., V. 46, p. 988. Tjioe & Hurtubise, *Anal. Lett*., V. 26, p. 557.
sodium chloride (NaCl)	1989 1992 1993	Hurtubise, et al. *Microchem. J*., V. 40, p. 317. Purdy & Hurtubise, *Appl. Spectr*., V. 46, p. 988. Tjioe & Hurtubise, *Anal. Lett*., V. 26, p. 557.
sodium bromide (NaBr)	1979 1988 1989 1992 1993	Vo-Dinh, et al., *Anal. Chem*., V. 51, p. 1915. Khasawneh, et al., *Anal. Lett*., V. 21, p. 125. Hurtubise, et al. *Microchem. J*., V. 40, p. 317. Purdy & Hurtubise, *Appl. Spectr*., V. 46, p. 988. Tjioe & Hurtubise, *Anal. Lett*., V. 26, p. 557.
silver nitrate ($AgNO_3$)	1978 1979	Bower, et al., *Anal. Chim. Acta*, V. 102, p. 1. Vo-Dinh, et al., *Anal. Chem*., V. 51, p. 1915.
cesium iodide (CsI)	1979	Vo-Dinh, et al., *Anal. Chem*., V. 51, p. 1915.
lead (II) acetate ($Pb(C_2H_3O_2)_2$)	1977 1979 1994	Jakovljevic, *Anal. Chem*., V. 49, p. 2048. Vo-Dinh, et al., *Anal. Chem*., V. 51, p. 1915. Li & Yang, *Anal. Chim. Acta*, V. 296, p. 99.
lead (IV) acetate ($Pb(C_2H_3O_2)_4$)	1977	Jakovljevic, *Anal. Chem*., V. 49, p. 2048.
lead nitrate ($Pb(NO_3)_2$)	1978 1994	Bower, et al., *Anal. Chim. Acta*, V. 102, p. 1. Li & Yang, *Anal. Chim. Acta*, V. 296, p. 99.
lead borate ($Pb(BO_2)_2 \cdot H_2O$)	1977	Jakovljevic, *Anal. Chem*., V. 49, p. 2048.
lithium perchlorate ($LiClO_4$)	1979	Vo-Dinh, et al., *Anal. Chem*., V. 51, p. 1915.
mercury (II) chloride ($HgCl_2$)	1978	Bower, et al., *Anal. Chim. Acta*, V. 102, p. 1.

Table 1 (continued). Salts that have been investigated as potential external heavy-atom phosphorescence enhancers.

mercury (II) nitrate ($Hg(NO_3)_2$)	1978	Bower, et al., *Anal. Chim. Acta*, V. 102, p. 1.
thallium nitrate ($TlNO_3$)	1988 1989 1989 1994 1996	Khasawneh, et al., *Anal. Lett*., V. 21, p. 125. Perry, et al., *Anal. Chem*., V. 61, p. 2328. Perry, et al., *Anal. Chim. Acta*, V. 225, p. 415. Corley & Hurtubise, *Appl. Spectr*., V. 48, p. 747. Chu & Hurtubise, *Appl. Spectr*., V. 50, p. 476.
thallium (I) acetate ($TlC_2H_3O_2$)	1977 1978 1987 1993 1994	Jakovljevic, *Anal. Chem*., V. 49, p. 2048. Bower, et al., *Anal. Chim. Acta*, V. 102, p. 1. Suter, et al., *Anal. Chem*., V. 59, p. 1644. Tjioe & Hurtubise, *Anal. Lett*., V. 26, p. 557. Corley & Hurtubise, *Appl. Spectr*., V. 48, p. 747.
thallium (III) acetate ($Tl(C_2H_3O_2)_3$)	1977	Jakovljevic, *Anal. Chem*., V. 49, p. 2048.
thallium fluoride (TlF)	1977 1994	Jakovljevic, *Anal. Chem*., V. 49, p. 2048. Corley & Hurtubise, *Appl. Spectr*., V. 48, p. 747.
thallium chloride (TlCl)	1978 1994	Bower, et al., *Anal. Chim. Acta*, V. 102, p. 1. Corley & Hurtubise, *Appl. Spectr*., V. 48, p. 747.
potassium iodide (KI)	1988	Khasawneh, et al., *Anal. Lett*., V. 21, p. 125.
thorium chloride ($ThCl_4$)	1988	Khasawneh, et al., *Anal. Lett*., V. 21, p. 125.
cadmium acetate ($Cd(C_2H_3O_2)_2$)	1995	Liu, et al., *Appl. Spectr*., V. 49, p. 320.
zinc acetate ($Zn(C_2H_3O_2)_2$)	1995	Liu, et al., *Appl. Spectr*., V. 49, p. 320.
indium sulfate ($In_2(SO_4)_3$)	1995	Liu, et al., *Appl. Spectr*., V. 49, p. 320.
barium acetate ($Ba(C_2H_3O_2)_2$)	1995	Liu, et al., *Appl. Spectr*., V. 49, p. 320.
sodium nitrate ($NaNO_3$)	1994	Corley & Hurtubise, *Appl. Spectr*., V. 48, p. 747.
sodium iodate ($NaIO_3$)	1988	Khasawneh, et al., *Anal. Lett*., V. 21, p. 125.

useful external heavy-atom phosphorescence enhancers that have been reported in the literature. Nevertheless, the reader is advised that very few of the salts listed in Table 1 are universally suitable for all SSRTP investigations. A particular heavy-atom salt that is responsible for significantly improving the phosphorescence quantum yield of a single model analyte may in fact offer no phosphorescence enhancement when used in conjunction with other phosphors.

Tjioe and Hurtubise have reported that strong RTP can be detected without adding a heavy-atom if the analyte is immobilized on Whatman™ 1PS filter paper.[35] The Whatman™ 1PS filter paper is a water repellent paper that has been used for the partition of phases in place of conventional separatory funnels. The paper is specially formulated by Whatman to allow for the separation of aqueous solvents from water immiscible solvents. It is impregnated with a special silicone and contains a tin complex to enhance stability. The authors acknowledge that the tin complex found therein may be an active participant in the RTP enhancement of the analyte.

2.2.2 General Considerations: Quenching Effects

Oxygen

Oxygen is one of the most efficient phosphorescence quenching agents. It can also decrease fluorescence yield, but the quenching of phosphorescence is much more drastic as a result of the long triplet lifetimes encountered. Typically, the primary effects of oxygen on aromatic phosphors are:

1). a decrease in the phosphorescence intensity (k_P),
2). a decrease in the phosphorescence lifetime (τ_P),
3). an appearance of absorption bands due to charge-transfer complexes, and
4). an increase in $S_0 \rightarrow T_1$ absorption.

Various theoretical models of this phenomenon have been proposed. One explanation has attributed oxygen quenching to an *intermolecular exchange interaction*.[20] A potential mechanism of *contact charge transfer* has been discussed as well.[36] A theoretical study of the quenching of the T_1 state of a phosphor by oxygen has been reported by Kawaoka and colleagues.[37] They propose that the most likely quenching mechanism deactivates the molecule from T_1 to its singlet ground state whereas oxygen undergoes a transition from its triplet ground state to an excited singlet state.

Moisture

Studies have shown that RTP intensities are reduced for samples that are exposed to ambient moisture (such as humidity).[34,38,39] The quenching process by moisture is so efficient that RTP intensities will often be rendered undetectable within less than a minute. It is generally agreed by the RTP community that the water molecules compete with the analytes for bonding

---

[35] S.W. Tjioe and R.J. Hurtubise, *Talanta*, 1994, V. 41, p. 595.
[36] H. Tsubomura and R.S. Mulliken, *J. Am. Chem. Soc.*, 1960, V. 82, p. 5966.
[37] K. Kawaoka, A.U. Khan, and P.R. Kearns, *J. Chem. Phys.*, 1967, V. 46, p. 1842.
[38] E.M. Schulman and C. Walling, *J. Phys. Chem.*, 1973, V. 77, p. 902.
[39] S.L. Wellons, R.A. Paynter, and J.D. Winefordner, *Spectrochim. Acta*, 1974, V. 30A, p. 2133.

sites on the solid supports. This would have the effect of decreasing the phosphor-support adsorption process and yielding an increased probability of collisional and vibrational quenching.

Schulman and Parker published a thorough study of the influence of moisture, oxygen, and support-phosphor interactions on RTP in 1977.[40] They found that the degree of oxygen quenching increased significantly with the relative humidity. They suggested that moisture allows an increase in RTP quenching by oxygen because it disrupts hydrogen bonds and can facilitate the diffusion of oxygen into the solid support material. A number of researchers have attempted to combat these effects by filling the channels and interstices of filter paper substrates with various salts and sugars, thus preventing the transport of oxygen into the matrix.[41,42]

Chen, Tjioe, and Hurtubise have proposed that at least two mechanisms are involved with the quenching of phosphors adsorbed on filter paper.[43] During their investigations, dynamic quenching of the phosphor was minimal, but matrix quenching was discovered to be considerable after a certain amount of moisture was adsorbed by the filter paper support. Based on these early studies, the researchers have further proposed that the changes in phosphorescence due to the adsorption of moisture on filter paper are caused primarily by alterations of the hydrogen-bonding network in the "amorphous regions" of the filter paper.[44] These reports serve to illustrate the importance of protecting RTP samples from the quenching effects of oxygen and moisture.

2.2.3 General Considerations: Solvent Effects

Low Temperature Studies

The selection of solvents for low-temperature phosphorescence measurements has been given careful consideration. In 1941, Lewis et al. reported that when a liquid is cooled, the intensity of phosphorescence increases as viscosity increases.[45] Additionally, they consistently used solvents that contain many hydroxyl groups. It was proposed that the hydrogen bonds allowed the "solvent molecules to be *clamped* tightly to one another and to the phosphor molecules as well". They found that phosphorescence was measurable from dilute solutions of fluorescein in any acid solvent which had been cooled without crystallization to a glassy state.

Winefordner and colleagues have provided thorough reviews of the potential solvents that are suitable for use in low temperature phosphorescence (LTP) studies.[46,47,48] They have advised that fluorescence-grade solvents are generally excellent solvents for LTP. The extreme sensitivity of this method places severe demands on the purity of solvents and other reagents

---

[40] E.M. Schulman and R.T. Parker, *J. Phys. Chem*., 1977, V. 81, p. 1932.
[41] G.L. Niday and P.G. Seybold, *Anal. Chem*., 1978, V. 50, p. 1577.
[42] D.L. McAleese, R.S. Freedlander, and R.B. Dunlap, *Anal. Chem*., 1980, V. 52, p. 2443.
[43] J. Chen, S.W. Tjioe, and R.J. Hurtubise, *Appl. Spectr*., 1994, V. 48, p. 1242.
[44] J. Chen and R.J. Hurtubise, *Appl. Spectr*., 1995, V. 49, p. 98.
[45] G.N. Lewis, D. Lipkin, and T.T. Magel, *J. Am. Chem. Soc*., 1941, V. 63, p. 3005.
[46] J.D. Winefordner, W.J. McCarthy, and P.A. St. John, *Methods of Biochemical Analysis*, 1967, V. 15, p. 369.
[47] J.D. Winefordner, P.A. St. John, and W.J. McCarthy, in **Fluorescence Assay in Biology and Medicine II**(S. Udenfriend, ed.), New York: Academic Press, Inc., 1969.
[48] C.M. O'Donnell and J.D. Winefordner, *Clin. Chem*., 1975, V. 21, p. 285.

utilized for LTP. Good low temperature phosphorimetry solvents should neither absorb strongly nor emit light in the spectral regions of interest.

Room Temperature Investigations

Hilsenbeck and Haustein have studied the effects of solvents on room temperature phosphorescence measurements.[49] Although the solvent is typically removed prior to SSRTP measurements, they noted that the nature of the solvent can affect the intensity of the resulting phosphorescence on a solid cellulose substrate. The model phosphor-substrate combination selected for their studies was p-aminobenzoic acid (PABA) and Schleicher and Schuell™ filter paper. The solvents studied included methanol, acetone, 1-propanol, 2-butanone, phenol, methylene chloride, carbon tetrachloride, and water. The investigators proposed that solvent volatility has little correlation with RTP intensity and that solvents with high dielectric constants will generally allow for more intense phosphorescence signals. The former claim is unexpected considering the high probability of intermolecular collisional quenching due to unfavorable phosphor-solvent interactions.

In many instances, the selection of solvent can add an additional variable to the analyte-matrix-heavy-atom combination. For instance, Senthilnathan and Hurtubise advise that "it is important to consider both the initial wet chemistry and the final dried matrix for phosphorescent compounds...". They found that the adsorption of PABA on sodium acetate using ethanol as the solvent yielded strong RTP signals; whereas, when the solvent was changed to acetone or ether, no RTP was observed from the analyte.[50]

Gaye and Aaron have studied the effect of pH on the RTP properties of several purine and pyrimidine derivatives adsorbed on filter paper.[51] It was discovered that RTP excitation and emission wavelengths do not vary significantly with pH. For most compounds, the use of basic (pH ~ 13) solutions yield stronger RTP signals than the use of neutral or acidic (pH ~ 1.6) solutions. Exceptions were adenine, theobromine, and theophylline, which give more intense RTP signals when found in neutral, rather than basic, conditions.

2.2.4 General Considerations: Temperature-Induced Effects

Typically, phosphorescence spectra obtained at room temperature are of lower resolution than their counterparts measured at liquid nitrogen temperatures. Additionally, phosphorescence quantum yields generally increase as the temperature of the sample is decreased. Schulman and Parker observed that RTP intensities are decreased as the sample temperature is increased in the range of 13° to 38° C.[40] De Lima and de M. Nicola found that RTP intensities decreased between 30% and 80% for various 1,8-naphthyridine derivatives adsorbed on filter paper as the sample temperature was increased from 25° to 65° C.[52] Jones and Siegel have studied the effect of temperature on the phosphorescence lifetimes of various polyaromatic hydrocarbons in

[49] S.J. Hilsenbeck and C. Haustein, *J. Iowa Acad. Sci.*, 1988, V. 95, p. 38.
[50] V.P. Senthilnathan and R.J. Hurtubise, *Anal. Chem.*, 1985, V. 57, p. 1227.
[51] M.D. Gaye and J.J. Aaron, *Talanta*, 1989, V. 36, p. 445.
[52] C.G. De Lima and E.M. de M. Nicola, *Anal. Chem.*, 1978, V. 50, p. 1658.

conjunction with solid substrates such as poly(methylmethacrylate).[53] Lehotay and colleagues have used temperature control to study the RTP of rhodamine 6G, warfarin, and PABA on filter paper.[54] They reported that the phosphorescence of PABA could only be observed below 25° C.

Hurtubise, et al. have reported the results of their investigations of the effect of temperature on the RTP of PABA immobilized on sodium acetate substrates.[55,56] Quantum yield values were obtained for the anion of PABA adsorbed on sodium acetate from +23° to -180° C. Phosphorescence lifetime data was also acquired from +23° to -196° C for the adsorbed anion. It is not surprising that the phosphorescence quantum yield values were substantially increased at lower temperatures. Phosphorescence lifetimes were also extended at the lower temperatures.

The Hurtubise group has investigated the effects of temperature on the RTP properties of 4-phenylphenol (4-PP) and benzo[*f*]quinoline (B[*f*]Q) adsorbed on filter paper.[57,58] For each analyte, experimental values of phosphorescence quantum yield and phosphorescence lifetime were acquired at temperatures between 23° to -180° C. Results indicated that the phosphors are not as strongly held on filter paper at room temperature as they are at low temperatures. Significant phosphorescence quantum yield improvements were achieved (a 9.2-fold increase for the B[*f*]Q and a 26.5-fold increase for the 4-PP) as the samples were cooled from 23° to -180° C. Based on these results and supporting work by Nissan[59], the investigators proposed that as the temperature increases for a cellulose-based material, the number of hydrogen bonds in the cellulose network decreases and the matrix becomes less rigid. Thus, the enhancement of phosphorescence quantum yield at reduced temperatures can best be explained in terms of an increase in modulus of the solid matrix.

2.2.5 Low Temperature Phosphorescence (LTP)

Traditionally, phosphorimetry has been performed at liquid nitrogen temperatures (77K) in order to minimize the radiationless deactivation of the triplet state molecule.[11] Low temperature phosphorimetry (LTP) involves the trapping of analytes within a frozen organic solvent which serves as a rigid glass-like matrix. Since this technique provides significant improvements in quantum yield, most of the past work in phosphorimetry has been performed in this fashion.[60] At this time, only one report in the literature has indicated that solid-matrix luminescence at room temperatures is superior to LTP for improved quantum yields.[61] LTP has

---

[53] P.F. Jones and S. Siegel, *J. Chem. Phys*., 1969, V. 50, p. 1134.
[54] S.J. Lehotay, B.T. Jones, M.A. Mignardi, L.A. Files, and J.D. Winefordner, *Microchem. J*., 1987, V. 36, p. 235.
[55] S.M. Ramasamy and R.J. Hurtubise, *Anal. Chem*., 1987, V. 59, p. 432.
[56] R.J. Hurtubise, S.M. Ramasamy, J.M. Bello, G.J. Burrell, and L.A. Citta, in **Luminescence Applications in Biological, Chemical, Environmental, and Hydrological Sciences** (M.C. Goldberg, ed.), ACS Symposium Series 383, American Chemical Society, 1989, p. 155.
[57] S.M. Ramasamy and R.J. Hurtubise, *Talanta*, 1989, V. 36, p. 315.
[58] S.M. Ramasamy and R.J. Hurtubise, *Appl. Spectr*., 1989, V. 43, p. 616.
[59] H. Nissan, *Macromol*., 1976, V. 9, p. 840.
[60] J.D. Winefordner, W.J. McCarthy, and P.A. St. John, *Methods of Biochemical Analysis*, 1967, V. 15, p. 369.
[61] S.M. Ramasamy and R.J. Hurtubise, *Appl. Spectr*., 1993, V. 47, p. 116.

traditionally been the favored technique when spectra of high resolution and maximum intensity are required.

The most commonly used solvents include pure ethanol and EPA (a mixture of ethanol, isopentane, and ether, 2:5:5 v/v/v). Other pure solvents suitable for this purpose, and useful mixtures of those solvents, have been reported in the literature.[62] There are a number of problems associated with this technique including frosted or opaque matrices, sample non-uniformity, and cracked cryogenic matrices. Extreme care must be taken during the introduction of the sample into the liquid nitrogen-filled Dewar in order to avoid those problems. These extensive sample preparation procedures are inconvenient and time-consuming for the analyst. The numerous disadvantages associated with LTP measurements have been discussed in the literature.[63,64,65] The primary factor contributing to the lack of wide-spread use of this technique at present is the requirement that frozen matrices be utilized to immobilize the compounds to be analyzed.

2.2.6 Room Temperature Phosphorescence in Liquid Solutions (RTPL)

Although phosphorescence has been observed in liquid solutions at room temperature (RTPL), it is generally accepted that the phosphorescence intensities are too low to be useful for analytical purposes. There are a number of phosphorescence quenching processes that typically deactivate the triplet state via a nonradiative pathway. Intermolecular collisional quenching and quenching by dissolved oxygen are merely two of the factors which may contribute to very weak or undetectable phosphorescence signals. Parker has reported that the first quantitative measurements of phosphorescence from fluid solution were obtained in 1930.[66] A visual phosphoroscope was used to observe the photoluminescence from solutions of eosin in glycerol at room temperature. A number of investigators have attempted to use highly purified solvents and nitrogen-purged systems in order to combat the phosphorescence quenching of analytes in liquid solutions; however, these techniques have met with limited success.[67,68,69,70] RTPL has often been reported as *anomalous emission bands at room temperature in fluid solution*.[71,72] Weinberger, Rembish, and Cline Love have published a comparison of techniques for generating

---

[62] J.D. Winefordner, P.A. St. John, and W.J. McCarthy, *Phosphorimetry as a means of Chemical Analysis* in **Fluorescence Assay in Biology and Medicine**, New York: Academic Press, 1969.
[63] J.L. Ward, G.L. Walden, J.D. Winefordner, *Talanta*, 1981, V. 28, p. 201.
[64] G.G. Guilbault, **Practical Fluorescence: Theory, Methods, and Techniques**, New York: Marcel Dekker, 1974.
[65] P.A. St. John and J.D. Winefordner, *Anal. Chem.*, 1963, V. 35, p. 2211.
[66] C.A. Parker, **Photoluminescence of Solutions**, New York: Elsevier, 1968.
[67] J. Langelaar, G.A. de Vries, and D. Bebelaar, *J. Sci. Instrum.*, 1969, V. 2, p. 149.
[68] M. Almgren, *Photochem. Photobiol.*, 1967, p. 829.
[69] C.A. Parker and T. A. Joyce, *Trans. Faraday Soc.*, 1969, V. 65, p. 2823.
[70] N.J. Turro, K.C. Liu, M.F. Chow and P. Lee, *Photochem. Photobiol.*, 1978, V. 27, p. 523.
[71] R.B. Bonner, M.K. DeArmond, and G.H. Wahl, Jr., *J. Am. Chem. Soc.*, 1972, V. 94, p. 988
[72] E. Vander Donckt, M. Matagne, and M. Sapir, *Chem. Phys. Lett.*, 1973, V. 20, p. 81.

RTP in fluids.[73] Their report discusses four techniques including microcrystalline/colloidal RTP, cyclodextrin-induced RTP, sensitized/quenched RTP, and MSRTP.

2.2.7 Micelle-Stabilized Room Temperature Phosphorescence (MSRTP)

In 1977 researchers discovered that phosphorescence could be observed in aqueous micelle solutions at room temperature.[74] Micelle-stabilized phosphorescence emission has been extensively investigated since that time.[75,76,77,78,79,80,81,82,83,84,85,86] There are a number of ways in which RTP is enhanced by trapping the phosphors in a micellar environment.

1). The micelle structure protects the excited analytes from external quenching agents.
2). The immobilization of the analyte within the micelle interior will reduce the probability of collisional quenching.
3). S-O coupling between the phosphors and heavy-atoms is increased as a result of their close proximity within the micelle.[87]

Disadvantages associated with the MSRTP technique include sample preparation procedures that are time-consuming and the limited ability of micelle solutions to trap non-polar or weakly polar analytes. Although the technique of MSRTP has matured rapidly, further research is necessary in order to determine the effects of various heavy-atoms in the micellar microenvironment. Additionally, the nature of temperature influences on MSRTP still remain somewhat unclear. Nevertheless, MSRTP is the most commonly used method of performing RTP in solution at this time.

---

[73] R. Weinberger, K. Rembish, and L.J. Cline Love, in **Advances in Luminescence Spectroscopy**, ASTM STP 863, L.J. Cline Love and D. Eastwood, Eds., Philadelphia: American Society for Testing and Materials, 1985.
[74] K. Kalyanasundaram, F. Grieser, and J.K. Thomas, *Chem. Phys. Lett.*, 1977, V. 51, p. 501.
[75] R. Humphry-Baker, V. Moroi, and M. Grätzel, *Chem. Phys. Lett.*, 1978, V. 58, p. 207.
[76] M. Almgren, F. Grieser, and J.K. Thomas, *J. Am. Chem. Soc.*, 1979, V. 101, p. 279
[77] L.J. Cline Love, M. Skrilec, and J.G. Habarta, *Anal. Chem.*, 1980, V. 52, p. 754.
[78] L.J. Cline Love and M. Skrilec, *Anal. Chem.*, V. 52, p. 1559.
[79] L.J. Cline Love and M. Skrilec, in **Solution Behavior of Surfactants**, Vol. 2, K.L. Mittal and E.J. Fendler (Eds.), New York: Plenum, 1982.
[80] S. Scypinski and L.J. Cline Love, *Anal. Chem.*, 1984, V. 56, p. 322.
[81] R.A. Femia and L.J. Cline Love, *Anal. Chem.*, 1984, V. 56, p. 327.
[82] M.E. Díaz García and A. Sanz-Medel, *Anal. Chem.*, 1986, V. 58, p. 1436.
[83] J.D. Bolt and N.J. Turro, *J. Phys. Chem.*, 1981, V. 85, p. 4029.
[84] H. Kim, S.R. Crouch, M.J. Zabik, and S.A. Selim, *Anal. Chem.*, 1990, V. 62, p. 2365.
[85] A.G. Mwalupindi, L.A. Blyshak, T.T. Ndou, and I.M. Warner, *Anal. Chem.*, V. 63, p. 1328.
[86] S. Panadero, A. Gómez-Hens, and D. Pérez-Bendito, *Anal. Chem.*, 1994, V. 66, p. 919.
[87] R. von Wandruszka, *Crit. Rev. in Anal. Chem.*, 1992, V. 23, p. 187.

2.2.8 Solid-Surface Room Temperature Phosphorescence (SSRTP)

Discovery

Lloyd and Miller have observed that the RTP of molecules adsorbed on solid surfaces seems to have been "discovered" no less than four times.[88] In 1972 Schulman and Walling published their findings regarding the phosphorescence of adsorbed ionic organic molecules at room temperature in *Science*.[89] They were surprised to observe that many organic molecules exhibit intense RTP when adsorbed on paper, silica, alumina, asbestos, glass fibers, and other supports. The researchers indicated at that time that they had been unable to find any comparable observations in the literature.

Lloyd and Miller have pointed out that several observations of RTP did in fact exist prior to the work of Schulman and Walling. The first observation of which they are aware was made by Millson in 1944, but apparently his findings were not widely published prior to being quoted in a 1954 text.[90,91] Millson observed that various cottons and other fibers would phosphoresce at room temperature when "bone dry". Apparently the phosphorescence was due to contaminants adsorbed on the cotton. Highly purified cotton does not exhibit the effect.

The next observation of RTP was recorded in 1958.[92] D.J. Brown observed that 2-mercaptonaphth[2,3]iminazole immobilized on a paper chromatogram would show in ultraviolet light a brilliant yellow phosphorescence for several seconds after the light source was extinguished, whereas 2-mercaptobenziminazole would not. Parker and colleagues have reported that their literature searches have revealed that phosphorescence was observed from dyestuffs adsorbed on solid gels (such as gelatine) as early as 1896.[93] They also found that Franck and Pringsheim had reported on their observations of RTP from trypaflavine adsorbed on silica gel, paper, and gelatine in 1943.[94]

In 1967, Roth published the results of fundamental RTP studies involving a wide variety of aromatics on several different solid supports.[95] Seventeen compounds were found to be sufficiently phosphorescent on cellulose surfaces to be detectable at microgram or submicrogram levels. It was emphasized that the technique was valuable as a simple, selective, and non-destructive method for studying chromatograms and electropherograms. Roth's early RTP investigations were eventually acknowledged by Schulman and Parker.[40]

---

[88] J.B.F. Lloyd and J.N. Miller, *Talanta*, 1979, V. 26, p. 180.
[89] E.M. Schulman and C. Walling, *Science*, 1972, V. 178, p. 53.
[90] H.E. Millson, *The Phosphorescence of Textile Fibers and Other Substances* in **Calco Tech. Bull. 753**, American Cyanamid Co., 1944.
[91] H.R. Mauersberger, in **Matthew's Textile Fibers -- 6th Edition**(H.R. Mauersberger, Ed.), New York: Wiley, p. 38.
[92] D.J. Brown, *J. Chem. Soc*., 1958, p. 1974.
[93] R.T. Parker, R.S. Freedlander, and R.B. Dunlap, *Anal. Chim. Acta*, 1980, V. 119, p. 189.
[94] J. Franck and P. Pringsheim, *J. Chem. Phys*., 1943, V. 11, p. 21.
[95] M. Roth, *J. Chromatog*., 1967, V. 30, p. 278.

Theoretical Aspects of SSRTP Analysis

The present theories concerning SSRTP are intimately linked to continuum theories that have been proposed for reflectance spectroscopy. Statistical theories have also been used to describe reflectance spectroscopy; however, these models have not yet been applied to SSRTP. Of the many continuum theory variations, the Kubelka-Munk theory is the one that has been given the most attention by SSRTP practitioners.[96,97,98] Although this theory and its derivatives have not yet suitably described SSRTP, a few of the pertinent concepts are nevertheless mentioned here.

The Kubelka-Munk theory is primarily concerned with the absorption and scattering of light. For most SSRTP support materials, it is likely that both the excitation radiation and emission radiation will be scattered. In addition to the excitation radiation absorbed by the analyte, it is also possible for the solid support material to absorb a portion of this energy. Listed below are a few assumptions made by the Kubelka-Munk theory that pertain to the interaction of light and solid substrates.

- The direction of the excitation radiation is perpendicular to the surface.
- Light within the substrate propagates only in the forward and backward directions. The propagation is perpendicular to the plane-parallel front and rear surfaces of the substrate.
- Once it reaches the surface of the substrate, light is scattered in all directions.
- The parameters that characterize the optical properties of the substrate are k, the absorption coefficient of the excitation radiation; s, the scattering coefficient of the excitation radiation; S, the scattering coefficient of the emitted radiation; and X, the thickness of the scattering material.
- The material is assumed to be homogeneous between its front and rear surfaces. Thus, theoretically, the absorption coefficient and scattering coefficients are not dependent on the thickness of the substrate.

Obviously, many of these assumptions do not hold for real-world SSRTP substrates. For example, in modern luminescence spectrometers, the direction of the excitation radiation is rarely perpendicular to the front surface of the support material. It is also unlikely that the light within an SSRTP substrate will travel only perpendicularly to the front and rear surfaces of the matrix.[99] Finally, most SSRTP supports are not perfectly homogeneous between their boundary surfaces. Thus, the absorption coefficients and scattering coefficients would indeed be dependent on the thickness of the substrate.

---

[96] P. Kubelka, *J. Opt. Soc. Amer*., 1948, V. 38, p. 448.

[97] G. Kortum, **Reflectance Spectroscopy**, New York: Springer-Verlag, 1969.

[98] W.W. Wendlandt and H.G. Hecht, **Reflectance Spectroscopy**, New York: Interscience Publishers, 1966.

[99] H.G. Hecht, *The Interpretation of Diffuse Reflectance Spectra*, in **Standardization in Spectrophotometry and Luminescence Measurements, NBS Special Publication 466**(K.D. Mielenz, R.A. Velapoldi, and R. Mavrodineanu, Eds.), Washington D.C.: U.S. Government Printing Office, 1977.

Modified equations based on the Kubelka-Munk theory have been discussed by Goldman and Goodall during their fluorescence densitometry investigations.[100] Pollak and Boulton have also developed equations based on the Kubelka-Munk theory during their research involving fluorescence from thin-layer chromatograms.[101] In each case, the investigators provided no experimental data to support their theoretical conclusions. Additionally, only a very limited amount of theoretical data was provided. Therefore, a firm conclusion cannot be made as to which approach is more applicable to solid-surface phosphorescence analysis until additional theoretical and experimental work is completed. The possibility also exists that both of the approaches will have to be extensively modified.

Zweidinger and Winefordner have proposed theoretical intensity expressions for LTP investigations using frozen organic solvents, cracked cryogenic glasses, and snowed matrices.[102] Although their equations were experimentally verified for low-temperature analyses, it has been noted that extensive experimental corroboration will be necessary before the intensity equations can be modified for SSRTP work.[2] Hurtubise has recently used RTP data obtained from model compounds adsorbed on filter paper to derive equations that describe the phosphorescence quantum yield for this system. The equations are based on phosphorescence rate constants, activation energies, and analysis temperatures.[103]

Practical Aspects of SSRTP Analysis

There are a number of practical considerations to be addressed prior to performing an SSRTP analysis. Decisions must be made regarding choice of substrate, solvents, and other experimental conditions. Vo-Dinh has reported that "Developing an RTP assay for the first time can be laborious, time-consuming, and sometimes frustrating.". However, by careful planning and optimization of each step in the analysis, potential pitfalls can be easily avoided. Table 2 details the key features of an SSRTP assay and the associated optimization considerations that must be addressed.

[100] J. Goldman and R.R. Goodall, *J. Chromatogr.*, 1968, V. 32, p. 24.
[101] V. Pollak and A.A. Boulton, *J. Chromatogr.*, 1972, V. 72, p. 231.
[102] R. Zweidinger and J.D. Winefordner, *Anal. Chem.*, 1970, V. 42, p. 639.
[103] S.M. Ramasamy and R.J. Hurtubise, *Appl. Spectr.*, 1991, V. 45, p. 555.

Table 2. Optimization of a generic SSRTP analysis

	Variable:	Considerations:
Step #1	Solvent	Degrades substrate? Dissolves heavy-atom perturber? Dissolves analyte? Volatility Purity Toxicity
Step #2	Heavy-Atom Perturber (or other additives)	Necessary? Soluble? Interaction with analyte Purity Toxicity
Step #3	Substrate	Degraded by solvent? Immobilizes heavy-atom? Immobilizes analyte? Availability Cost Ease of use Toxicity
Step #4	Sample Delivery	Sample concentration Reproducibility
Step #5	Drying Operation	Analyte stability Substrate stability Temperature regulation Duration Method
Step #6	RTP Measurement	Duration of instrument *warm-up* Use purge gas? If so, which one? Duration of purge Sample positioning Determine excitation wavelength (pre-scan?) Emission wavelength range to monitor Monochromator slit widths Scan speed Delay time (t_d) Gate time (t_g) Detector sensitivity (PMT voltage)

(table adapted from Vo-Dinh, *Room Temperature Phosphorimetry for Chemical Analysis*)[12]

A wide variety of substrates for RTP investigations have been reported in the literature. In addition to two fundamental texts on solid surface luminescence techniques, a number of review papers are especially useful for surveying the assortment of solid substrates that have already been investigated.[12,93,104,105,106] Nevertheless, at this time no clear-cut choice of a general, all-purpose matrix material for SSRTP can be made since the physical and chemical interactions involved are complex. This is an important consideration since the choice of support material can be critical to the successful observation of RTP. A compound might prove to be an intense phosphor when adsorbed on one support material and offer minimal RTP (or no phosphorescence whatsoever) when combined with a different substrate. With a little luck, the novice may be able to identify the optimum support materials for a particular analysis by carefully searching the pertinent SSRTP literature. On the other hand, Vo-Dinh has advised that "A certain amount of trial and error is inevitable in the search for a good substrate for a new compound.". Table 3 further illustrates the importance of careful SSRTP sample support selection.

Table 3. A few examples of sample-substrate interactions

phosphor	filter paper	sodium acetate	silica gel
4-biphenylcarboxylate	strong RTP	no RTP	---
terephthalic acid	---	no RTP	intense RTP
carbazole	strong RTP	---	no RTP
indole	strong RTP	---	no RTP
PABA	strong RTP	strong RTP	---

(table adapted from Vo-Dinh, *Room Temperature Phosphorimetry for Chemical Analysis*)[12]

Filter Paper Supports

At present, the most commonly used solid substrate for RTP work is filter paper. As an SSRTP matrix, filter paper is inexpensive, widely applicable, and easily prepared. Except for proprietary "binders" that are sometimes added, it has been reported that filter papers are primarily comprised of pure cellulose.[107] Cellulose is an unbranched glucosyl biopolymer containing β-(1-4) linkages [Figure 6]. It is considered to be the most abundant macromolecule present in nature and is ordinarily obtained from two major sources: wood and cotton.

The primary constituents of wood are cellulose, hemicellulose, and lignin. Approximately 55% of wood is cellulose; however, the composition will vary depending on the botanical source. Although cellulose is essential for the production of paper, lignin is an

[104] R.J. Hurtubise, **Solid Surface Luminescence Analysis: Theory, Instrumentation, Applications**, New York: Marcel Dekker, Inc., 1981.
[105] R.T. Parker, R.S. Freedlander, and R.B. Dunlap, *Anal. Chim. Acta*, 1980, V. 120, p. 1.
[106] M. Gunshefski, J.J. Santana, J. Stephenson, and J.D. Winefordner, *Appl. Spectr. Rev.*, 1992, V. 27, p. 143.
[107] R.P. Bateh and J.D. Winefordner, *Talanta*, 1982, V. 29, p. 713.

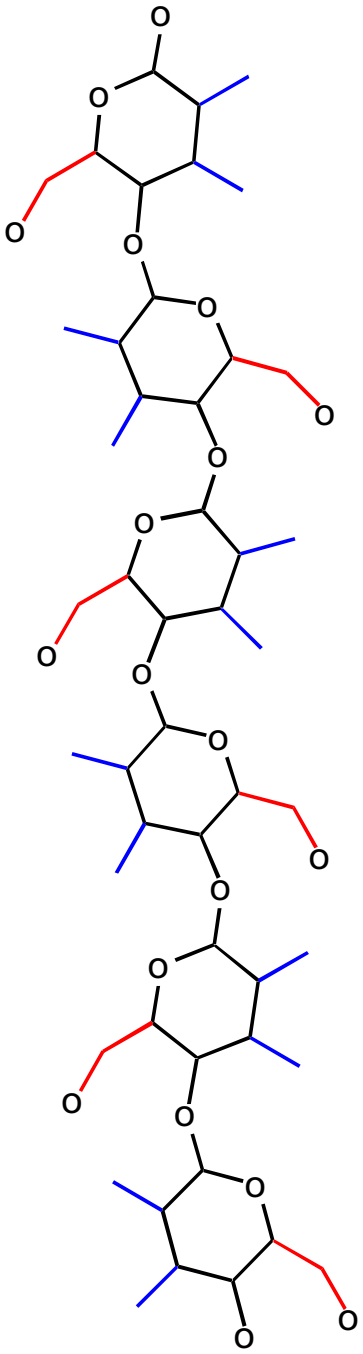

Figure 6. Cellulose Structure.

undesirable component and efforts are made to remove it during the pulping and bleaching process. Depending on the pulping methods utilized, the resulting wood pulps may approach 90% cellulose. Cotton fibers, on the other hand, are approximately 95% cellulose with minor amounts of waxes, pectins, and lignin present. The chemical processing of cotton can result in >99% yields of cellulose.

Bateh and Winefordner have reported that "Contrary to popular belief, the vast majority of filter-paper companies marketing products in the clinical fields do not add special luminescent chemicals (such as optical whiteners and sizing agents) to their pulps".[107] Companies are instead able to achieve the desired characteristics of their papers by chemical treatment (caustic cooking/extracting and inorganic bleaching followed by extensive washing with purified water) and physical processing (such as refining and beating) of the pulps. Nevertheless, researchers have insisted that filter paper cannot be 100% pure cellulose because even cotton fibers will contain trace amounts of hemicellulose and lignins. Bateh and Winefordner have agreed that it would be possible for the hemicellulose fractions (mainly β-1,3-glucans) to contain chemical species that luminesce.

As discussed earlier in this section, Roth is credited with the first analytical SSRTP measurements using a variety of solid supports such as filter paper, plain cellulose, a silica gel-starch mixture, pure alumina, and pure silica gel. The cellulose-based matrices were found to be necessary for RTP to be successfully measured. Minimal RTP was observed when the analytes were adsorbed on a silica gel-starch layer and no phosphorescence was detected when alumina or silica gel surfaces were used.

Schulman and Walling briefly reported their findings involving SSRTP on filter paper and other supports in 1972.[89] They observed that many salts of polynuclear carboxylic acids, phenols, amines, and sulfonic acids adsorbed on filter paper, silica, alumina, asbestos, and glass fibers exhibited strong triplet RTP with no evidence of quenching by oxygen. No phosphorescence was observed for nonionic materials. In 1973 they followed up their preliminary investigation with a more detailed publication citing that filter paper was the best substrate investigated.[38] They indicated that the RTP appeared to involve molecules that were surface-adsorbed, since phosphorescence could not be detected from finely ground samples of pure salts or from crystals grown from solutions. Alternatively, the same samples yielded excellent RTP when impregnated onto paper and slowly dried under an infrared lamp.

The researchers also discovered that dryness was essential. Samples adsorbed on paper would yield no RTP when exposed to a humid atmosphere; however, they would phosphoresce once again following the drying of the sample by heating or desiccation. They claimed that the RTP was completely oxygen insensitive. No difference in RTP intensity was observed for samples stored for weeks under pure atmospheres of dry oxygen, nitrogen, or air. Schulman and Walling proposed that the surface adsorption of the organic molecules was immobilizing them to an extent that their typical nonradiative decay would be minimized. They also attributed the lack of oxygen quenching of the analyte to this surface adsorption although they could not propose an explanation for their theory.

In 1974 Paynter, Wellons, and Winefordner described a "new method of analysis based on RTP".[108] Their study indicated that SSRTP was possible from a wide variety of ionic organic molecules and that the technique could have quantitative and qualitative identification purposes. They provided analytical figures of merit for samples that are representative of a wide variety of polynuclear carboxylic or sulfonic acids, phenols, and amines. Their conclusion was that virtually any salt of these compounds can be expected to phosphoresce at room temperature. Although they could not explain why these ionic aromatic species yielded analytically useful RTP signals, they suggested that the ionic state of the molecules was responsible for providing stronger adsorptions to the filter paper thereby reducing the magnitude of the radiationless decay due to collisional deactivation.

Numerous researchers have used spectral techniques other than RTP to study the interaction of aromatic hydrocarbons with filter paper. Following investigations involving ultraviolet diffuse reflectance and infrared spectrometry, Dalterio and Hurtubise proposed that individual phosphors can act as hydrogen donors, hydrogen accepting species, or as both hydrogen donors and hydrogen acceptors. The results of their work strongly support the concept that hydrogen bonding interactions occur between select phosphors and solid surfaces.[109]

Although an ideal X-ray photoelectron spectroscopy (XPS) probe for the study of filter paper/phosphor interaction has yet to be found, Winefordner and colleagues have utilized this technique to study the surface of Whatman™ No. 1 filter paper before and after the spotting of a phosphor and heavy-atom onto the surface of the paper.[110] The investigators confirmed that the heavy-atoms and the phosphors are sorbed into the bulk of the cellulose matrix. Additionally, it was reported that the extent of penetration of the heavy-atoms into the filter paper appeared to exceed that of the phosphors.

Filter paper has been treated with cyclodextrins in order to enhance RTP intensities. Vo-Dinh and colleagues have studied the selective enhancement of RTP using cyclodextrin-treated cellulose substrates.[111,112,113] Cyclodextrins can form inclusion complexes with compounds that can fit into their hydrophobic cavities. The stabilities of the cyclodextrin-phosphor inclusion complexes are governed by factors such as hydrogen bonding, hydrophobic interactions, and solvation effects as well as the size of the guest molecule.

Cyclodextrins (CD's) are prepared by enzymatically modifying starches. The final product consists of a small number of glucopyranose units joined together to form what is often described as a "doughnut-like structure".[114] Three types of CD's are readily available commercially: an alpha (α) form consisting of six glucose units, a beta (β) form consisting of seven glucose units, and a gamma (γ) form consisting of eight glucose units [Figure 7]. A fourth CD, not as readily available as the others, consists of nine glucose residues (the delta (δ) form). Additional higher-order cyclodextrins have been identified, but the isolation of those structures

---

[108] R.A. Paynter, S.L. Wellons, and J.D. Winefordner, *Anal. Chem.*, 1974, V. 46, p. 736.
[109] R.A. Dalterio and R.J. Hurtubise, *Anal. Chem.*, 1984, V. 56, p. 336.
[110] M.M. Andino, M.A. Kosinski, and J.D. Winefordner, *Anal. Chem.*, 1986, V. 58, p. 1730.
[111] A.M. Alak and T. Vo-Dinh, *Anal. Chem.*, 1988, V. 60, p. 596.
[112] A.M. Alak, N. Contolini, and T. Vo-Dinh, *Anal. Chim. Acta*, 1989,V. 217, p. 171.
[113] T. Vo-Dinh and A. Alak, *Appl. Spectr.*, 1987, V. 41, p. 963.
[114] M.L. Bender and M. Komiyama, **Cyclodextrin Chemistry**, New York: Springer-Verlag, 1978.

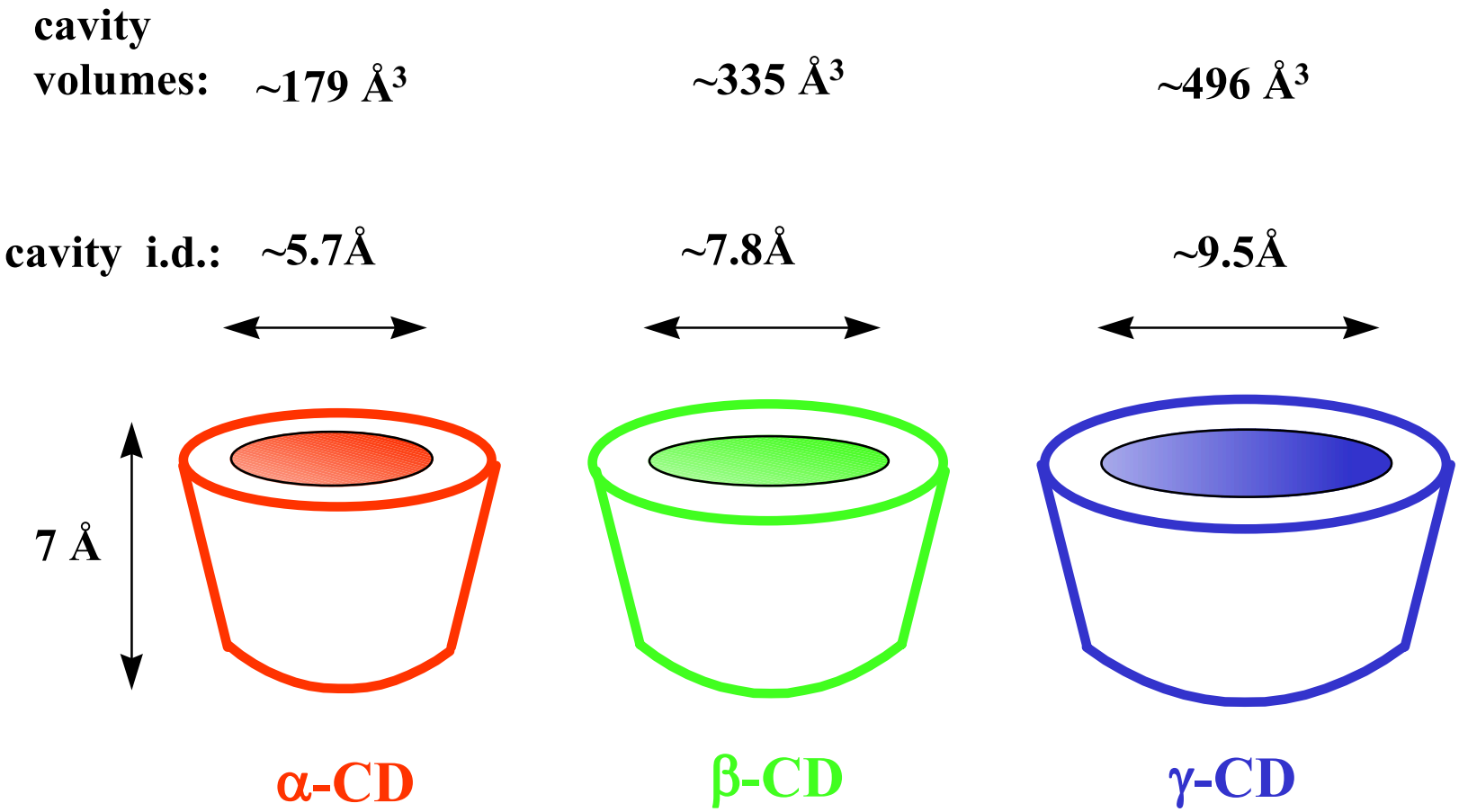

Figure 7. The Cyclodextrins

has proven difficult. Cyclodextrins having fewer than six glucose residues are not known to exist, probably because of steric hindrance.

All of the CD's are crystalline, non-hygroscopic, and they feature a macrocyclic ring structure which has a large internal axial cavity. The outer surface of a CD molecule is hydrophilic as a result of the hydroxyl groups lining the edges of the cylinder, but the internal cavity is hydrophobic in nature as a result of the glycosidic oxygen bridges connecting the monomeric units. It has been shown that the cyclodextrins will form inclusion complexes with many molecules, both organic and inorganic.[115] Table 4 summarizes a few of the physical properties of the cyclodextrins.

Table 4. Physical properties of the cyclodextrins

CD	# of glucose residues	molecular weight (calculated)	water solubility (g/100 mL)	cavity internal diameter[a] (Å)	cavity outer diameter[a] (Å)	cavity depth[a] (Å)	cavity volume[b] ($Å^3$)
α	6	972	14.5	≈5.7	≈13.7	≈7.0	≈179
β	7	1,135	1.85	≈7.8	≈15.3	≈7.0	≈335
γ	8	1,297	23.2	≈9.5	≈16.9	≈7.0	≈496
δ	9	1,459	very soluble	--	--	--	--

[a]Note: values are approximate and may vary considerably depending on literature source.
[b]Cavity volumes calculated from cavity internal diameter and cavity depth values using $\pi r^2 h$.
(adapted from the American Maize-Products Company *Cyclo-dextrins Marketing Briefs*)[116]

Ramasamy and Hurtubise have developed equations that relate changes in SSRTP lifetimes and other phosphorescence parameters to the Young's modulus values of filter paper.[117] The basis for the equations is a theory that describes the change in Young's modulus (E) as a function of temperature in terms of hydrogen bonding in cellulose. Three model compounds were utilized in the investigation (PABA anion, B[*f*]QH^+, and 4-PP). For all systems investigated, linear relationships were obtained between $\ln(\tau_p)$ and $\ln(E)$. They proposed that these investigations form the basis of a fundamental theory for the RTP of compounds adsorbed on filter paper supports.

Nishigaki and colleagues have proposed that filter paper consists of *cages* made by overlapping cellulose chains.[118] According to the authors, phosphors are trapped within these

[115] W. Saenger, *Angew. Chem. Int. Ed. Engl.*, 1980, V. 19, p. 344.
[116] Amaizo American Maize-Products Company, 1100 Indianapolis Boulevard, Hammond, Indiana, 46320-1094. Toll-free: 1-800-348-9896. In Indiana: 1-219-552-9793.
[117] S.M. Ramasamy and R.J Hurtubise, *Appl. Spectr.*, 1991, V. 45, p. 1126.
[118] A. Nishigaki, A. Uchida, I. Oonishi, and S. Ohshima, *Polycylic Aromatic Compounds*, 1996, V. 9, p. 323.

cages in a host-guest arrangement. Small molecules such as vanillin move about easily within the cages; whereas, larger molecules such as 9-anthracenemethanol fit perfectly within the cage and thereby avoid collisional deactivation. Furthermore, the researchers have suggested that there exists an optimum concentration of phosphor molecules that can be trapped by filter paper. As the number of analyte molecules exceeds the number of adsorption sites, the probability of collisional quenching is increased and RTP intensities are reduced.[118]

Paper-based solid substrates are presently the most widely used support materials in the SSRTP field. These supports, or the modified forms thereof, have allowed investigators to develop immunoassays,[119] detect pesticides,[120,121] study pharmaceuticals,[122,123] screen polychlorinated biphenyls (PCBs), [124,125,126] and monitor petroleum permeation through protective clothing.[127] In addition to allowing for the analysis of multicomponent mixtures,[128,129,130] numerous researchers have utilized RTP detection for paper electrophoresis[131] and paper chromatography[52] separations.

At this time, filter paper is the most popular, universal, and convenient substrate in use. However, it suffers from a relatively high background (~400-600 nm) that can interfere with the possibility of lowering the detection limits for most analytes. A few attempts to reduce the background RTP emissions from filter paper have been reported.[107,132,133,134]

---

[119] M.R. Glick and J.D. Winefordner, *Anal. Chem.*, 1988, V. 60, p. 1982.
[120] A.D. Campiglia and C.G. de Lima, *Anal. Chem.*, 1987, V. 59, p. 2827.
[121] S.Y. Su, E.B. Asafu-Adjaye, and S. Ocak, *Analyst(London),* 1984, V. 109, p. 1019.
[122] I.M. Khasawneh, M.C. Garcïa Alvarez-Coque, G. Ramis Ramos, and J.D. Winefordner, *J. Pharm. & Biomed. Anal.*, 1989, V. 7, p. 29.
[123] M.D. Gaye-Seye and J.J. Aaron, Anal. Chim. Acta, 1994, V. 290, p. 166.
[124] W. Watts, A. Pal, L. Ford, G.H. Miller, T. Vo-Dinh, D. Eastwood, and R. Lidberg, *Appl. Spectr.*, 1992, V. 46, p. 1235.
[125] A. Pal, W. Watts, J. Caraway, and T. Vo-Dinh, *Analusis*, 1992, V. 20, p. 149.
[126] T. Vo-Dinh, W. Watts, G.H. Miller, A. Pal, D. Eastwood, and R. Lidberg, in **SPIE -- International Conference on Monitoring of Toxic Chemicals and Biomarkers**, T. Vo-Dinh and K. Cammann, Eds., 1992, V. 1716, p. 490. SPIE -- The International Society for Optical Engineering, P.O. Box 10, Bellingham, Wash. 98227-0010.
[127] D.A. White and T. Vo-Dinh, *Appl. Spectr.*, 1988, V. 42, p. 285.
[128] V.P. Senthilnathan and R.J. Hurtubise, *Anal. Chim. Acta*, 1985, V. 170, p. 177.
[129] E.B. Asafu-Adjaye, J.I. Yun, and S.Y. Su, *Anal. Chem.*, 1985, V. 57, p. 904.
[130] E.B. Asafu-Adjaye and S.Y. Su, *Anal. Chem.*, 1986, V. 58, p. 539.
[131] Y.F. Cheng and T. Vo-Dinh, *Anal. Lett.*, 1990, V. 23, p. 941.
[132] J.L. Ward, E.L. Yen-Bower, and J.D. Winefordner, *Talanta*, 1981, V. 28, p. 119.
[133] D.L. McAleese and R.B. Dunlap, *Anal. Chem.*, 1984, V. 56, p. 600.
[134] J. de Ribamar F., Jr. and A.D. Campiglia, *Microchem. J.*, 1995, V. 52, p. 101.

A Survey of the Conventional SSRTP Support Materials

In addition to filter paper, a number of other substrates have been investigated in order to determine their usefulness as SSRTP sample matrices. A survey of the literature provided the listing of materials in table 5. The reader is advised that not all of the listed substrates were suitable for SSRTP work. Many of the phosphor-adsorbed matrix materials yielded either very weak RTP intensities or, in many cases, no measurable RTP signal whatsoever. All previously investigated substrates are listed for the following reason: often a selection of different phosphor or a substitution of heavy-atom perturber will result in a significantly improved performance of the matrix material. There are at least three independent variables to be considered including analyte, substrate, and heavy-atom perturber. Additionally, quenching agents were often not accounted for in many early investigations. By minimizing the ambient oxygen and moisture surrounding a sample, it is often possible to convert an ineffective substrate into a favorable one.

Table 5. Materials investigated as potential substrates for SSRTP

Matrix Material	Year	Reference
gelatine	1896	Wiedemann, et al., *Ann. Phys.*, V. 58, 103.
	1943	Franck & Pringsheim, *J. Chem. Phys*., V. 11, 21.
cotton fabrics	1944	H.E. Millson, *Calco Tech. Bull*. V. 753.
	1982	J.B.F. Lloyd, *J. Forensic Sci. Soc*., V. 22, 161.
chromatography paper	1958	D.J. Brown, *J. Chem. Soc*., 1958, 1974.
	1984	McAleese & Dunlap, *Anal. Chem*., V. 56, 2244.
paper	1943	Franck & Pringsheim, *J. Chem. Phys*., V. 11, 21.
	1972	Schulman & Walling, *Science*, V. 178, 53
filter paper	1967	M. Roth, *J. Chromatog*., V. 30, 278.
	1973	Schulman & Walling, *J. Phys. Chem*., V. 77, 902.
	1974	Winefordner, et al., *Anal. Chem*., V. 46, 736.
	1977	Schulman & Parker, *J. Phys. Chem*., V. 81, 1932
	1977	Vo-Dinh, et al., *Talanta*, V. 24, 146.
	1977	Vo-Dinh, et al., *Anal. Chem.*, V. 49, 1126.
	1982	Bateh & Winefordner, *Talanta*, V. 29, 713.
	1982	Su & Winefordner, *Microchem. J*., V. 27, 151.
	1986	Hurtubise, et al., *Anal. Chem*., V. 58, 612.
	1986	Vo-Dinh, et al., *J. Phys. Chem*., V. 90, 4941.
	1987	Campiglia & de Lima, *Anal. Chem*., V. 59, 2822.
	1988	Winefordner, et al., *Microchem. J*., V. 37, 77.
	1988	Hilsenbeck, et al., *J. Iowa Acad. Sci*., V. 95, 38.
	1989	Gaye & Aaron, *Talanta*, V. 36, 445.
	1990	Gaye, Delamar, and Aaron, *Analusis*, V. 18, 571.
	1994	Li & Yang, *Anal. Chim. Acta*, V. 296, 99
filter paper with surfactant salt (thallium lauryl sulfate)	1988	Winefordner, et al., *Anal. Chem*., V. 60, 416.
	1989	Winefordner, et al., *Anal. Chem*., V. 61, 2328.
	1989	Winefordner, et al., *Anal. Chim. Acta*, V. 225, 415
chromatography paper with surfactants	1994	Campiglia, et al., *Anal. Chim. Acta*, V. 287, 89.
zeolite-modified filter paper	1993	Cabalin, et al., *Fres. J. Anal. Chem*, V. 346, 1003.
silanized filter paper	1977	Schulman & Parker, *J. Phys. Chem*., V. 81, 1932
filter paper with silicone	1993	Tjioe & Hurtubise, *Anal. Lett*., V. 26, 557.
	1994	Tjioe & Hurtubise, *Talanta*, V. 41, 595.
filter paper treated with gelatin	1994	T. Vo-Dinh & T. Pal, *Unpublished results*.
	1994	T. Pal, *J. Chem. Ed*., V. 71, 679.

Table 5 (continued). Materials investigated as potential substrates for SSRTP

Matrix Material	Year	Reference
filter paper treated with cyclodextrins	1987 1988 1989 1989	Alak & Vo-Dinh, *Appl. Spectr*., V. 41, 963. Alak & Vo-Dinh, *Anal. Chem*., V. 60, 596. Vo-Dinh, et al. *Anal. Chim. Acta*, V. 217, 171. Hurtubise, et al., *Microchem. J*., V. 40, 317.
filter paper with polyacrylic acid	1984 1989	Hurtubise, et al., *Anal. Chim. Acta*, V. 157, 203. Citta & Hurtubise, *Microchem. J*., V. 34, 1989.
filter paper treated with sodium halide salts	1982	Dalterio & Hurtubise, *Anal. Chem*., V. 54, 224.
50/50 paper/polyethylene fiber blend	1977	Schulman & Parker, *J. Phys. Chem*., V. 81, 1932
paper lint/crushed quartz mixture	1978	J.B.F. Lloyd, *Analyst*, V. 103, 775.
pure cellulose	1967	M. Roth, *J. Chromatog*., V. 30, 278.
microcrystalline cellulose membranes	1997	Fu & Li, *Fenxi Shiyanshi*, V. 16, 84.
wood pulps	1982	Bateh & Winefordner, *Talanta*, V. 29, 713.
cotton linter pulps	1982	Bateh & Winefordner, *Talanta*, V. 29, 713.
carboxymethylcellulose	1988	Su, et al., *Anal. Chim. Acta*, V. 205, 279.
sodium acetate	1976 1977 1978 1982 1985 1987 1990 1990	Hurtubise, et al., *Anal. Chem*., V. 48, 1784. Hurtubise, et al., *Anal. Chem*., V. 49, 2164 Winefordner, et al., *Anal. Chim. Acta*, V. 102, 1. Malmstadt, et al., *Anal. Chem*., V. 54, 1853. Hurtubise, et al., *Anal. Chem*., V. 57, 1227. Hurtubise, et al., *Anal. Chem*., V. 59, 432. Hurtubise, et al., *Anal. Chem*., V. 62, 1060. Hurtubise, et al., *Appl. Spectr.*, V. 44, 1494.
silica	1972 1973 1988 1994	Schulman & Walling, *Science*, V. 178, 53. Schulman & Walling, *J. Phys. Chem*, V. 77, 902. Winefordner, et al., *Microchem. J*., V. 37, 77. Ciolino & Dorsey, *Anal. Chem*., V. 66, 3223.
silica gel	1943 1967 1978 1980 1990	Franck & Pringsheim, *J. Chem. Phys*., V. 11, 21. M. Roth, *J. Chromatog*., V. 30, 278. Ford & Hurtubise, *Anal. Chem*., V. 50, 610. Ford & Hurtubise, *Anal. Chem*., V. 52, 656 Gaye, Delamar, and Aaron, *Analusis*, V. 18, 571.

Table 5 (continued). Materials investigated as potential substrates for SSRTP

Matrix Material	Year	Reference
silica gel chromatoplates	1979 1980 1988 1988	Ford & Hurtubise, *Anal. Chem*., V. 51, 659. Ford & Hurtubise, *Anal. Chem*., V. 52, 656. Burrell & Hurtubise, *Anal. Chem*., V. 60, 564. Winefordner, et al., *Microchem. J*., V. 37, 77.
silica gel-starch mixture	1967	M. Roth, *J. Chromatog*., V. 30, 278.
alumina	1967 1972 1973 1983 1988 1990	M. Roth, *J. Chromatog*., V. 30, 278. Schulman & Walling, *Science*, V. 178, 53. Schulman & Walling, *J. Phys. Chem*, V. 77, 902. Oelkrug, et al., *J. Phys. Chem*., V. 87, 4872. Winefordner, et al., *Microchem. J*., V. 37, 77. Gaye, Delamar, and Aaron, *Analusis*, V. 18, 571.
glass-fibers	1972 1973	Schulman & Walling, *Science*, V. 178, 53. Schulman & Walling, *J. Phys. Chem*., V. 77, 902.
glass fiber "paper" (100% borosilicate)	1977	Schulman & Parker, *J. Phys. Chem*., V. 81, 1932
stainless steel	1977	Schulman & Parker, *J. Phys. Chem*., V. 81, 1932
sucrose	1977	Schulman & Parker, *J. Phys. Chem*., V. 81, 1932.
starch	1977 1982 1982 1988	Schulman & Parker, *J. Phys. Chem*., V. 81, 1932. Dalterio & Hurtubise, *Anal. Chem*., V. 54, 224. Su & Winefordner, *Microchem. J*., V. 27, 151. Su, et al., *Anal. Chim. Acta*, V. 205, 279.
chalk ($CaCO_3$ and a binder)	1982	Su & Winefordner, *Microchem. J*., V. 27, 151.
α-, β-, and γ-cyclodextrins	1982 1983	Turro, et al., *Photochem. Photobiol*., V. 35, 69. Turro, et al., *Photochem. Photobiol*., V. 37, 149.
α-, β-, or γ-cyclodextrin / salt mixtures	1986 1986 1989 1989 1991 1991 1994 1996 1996	Bello and Hurtubise, *Appl. Spectr*., V. 40, 790. Bello and Hurtubise, *Anal. Lett*., V. 19, 775. Hurtubise, et al., *Anal. Chem*., V. 61, 2643. Hurtubise, et al., *Appl. Spectr*., V. 43, 810. Hurtubise, et al., *Anal. Chem*., V. 63, 169. Hurtubise, et al., *Anal. Chem*., V. 63, 1073. Hurtubise, et al., *Appl. Spectr.*, V. 48, 747. Hurtubise, et al., *Appl. Spectr*., V. 50, 115. Hurtubise, et al., *Appl. Spectr.*, V. 50, 1140.
β-cyclodextrin with Triton X-100 (as second guest)	1996	Du, et al., *Appl. Spectr*. V. 50, 1273.
sol-gel glass	1986 1997	Avnir, et al., *J. Non-Cryst. Solids*, V. 82, 103. Costa-Fernández, et al., *Sens. Act. B*, V. 38-39, 103

Table 5 (continued). Materials investigated as potential substrates for SSRTP

Matrix Material	Year	Reference
sugar-based glasses (glucose and trehalose) (glucose)	 1996 1997	 Wang & Hurtubise, *Appl. Spectr*., V. 50, 53. Wang & Hurtubise, *Anal. Chem*., V. 69, 1946.
polyamide membrane with sucrose	1996	Wei, et al., *Anal. Chim. Acta*, V. 319, 239.
95% poly(vinyl alcohol) + 5% cellulose	1995 1996	Kitade, et al., *Anal. Chem*., V. 67, 3806. Kitade, et al., *Anal. Sci*., V. 12, 439.
polymers	1968 1969 1991 1995 1996 1997	P.F. Jones, *Polym. Lett*., V. 6, 487. Jones & Siegel, *J. Chem. Phys*., V. 50, 1134. Soutar & Swanson, *Polymer Comm*., V. 32, 264. Song, et al., *Macromol*., V. 28, 5581. Dreger, et al., *J. Phys. Chem.*, V. 100, 4637. Nakashima et al., *J. Photochem. Photobiol A.* V. 111, 249.
polymer-salt mixtures	1982	Dalterio & Hurtubise, *Anal. Chem*., V. 54, 224.
polyethylene fiber "paper"	1977	Schulman & Parker, *J. Phys. Chem*., V. 81, 1932
H_3BO_3, $CaHPO_4$, Na_2HPO_4, $CaSO_4$	1982	Su & Winefordner, *Microchem. J*., V. 27, 151.
sodium propionate sodium butyrate sodium valerate sodium oxalate sodium tartrate sodium formate sodium adipate sodium pimelate	1977	von Wandruszka & Hurtubise, *Anal. Chem*., V. 49, 2164
$Mg(OH)_2$, $Ba(OH)_2$, $Ca(OH)_2$, $C_2H_3LiO_2$	1977	von Wandruszka & Hurtubise, *Anal. Chem*., V. 49, 2164
pure alkali halides	1995	Schutt & Li, *Anal. Lett.*, V. 28, 307.
Quaternary ammonium ion exchange resin	1977	von Wandruszka & Hurtubise, *Anal. Chem*., V. 49, 2164
poly(acrylic acid)-salt mixtures	1982 1982 1983 1993 1993	Smith & Hurtubise, *Anal. Chim. Acta,* V. 139, 315. Dalterio & Hurtubise, *Anal. Chem*., V. 54, 224. Dalterio & Hurtubise, *Anal. Chem*., V. 55, 1084. M.M. O' Leary, et al., *Anal. Proc*., V. 30, 147. M.M. O' Leary, et al., *Anal. Proc*., V. 30, 475.
asbestos	1972 1973	Schulman & Walling, *Science*, V. 178, 53 Schulman & Walling, *J. Phys. Chem*., V. 77, 902.

Table 5 (continued). Materials investigated as potential substrates for SSRTP

Matrix Material	Year	Reference
zeolites	1989	Ramamurthy, et al., *J. Photochem and Photobiol. A*, V. 50, 157.
	1990	Ramamurthy, et al., *Tetr. Lett*., V. 31, 1097.
	1990	Ramamurthy, et al., *Coord. Chem. Rev*, V. 97, 225.
	1992	Ramamurthy, et al., *JACS*, V. 114, 3882.
ion exchange membrane	1997	Fu & Li, *Fenxi Shiyanshi*, V. 16, 84.
ion exchange chromatographic papers	1984	Su, Asafu-Adjaye, & Ocak, *Analyst(London),* V. 109, 1019.

Sodium Acetate

Sodium acetate is another support material that has received considerable attention. Hurtubise and von Wandruszka have investigated the interactions of p-aminobenzoic acid with a sodium acetate surface in detail.[135] It was discovered that the adsorption involved hydrogen bonding and the formation of the sodium salt of PABA on the sodium acetate surface. The researchers also studied the ability of sodium acetate to serve as a universal SSRTP matrix by monitoring the RTP intensities of approximately fifty analytes. Of these fifty compounds, only thirteen yielded a measurable RTP signal when immobilized on sodium acetate supports. With a success-to-failure ratio of one to four, sodium acetate can hardly be regarded as a dependable RTP substrate.

Numerous other researchers have investigated the use of sodium acetate as an SSRTP matrix. Winefordner and colleagues have reported that sodium acetate is advantageous since it contributes very little phosphorescence background to the analytical signal. On the other hand, it has also been acknowledged that sodium acetate is actually a poor SSRTP support material since very few compounds give adequate RTP signals when immobilized on the substrate.[106]

Silica Gel

Silica Gel is another material that has been useful for SSRTP measurements under certain conditions. More commonly used for chromatographic purposes, it is an amorphous, highly porous, partially hydrated form of silica that was first prepared by a gelling process in 1861 by Sir Thomas Graham.[136] The primary particles of silica gel which are formed during the gelling process can vary from a few Angstroms to several hundred Angstroms in diameter. Consequently, the pores of the silica gel will have similar dimensions. For chromatographic methods, this porosity allows for size-exclusion separations of various analytes on the basis of their molecular size. Adsorption mechanisms of various compounds on silica gel have been investigated by UV and IR absorption techniques.[137] It was determined that these model adsorbates could associate with the silica gel via a nonspecific interaction with the whole sorbent and/or a specific interaction with the active surface hydroxyls. Multicomponent mixtures on silica gel chromatoplates have been analyzed successfully by RTP methods.[138]

Compounds that have the potential to strongly hydrogen bond to silica gel exhibit greater RTP intensities than similar compounds having less polar functional groups and consequently weaker hydrogen bonding ability. Ford and Hurtubise have extensively investigated the utility of several brands of silica gel for the ability to yield RTP from benzo[*f*]quinoline and terephthalic acid.[139,140,141] They found that the salt of polyacrylic acid, a binding agent in certain brands of silica gel, is often one of the main components for inducing strong RTP for analytes adsorbed on

---

[135] R.M.A. von Wandruszka and R.J. Hurtubise, *Anal. Chem.*, 1977, V. 49, p. 2164.

[136] R.P.W. Scott, **Silica Gel and Bonded Phases: Their Production, Properties and Use in LC** New York: John Wiley & Sons, Ltd., 1993.

[137] P.A. Leermakers, H.T. Thomas, L.D. Weis, and F.C. James, *J. Am. Chem. Soc.*, 1966, V. 88, p. 5075.

[138] V.P. Senthilnathan and R.J. Hurtubise, *Anal. Chem.*, V. 56, p. 913.

[139] C.D. Ford and R.J. Hurtubise, *Anal. Chem.*, 1980, V. 52, p. 656.

[140] C.D. Ford and R.J. Hurtubise, *Anal. Chem.*, 1979, V. 51, p. 659.

[141] C.D. Ford and R.J. Hurtubise, *Anal. Chem.*, 1978, V. 50, p. 610.

silica gel chromatoplates. Burrell and Hurtubise have continued those studies.[142] Although the use of silica gel finds some application in the analysis of phosphors in conjunction with TLC analysis, reported RTP intensities tend to be lower than those from filter paper by a factor of 1.6 or more.

Polymer-salt mixtures

Polymer-salt mixtures have been extensively investigated as potential substrates for SSRTP measurements. Although polymers alone will typically not yield suitable RTP intensities, they have been found to perform well when mixed with an inorganic salt. Hurtubise and Smith have studied polyacrylic acid-NaCl mixtures in conjunction with terephthalic acid.[143] They have proposed that it is possible that the terephthalic acid forms hydrogen bonds with the polyacrylic acid.

Dalterio and Hurtubise have used polyacrylic acid in conjunction with NaBr, LiCl, KCl, and NaCl to measure the RTP of a number of hydroxyl aromatics such as 4-PP, 4,4′-biphenol, and 2-naphthol.[18,144] Their comparison of the RTP of several analytes adsorbed on 1% polyacrylic acid-NaBr and on Whatman™ filter paper has shown that filter paper is a more convenient and more effective support material than the polymer-salt substrate.

Silica

Contrary to prior reports in the literature, Ciolino and Dorsey have reported that bare silica will provide higher sensitivity for RTP than filter paper when the specific surface areas of the two substrates are similar.[145] The silicas used for the RTP studies were 10-μm Lichrospher silica Si 300 (E.M. Science) and a 1.5-μm non-porous silica (Keystone). The surface area of the Keystone silica was determined to be 2.04 m^2/g (BET analysis, krypton adsorption).

The researchers prepared thin-layer phases from a slurry comprised of keystone silica and a binder material by casting the mixture onto a sheet of polyethylene terephthalate. Ordinary cornstarch ("Argo Pure" – purchased from the local grocery) or Carbopol 934 (cross-linked polyacrylic acid, B.F. Goodrich) were used as binders. The casting slurry was comprised of the silica plus an aqueous gel of the binder. For the cornstarch system, 1.5-2.0 g. of silica were mixed with 1.0-1.5 g. of a 2% aqueous cornstarch dispersion. After casting, the substrates were allowed to air-dry and desiccated overnight prior to measurement.

Ciolino and Dorsey proposed that the specific surface areas of the silica substrates were directly linked to their performance as useful RTP matrices. It was estimated that the surface area available for adsorption was 0.003 m^2 for filter paper (Whatman No. 42) and 0.008 m^2 for the Keystone silica phase. It is unknown if the researchers considered the potential contributions of the polyacrylic acid and "inert" starch materials that were utilized as binders within the thin-layer phase substrates.

---

[142] G.J. Burrell and R.J. Hurtubise, *Anal. Chem.*, 1988, V. 60, p. 564.
[143] C.A. Smith and R.J. Hurtubise, *Anal. Chim. Acta*, 1982, V. 139, p. 315.
[144] R.A. Dalterio and R.J. Hurtubise, *Anal. Chem.*, 1982, V. 54, p. 224.
[145] L.A. Ciolino and J.G. Dorsey, *Anal. Chem.*, 1994, V. 66, p. 3223.

Cyclodextrins

In addition to the use of cyclodextrin-treated filter paper in order to enhance RTP intensities, Hurtubise and colleagues have extensively studied the use of cyclodextrin-salt mixtures to prepare solid supports for RTP measurements. Bello and Hurtubise reported the first CD-RTP results for this system in 1986.[146] During this initial study, they investigated fifty-five organic compounds of various sizes and functionalities for SSRTP on an 80% α-cyclodextrin-NaCl matrix. Thirty-four of those compounds yielded measurable RTP intensities. This was primarily attributed to their ability to form inclusion complexes with the α-CD hydrophobic cavities.

The cyclodextrins have proven to be potentially useful RTP support materials; however, one of the most significant disadvantages associated with the use of these host molecules rests with their respective costs. Table 6 lists a representative pricing scheme for the most commonly used cyclodextrins.

Table 6. Cyclodextrin costs (1996 $)

CD	100 mg	500 mg	1 g	5 g	25 g
α	--	--	10.20	29.50	132.70
β	--	--	4.65	8.65	26.50
γ	21.60	70.95	113.40	449.10	--

(table prepared from *Biochemicals and Organic Compounds for Research*, Sigma Chemical Company)[147]

Sol-Gel Glasses

Glasses derived from the sol-gel process have allowed researchers to study a new SSRTP matrix. Until recent years, glasses have been prepared by melting their components at very high temperatures. This has limited the use of additives (such as coloring agents) to inorganic compounds which can withstand the glass production temperatures. Organic dyes could not be used as additives because of their low decomposition temperatures; however, it is now possible to incorporate organic molecules into an inorganic oxide glass via the *sol-gel* process.[148]

The typical sol-gel process is seemingly straightforward -- a metal alkoxide, water, a solvent, and frequently a catalyst are stirred together thoroughly in order to achieve a homogenous mixture on a molecular scale.[149] Chemical reactions (hydrolysis and condensation-polymerization) lead to the formation of a viscous gel, which is an amorphous porous material

---

[146] J. Bello and R.J. Hurtubise, *Appl. Spectr.*, 1986, V. 40, p. 790.

[147] 1996 Catalog, **Biochemicals and Organic Compounds for Research**, Sigma Chemical Company, P.O. Box 14508, St. Louis, Mo. 63178.

[148] C.J. Brinker and G.W. Scherer, **Sol-Gel Science: The Physics and Chemistry of Sol-Gel Processing** Boston: Academic Press, Inc., 1990.

[149] A.M. Buckley and M. Greenblatt, *J. Chem. Ed.*, 1994, V. 71, p. 599.

containing liquid solvents in the pores. A low temperature drying period allows for the removal of the excess solvent from the gel (usually < 100º C). Further curing at elevated temperatures yields a collapse of the porous structure and results in a densification of the glass. A commonly cited sol-gel reaction involves the use of tetraethyl orthosilicate (TEOS), ethanol, water, and hydrochloric acid for controlling the pH of the mixture:
$Si(OC_2H_5)_4 + C_2H_5OH + H_2O$ (pH ~ 1) $\rightarrow$ (-Si-O-Si)$_n$.

Kaufman, Levy, and Avnir first described the used of sol-gel as an RTP matrix in their report detailing the photophysical studies of the sol/gel transition in silica.[150] The researchers were able to trap pyrene in a sol-gel matrix in the presence of NaI. It was reported that the RTP intensity and life-time increased with gel shrinkage and dryness.

Levy, Avnir, and colleagues have more recently investigated the room temperature phosphorescence of organic molecules trapped in silica sol-gel glasses.[151,152,153] They reported that phosphorescence lifetimes of up to several seconds are possible and the conditions required for the observation of RTP are variable. In some cases, co-trapping of a heavy-atom is necessary. In others, RTP may supposedly be observed even in wet gels without a heavy-atom. The sol-gel samples required five days of drying time prior to being used for these studies. Studies involving the wet gels were performed after the gels had reached a constant weight (21 days).

Qualitative SSRTF and SSRTP spectra were published for a variety of entrapped analytes. However, emission units were *arbitrarily* specified for these particular plots. Thus, in each case, the fluorescence spectra appear to be no greater in intensity than the corresponding phosphorescence spectra. Such results are atypical for fluorescence and phosphorescence analyses. Additionally, analytical figures of merit were not reported; therefore, it is not possible to directly compare the performance of the sol-gel matrix to the performance of other solid supports such as filter paper, silica gel, and so on.

There are a number of significant problems associated with the sol-gel method that render it unsuitable for conventional use as an SSRTP matrix. At this time, there is no universally-accepted method suggested for the preparation of these glasses. The optimization of the process is left to the end-user and the amount of time required to achieve this goal must not be underestimated. The sample preparation step itself is tedious and time-consuming. For instance, the sol-gel to microporous glass curing phase will typically require a waiting period of several days (if not several weeks). Alternatively, the approximate sample preparation time for an analyte to be immobilized on a more conventional RTP substrate (such as filter paper) is on the order of minutes. Comparatively, this puts the sol-gel process at a severe disadvantage if the analyst wishes to perform rapid RTP analyses.

Another difficulty involves the inherent brittleness and potential for fracture of the porous glasses during the sol-gel drying phase. As solvent is removed from the gel, the exterior tries to shrink faster than the interior. This yields significant tensile stresses that can fracture the network at the exterior. Investigators have found that supercritical drying can alleviate some of

---

[150] V.R. Kaufman, D. Levy, and D. Avnir, *J. Non-Cryst. Solids*, 1986, V. 82, p. 103.
[151] D. Levy and D. Avnir, *J. Photochem. Photobiol. A: Chem.*, 1991, V. 57, p. 41.
[152] D. Avnir, S. Braun, and M. Ottolenghi, in **Supramolecular Architecture: Synthetic Control in Thin Films and Solids**, ACS Symposium Series 499, American Chemical Society, 1992, p. 384.
[153] D. Levy, *J. Non-Cryst. Solids*, 1992, V. 147& 148, p. 508.

these problems.[154] Typically, an apparatus such as an autoclave is used for the provision of suitable temperatures and pressures within the drying environment. Other investigators have advised the use of drying control chemical additives (DCCA) such as formamide in order to minimize cracking.[155] Obviously, the drying process must be carefully controlled in order to minimize the possibility of loss or degradation of analyte. Additionally, the potential for analytical interferences must be considered if the investigator wishes to formulate and incorporate DCCA agents.

Starch

Roth first used silica gel-starch mixtures for RTP investigations in 1967.[95] It was reported that "La phosphorescence est plus faible sur support de silice mêlée à de l'amidon" (The support mixture of starch and silica gel yields the weakest phosphorescence). It was concluded that cellulose was a superior RTP support in comparison to the silica gel-starch mixture. However, no data was published in conjunction with the silica gel-starch investigations. Additionally, starch was not studied as an SSRTP support independent of the silica gel. Other investigators have apparently used starch as an RTP support or binder material. However, in many cases, there has been insufficient data and its merit as an RTP support have not been suitably evaluated.[40,144,156,157]

[154] S.S. Kistler, *J. Phys. Chem.*, 1932, V. 36, p. 52.
[155] L.L. Hench and D.R. Ulrich, eds., **Science of Ceramic Chemical Processing** New York: Wiley, 1986.
[156] S.Y. Su and J.D. Winefordner, *Microchem. J.*, 1982, V. 27, p. 151.
[157] W.J. Long, S.Y. Su, and H.T. Karnes, *Anal. Chim. Acta*, 1988, V. 205, p. 279.

3.0 Cellulose

In 1838, Anselme Payen extracted a fibrous substance from plant tissue, cotton linters (cotton fibers too short to be spun), root tips, and the pith of trees.[158] The substance was further isolated and the elemental composition determined. From this data, Payen concluded that the empirical formula was $C_6H_{10}O_5$ and that the substance was an isomer of starch. It was not Payen, but the French Academy who proposed the term *cellulose* in 1839.[159]

Although certain types of bacteria, fungi, and algae can synthesize cellulose, plants and trees are by far the most common sources of cellulose. In wood, cellulose is intimately associated with other polysaccharides and lignin. Following intensive chemical treatment it is possible to isolate the desired cellulose component. Nevertheless, the resulting extract is still considered to be impure. To obtain 100% pure cellulose from wood, the extract must be subjected to further treatments such as hydrolysis, dissolution, and precipitation. Native cellulose can have up to 14,000 cellobiose repeating units, but the purified product consists of short molecular chains on the order of 2,500 repeating units.[160]

Because cellulose is the basis of many commercial products such as paper, films, and fibers, it is primarily isolated from wood via large-scale pulping processes. Chemical and physical modifications of the process allow for the production of pulps having a wide variety of properties. If these pulps are to be used for the production of films, fibers, and cellulose derivatives, then the raw material is further purified by a bleaching process.

3.1 Molecular Properties

Cellulose is composed of β-D-glucopyranose *monomer*s that are joined to form a biopolymer.[161,162] The monomeric unit of the cellulose chain has a length of 1.03 nm and each of these monomers are attached to their neighbors by β-(1→4)-glycosidic linkages.[163] Two adjacent glucose units are linked by the elimination of one molecule of water at carbons C1 and C4.[164]

---

[158] A. Payen, *C.R. Hebd. Seances Acad. Sci.*, 1838, Vol. 7, p. 1052.
[159] A. Brongniart, T.J. Pelouze, and A.B. Dumas, *C.R. Hebd. Seances Acad. Sci.*, 1839, Vol. 8, p. 51.
[160] G. Jayme and H. Knolle, *Holz, Roh-Werkst*, 1965, Vol. 23, p. 438.
[161] W.N. Haworth, *Helv. Chim. Acta*, 1928, Vol. 11, p. 534.
[162] H. Staudinger, **Die hochmolekularen organischen Verbindungen -- Kautschuk und Cellulose**, Berlin: Springer Verlag, 1932.
[163] H.A. Krassig, **Cellulose: Structure, Accessibility, and Reactivity** in *Polymer Monographs Vol. 11*, M.B. Huglin, Ed., USA: Gordon and Breach Science Publ., 1993.
[164] K. Freudenberg, *Chem. Ber.,* 1967, Vol. 100, p. 172.

3.1.1 Conformation

When fully extended, the cellulose molecule exists in the form of a flat ribbon [Figure 8]. Hydroxyl groups protrude laterally from the ribbon and are capable of forming both inter- and intra-molecular hydrogen bonds. The surface of the ribbon consists primarily of hydrogen atoms linked directly to carbon. Due to this arrangement, the cellulose surface tends to be hydrophobic.[165] These features determine many of the chemical and physical properties of the cellulose as well as its supramolecular structure.

The monomeric units in the cellulose ribbon are arranged in a single plane. There are three fundamental reasons for this arrangement. The first involves the β-(1→4)-glycosidic linkage. If there were an α-hydroxyl and an α-(1→4)-glycosidic linkage, this would result in the formation of a helical molecular chain (as is the case for the amylose biopolymer found in starch).[166] The second reason involves the conformation of the pyranose ring.[167] Bent hexagonal rings are found in various conformations -- the extreme forms being the *chair* and *boat*. The most stable form (lowest energy) is the chair, whereas the half-chair and boat forms are of higher energy and greater instability. At moderate temperatures, bent hexagonal rings assume the most stable form and, as a result, the glucopyranose units of the cellulose have the chair conformation.[168] The final reason also involves ring conformation: if hydroxyl groups are taken into consideration there are two possible chair forms. The -OH groups can either be positioned above and below the ring (axial position) or in the plane of the ring (equatorial position). Of the two forms, the latter arrangement is the conformation of lower energy. Because this conformation offers the highest stability, the $-CH_2OH$ and -OH groups (as well as the glycosidic bonds) are all presumed to be equatorial with respect to the plane of the ring.[169,170]

3.1.2 Hydrogen Bonding

Hydroxyl groups are able to form hydrogen bond linkages between each other and with -O, -N, and -S atoms. The supramolecular structures of most natural and synthetic polymers are based on the hydrogen bond. Additionally, the supramolecular arrangements in liquid water and the crystalline structure in ice are due to the formation of hydrogen bonds between water molecules. In this case, hydrogen bonds can occur as the result of close contact between a hydrogen (on a given hydroxyl) and the lone pair electrons of another oxygen atom.

---

[165] It is interesting to note that amylose has a much greater affinity for water due to its α-(1→4)-glycosidic linkages. Compared to cellulose, the stereochemistry of the resulting amylose helix allows a greater proportion of the hydroxyl groups to be available for solvation.

[166] D.A. Rees, **Polysaccharide Shapes**, New York: John Wiley & Sons, 1977.

[167] I.A. Tarchevsky and G.N. Marchenko, *Cellulose Conformation* in **Cellulose: Biosynthesis and Structure**, New York: Springer-Verlag, 1991.

[168] V.S.N. Rao, P.R. Sundaraajan, C. Ramakrishnan, and G.N. Ramachandran, **Conformation of Biopolymers** (G.N. Ramachandran, Ed.), London: Academic Press, 1957.

[169] A.J. Mitchell and H.G. Higgins, *Tetrahedron*, 1965, Vol. 21, p. 1109.

[170] G.D. Goebel, C.E. Harwie, and D.A. Brant, *Appl. Polymer Symp.*, 1976, Vol. 28, p. 671.

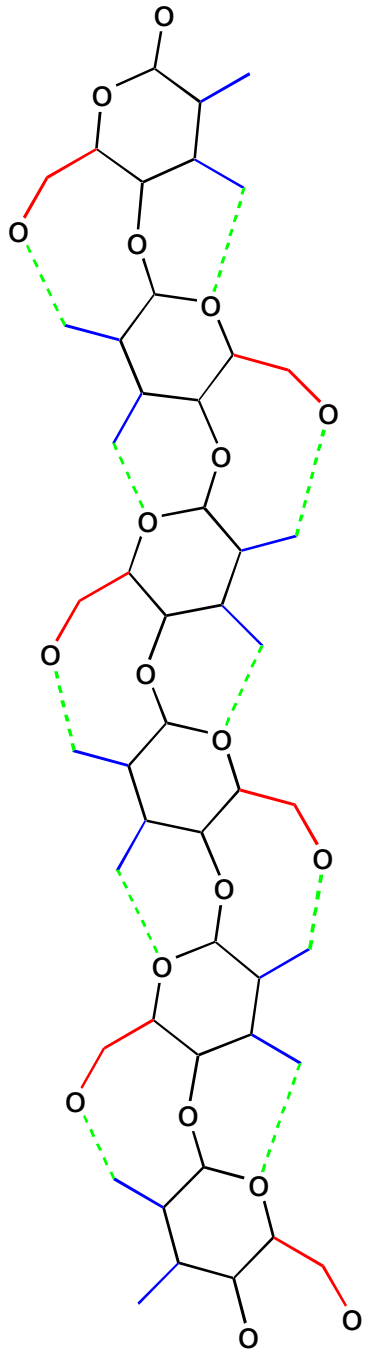

Figure 8. Ribbon conformation of cellulose.

A hydrogen bond is characterized by:

a). the strength of the binding energy (which depends on the charge density and the angle between the linked atoms),
b). steric factors that cause an asymmetrical distribution of the electrons,
c). and the frequency with which the hydroxy groups oscillate and the protons change position.[171,172,173]

Hydrogen bonds are approximately 100 times stronger than van der Waals forces. On the other hand, they are approximately 26 times weaker than covalent bonds. Table 7 compares the energies of a few such linkages. It can be assumed that the binding energy between the hydroxy groups of cellulose are about the same or slightly higher than the binding energy of hydroxy groups in alcohols.

Table 7. Energy of various molecular linkages.

Linkage	Compound	Energy (kJ/mol)
van-der-Waals	$H_2O_{liq.}$	0.155
O—H···O	$H_2O_{liq.}$	15
O—H···O	$C_nH_{2n+1}OH$	28
N—H···O	Melamin	25
O—H	--	460
C—O	--	356
C—H	--	414
C—C	--	347

Table adapted from: **Wood: Chemistry, Ultrastructure, Reactions** by D. Fengel and G. Wegener.

Depending on their location, the -OH groups of cellulose molecules are able to form two types of hydrogen bonds. There are *intramolecular* hydrogen bonds between -OH groups of adjacent glucose units in the same cellulose molecule.[174] These linkages add *stiffness* to a cellulose ribbon. There are also *intermolecular* hydrogen bonds between -OH groups of adjacent cellulose ribbons. These linkages are responsible for the formation of supramolecular structures.

As a result of this extensive hydrogen bonding, bundles of cellulose molecules (*elementary fibrils*) can aggregate together to form *microfibrils*. Microfibrils, in turn, form *fibrils*. It is the fibrils that are responsible for the ultimate formation of cellulose fibers that

[171] W. Luck, *Naturwissenschaften*, 1965, Vol. 52, p. 25.
[172] W. Luck, *Naturwissenschaften*, 1965, Vol. 52, p. 49.
[173] W. Luck, *Naturwissenschaften*, 1967, Vol. 54, p. 601.
[174] L.M.J. Kroon-Batenburg, J. Kroon, and M.G. Northolt,*Polym. Comm.*, 1986, Vol. 27, p. 290.

comprise the layers of the plant cell wall. Additionally, the mechanical properties of a pulp or paper sheet are determined by fiber-fiber bonds which are the result of hydrogen bonds between fiber surfaces.[175,176] The number of hydroxyl groups on the surface of a fiber that are capable of forming fiber-fiber bonds determine the strength of the paper.[177,178] The fibrillar structure of cellulose has been extensively studied and additional details may be found elsewhere.[179,180,181]

In addition to the hydrogen bonds formed between cellulose hydroxyls, hydrogen bonds can also be formed between the cellulose hydroxyls and water. Single water molecules or clusters can be linked to the edges of the cellulose ribbon in this manner.[182] The energy of the hydrogen bonds between water and cellulose has been calculated to be 25 kJ/mol.[183]

3.2 Adsorption of Liquids

Robertson has studied the nature and extent of cellulose-liquid interactions for thirty-nine different solvents (including water).[184,185] Although the cellulose structure will swell significantly when exposed to water, most liquids swell cellulose to a lesser extent. It has been reported that the sorption of alcohols (such as methanol and ethanol) by cellulose decreases regularly as the molecular weight of the alcohol increases.[186] On the other hand, sorption by cellulose becomes practically negligible for butanol and larger alcohols. Table 8 illustrates these trends.

---

[175] G. Jayme, *Papier*, 1961, Vol. 15, p. 581.
[176] A.H. Nissan and S.S. Sternstein, *Tappi*, 1964, Vol. 47, p. 1.
[177] R.W. Davison, *Tappi*, 1972, Vol. 55, p. 567.
[178] U.B. Mohlin, *Svensk Papperstid.*, 1974, Vol. 77, p. 131.
[179] D. Fengel and G. Wegener, **Wood: Chemistry, Ultrastructure, Reactions**, New York: Walter de Gruyter, 1989.
[180] H.A. Krassig, **Cellulose: Structure, Accessibility, and Reactivity** in *Polymer Monographs Vol. 11*, M.B. Huglin, Ed., USA: Gordon and Breach Science Publ., 1993.
[181] J.O. Warwicker, *Cellulose as a Matrix Material* in **Cellulose and its Derivatives: Chemistry, Biochemistry, and Applications** (J.F. Kennedy, G.O. Phillips, D.J. Wedlock, and P.A. Williams, Eds.), New York: John Wiley & Sons, 1985.
[182] R.J. Dobbins, *Tappi*, 1970, Vol. 53, p. 2284.
[183] J.L. Morrison and M.A. Dzieciuch, *Can. J. Chem.*, 1969, Vol. 37, p. 1379.
[184] A.A. Robertson, *Pulp Paper Mag. Can.*, 1964, Vol. 65, p. T171.
[185] A.A. Robertson, *Tappi*, 1970, V. 53, p. 1331.
[186] S.E. Sheppard and P.T. Newsome, *J. Phys. Chem.*, 1932, Vol. 36, p. 2306

Table 8. Sorption of Vapors by Cotton Cellulose (approximate)

Liquid	Max. Vapor Sorbed (g/100g) [20% relative vapor pressure]	Max. Vapor Sorbed (g/100g) [90% relative vapor pressure]
water	2.2	10.1
methanol	0.6	7.5
ethanol	0.5	4.7
n-propanol	0.2	0.85
n-butanol	0.0	0.0
ethyl ether	0.37	0.37
acetone	0.04	3.0
acetic acid	0.13	10.8
benzene	1.0	1.2
chloroform	0.91	1.1
carbon tetrachloride	1.0	1.2

Table adapted from: **Cellulose and Cellulose Derivatives -- Part I, 2nd Edition**. E. Ott, H.M. Spurlin, and M.W. Grafflin, Eds.

Robertson has also reported that inert (i.e. non-polar) liquids have the ability to decrease the tensile strength of paper as the cohesive energy densities of the solvents are increased.[187] Robertson suggests that "It must be supposed from the reduction in bonding by such liquids that at least some of the inter-fibre bonding depends on dispersion forces; and hydrogen bonding or strong dipolar interactions are not required for their weakening. Similar inert liquids do not appreciably change the accessibility as measured by the methoxyl content nor do they produce swelling.".[187]

Many attempts have been made to correlate the adsorption and swelling of cellulose fibers with dielectric constant, surface tension, or dipole moment of the liquid. However, such correlation is usually only possible within families of compounds.[188] Stamm and Tarkow have proposed that the extent to which a given liquid will penetrate cellulose is dependent upon the molecular volume of the liquid and its ability to form hydrogen bonds with the cellulose hydroxyl groups.[188] Thus, small molecules that form hydrogen bonds will be strongly sorbed by cellulose and the sorption will decrease with increasing molecular volume (or other steric effects). Larger molecules, regardless of hydrogen bonding ability, can be readily sorbed in a fiber which has been pre-swollen with a liquid in which they are miscible. Small molecules with small hydrogen bonding tendencies will neither swell cellulose fibers or be strongly sorbed by them.[189]

---

[187] A.A. Robertson, *Pulp Paper Mag. Can.*, 1964, Vol. 65, p. T176.
[188] A.J. Stamm and H. Tarkow, *J. Phys. & Colloid Chem.*, 1950, Vol. 54, p. 745.
[189] T.P. Nevell and S.H. Zeronian, Eds., **Cellulose Chemistry and its Applications**, New York: John Wiley & Sons, 1985.

If cellulose is immersed in aqueous solutions with certain inorganic salts, swelling beyond the water-swollen state results. It has been proposed that the swelling ability depends on the state of hydration of the ions.[163] According to Stamm, the swelling power increases for various cations and anions in the following order:

cations: $K^+ < NH_3^+ < Na^+ < Ba^{+2} < Mg^{+2} < Ca^{+2} < Li^+ < Zn^{+2}$

anions: $ClO_3^- < SO^{-2} < NO_3^- < Cl^- < Br^- < PO_4^{-3} < I^- < SCN^-$

Aqueous solutions of the iodides of lithium, sodium, and potassium are reported to be swelling agents for cellulose.[190,191,192,193] A detailed account of the swelling ability of inorganic salt solutions has been provided by Warwicker and colleagues.[194]

Thode and Guide have provided a thermodynamic interpretation of the swelling of cellulose in organic liquids.[195] The researchers discovered that the apparent total surface area of cellulose (by nitrogen adsorption) is a function of the cohesive energy density of the solvent from which it is dried. Thode and Guide cited two supporting reasons for this claim: "First, the more the polymer elements are swollen, the more conformable they are, leading to a greater collapse of internal pore structure upon drying. Second, the greater the cohesive energy density of the solvent, the greater the ability of the retreating solvent layer to pull elements of the polymer structure together.".[195]

Philipp and colleagues have studied the influence of cellulose structure on the swelling of cellulose in organic liquids.[196] By adopting a "pore and void" model of cellulose structure, the researchers discovered that swelling depends on a). the polar and hydrogen-bonding components of the cohesive energy densities of the liquids, b). the molar volumes of the liquids, and c). the cellulose structure with respect to the width and distribution of voids. Mantanis and colleagues confirmed these findings and reported that the hydrogen-bonding ability of the swelling liquid is the most important factor in the swelling of compressed cellulose fiber webs.[197]

---

[190] R. Haller, *Kelpzig's Textilz*, 1941, Vol. 44, p. 645.
[191] S.V. Bleshinskii, *Izv. Kirgiz Filial. Akad., Nauk SSSR*, 1954, Vol. 453, p. 19.
[192] R.O. Herzog and F. Beck, *Hoppe-Seyler's Z. Physiol.*, 1920, Vol. 111, p. 287.
[193] S.V. Bleshinskii, *Izv. Akad. Nauk Kirgiz. SSSR, Ser. Estestven Tekh. Nauk*, 1962, Vol. 4, p. 41.
[194] J.O. Warwicker, *Swelling* in **Cellulose and Cellulose Derivatives**(N.M. Bikales and L. Segal, Eds.), Vol. V, New York: John Wiley & Sons, 1971.
[195] E.F. Thode and R.G. Guide, *Tappi*, 1959, Vol. 42, p. 35.
[196] B. Philipp, H. Schleicher, and W. Wagenknecht,*J. Polym. Sci.*, 1973, Symp. No. 42, p. 1531.
[197] G.I. Mantanis, R.A. Young, and R.M. Rowell, *Cellulose*, 1995, V. 2, p. 1.

3.2.1 Inclusion Celluloses

The formation of inclusion compounds between organic solvents and cellulose has been extensively studied.[198,199,200,201,202,203,204,205,206] If cellulose is swollen with water and then dried by a series of solvent exchanges with liquids of decreasing polarity, then the final solvent can become trapped within the cellulose structure. Compounds such as benzene, pyridine, hexane, and tetrahydrofuran can be trapped by cellulose. The resulting complex is often referred to as an *inclusion cellulose*. It has been proposed that the organic solvent will enter the capillaries, pores, and interfibrillar interstices within the cellulose matrix. Upon drying, the solvent is trapped when the swollen cellulose structure partly collapses.[189] Studies have shown that the trapped solvent cannot be removed even if the inclusion cellulose is heated to temperatures higher than the boiling point of the liquid. However, the trapped solvent will be released from the complex if water is introduced to the inclusion cellulose.

Supposedly, there is no specific molecular requirement for the ability of an organic compound to form an inclusion cellulose. If the cellulose is sufficiently swollen, almost any organic molecule that is not too large can be introduced into the cellulose. The amount to be included depends primarily on the volume of the internal surface of the cellulosic substrate and the molecular volume of the organic compound of interest.[163]

3.2.2 Drying of Cellulose

Following water adsorption and swelling of the cellulose, the reverse process involves the removal of the moisture and subsequent shrinkage of the matrix. Researchers have typically examined this drying process in stages. The first stage involves the cleavage of the hydrogen bonds between water molecules. Some of the water is removed and the cellulose surfaces approach each other. The process continues until a monolayer of water remains between the two cellulose ribbons. Finally, the remaining water-cellulose hydrogen bonds are broken and new hydrogen bonds form a bridge between the cellulose surfaces.

McAleese and Dunlap have noted that water can swell the size of the submicroscopic pores (estimated at 5 to 1000 Å) in cellulose fibers more than 10-fold.[207] Following a drying step, the fibers collapse and nearly all of the water-cellulose hydrogen bonds are replaced with cellulose-cellulose hydrogen bonds, thereby trapping any "guests" between the cellulose chains.[93,143]

---

[198] S.S. Kistler, *J. Phys. Chem*, 1932, Vol. 36, p. 52.
[199] R.T. Mease, *Ind. Eng. Chem. Anal. Ed.*, 1933, Vol. 5, p. 317.
[200] J. Wiertelak and.I. Garbaczowna, *Ind. Eng. Chem. Anal. Ed.*, 1935, Vol. 7, p. 110.
[201] P.H. Hermans and A.J. Leeuw, *Kolloid Z.*, 1938, Vol. 82, p. 58
[202] H. Staudinger, W. Döhle, and O. Heick, *J. Prakt. Chem.*, 1943, Vol. 161, p. 191.
[203] H. Staudinger and W. Döhle, *J. Prakt. Chem.*, 1943, Vol. 161, p. 219.
[204] H. Staudinger, K.H. In den Birken, and M. Staudinger, *Makromol. Chem.*, 1953, Vol. 9, p. 148.
[205] H. Staudinger and W. Döhle, *Makromol. Chem.*, 1953, Vol. 9, p. 188.
[206] H. Staudinger and Th. Eicher, *Makromol. Chem.*, 1953, Vol. 10, p. 254.
[207] D.L. McAleese and R.B. Dunlap, *Anal. Chem.* 1984, V. 56, p. 2246.

Merchant has examined the effects of varying the final solvent from which cellulose is dried.[208] According to Merchant, "Before a liquid hydrocarbon evaporates from a fiber pore, a meniscus appears at the pore entrance and thus the internal tension of the liquid tends to collapse the pores. These pores, or capillaries, have neighboring structural limits such as fibrils or microfibrils as boundaries… The extent to which pores collapse or new contacts between structural units are made will be a function of surface tension, other factors remaining constant… As surface tension increases, the total pore volume decreases, whereas the amount of enmeshed or retained liquid increases."[209]

3.3 Supramolecular Structure

Although the chemical structure of cellulose is well-understood, its supramolecular form (including its crystalline and fibrillar structure) is still open to much debate.[210,211] For example, theoretical studies have provided numerous models of cellulose helix conformations.[189,212,213] Although many of the proposed helical forms have not yet been observed, A.D. French has described the formation of a deep blue-colored complex between cellulose and iodine. This complex may be similar to the well-known host-guest inclusion complex that can occur between an amylose helix and iodine.[214,215] Although their X-ray diffraction studies remain unconfirmed, Viswanathan and Shenouda have proposed a helical form of cellulose with seven cellobiose residues per turn.[216,217]

The crystalline structure of cellulose has been characterized by X-ray diffraction, infrared spectroscopy, high-resolution NMR, and diffraction contrast electron microscopy.[218] The unit cell of *native cellulose* (**cellulose I**) consists of four D-glucose residues. Recall that in the chain direction, the monomeric unit is a cellobiose residue (1.03 nm). Because every glucose residue is

---

[208] M.V. Merchant, *Tappi*, 1957, V. 40, p. 771.
[209] M.V. Merchant, *Tappi*, 1957, V. 40, p. 771.
[210] A. Sarko, *Cellulose - How much do we know about its structure?* in **Cellulosics: Chemistry, Biochemistry, and Material Aspects** (J.F. Kennedy, G.O. Phillips, and P.A. Williams, Eds.), New York: E. Horwood, 1993.
[211] A.F. Turbak and A. Sakthivel, *CHEMTECH*, July 1990, p. 444.
[212] A.D. French, *Physical and theoretical methods for determining the supramolecular structure of cellulose* in **Cellulose Chemistry and its Applications** (T.P. Nevell and S.H. Zeronian, Eds.), New York: John Wiley & Sons, 1985.
[213] I.A. Tarchevsky and G.N. Marchenko, *Cellulose Conformation* in **Cellulose: Biosynthesis and Structure**, New York: Springer-Verlag, 1991.
[214] R.C. Teitelbaum, S.L. Ruby, and T.J. Marks, *J. Am. Chem. Soc.*, 1978, Vol. 100, p. 3215.
[215] T.L. Bluhm and P. Zugenmaier, *Carbohydr. Res.*, 1981, Vol. 89, p. 1.
[216] A. Viswanathan and S.G. Shenouda, *J. Appl. Polym. Sci.*, 1971, Vol. 15, p. 519.
[217] A. Viswanathan and S.G. Shenouda, *The Helical Structure of Cellulose I* in **Proceedings of the Technological Conference -- Ahmedabad Textile Industry's Research Association** (Radhakrishnan, Ed.), 1971, p. 227.
[218] R.H. Marchessault and P.R. Sundararajan, *Cellulose* in **The Polysaccharides Vol. 2** (G.O. Aspinall, Ed.), New York: Academic Press, 1983.

displaced 180º with respect to its neighbors, cellulose I has a 2-fold screw axis.[219] It is generally agreed that all chains in native cellulose microfibrils are oriented in the same direction (parallel). For this configuration [Figure 9], there are two hydrogen bonds within each cellulose chain (from O(6) in one glucose residue to O(2) in the adjacent glucose and also from O(3)H to the ring oxygen). In one of the crystallographic planes, the chains form a layer and are held together by hydrogen bonds from O(3) in one chain to O(6) in the other. There are no hydrogen bonds in cellulose I between the layers -- only weak van der Waals forces are present. Thus, native cellulose has both a chain lattice and a layer lattice.

Regenerated cellulose (**cellulose II**) has essentially the same chain conformation as native cellulose. However, regenerated cellulose has antiparallel chains [Figure 10]. According to Reese, the cellulose chains are "piled on top of each other with more resemblance to planks in a timberyard than to bricks in a wall.".[166] Cellulose II is formed whenever the lattice of cellulose I is disrupted. Common pathways involve either dissolution or swelling of the cellulose with strong alkali (*mercerization*). The degree of swelling determines the degree of lattice transformation. Additionally, because the cellulose II form is more thermodynamically stable than the cellulose I conformation, the process is irreversible.

All naturally occurring cellulose is found in the cellulose I conformation. Additional supramolecular structures of cellulose (III and IV) are produced only when cellulose I and II are subjected to further chemical and physical treatments (for instance, with liquid ammonia @≥ 200 °C). Sjöström has reported that the proportions of the ordered and disordered regions of cellulose vary considerably depending on the origin of the sample.[220] For instance, cotton cellulose is slightly more crystalline than cellulose from wood sources.[221,222,223]

---

[219] J. Blackwell, F.J. Kolpak, and K.H. Gardner, *Structures of Native and Regenerated Celluloses* in **Cellulose Chemistry and Technology --ACS Symposium Series V. 48**, Washington, DC: American Chemical Society, 1977.

[220] E. Sjöström, **Wood Chemistry: Fundamentals and Application, 2nd Ed** New York: Academic Press, Inc., 1993.

[221] A.M. Hindeleh and D.J. Johnson, *Polymer*, 1972, Vol. 13, p. 423.

[222] A.M. Hindeleh and D.J. Johnson, *Polymer*, 1974, Vol. 15, p. 697.

[223] G. Jayme, *Cell. Chem. Technol.*, 1975, Vol. 9, p. 477.

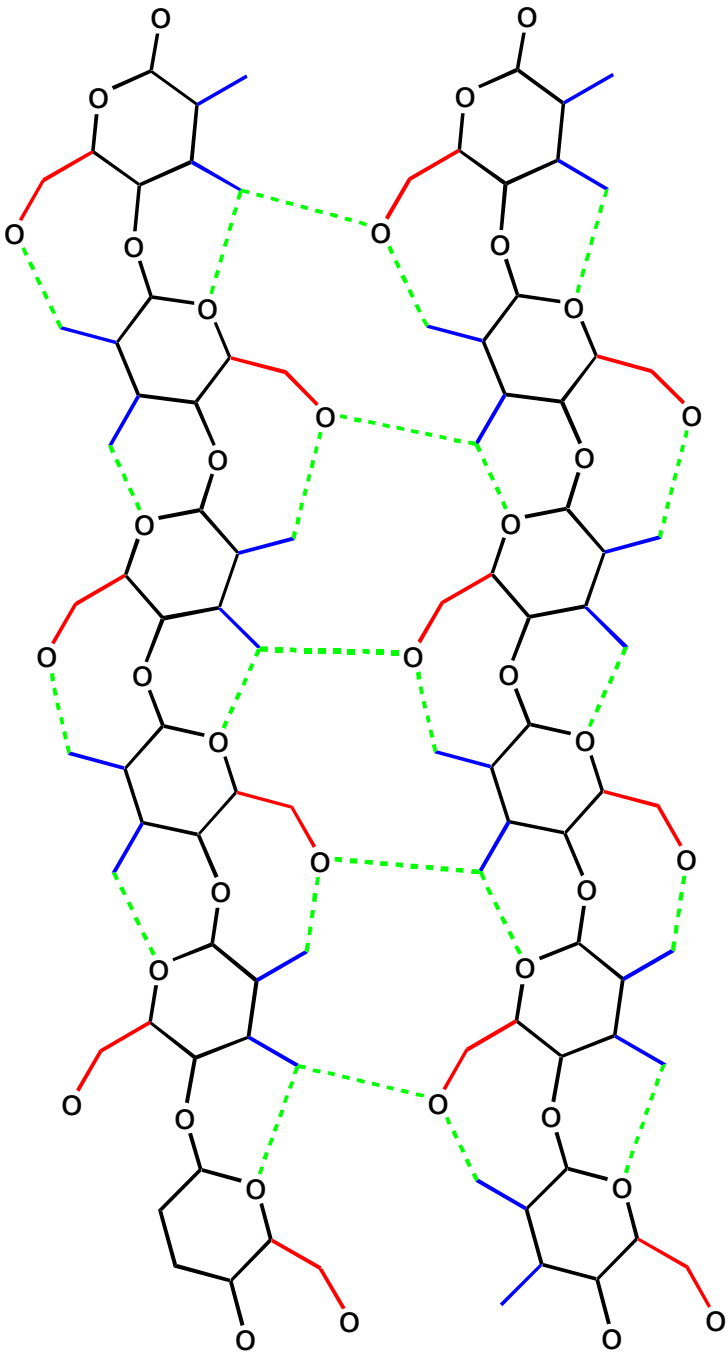

Figure 9. Native Cellulose (cellulose I).

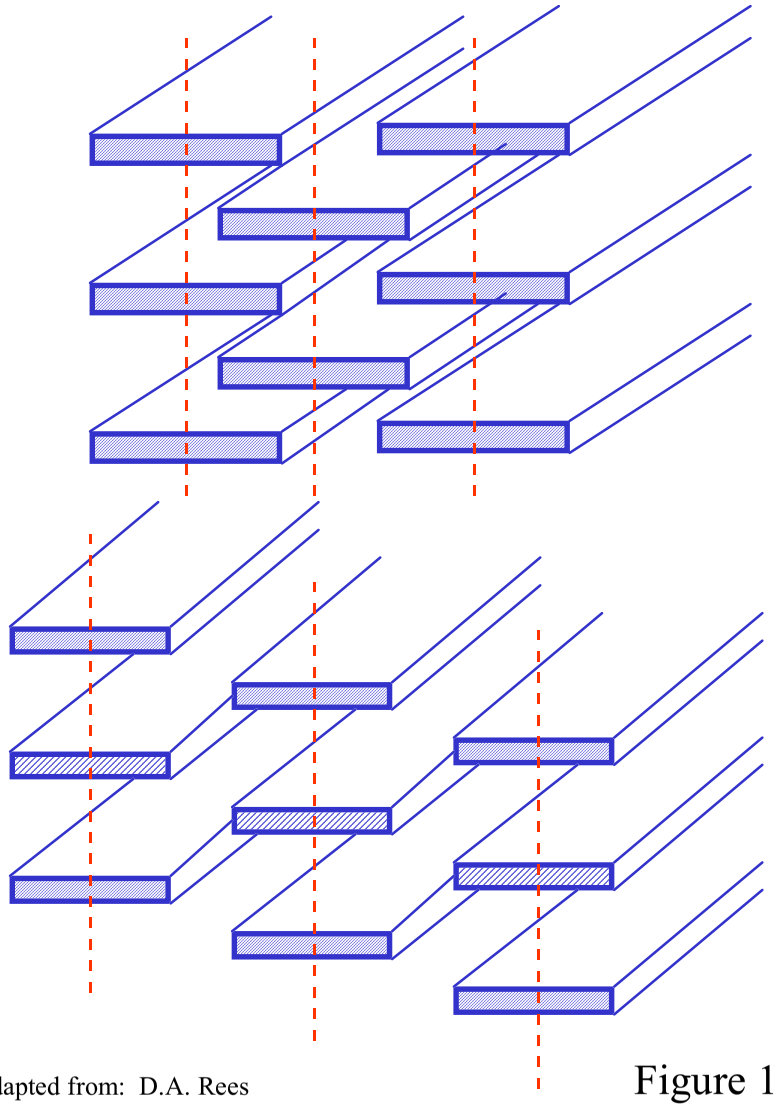

Cellulose I (parallel)

Cellulose II (anti-parallel)

adapted from: D.A. Rees
Polysaccharide Shapes,
John Wiley & Sons, 1977.

Figure 10. Packing of cellulose chains:
native cellulose (I) vs. regenerated cellulose (II).

3.4 Interaction of Light and Cellulose

Many studies have been concerned with the degradation of cellulose by UV light and solar irradiation.[224,225,226,227,228] However, there are surprisingly few investigations that address the penetration depth of UV and visible light into cellulose. Hon and Ifju have studied the penetration of light through radial and tangential microtome sections of Douglas fir, redwood, southern pine, and western red-cedar.[229] The principle constituents of wood are cellulose, hemicellulose, lignin, and numerous polyphenolic substances. Of these components, cellulose absorbs UV light strongly at wavelengths shorter than 200 nm (with limited absorption between 200 and 300 nm).[226,230] In addition to absorption through the visible region, lignin and the polyphenolic substances absorb strongly at wavelengths shorter than 200 nm and have a strong absorption maxima at 280 nm.[231] Therefore, light does not easily penetrate wood due to the variety of chromophoric groups associated with its basic composition.

In order to measure the penetration of light into the wood, Hon and Ifju relied on conventional UV transmission spectroscopy and the measurement of free radical concentration in the samples via electron spin resonance (ESR).[229] Based on their experimental findings, UV light was unable to penetrate into wood beyond 75 μm. The majority of visible light could only penetrate to approximately 100 to 150 μm and only small amounts of visible light could penetrate beyond 150 μm. The free radical study via ESR revealed that light can penetrate into wood no deeper than 200 μm.

Forsskåhl and colleagues have depth profiled photochemically-yellowed paper using UV-visible reflectance and fluorescence spectroscopy.[232] When absorbed in the outer layers of pulp and paper, UV light (< 300 nm) causes yellowing; whereas visible light causes photobleaching.[233] These researchers reported that 25% of the yellowing occurs at a depth of 10-12 μm, 50% at 15-20 μm, and 75% at 25-30 μm. For this study, no photochemical yellowing was found at depths greater than 110 μm from the surface of the paper.

Based on these results, it is not unreasonable to assume that UV radiation can penetrate the surface of a cellulosic material up to a depth of approximately 100 μm. However, this assumption depends on a number of variables including the purity of the cellulose, nature of its manufacture, chemical treatments, and density (or surface weight) of the material. Future experiments by pulp and paper scientists will hopefully confirm this proposal.

---

[224] R.L. Desai, *Text. Res. J.*, Sept. 1969, p. 882.
[225] N.-S. Hon, *J. Macromol. Sci. - Chem.*, 1976, Vol. A10, p. 1175.
[226] N.-S. Hon, *J. Polym. Sci. Polym. Chem. Ed.*, 1976, Vol. 14, p. 2497.
[227] C.Q. Yang and J.M. Freeman, *Appl. Spectr.*, 1991, V. 45, p. 1695.
[228] K. Fischer, H. Koch, and M. Beyer, Proceedings of **The 8th International Symposium on Wood and Pulping Chemistry Vol. 1: Oral Presentations**, June 6-9, 1995, Helsinki, Finland, p. 429.
[229] D.N.-S. Hon and G. Ifju, *Wood Sci.*, 1978, Vol. 11, p. 118.
[230] N.-S. Hon, *J. Polym. Sci. Polym. Chem. Ed.*, 1975, Vol. 13, p. 1347.
[231] O. Goldschmid, *Ultraviolet Spectra* in **Lignins: Occurrence, Formation, Structure, and Reaction** (K.V. Sarkanen and C.H. Ludwig, Eds.), New York: Wiley-Interscience, p. 241.
[232] I. Forsskåhl, C. Olkkonen, and H. Tylli, *Appl. Spectr.*, 1995, Vol. 49, p. 92.
[233] H. Tylli, I. Forsskåhl, and C. Olkkonen, *J. Photochem. Photobiol. A: Chem.*, 1993, Vol. 76, p. 143.

Although the origin of the fluorescence emission from pure cellulose is not yet understood, numerous investigations have been reported.[234] Zhu and Gray have studied both the room-temperature fluorescence and phosphorescence from handsheets prepared from both bleached and unbleached lignin-rich pulps.[235] For bleached pulps, they found that the intensity of the phosphorescence is less than 10^{-4} of that of the fluorescence ($\lambda_{em} \cong 500$ nm; $\tau = 10\text{-}20$ mS). Additionally, they confirmed that Whatman™ No. 1 filter paper yields a broad fluorescence peak at 415-435 nm when excited at a wavelength of 320 nm. For each of the pulp materials investigated, emission was found to be very inefficient for excitation with near-UV wavelengths between 300 and 360 nm.

Tylli and colleagues have also studied the influence of photo-irradiation on cellulose via fluorescence, FT-IR, and UV-visible reflectance spectroscopy. Munktell OOM™ and Whatman 40™ filter papers were used in these studies. The researchers reported that they were able to visually observe a yellowing of the samples during the fluorescence study. This discoloration has been attributed to the formation of aldehyde groups on the anhydroglucose units within the cellulose chain.[236]

3.5 Cellulose Ethers

Many commercially important cellulose derivatives have been prepared via the chemical modification cellulose. In his historical review of cellulose derivatives, Durso indicates that the *cellulose ethers* were first prepared and patented in the early 1900's by L. Lilienfield.[237,238] Today millions of pounds of cellulose ethers are produced annually including such derivatives as carboxymethylcellulose (CMC), ethylcellulose (EC), methylcellulose (MC), hydroxyethylcellulose (HEC), hydroxypropylcellulose (HPC), and hydroxypropylmethylcellulose (HPMC). Cellulose ethers are commonly used in adhesives, agricultural chemicals, detergents, food products, specialty chemicals, cosmetics and toiletries, latex paint, paint removers, paper products, pharmaceuticals, printing inks, elastomers, and textiles.[239,240,241,242] They function as thickeners, binders, film formers, and water retention agents. The cellulose ethers can also serve as suspension aids, surfactants, lubricants, protective colloids, and emulsifiers.

The preparation of alkali cellulose (AC) is the first step in the manufacture of cellulose ethers. Sodium hydroxide (NaOH) is used almost exclusively to swell and decrystallize the raw

---

[234] S. Toner and K. Plitt, *Tappi*, 1962, Vol. 45, p. 681.
[235] J.H. Zhu and D.G. Gray, *J. Photochem. Photobiol. A: Chem.*, 1993, Vol. 73, p. 67.
[236] H.A. Carter, *J. Chem. Ed.*, 1989, Vol. 66, #11, p. 883.
[237] D.F. Durso, *Chemical Modification of Cellulose: A Historical Review* in **Modified Cellulosics** (R.M. Rowell and R.A. Young, Eds.), New York: Academic Press, 1978.
[238] L. Lilienfeld, US Patent 1,188,376, 1916.
[239] R.L Davidson, Ed., **Handbook of Water-Soluble Gums and Resins**, New York: McGraw-Hill, 1980.
[240] R.L. Whistler and J.N. BeMiller, **Industrial Gums: Polysaccharides and their Derivatives, 3rd Ed**, New York: Academic Press Inc., 1993.
[241] A.B. Savage, A.E. Young, and A.T. Maasberg in **Cellulose and Cellulose Derivatives 2nd Ed** (E. Ott, H.M. Spurlin, and M.W. Grafflin Eds.), Part II, New York: Interscience, 1954.
[242] A.B. Savage in **Cellulose and Cellulose Derivatives** (N.M. Bikales and L. Segal, Eds.), Part V, New York: Interscience, 1954.

material (typically wood pulp or cotton linters). The sodium hydroxide (35-60%) can be directly applied to the cellulose by dipping, spraying, slurrying, or mixing.[243] Studies have shown that this *Mercerization* process only disrupts a portion of the fibrillar assemblies.[244,245] The alkalization step does not permit complete accessibility to the cellulosic fiber matrix on the molecular level. Cellulose molecules inside fibrils or fibrillar assemblies are not available to participate in the etherification reaction. As a result, portions of the cellulose that are not properly swollen by the NaOH do not react and appear as insolubles when the subsequent cellulose ether is dissolved. Therefore, the process is usually monitored either by spectroscopic or X-ray methods in order to insure uniform swelling and decrystallization. Although the added expense may partially explain their limited use, quaternary organic bases have been shown to offer a higher swelling potential. In this manner, cellulose substrates are opened to an extent that both interfibrillar and intrafibrillar cellulose is available for reaction. The chemical structure of hydroxypropylmethylcellulose (HPMC) is illustrated in figure 11.

HPMC is prepared by reaction of the alkali cellulose with mixtures of methyl chloride and propylene oxide.[246] On a large scale, the starting materials are loaded into a jacketed, nickel-clad reaction vessel and heated under controlled conditions to a maximum pressure of 1.38 MPa (200 psig).[243] The concentrations of the reactants determine the relative amounts of methyl and hydroxypropyl substitution and thus directly affect the properties of the final product. The distribution of these substituents is also affected by the reactivity of the cellulose hydroxyls. Methylation and hydroxypropylation occur preferentially at sites C2 and C6. The enhanced reactivity of the secondary C2 hydroxyl is traditionally explained in terms of its higher acidity which results in the preferential interaction with the alkoxide. The primary C6 site is methylated or hydroxypropylated as a result of its exposed position.

Due to the widespread adoption of the fibrillar network view of cellulose fiber architecture, greater emphasis must now be placed on the structural aspects that influence chemical interactions on fiber substrates. If the fiber matrix is properly activated following the alkalization step, etherification agents can enter into the substrate through swollen capillaries. The movement of the reactants to the accessible surfaces of fibrils or fibrillar aggregates is diffusion controlled. The agents interact primarily with the reactive, non hydrogen-bonded hydroxyls that protrude from the accessible surfaces of fibrils or fibrillar aggregations. On fibrillar surfaces, the number of protruding, non hydrogen-bonded secondary hydroxyls is in theory twice as great as the number of primary hydroxyls freely available for reaction. Experimental observations have shown that the secondary hydroxyls show a doubled reactivity over primary hydroxyls. Additionally, the secondary hydroxyls are initially derivatized with an approximate 2:1

---

[243] R.L. Davidson, **Handbook of Water-Soluble Gums and Resins**, New York: McGraw-Hill, 1980.
[244] J.F. Mahoney and C.B. Purves, *J. Am. Chem. Soc.*, 1942, V. 64, p. 15.
[245] T. Timell, *Studies on Cellulose Reactions*, Esselte Akt., Stockholm, 1950.
[246] Although HPMC is readily available through numerous commercial channels, a small-scale, laboratory preparation has been described. See M.D. Nicholson and F.M. Merritt, *Cellulose Ethers* in **Cellulose Chemistry and its Applications** (T.P. Nevell and S.H. Zeronian, Eds.), New York: John Wiley & Sons, 1985, p.376.

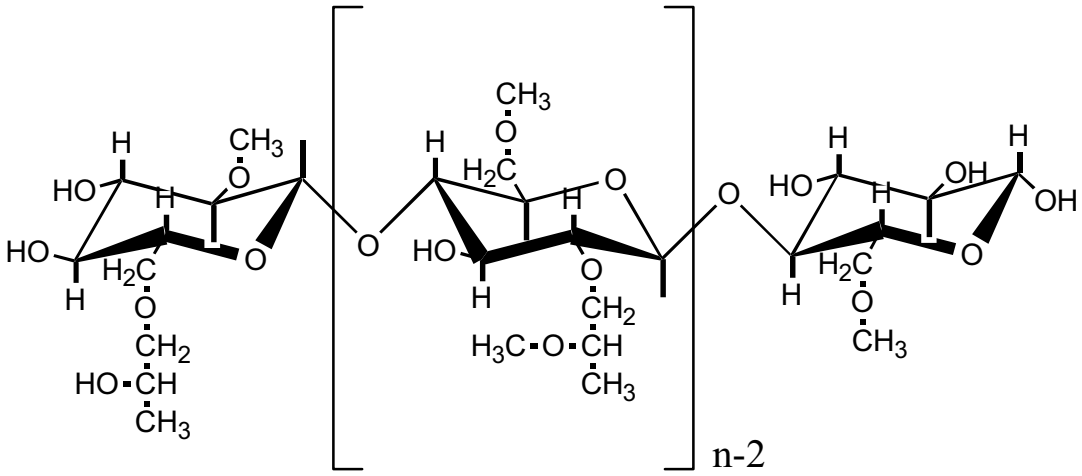

Figure 11. HPMC Structure

preference over the primary hydroxyls.[163] Recent efforts have attempted to carry out the etherification reactions on celluloses dissolved in solution. As expected, when initiated within these homogeneous conditions, the primary cellulose hydroxyls exhibit enhanced reactivities in comparison to the secondary hydroxyls.

Since HPMC is insoluble in hot water, the reaction by-products are removed by slurrying the product in water heated to greater than 90 °C and then filtering. The purified fibrous product is then dried and ground to a fine, uniform powder prior to packaging. Table 9 lists a few properties of four commercially available HPMC products.

Table 9. Representative hydroxypropylmethylcellulose products (Dow Chemical Company)

substitution, % methoxyl	substitution, % hydroxypropyl	Gel Point (°C)	Viscosity Range (cP) 2% soln; 20 °C	Tradename
28-30	7-12	60	15-4,000	Methocel E™
27-30	4-7.5	65	50-4,000	Methocel F™
19-24	7-12	75	35-15,000	Methocel K™
16.5-20	23-32	≈70	5,000-75,000	Methocel J™

Premium-grade HPMC products have been used by the food, pharmaceutical, and cosmetic industries for many years.[247] They are odorless, tasteless, white granular powders and are considered to be physiologically inert. While a significant exposure to HPMC might cause temporary irritation to skin and eyes, exposure to normal amounts presents no major health hazards from either contact or inhalation. HPMC products are environmentally-friendly and may be disposed of in landfills or by incineration.[247] Although the characteristics of HPMC in solution have been widely reported, this research is primarily concerned with the exhibited properties of HPMC in the dry, powder form [Table 10].

[247] **Methocel Cellulose Ethers Technical Handbook**, Dow Chemical U.S.A., an operating unit of the Dow Chemical Company, Chemicals and Performance Products Department, Midland, MI 48674. (*out of print*)

Table 10. Hydroxypropylmethylcellulose properties.

Chemical names and CAS Registry Number	Cellulose, 2-Hydroxypropylmethylether Cellulose, Hydroxypropylmethylether [9004-65-3]
Empirical Formula	$C_8H_{15}O_6$ — $(C_{10}H_{18}O_6)n$ — $C_8H_{15}O_5$
Molecular Weight	Approx. 86,000 (96,000 also reported in the literature)[248,249]
particle size and morphology	see figures 12 & 13
Bulk Density (ρ)[250]	0.25-0.70 g/cm^3
Browning Temperature	190-200 °C
Charring Temperature	225-230 °C
Ionic Charge	No ionic charge.
Solubility	Soluble in cold water; insoluble in hot water, ether and chloroform. Certain grades are soluble in aqueous acetone, mixtures of methylene chloride and alcohols, and other organic solvents. Soluble in 70% ethanol.[251]
Stability	Very stable in dry conditions.
Equilibrium Moisture (25 °C)	2-13% (10 to 85% relative humidity); 25% @ 93% relative humidity

Table adapted from: *Hydroxypropylmethylcellulose* in the **Handbook of Pharmaceutical Excipients**, American Pharmaceutical Association, 2215 Constitution Ave., NW, Washington, DC, 20037.

Figures 12 and 13 are electron micrographs of Methocel™ HPMC in its native dry, granular form. The samples were analyzed in the Chemistry Department Surface Analysis Laboratory at Virginia Tech on an I.S.I. SX40 scanning electron microscope by Mr. Frank Cromer.

[248] R.T.C. Ju, P.R. Nixon, and M.V. Patel, *J. Pharm. Sci.*, 1997, V. 86, p. 1293.
[249] R.T.C. Ju, P.R. Nixon, and M.V. Patel, *J. Pharm. Sci.*, 1995, V. 84, p. 1455.
[250] This range of densities applies to all of Dow's Methocel™ products. Individual densities are not reported (1-800-258-CHEM).
[251] E. Doelker, *Swelling Behavior of Water-Soluble Cellulose Derivatives* in **Absorbent Polymer Technology**(L. Brannon-Peppas and R.S. Harland, Eds.), New York: Elsevier, 1990.

Figure 12. Electron Micrograph of K4M PREM HPMC (20x)

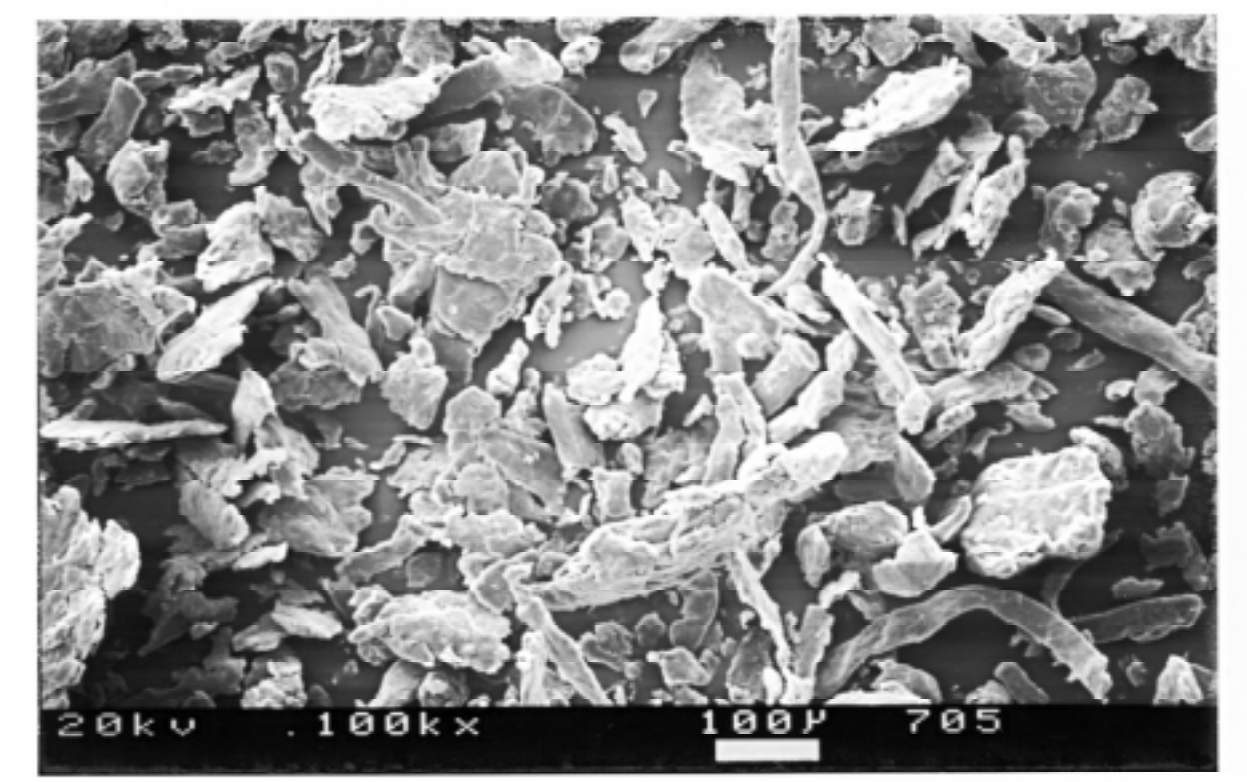

Figure 13. Electron Micrograph of K4M PREM HPMC (100x)

Although studies regarding the swelling of HPMC substrates by organic solvents were not found in the literature, related studies have attempted to model the prolonged drug release of pharmaceutical tablets in aqueous environments.[248,249,252,253,254,255] Mitchell and colleagues have observed that the rate of water-induced swelling of *K4M* HPMC is temperature dependent during the first ten minutes of exposure.[256] At all temperatures, the matrices actually decreased in size slightly before beginning to swell and, in some instances, the rate of swelling was so rapid that the tablets disintegrated. Numerous theories exist with respect to the transport of fluids through porous polymers[257], but as E. Doelker has noted "more experimental systems need to be investigated and more basic data are needed.".[251]

Nokhodchi et al. have used the Young and Nelson equations to describe three locations (monolayer adsorption, externally adsorbed moisture, and internally absorbed moisture) of sorbed moisture in different viscosity grades of HPMC.[258] Their experimental approach was used to examine the moisture sorption hysteresis of each cellulose ether. The researchers found that there was a higher amount of sorbed moisture remaining during desorption than attained during sorption. Multiple explanations have been proposed, including changes in polymer chain conformation (irreversible swelling), an increase in the strength of solid-liquid bonding (enthalpy effect), molecular ordering (entropy effect), or a combination of effects determined by the entry of water into the polymeric matrix. Nokhodchi and colleagues also determined that the tensile strength of *K4M* HPMC tablets will increase as relative humidity surrounding the granulated excipient material is increased (prior to tableting). Water molecules initially absorbed on the granule surfaces may form a monomolecular layer and increase the van der Waals forces present, thereby smoothing out the surface microirregularities and reducing interparticle separation. The development of additional bonds by plastic deformation and/or melting of powder particles may also be a factor.[258] Unfortunately, although higher levels of ambient moisture will increase the tensile strength of the HPMC pellet, water is also regarded as a prime offender in the arena of RTP-quenching agents.

Sadek and Olsen have determined the water-adsorption isotherms of methylcellulose and HPMC using a quartz crystal microbalance approach.[259] They discovered that HPMC exhibits a "Type II" adsorption isotherm. According to the researchers, a Type II isotherm is encountered when adsorption occurs on non-porous surfaces or on microporous surfaces that allow a multimolecular layer of adsorbate to be bound to the surface. Both cellulose ethers exhibited a hysteresis loop. Numerous theories have been proposed in order to explain this phenomenon by

---

[252] K. Mitchell, J.L. Ford, D.J. Armstrong, P.N.C. Elliott, J.E. Hogan, and C. Rostron,*Int. J. Pharm.*, 1993, V. 100, p. 175.
[253] P. Gao, J.W. Skoug, P.R. Nixon, T.R. Ju, N.L. Stemm, and K.C. Sung,*J. Pharm. Sci.*, 1996, V. 85, p. 732.
[254] A.T. Pham and P.I. Lee,*Pharm. Res.*, 1994, V. 11, p. 1379.
[255] P. Colombo, P.L. Catellani, N.A. Peppas, L. Maggi, and U. Conte,*Int. J. Pharm.*, 1992, V. 88, p. 99.
[256] K. Mitchell, J.L. Ford, D.J. Armstrong, P.N.C. Elliott, J.E. Hogan, and C. Rostron,*Int. J. Pharm.*, 1993, V. 100, p. 143.
[257] W.M. Saltzman, *Transport in Porous Polymers* in **Absorbent Polymer Technology**(L. Brannon-Peppas and R.S. Harland, Eds.), New York: Elsevier, 1990.
[258] A. Nokhodchi, J.L. Ford, and M.H. Rubinstein,*J. Pharm. Sci.*, 1997, V. 86, p. 608.
[259] H.M. Sadek and J.L. Olsen,*Pharm. Technol.*, February 1981, p. 40.

considering many of the potential differences in the state of the adsorbate during adsorption and desorption.[259]

3.6 Pelletization

A direct compression technique was used in order to prepare the HPMC pellets for this project. This approach enhanced the uniformity of each substrate with respect to size, compaction density, and macroscopic surface morphology. Sadlik has noted that direct compression methods have been used since the 1800's for the preparation of solid oral dosage forms (pharmaceutical *tablets*).[260] Manufacturers of pharmaceuticals are fond of the direct compression technique because it lends itself to rapid mass production and is the least expensive method of producing solid dosage forms. Advantages of the direct compression method include its overall simplicity, elimination of solvents (and subsequent drying steps), minimization of materials handling, and rapidity of tablet manufacture.[261]

The term *direct compression* was initially used to describe the compression of a single crystalline compound. For example, potassium bromide (KBr) pellets may be prepared by direct compression for use in infrared spectroscopic investigations. However, very few chemicals possess the necessary flow, cohesion, and lubricating properties required for the preparation of a pellet by this method. Today, the term *direct compression* is used to define the process by which pharmaceutical tablets are compressed directly from powder blends of an active ingredient and excipient materials. Each component must flow uniformly into a die cavity and provide for the formation of a solid compact.[262]

Compressed tablets are manufactured by compressing the powder blend in a die between two punches under loads of a thousand pounds or more.[261] One of the most critical factors in pellet or tablet making is the tooling (punches and dies) that are used for their manufacture. The tooling utilizes hardened steel and the parts are machined precisely to close tolerances. For a well-written and detailed account of the physics of tablet compression, the reader is referred to **Solid Pharmaceutics** by J.T. Carstensen.[263]

Typically, powders resist compression into tablet form because of two factors: entrapped air and poor particle-particle adhesion following compression. As a result, the tablets tend to be soft and of poor appearance regardless of the compression pressure used. There are a number of essential qualities of a good tablet. Among these are: accurate and uniform weight, content uniformity, homogeneity, absence of incompatibilities, tablet hardness, disintegration

---

[260] F. Sadlik, *Tablets* in **Dispensing of Medication: A practical manual on the formulation and dispensing of pharmaceutical products, 9th Ed** (R.E. King, Ed.), Easton, PA: Mack Publishing Co., 1984.

[261] G.S. Banker, *Tablets and Tablet Product Design* in **Sprowl's American Pharmacy: An introduction to Pharmaceutical Techniques and Dosage Forms, 7th Ed** (L.W. Dittert, Ed.), Philadelphia: J.B. Lippincott Company, 1974.

[262] R.F. Shangraw, *Compressed Tablets by Direct Compression* in **Pharmaceutical Dosage Forms: Tablets, 2nd Ed.** (H.A. Lieberman, L. Lachman, and J.B. Schwartz, Eds.), New York: Marcel Dekker, Inc., 1989.

[263] J.T. Carstensen, **Solid Pharmaceutics: Mechanical Properties and Rate Phenomena**, New York: Academic Press, 1980.

characteristics, dissolution properties, and overall stability. The majority of these considerations are also pertinent to the preparation of suitable RTP substrates via direct compression methods.

The term *excipient* refers to all of the materials in a compressed pellet or tablet except for the active ingredient. For pharmaceutical tablets, the excipient is an inert substance that provides the compact with suitable form or consistency. The excipients used in the manufacture of compressed tablets are typically assigned a function in the process and can be classified accordingly. For instance, excipients can serve as diluents, binders, disintegrants, lubricants, coloring agents, or flavoring agents.[264] Often, a single excipient material can serve more than one function (for example, corn starch can serve as a diluent, a disintegrant, and a lubricant).

The purpose of a diluent (sometimes referred to as a *filler*) is to provide tablet bulk. Binders are materials that are added as dry powders to the mixture in order to provide bonding and cohesion of the components. With regard to pharmaceutical applications, hydroxypropylmethylcellulose has primarily been classified as a tablet binder.[265] Disintegrants are additives that cause tablets to break up and fragment after ingestion. Lubricants are excipient materials that serve two purposes: to reduce adhesion or sticking of the powdered mixture to the punch faces and to reduce the ejection force needed to remove the compressed tablets from the die. Following compression, unlubricated mixtures produce tablets that have high die wall friction during ejection. The friction can cause tablets to fracture and the die walls may be scored. Over long periods of time, this will cause excessive wear in the bore of the die. These substances have been further classified according to their primary function. *Lubricants* reduce the friction between surfaces (in this case between the side of the tablet and the wall of the die). *Anti-adherents* reduce adhesion and sticking of the components to the faces of the punch. *Glidants* reduce inter-particle friction and promote particle flow. Additional details regarding the fundamental properties of excipient materials can be found elsewhere.[262,266,267]

For this work, the preparation of HPMC pellets did not require the addition of fillers. Because HPMC is relatively inexpensive, it can be used alone to provide suitable tablet bulk. Disintegrants were also not required. Solid RTP substrates that readily disintegrate upon wetting are to be avoided. If HPMC pellets were to be prepared via automated methods on a large scale, then perhaps a lubricant would be necessary. However, it was discovered during this project that HPMC does not adhere strongly to the surfaces of the punch and die. If pellets are manufactured manually using compression forces less than or equal to 17K PSI, then a lubricant should be unnecessary.

---

[264] E.W. Martin and J.E. Hoover, Eds. **Husa's Pharmaceutical Dispensing: A textbook and reference manual on drug development, pharmaceutical compounding, and dispensing, 6th Ed**, Easton, PA: Mack Publishing Co., 1966.

[265] *Hydroxypropylmethlycellulose* in the **Handbook of Pharmaceutical Excipients**, American Pharmaceutical Association, 2215 Constitution Ave, NW, Washington, DC, 20037.

[266] M.R. Harris and I. Ghebre-Sellassie, *Formulation Variables* in **Pharmaceutical Pelletization Technology** (I. Ghebre-Sellassie, Ed.), New York: Marcel Dekker, Inc., 1989.

[267] **Handbook of Pharmaceutical Excipients**, American Pharmaceutical Association, 2215 Constitution Ave, NW, Washington, DC, 20037.

4.0 Instrumentation

This section of the dissertation will discuss a series of topics associated with the design, construction, and use of a phosphorimeter. More specifically, a discussion of xenon arc lamps, excitation and emission monochromators, sample holders, photodetectors, and phosphoroscope attachments will be presented.

A basic luminescence spectrophotometer consists of the following elements:

1). an optical radiation source
2). wavelength selection devices (usually monochromators)
3). a sample compartment and sample holder
4). a photodetector (usually a photomultiplier tube), and
5). a read-out device (frequently a computer-based data acquisition system).

Figure 14 is a block diagram of such an instrument. The light source is typically a high-intensity xenon arc lamp. Following collimation, optical radiation from the source is focused on the entrance slit of an excitation monochromator. The gratings found in commercial instruments will normally have rulings of either 600 or 1200 grooves/mm. After passing through the excitation monochromator, the light enters the sample compartment and strikes the sample. The luminescence produced by the sample is then collected and focused onto the entrance slit of the emission monochromator. The excitation path and emission pathway are usually arranged in a right angle configuration in order to minimize interference due to scattered light. In most modern instruments, the gratings within the monochromators are motor-driven. The entrance and exit slits are also automated on certain instruments. After passing through the emission monochromator, the optical radiation strikes a photomultiplier tube (PMT). The PMT is an elegant device that efficiently converts photons into electrons. It then amplifies the number of electrons and provides an output in the form of electrical current that is proportional to the intensity of light which strikes it. The electrical current is typically converted to a voltage signal that may be monitored by an analog-to-digital (A/D) converter. The A/D device will convert the analog voltage into a digital form that can be subsequently manipulated by a computer.

The instrument that has been described is conventionally called a *fluorimeter*. It is suitable for measuring the short-lived, photoluminescence that results from $S_1 \Rightarrow S_0$ transitions. In order for this instrument to be useful in acquiring $T_1 \Rightarrow S_0$ photoluminescence data, a modification is required so that the long-lived phosphorescence emissions can be fully isolated from the quickly decaying fluorescence emission. Older instruments were equipped with what is commonly called a *phosphoroscope*. The phosphoroscope is a mechanical device that serves two useful purposes: 1). it insures that the phosphorescence measurement step is always out of phase with the excitation of the sample and 2). that the photoluminescence is essentially *gated* so that any fluorescence emission from the sample will be physically blocked and only phosphorescence

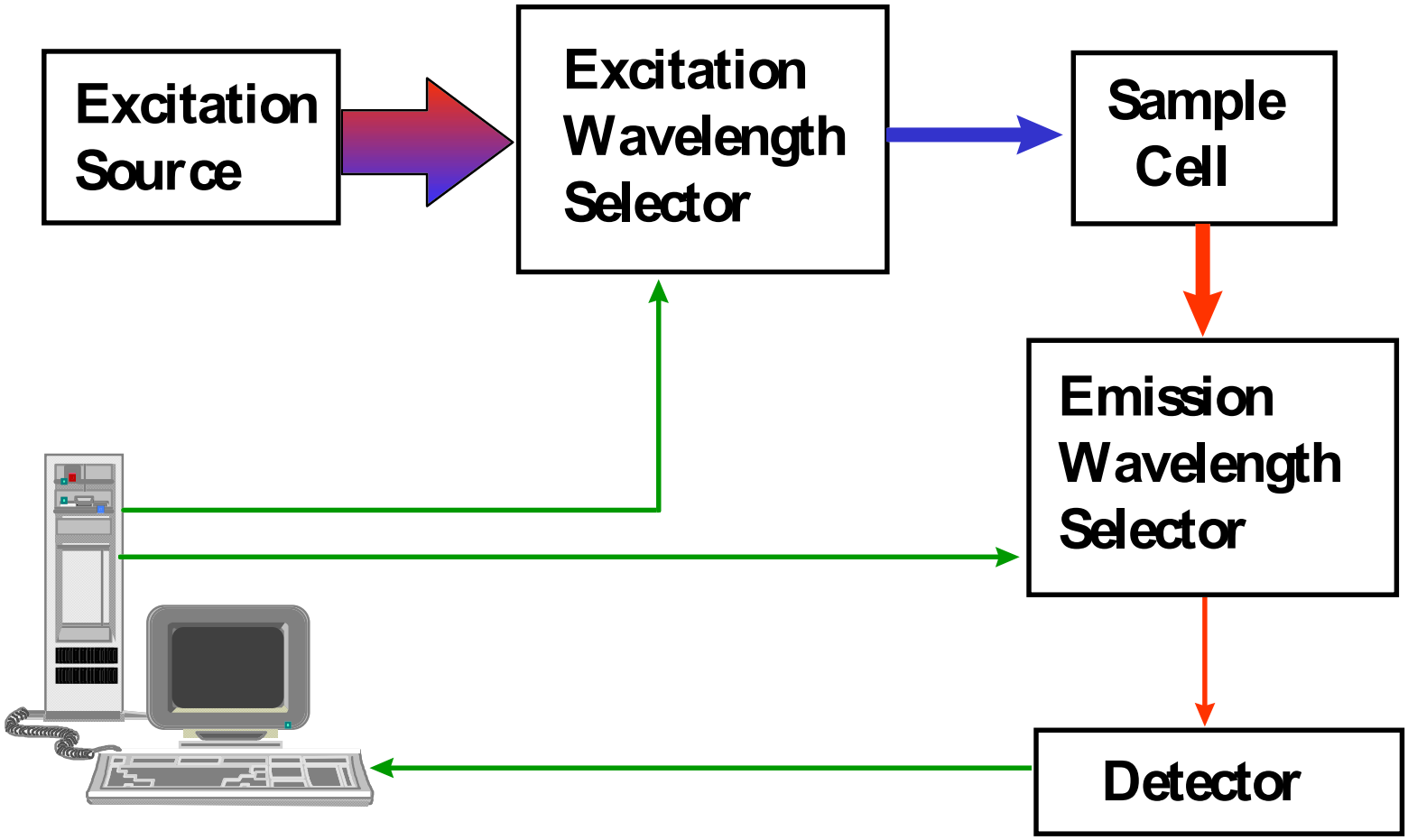

Figure 14. Block Diagram of a Simple Luminescence Spectrophotometer

emission will be allowed to arrive at the PMT. Modern computer-controlled instruments are usually pulsed-source/gated-detector instruments. If the excitation and detection steps are automated in this manner, the mechanical phosphoroscope may be eliminated from the instrument. Figure 15 is a block diagram of a pulsed-source/gated-detector phosphorimeter.

4.1 Optical Radiation Source

Ultraviolet (UV) light is usually required for the excitation of RTP analytes. The most commonly used optical radiation source for this purpose is the xenon arc lamp. The xenon arc lamp produces an intense continuum of radiation ranging from the UV (< 200 nm) to the near infrared (> 1000 nm). A few broad bands are present at approximately 450-500 nm. The lamps consist of two tungsten electrodes surrounded by high pressure xenon gas within a quartz enclosure. The operation of these lamps requires special care and handling. It is best to power Xe-arc lamps with highly regulated DC power supplies in order to provide lamp stability. The infrared output of the lamp can produce a significant amount of heat that must be removed. A thirty minute warm-up period of the lamp is always required. There is some tendency for the arc to change its location within the lamp during the first half hour of operation. If the arc should wander during an analysis, sudden variations in observed intensity may occur. This can be especially troublesome when the image of the arc is focused onto a small entrance slit.

4.2 Wavelength Selection

Most modern phosphorimeters utilize excitation and emission monochromators for wavelength selection. Grating monochromators are more commonly used than prism monochromators as a result of their higher resolution. They are also convenient to use because their spectral dispersion is linear with respect to wavelength. Diffraction gratings were first refined in the late 1800's by the American physicist, Henry Rowland. They consist of a large number of grooves that are ruled onto a highly polished surface.[268]

The functional characteristics of a grating are determined by the number and shape of the grooves found on its surface. With an increasing number of grooves per millimeter, the throughput and resolution of the grating are improved. The width of the groove should be approximately equal to the wavelength of the light to be dispersed. The shape of the groove should be arranged such that the maximum amount of light at a given wavelength is concentrated at only one specific angle for each order. It is the design and construction of the grating that determines additional properties of the monochromator such as radiance throughput and stray light rejection.

The general diffraction grating formula follows:

$$\sin\theta + \sin\theta' = k\cdot\lambda/d = k\cdot n\cdot\lambda$$

where θ is the angle of incidence, θ' is the angle of diffraction, n is the number of grooves per unit length ($1/d$), d is the groove spacing, and k is the dispersion order. As seen by the diffraction grating formula, light is dispersed by the grating because θ' is dependent on λ. A spectrum is

[268] A.D. Moore, *Sci. Am.*, Feb. 1982, p. 150.

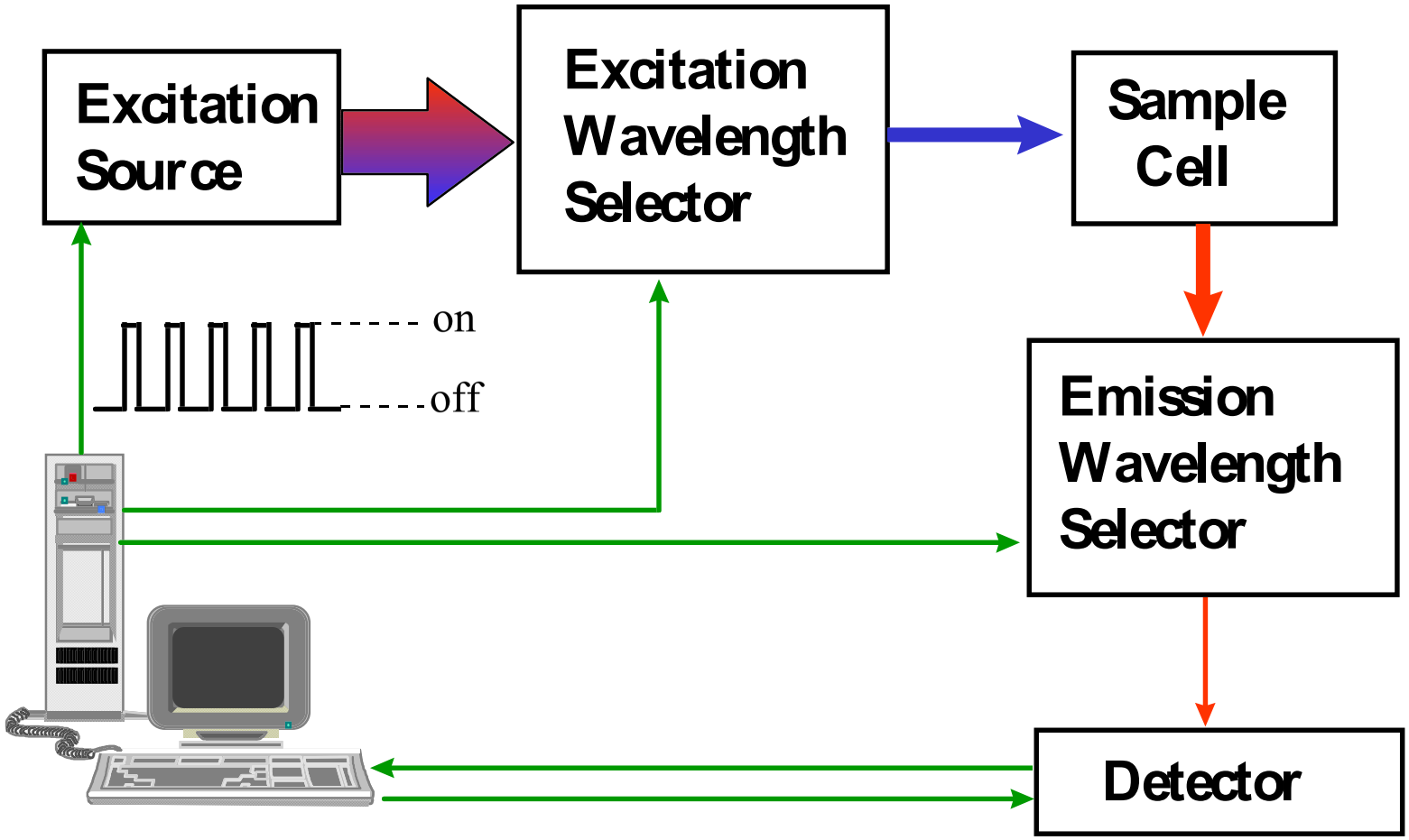

Figure 15. Block Diagram of a pulsed-source/gated-detector Phosphorimeter

obtained for each value of *k*. As a consequence of this, gratings can also produce second- and higher-order dispersions that can overlap the lower-order emission of interest. For solid surface fluorescence analyses, this effect commonly results in the appearance of anomalous maxima within the emission spectra acquired. Such peaks are often ambiguously described as resulting from "second-order scatter". One easy way to overcome this problem is to insert an appropriate cutoff filter within the optical path of the instrument (usually at the expense of considerable reduction of signal intensity). As a result of the gated-detector operation of all phosphorimeters, second- and higher-order emissions will never reach the PMT. This is one particular instance where the SSRTP technique is superior to that of SSRTF.

The light throughput for various standard gratings varies between 50 and 90% and increases with groove density. For conventionally ruled gratings, this density has a practical limit above which it may produce too much stray light and *ghosts* (spurious spectral lines caused by periodic imperfections in the gratings). Lasers and holography have made it possible to produce holographic gratings that have a very high throughput and produce minimal stray light.

4.3 Phosphoroscope Devices

A phosphoroscope can serve two primary purposes: to reject any scattered excitation light and prevent fluorescence emissions from reaching the detector. The amount of scattered light is usually negligible when the sample consists of a transparent liquid; however, certain solid samples or solid substrates can be highly scattering. Additionally, most organic phosphors yield strong fluorescence emission spectra when immobilized on solid support materials. The phosphoroscope prevents all short-lived fluorescence emissions from arriving at the PMT.

The most commonly used phosphoroscope devices are mechanical choppers. A suitable chopper will periodically interrupt the excitation radiation and the phosphorescence emission will be observed only after a short time delay which follows the excitation step. Common arrangements are the Becquerel discs,[11,269,270] the rotating can,[52,271,272,273] the rotating mirror,[274] and the single disc chopper.[140,275,276] The rotating mirror assembly is an especially interesting phosphoroscope configuration that allows for the RTP measurement of *overhead* samples. Vo-Dinh and colleagues were able to use this unique geometry to their advantage by obtaining RTP measurements from a continuous strip of filter paper that could be pulled across the top of the phosphoroscope. This was the first report of a significant effort to fully automate the SS-RTP technique.

The maximum rotating speed of most commercial mechanical phosphoroscopes is approximately 6000 rpm. Vo-Dinh cautions that compounds having very fast RTP decays ($\tau < 1$

---

[269] E. Becquerel, *Ann. chim. et. phys.*, 1871, V. 27, p. 539.
[270] L. Langouet, *Appl. Optics*, 1972, V. 11, p. 2358.
[271] T.C. O'Haver and J.D. Winefordner, *Anal. Chem.*, 1966, V. 38, p. 602.
[272] J.D. Winefordner, *Accounts Chem. Res.*, 1969, V. 2, p. 361.
[273] P.F. Lott and R.J. Hurtubise, *J. Chem. Ed.*, 1974, V. 51, p. A315.
[274] T. Vo-Dinh, G.L. Walden, and J.D. Winefordner, *Anal. Chem.*, 1977, V. 49, p. 1126.
[275] H.C. Hollifield and J.D. Winefordner, *Chem. Instr.*, 1969, V. 1, p. 341.
[276] H. Kim, M.J. Zabik, and S.R. Crouch, *Appl. Spectr.*, 1989, V. 43, p. 611.

msec) and low phosphorescence quantum yields ($\phi_P < 0.01$) could possibly have completely decayed before the aperture of a mechanical chopper has rotated to the viewing position.[12] At higher speeds, mechanical phosphoroscopes must be carefully balanced or violent vibrations may result as the assembly and motor shaft are forced off-axis. This is especially true for the rotating can and rotating mirror configurations.

Modern instruments use pulsed sources and gated detectors instead of the mechanical phosphoroscopes discussed above.[277,278,279,280] According to Fisher and Winefordner, this allows for a distinct sensitivity and selectivity advantage over the mechanically modulated systems.[281] Additionally, this arrangement will not restrict the sample compartment geometry and it is a simple matter to convert from a measurement of phosphorescence to one of fluorescence.

Figure 16 shows the sequence of events that occur during an excitation/emission cycle of a pulsed-source/gated-detector instrument. For an instrument such as the Perkin-Elmer LS-50, the pulsed xenon arc lamp will produce a band of energy with a width at half peak intensity (t_f) of less than 10 μs. During this period, the phosphorescence increases to a peak value (I_o) and then decays exponentially to zero. The gating of the PMT is delayed by a short period of time (t_d) so that it will not intercept the flash of the Xe-arc lamp. If t_d is set to greater than 0.1 ms, then prompt fluorescence from the sample will also not interfere with the desired RTP measurements. The gate width (t_g) is the duration of PMT exposure to the phosphorescence emitted by the sample.

[277] J.L. Charlton and B.R. Henry, *J. Chem. Ed.*, 1974, V. 51, p. 753.
[278] E.L. Yen, G.D. Boutilier, and J.D. Winefordner, *Can. J. Spectr.*, 1977, V. 22, p. 120.
[279] M.C. Piton, W. Panning, and M.A. Winnik, *Rev. Sci. Instrum.*, 1990, V. 61, p. 3726.
[280] J.R. Herman, T.R. Londo, N.A. Rahman, and B.G. Barisas, *Rev. Sci. Instrum.*, 1992, V. 63, p. 5454.
[281] R.P. Fisher and J.D. Winefordner, *Anal. Chem.*, 1972, V. 44, p. 948.

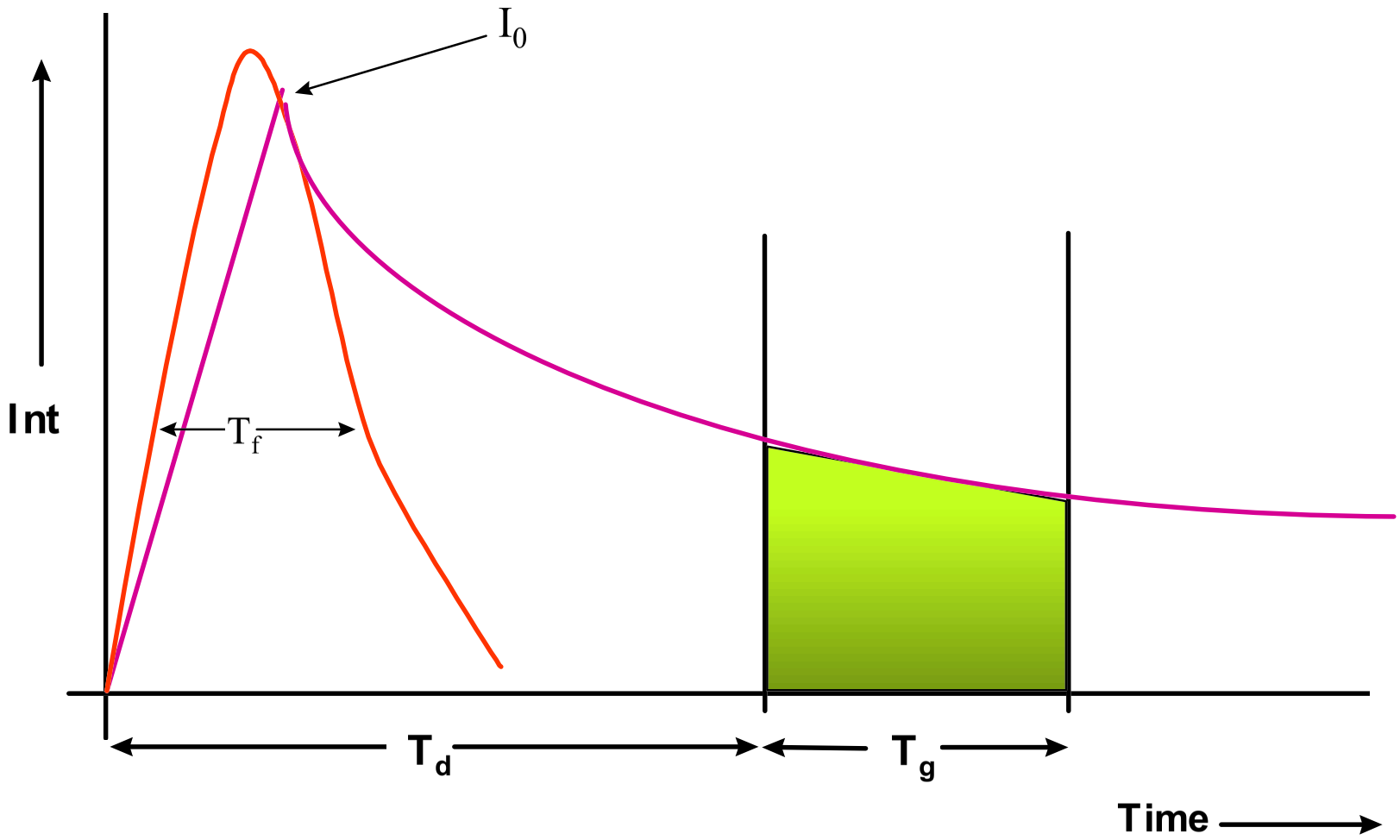

Figure 16. Excitation Pulse and Phosphorescence Decay

4.4 Sample Holders

It is sometimes possible for a phosphorescence researcher to purchase specialized front surface accessories from their instrument vendor in order to facilitate the examination of solids. However, these accessories are typically quite expensive and often require further in-house modification before they are suitable for phosphorescence investigations. Therefore, most SSRTP sample holders have been fabricated in-house. These devices are literally the "heart" of the phosphorimeter and their importance is not to be underestimated. The literature describes a multitude of diverse sample holder configurations. Between laboratories, the devices tend to differ significantly in both complexity and utility.[34,108,144,282,283,284,285,286,287,288,289,290,291]

Scharf and colleagues designed one particularly elegant sample holder for the Perkin-Elmer LS-5 fluorimeter.[292] In addition to providing for four samples and an analytical blank, a special feature of the device is that it may be used for both RTP (25 °C) and LTP (-65 °C) investigations. After obtaining excitation and emission spectra for samples immobilized on filter papers and cellulose TLC plates, the researchers advised that analytical LTP with solid substrates would be most useful for those molecular species that yield very weak phosphorescence (or no phosphorescence) at room temperatures.

Campiglia and colleagues have described an automatic sampling system for use in SS-RTP analyses.[293] Samples are sprayed onto a moving strip of filter paper by means of a conventional atomic absorption nebulizer. A custom sample holder was designed and built in-house for use in this system. Reasonable results were obtained for three model phosphors. However, a significant disadvantage was that high concentrations of heavy-atom salts would clog the nebulizer. A subsequent paper published by the same group described the use of a two-nebulizer system that solved the clogging problem.[294] Using the modified system, the tedious procedure of pre-mixing solutions was avoided. It was reported that sixteen to twenty RTP measurements could be taken within one minute using this automated system.

L.F. Capitán-Valvey et al. have developed a new RTP measurement system that relies on the detection of diffuse transmitted phosphorescence emitted from the unexcited surface of a filter paper support.[295] A homemade sample holder was designed to be inserted into the sample

---

[282] T. Vo-Dinh and J.D. Winefordner, *Appl. Spectr. Rev.*, 1977, V. 13, p. 261.
[283] E. Lue-Yen Bower and J.D. Winefordner, *Anal. Chim. Acta*, 1978, V. 101, p. 319.
[284] T. Vo-Dinh and J.R. Hooyman, *Anal. Chem.*, 1979, V. 51, p. 1915.
[285] T. Vo-Dinh and P.R. Martinez, *Anal. Chim. Acta*, 1981, V. 125, p. 13.
[286] J.L. Ward, R.P. Bateh, and J.D. Winefordner, *Analyst*, 1982, V. 107, p. 335.
[287] M.W. Warren II, J.P. Avery, and H.V. Malmstadt, *Anal. Chem.*, 1982, V. 54, p. 1853.
[288] J.M. Bello and R.J. Hurtubise, *Anal. Lett.*, 1986, V. 19, p. 775.
[289] S.M. Ramasamy, V.P. Senthilnathan, and R.J. Hurtubise, *Anal. Chem.*, 1986, V. 58, p. 612.
[290] G.J. Burrell and R.J. Hurtubise, *Appl. Spectr.*, 1988, V. 42, p. 173.
[291] S.W. Tjioe and R.J. Hurtubise, *Talanta*, 1995, V. 42, p. 971.
[292] G. Scharf, B.W. Smith, and J.D. Winefordner, *Anal. Chem.*, 1985, V. 57, p. 1230.
[293] A.D. Campiglia, L.M. Perry, and J.D. Winefordner, *Appl. Spectr.*, 1989, V. 43, p. 1341.
[294] A.D. Campiglia, L.M. Perry, and J.D. Winefordner, *Appl. Spectr.*, 1990, V. 44, p. 729.
[295] L.F. Capitán-Valvey, F. Ojeda, M. del Olmo, R. Avidad, A. Navalón, and T. Vo-Dinh, *Appl. Spectr.*, 1998, V. 52, p. 101.

compartment of the Perkin-Elmer LS-5 spectrometer. The analyte of choice was nalidixic acid, an antibacterial agent used for the prevention and treatment of Gram-negative urinary-tract infections and for the control of infections in chickens. According to the researchers, the diffuse transmission configuration was superior to conventional RTP systems based on reflected intensity.

4.5 Photodetectors

Although the naked eye was often a sufficient detector for many early qualitative phosphorescence studies, modern photodetectors such as the photomultiplier tube have allowed for the quantitation of emissions as well. PMTs are vacuum tubes that contain a cathode, a series of dynodes (typically seven to twelve), and an anode. The metal-oxide cathode is sensitive to photons. As a result of the photoelectric effect, the photons that strike it are immediately converted to electrons. The dynodes are special types of electrodes that have their surfaces coated with a material that can emit several secondary electrons for each electron that strikes them. Thus, the *photoelectrons* provided by the cathode are able to cascade down the dynode chain in increasing number as a result of secondary emissions that occur at each dynode surface. The electrons are accelerated down the dynode chain by a potential that can be as high as 100 V from one dynode to the next. As a result of the cascading and amplification effects provided by the dynodes, a single photon at the cathode may result in as many as 10^9 electrons received at the anode. This amplification factor depends both on the PMT materials and the input voltage applied to the device.[296] The total current collected at the anode is proportional to the incoming photon flux and is linear over many orders of magnitude.

The spectral response of a PMT is determined by the materials used in the photocathode and the transmission characteristics of the window. The long-wavelength cutoff is determined by the photocathode material; whereas the short-wavelength cutoff is determined by the window material used in the enclosure surrounding the PMT. Manufacturers always provide spectral response curves in association with their PMT products.

A relatively new instrument design has cleverly allowed for the simultaneous measurement of prompt fluorescence and long-lived phosphorescence using dual balanced PMTs.[297] The gains of the PMTs are suppressed for the duration of the fluorescence emission, and subsequently returned to normal in order to maintain the fluorescence and phosphorescence signals at the same level. The suppression of the gain is controlled by a specially designed dual-channel PMT gain-suppression circuit. The signals from the PMTs are recorded by two digital oscilloscopes, one set at a fast sampling rate to measure the fluorescence and the other set to a slow sampling rate to measure the phosphorescence.

---

[296] J. Dakin and B. Culshaw, **Optical Fiber Sensors: Principles and Components** Boston: Artech House, Inc., 1988.

[297] L. Yang, D. McStay, A. Rogers, and P.J. Quinn, *Opt. Eng*., 1993, V. 32, p. 354.

5.0 Experimental

This chapter will examine the experimental parameters associated with this research. The reagents, apparatus, and laboratory procedures utilized during this investigation are specified. The primary analytical instrument used for this research is the Perkin-Elmer LS-50. The hardware specifications and signal handling features associated with this instrument will be examined. The construction of a unique, custom-built sample cell module is explained in detail. Additionally, a commercially-available front surface sample accessory was borrowed from Perkin-Elmer. Following limited modification, it was possible to use this accessory to determine if a direct relationship exists between sample substrate thickness and RTP intensity. Finally, the chapter closes with the presentation and analysis of the data collected during this project.

5.1 Supplies

Table 11 briefly summarizes pertinent information concerning the reagents, solvents, support materials, purge gases, and desiccant used during this project. If known, the purity or grade of each material is provided as well as information regarding specific vendors.

Table 11. Listing of reagents, solvents, support materials, purge gases, and desiccant.

Solvent	Purity or grade	Vendor
Ethanol; Absolute 200 Proof	U.S.P.	AAPER Alcohol and Chemical Co. DSP - KY - 417 Shelbyville, KY 40065
Support Material	**Purity or grade**	**Vendor**
Hydroxypropylmethylcellulose	Methocel™ *K4M PREM* Lot # MM93100201K	the Dow Chemical Company Midland, MI 48674 1-800-258-CHEM
Hydroxypropylmethylcellulose	Methocel™ E15LV PREM Lot # MM94101921E	the Dow Chemical Company Midland, MI 48674 1-800-258-CHEM
Hydroxypropylmethylcellulose	Methocel™ E3 PREM Lot # MM93021522E	the Dow Chemical Company Midland, MI 48674 1-800-258-CHEM
FisherBrand filter paper - P2 (manufactured by Whatman for Fisher)	porosity: fine flow rate: slow cat # 09-803-5C	Fisher Scientific Company Pittsburgh, PA 15219-4785 1-800-766-7000 Whatman Inc. Fairfield, NJ 07004 (201) 882-9277
Gases	**Purity or grade**	**Vendor**
AIRCO compressed nitrogen	N/A	Industrial Gas and Supply Co. Radford, VA (540) 639-9606
AIRCO compressed oxygen	N/A	Industrial Gas and Supply Co. Radford, VA (540) 639-9606
AIRCO compressed air	medical air, U.S.P. 21% O_2 79% N_2	Industrial Gas and Supply Co. Radford, VA (540) 639-9606

Table 11 (continued). Listing of reagents, solvents, support materials, purge gases, and desiccant.

Reagent	Purity or grade	Vendor
Naphthalene	scintillation grade >99% Lot # 250917 186	Fluka Chemie AG Industriestrasse 25 CH-9471 Buchs Switzerland 1-800-358-5287
2-Naphthol	99% Lot # 1011EK	Aldrich Chemical Company P.O. Box 335 Milwaukee, WI 53201 (414) 273-3850
2-Naphthoic Acid	99% Lot # 01503DT	Aldrich Chemical Company P.O. Box 335 Milwaukee, WI 53201 (414) 273-3850
Phenanthrene	Zone Refined Gold Label 99.5+% Lot # 8028DK	Aldrich Chemical Company P.O. Box 335 Milwaukee, WI 53201 (414) 273-3850
Triphenylene	>98%(HPLC) Lot # 2327711282	Fluka Chemie AG Industriestrasse 25 CH-9471 Buchs Switzerland 1-800-358-5287
Acenaphthene	>97%(HPLC) Lot # 219872185	Fluka Chemie AG Industriestrasse 25 CH-9471 Buchs Switzerland 1-800-358-5287
Salicylic Acid, sodium salt	99+% Gold Label Lot # 00426KJ	Aldrich Chemical Company P.O. Box 335 Milwaukee, WI 53201 (414) 273-3850
p-aminobenzoic acid (PABA)	Lot # 592634A	Eastman Kodak Company Rochester, NY 14650
Sodium Iodide	Certified Lot # 874655	Fisher Scientific Company Chemical Manufacturing Division Fair Lawn, NJ 07410

Table 11 (continued). Listing of reagents, solvents, support materials, purge gases, and desiccant.

Desiccant	Purity or grade	Vendor
Drierite™ (97% anhydrous $CaSO_4$ & 3% $CoCl_2$)	Stock #23001. Size: 8 mesh.	W.A. Hammond Drierite Company Xenia, Ohio. 1-513-376-2927

Naphthalene ($C_{10}H_8$) was the phosphor of choice for the majority of SSRTP investigations carried out during this project. Naphthalene has generally exhibited strong emission characteristics in prior solution and solid-state studies. It has frequently been used as a model compound by spectroscopists during investigations involving both fluorescence and phosphorescence. As a result of the simplicity of its structure, naphthalene's singlet- and triplet-state transitions have been well-characterized in the literature. Furthermore, naphthalene is easy to obtain, low-in-cost, and safe to work with in the laboratory.

Additional model compounds selected for the room temperature phosphorescence studies include: 2-naphthol ($C_{10}H_7OH$), 2-naphthoic Acid ($C_{10}H_7CO_2H$), phenanthrene ($C_{14}H_{10}$), triphenylene ($C_{18}H_{12}$), acenaphthene ($C_{12}H_{10}$), sodium salicylate (2-$(HO)C_6H_4CO_2Na$), and p-aminobenzoic acid ($H_2NC_6H_4CO_2H$). These analytes were chosen specifically as a result of their varied physical and chemical properties in order to determine if the proposed RTP support materials would be suitable for the analysis of a wide range of phosphors.

The use of the external heavy-atom effect for the increase of SSRTP intensity was first reported in 1975 by Seybold and White.[33] Sodium iodide was reported to strongly decrease the fluorescence signal and increase the phosphorescence intensity of 2-naphthalene sulfonate (sodium salt). For this project, the heavy-atom phosphorescence enhancer of choice was also sodium iodide (NaI). It has often been demonstrated by other laboratories that sodium iodide is a versatile and capable external heavy-atom phosphorescence enhancer. Since NaI was the only heavy-atom chosen for this project, one important variable in the extensive roster of analysis conditions could be held constant throughout the duration of the project.

Additionally, there have been no unfavorable reports in the literature suggesting that NaI interferes with the spectral characteristics of RTP emission. Experiments conducted during this project support prior observations that NaI is an excellent all-purpose phosphorescence enhancer. Safety considerations are also important factors that should be addressed by the SSRTP investigator as well. A few researchers have noted that the acetates of lead and thallium are suitable heavy-atom enhancers. On the other hand, the toxicity of these salts would preclude their usage on a regular basis for routine sample analysis.

As an added bonus, in addition to being a suitable external heavy-atom perturber, NaI is also an excellent swelling agent for cellulose. This feature is particularly desirable considering the nature of the solid supports investigated. Finally, sodium iodide was sufficiently soluble in

ethanol (42.57g. per 100 mL[298]) to allow for the preparation of a series of solutions having concentrations within the range of 0.01 M to 1.0 M (0.2% to 16.5% wt/wt). A series of RTP studies involving this series of sodium iodide solutions was undertaken and the results were particularly illuminating.

Three grades of hydroxypropylmethylcellulose were investigated as potential SSRTP support materials. *K4M PREM*, *E15LV PREM*, and *E3 PREM* Methocel™ are premium grades of HPMC intended for use by the food, pharmaceutical and cosmetic industries. *K4M PREM* Methocel™ is characterized by 19-24% methoxyl substitution and 7-12% hydroxypropyl substitution. *E15LV PREM* and *E3 PREM* varieties of Methocel™ are characterized by 28-30% methoxyl substitution and 7-12% hydroxypropyl substitution. Although often specified on the basis of their viscosity characteristics in solution, these particular Methocel™ products were chosen in part due to their high level of purity and suitable compression characteristics for the preparation of RTP substrates. Each of the HPMC samples were provided gratis courtesy of the Dow Chemical Company.

In order to test their stability, HPMC pellets were exposed to small volumes of different solvents. It was discovered that the following solvents tend to either fracture or disintegrate the HPMC pellets: chloroform ($CHCl_3$), dichloromethane (CH_2Cl_2), acetonitrile (CH_3CN), and tetrahydrofuran (C_4H_8O). HPMC pellets were found to be stable when exposed to small quantities of solvents such as tert-butyl methyl ether ($(CH_3)_3COCH_3$, hexane ($CH_3(CH_2)_4CH_3$), and methyl ethyl ketone ($C_2H_5COCH_3$). On the other hand, these solvents may offer only limited solubility for some phosphors and heavy-atom enhancers. Additionally, highly volatile solvents tend to introduce difficulties associated with the preparation and storage of volumetric samples.

The filter paper chosen for this study was FisherBrand "P2". This particular paper was chosen for its fine porosity (particle retention: 1-3 μm). Although the paper is marketed by the Fisher Scientific Company, it's actually manufactured by Whatman, Inc. The corresponding Whatman filter paper is specified as Grade #5 (particle retention: ≈ 2.5 μm). The thickness of the P2 paper was determined experimentally with an outside micrometer to be 0.018 cm. Given a sheet diameter of 9.0 cm, it was possible to determine the bulk density of the material by weighing five individual sheets and then calculating the average weight of the set. The "volume" of a single sheet was calculated using $\pi r^2 h$. The bulk density of the P2 paper was determined to be 0.55 g/cm^3 by this method. Fisher Scientific has qualitatively described their P2 paper as having a "smooth, dense texture", excellent retention characteristics, and limited wet strength.[299] Whatman has reported that their filter paper consists of an α-cellulose cotton fiber content of at least 98%.[300] Surprisingly, it has been reported that filter paper will swell to an extent almost three times greater than α-cellulose fibers when water is the solvent of choice (swelling measured as percent increase in thickness).[301]

---

[298] R.C. Weast, Ed., **Handbook of Chemistry and Physics, f^{t} Student Edition**, Boca Raton, FL: CRC Press, Inc., 1988.

[299] **Fisher Catalog 98/99**, p. 577, Fisher Scientific U.S. Headquarters, 585 Alpha Dr., Pittsburgh, PA 15238. Internet: http://www.fishersci.com. Phone: (412) 490-8300.

[300] **Whatman Catalog**, Whatman Inc., Fairfield, NJ 07004. Phone: (201) 882-9277.

[301] G.I. Mantanis, R.A. Young, and R.M. Rowell, *Cellulose*, 1995, V. 2, p. 14.

For these studies, absolute ethanol (U.S.P.; 200 proof) was the solvent of choice. It has been reported that ethanol is sufficiently capable of penetrating and swelling a cellulose matrix. These characteristics are particularly desirable considering the nature of the solid supports investigated herein. Small volumes of ethanol did not fracture or disperse the HPMC pellets used for this research. Additionally, each of the aforementioned analytes was soluble in ethanol and the heavy-atom enhancer was also fully soluble.

Due to ethanol's moderate boiling point (78.5 °C), only mild heating was required for the solvent to be removed from the solid substrate following sample delivery. Thus, sample drying times were very short (< 3 minutes per sample). On the other hand, this particular solvent is not so volatile that solution storage and sample handling become problematic.

Nitrogen, oxygen, and compressed air were chosen as the purge gases for this project. Although it is now generally agreed by SSRTP researchers that a dry, oxygen-free atmosphere is preferred so that maximum phosphorescence intensities may be achieved, many conflicting results have been reported in the literature. During this project, fundamental experiments using dry nitrogen gas, dry oxygen gas, and dry compressed air were designed and carried out to in order to measure the effect of each on SSRTP analyses. Additionally, a study was undertaken to determine the effect of RTP quenching by ambient moisture. Since nitrogen gas is not known to quench RTP, it was chosen as a carrier gas to transport the H_2O vapor through the sample cell module.

5.2 The Perkin-Elmer LS-50 luminescence spectrometer

For this project, a spectrometer was required that would be capable of acquiring room temperature phosphorescence spectra for a series of model compounds immobilized on a variety of solid support materials. The Perkin-Elmer LS-50 luminescence spectrometer was utilized for these studies.[302] The LS-50 is a versatile and reliable instrument that allows for the measurement of fluorescence, phosphorescence, and chemi- or bio-luminescence.[303] The following luminescence data can be obtained with the LS-50:

1). excitation (absorption) spectra
2). emission spectra
3). synchronous (excitation vs. emission) spectra
4). and luminescence lifetimes.

The instrument is controlled by a PC-compatible computer using the RS-232 serial interface. Instrument parameters are selected by the operator within Perkin-Elmer's custom Fluorescence Data Manager software. Digital Research Inc.'s GEM desktop for DOS has allowed for the creation of user-friendly *virtual benchtop* that allows for icon-based instrument control and data manipulation in a windows-like environment. At the time of manufacture, this particular

[302] The Perkin-Elmer Co., Norwalk, CT (SN #32801).
[303] **The Model LS 50 Luminescence Spectrometer User's Manual**, Perkin-Elmer Ltd., Maxwell Road, Beaconsfield, Buckinghamshire, England, HP9 1QA, January 1989.

instrument (SN #32801) was certified as ISO-9001 compliant by the British Standards Institution.

5.2.1 Hardware Specifications

The excitation source utilized in the LS-50 is a xenon flash lamp rated at a power equivalent to 20 kW for 8 μs duration. The lamp is pulsed at line frequency (60 Hz) and has a pulse width at half height of less than 10 μs. A small festoon lamp close to the excitation source allows for an even triggering of the xenon flash tube. Figure 17 depicts the optical layout and beam path of the LS-50 instrument. Optical radiation from the source is focused by the ellipsoidal mirror M(E)5 and reflected by the toroidal mirror onto the entrance slit of the excitation monochromator. This primary monochromator consists of an entrance slit, a reflection grating ruled at 1440 lines per mm, a spherical mirror, and an exit slit. The angle of the excitation monochromator grating is fully automated using a PC controlled stepper motor. The excitation monochromator can be scanned through a wavelength range of 200 to 800 nm. The majority of the excitation beam is transmitted to the sample via a focusing toroidal mirror. In order to obtain a reference signal, a small portion of this beam is reflected by a beam-splitter onto a reference PMT. To correct for the response of the reference PMT, a rhodamine correction curve is stored within the instrument. Rhodamine dye absorbs energy from 230 nm to 630 nm and fluoresces at 650 nm with nearly constant quantum efficiency.

Light emitted by the sample is focused by a toroidal mirror onto the entrance slit of the emission monochromator. This secondary monochromator consists of an entrance slit, a spherical mirror, a reflection grating ruled at 1200 lines per mm, and an exit slit. The emission monochromator grating is also automated using a stepper motor and may be scanned over the wavelength range of 200-900 nm. However, the standard PMT is only sensitive to 650 nm. An optional red-sensitive PMT must be installed in order to fully utilize the 650-900 nm wavelength range.

The excitation and emission monochromators can be scanned independently, synchronously, or driven to selected points within their ranges as specified by the operator. The wavelength accuracy and reproducibility of the monochromators are reported to be± 1.0 nm and ± 0.5 nm, respectively. Monochromator scanning speeds within the range of 10 to 1500 nm/min must be specified by the user. Both the excitation monochromator and the emission monochromator can be driven to a zero-order position. When analyzing unknowns, this feature is useful for the acquisition of photoluminescence pre-scan information. First, the emission monochromator is driven to zero-order to allow all emission wavelengths to be detected. The excitation monochromator is scanned between user-defined limits and the wavelength of maximum intensity is stored by the computer. When the excitation scan is complete, the excitation monochromator is driven to the wavelength of maximum intensity and the emission monochromator is scanned between user-specified limits. On completion of the emission scan, the emission monochromator is driven to the wavelength of maximum intensity. A pre-scan dialogue box is then presented to the operator that reports the excitation and emission wavelengths at maximum intensity and the intensity value at those wavelengths.

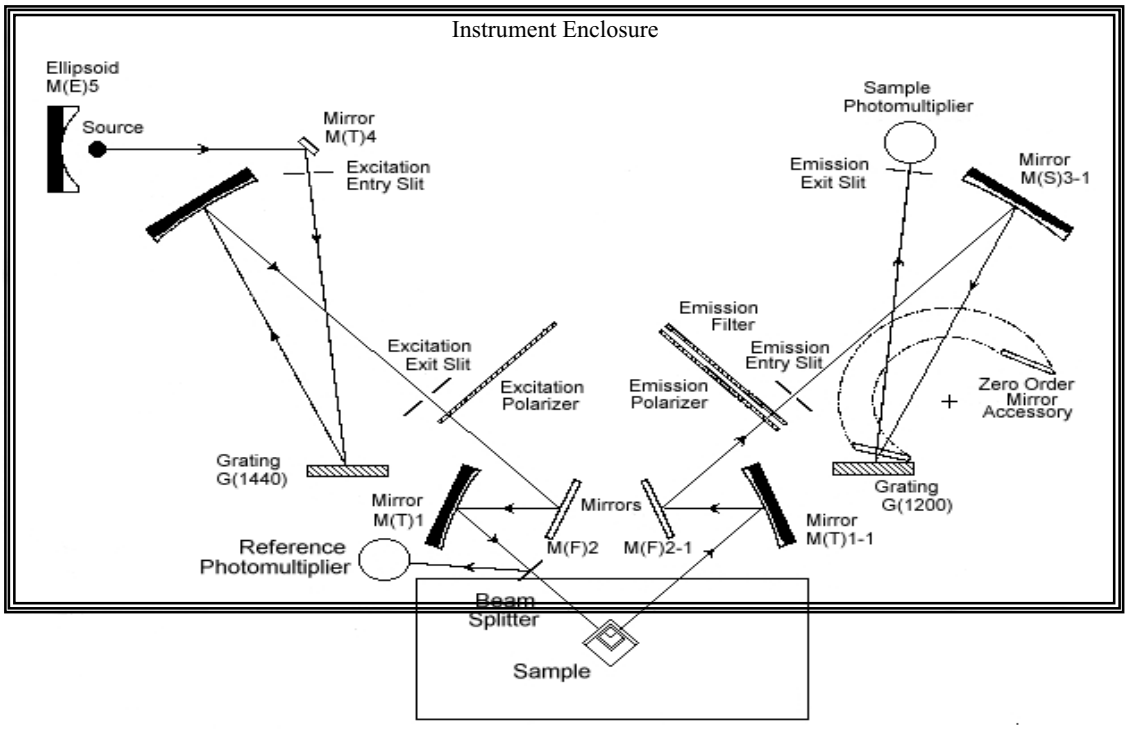

Figure 17. Optical Layout and Beam Path of the LS-50.
(figure adapted from The Perkin-Elmer Model LS-50 Luminescence Spectrometer User's Manual)

A synchronous scanning mode is also available to the user. In this mode, either a wavelength interval or frequency interval must be selected in order to define either the wavelength separation or energy separation between the two monochromators during scanning. Depending on the operating parameters selected, it is possible to obtain a series of spectra that may be utilized to prepare a 3-D *spectral fingerprint* representing the analyzed sample. This is a particularly useful mode of operation for the analysis of unknowns. Representative 3-D luminescence spectra may be found in dissertations recently completed by Ishihara and Asimopoulos.[304,305] Vo-Dinh has reported that synchronous luminescence spectroscopy is advantageous for multicomponent analyses; whereas, Winefordner and colleagues have discussed limitations associated with this application.[306,307,308]

The excitation and emission monochromator slits within the LS-50 are fully automated and may be adjusted in increments as small as 0.1 nm. The excitation slit widths are user-specified within the range of 2.5 to 15 nm. Similarly, the emission slit widths are user-specified and can be set within the range of 2.5 to 20 nm. A computer controlled emission filter wheel houses optical filters rated at 290 nm, 350 nm, 390 nm, 430 nm, and 530 nm. These cut-off filters may be used to minimize the undesirable second-order scatter effects that commonly appear within solid state fluorescence spectra. Also present are a blank (that serves as a shutter), a 1% attenuator, and a fully open slot that allows for a clear beam path. The PMT voltage may be selected either automatically or manually. If **AUTO** is chosen, the instrument selects the PMT voltage according to the current excitation slit width. If the operator wishes to manually set the PMT voltage, this parameter is software configurable within a range of 600 to 900 V (one volt increments minimum). For purposes of comparisons between RTP spectral acquisitions, it is particularly important for the operator to confirm that the t_d and t_g values, the slit widths, the scan speed, and the PMT voltage are consistent from one run to the next. The virtual benchtop allows optimized methods to be stored to disk by the operator for future use.

5.2.2 Signal Handling

Spectral data is acquired from the PMTs during each data collection cycle. The signals undergo integration, conversion, averaging, digital filtering, and ratioing in hardware prior to being received by the PC. Figures 18 and 19 are block diagrams that illustrate the signal handling and instrument control system associated with the LS-50. The PC is ultimately responsible for receiving and storing all luminescence data from the LS-50 in addition to providing full control over the instrumentation.

---

[304] F. Ishihara, **The use of Hadamard Transform as a Data Compression Technique in the Development of a 3-Dimensional Fluorescence Spectral Library for Qualitative Analysis** Dissertation, Virginia Polytechnic Institute and State University, Blacksburg, VA 24061, 1989.

[305] G. Asimopoulos, **Hartley Transform Based Algorithm for the Qualitative and Quantitative Analysis of Multi-component Mixtures with the use of Emission Excitation Matrices** Dissertation, Virginia Polytechnic Institute and State University, Blacksburg, VA 24061, 1992.

[306] T. Vo-Dinh, *Anal. Chem.*, 1978, V. 50, p. 396.

[307] T. Vo-Dinh and R.B. Gammage, *Anal. Chem.*, 1978, V. 50, p. 2054.

[308] H.W. Latz, A.H. Ullman, and J.D. Winefordner, *Anal. Chem.*, 1978, V. 50, p. 2148.

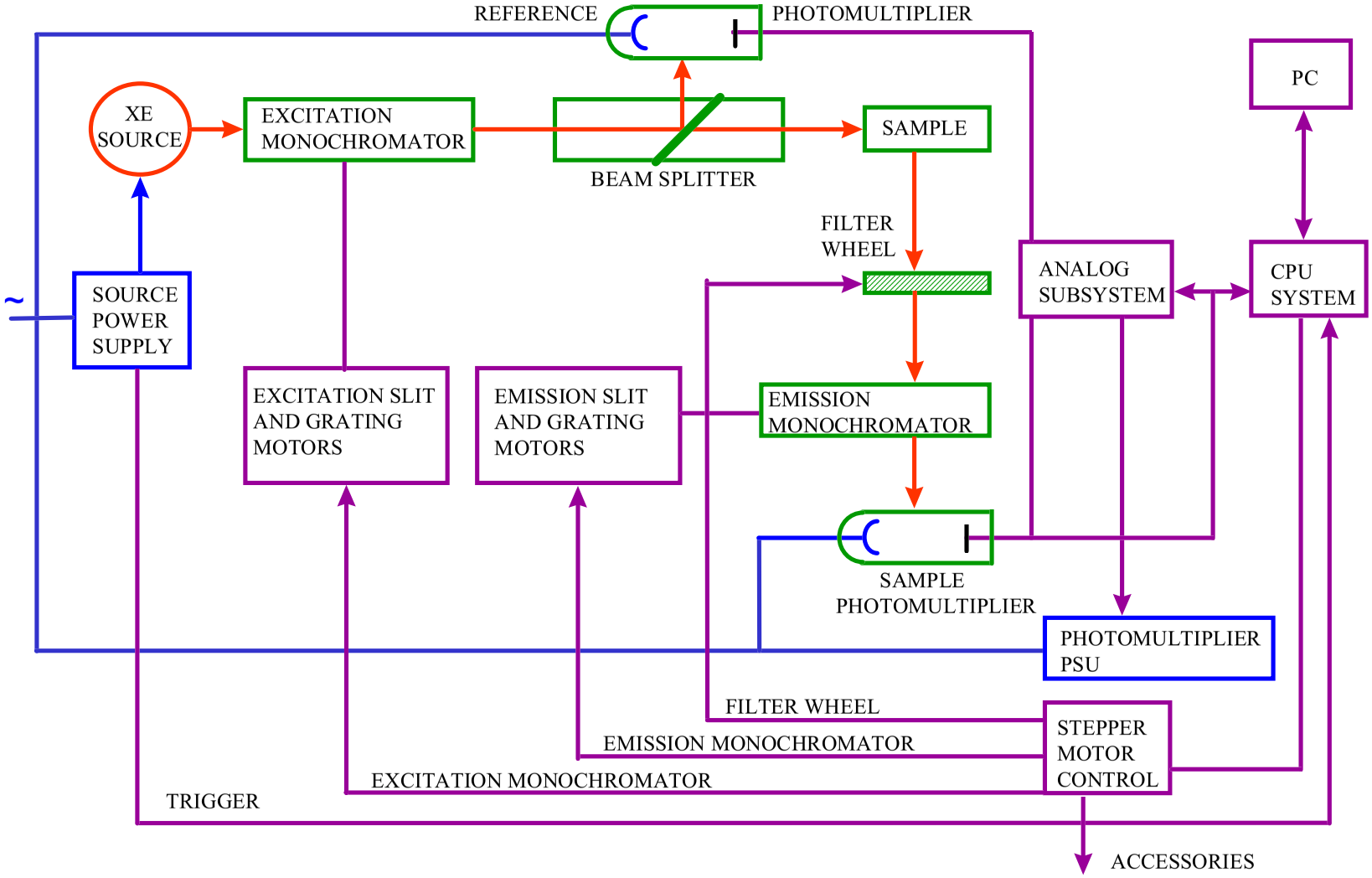

Figure 18. Block diagram of the LS-50 instrument control system.

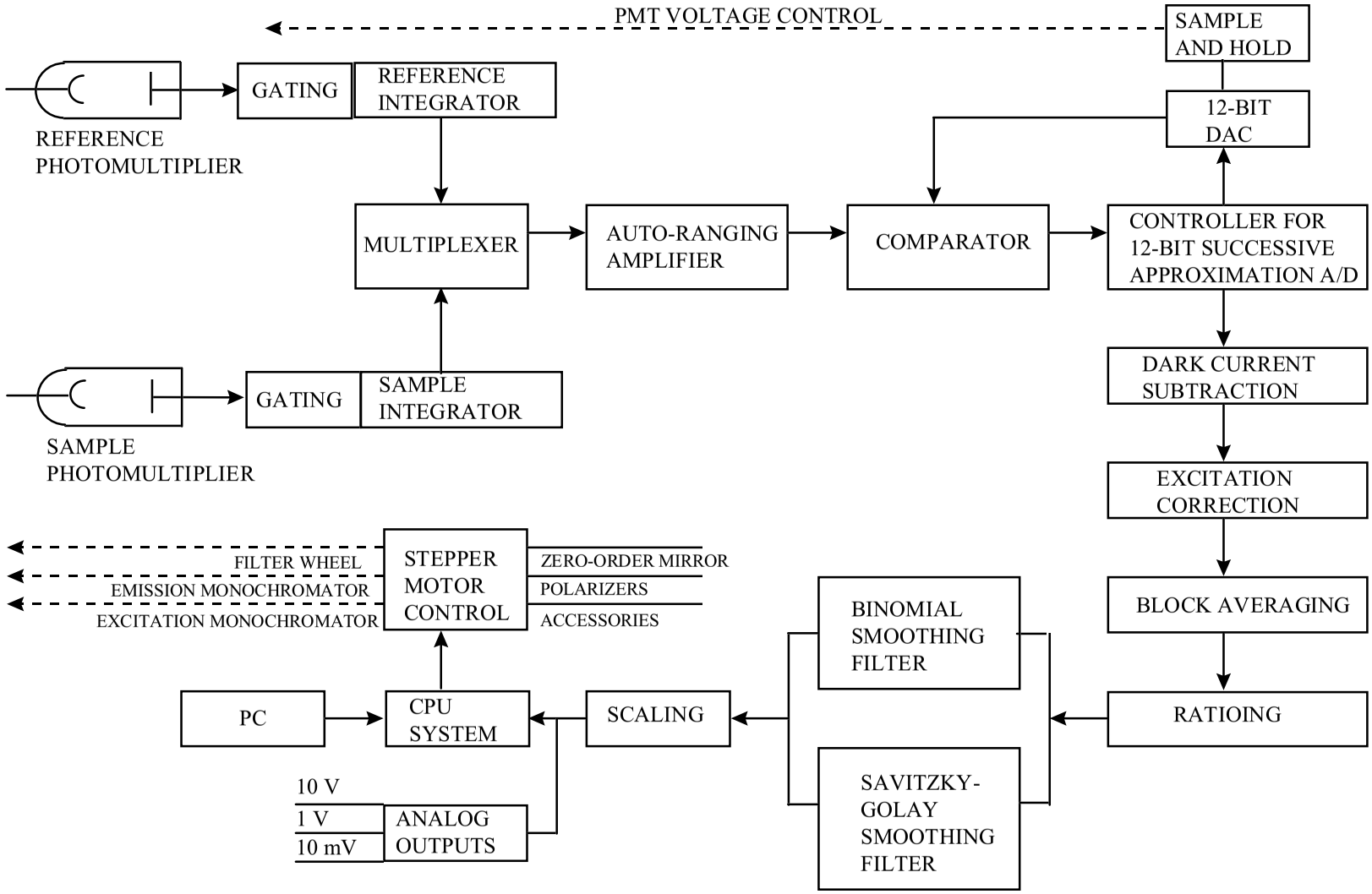

Figure 19. Perkin-Elmer LS-50 signal handling system.

When the instrument is operated in the fluorescence mode, four integrations are performed for every data collection cycle. Two integrations are taken from the emission channel and two from the excitation channel. The integrations are performed at fixed times with respect to the last flash of the xenon lamp. An integration of 80 µs is taken for both the excitation and emission primary signals. The effect of PMT dark current is eliminated by gating open both channels a second time just prior to the next flash and then integrating the acquired signal. These dark current signals are then subtracted from the main fluorescence signals to give a corrected signal.

When the instrument is operating in the phosphorescence mode, the emission integration time is not fixed. The integration can be started between 0 and 9490 ms after the start of the flash. This delay time (t_d) may be varied by the user within the Fluorescence Data Manager software. The time period over which the integration is performed is called the gate time (t_g). The gate time can be varied from 0.01 ms to 500 ms. If the sum of the delay and gate times exceeds 13 ms then the cycle time must be increased in order to allow a longer data collection period. On initiating a phosphorescence measurement, the dark current is measured and the resulting value is stored so that it may be subtracted from all sample signals.

Following integration, the photomultiplier signals are multiplexed, fed into an auto-ranging amplifier, and then into a 12-bit successive approximation A/D converter. The dark current is digitally subtracted from the reference signal and the sample signal to give a true zero. The signal is automatically block averaged depending upon the scan speed selected and the data interval. Table 12 lists representative block average widths assuming a default data interval of 0.5 nm.

Table 12. Block average width relative to monochromator scan speeds

scan speed (nm/min)	block average width (60 Hz)
30	60
120	15
480	3
1500	1

(table adapted from The Perkin-Elmer Model LS 50 Luminescence Spectrometer User's Manual)

After the sample and reference channels have been block averaged, they're ratioed to improve the signal to noise and to remove source-related artifacts. The ratioed output is then scaled to the wavelength range scanned to give the corrected result. The results are multiplied by the rhodamine correction curve stored in the instrument in order to correct for the spectral response of the PMTs and the transmission response of the beam splitter. The ratioed, corrected signal is then smoothed using either a binomial or a Savitzky-Golay filter. The width of the filter is determined by the resolution selected (via the slit width setting) and the data interval.

At power on, the instrument always automatically initializes with binomial filtering selected. However, the smoothing filters can be manually selected by the user from within a

mode menu available on the virtual benchtop. The binomial smoothing filter is a quadratic function of slit width and obeys the following equation:

$$S = AR^2 + BR + C$$

where S is the smoothing factor, R is the slit width, A = 0.04571, B = 0.2285, and C = 4.143. The value obtained from this equation is rounded to the nearest odd integer.

The Savitzky-Golay smoothing filter is a linear function of slit width and obeys the following equation:

$$S = MR + C$$

where S is the smoothing factor, R is the slit width, M = 1.257, and C = 3.857. Savitzky and Golay have prepared a classic paper that discusses this weighted digital filtering technique.[309] It should be noted that this original paper contains typographical errors concerning several of the convolution and normalization integers. A subsequent paper has discussed the method of determining these array errors.[310] The Savitzky-Golay smoothing algorithm assumes that data points occur at fixed uniform intervals along a chosen abscissa and that the data points describe a continuous function. The S/N is approximately proportional to the square root of the number of points used in the smooth.[311] The type of filtering to select depends on the particular aspects of the spectrum being acquired. Table 13 summarizes the advantages and disadvantages of these two filtering algorithms.

Table 13. Binomial vs. Savitzky-Golay filtering

digital filtering technique:	advantages	disadvantages
Binomial	Good noise reduction with minimum peak distortion.	Peaks may be flattened.
Savitzky-Golay	Good noise reduction with sharp peaks.	Peak edges may be distorted if there are rapid intensity changes.

(table adapted from The Perkin-Elmer Model LS 50 Luminescence Spectrometer User's Manual)

After spectra are acquired by the LS-50, they are stored in memory using a Perkin-Elmer binary data format. Until deleted, the data files will be represented as icons on the virtual benchtop. All spectral data files are given the extension **.SP** and all luminescence decay data files are given the file extension **.TD**. These files may be saved directly to hard disk or floppy disk for future use. Additionally, the data files may be converted and exported to either JCAMP format[312]

[309] A. Savitzky and M.J.E. Golay, *Anal. Chem.*, 1964, V. 36, p. 1627.
[310] H.H. Madden, *Anal. Chem.*, 1978, V. 50, p. 1383.
[311] J.N. Demas and S.E. Demas, **Interfacing and Scientific Computing on Personal Computers**, Boston: Allyn and Bacon, 1990.
[312] R.S. McDonald and P.A. Wilks, Jr., *Appl. Spectr.*, 1988, V. 42, p. 151.

or Lotus™ spreadsheet format (.wk1) prior to storage. This allows for greater flexibility in post-processing and analysis of the data.[313,314,315,316] During this project, all data files were converted to ASCII spreadsheet format prior to archiving so that they could be easily accessed at a later time using software such as Quattro Pro™ and Microsoft Excel™.[317,318]

5.2.3 The Sample Cell Module

The LS-50 sample compartment itself is found at the front and center of the instrument. The compartment cover is hinged on the underside and may be opened by using a finger grip found at the top of the compartment. The sample compartment was designed to accommodate a wide variety of accessories that are commercially available from the Perkin-Elmer Corporation.[319] The standard sample cell module packaged with the LS-50 instrument is a single-position cell holder (P-E Part No. L225 0140). This removable accessory accepts 12.5 mm square (10 mm path length) quartz cuvettes and is particularly useful for the analysis of liquid samples. The removal of this device is facilitated by the release of two spring-loaded quick-release fasteners. The module must be lifted vertically in order to free it from alignment pins. All that remains is a rugged, metal foundation that extends horizontally from the front of the instrument. This foundation serves as a platform upon which interchangeable accessories may be mounted.

A front-surface accessory is available from the Perkin-Elmer Corporation (P-E Part No. 5212 3130). This sample holder is designed for the analysis of samples existing in three forms: thin sheets, powdered samples, and liquid samples. This device is particularly useful for the measurement of solid-state room temperature fluorescence (SSRTF). However, the accessory does not offer the operator the ability to purge the sample environment with a dry gas. Phosphorescence quenching by moisture and/or oxygen will severely reduce the potential signal intensity. For analytes that exhibit very weak phosphorescence, it may not be possible to detect any signal at all if the sample remains exposed to the ambient surroundings. As a result of this design flaw, the Perkin-Elmer front surface sample holder is unsuitable for use in SSRTP investigations in its standard configuration.

In order to carry out this research project, it was necessary to design and manufacture a custom sample cell module in-house. The single most important feature associated with the design of the module was the incorporation of a dry gas purge system so that the sample and surrounding environment would be protected from moisture and oxygen. It was required that the accessory be designed so that it could be easily installed and removed from the instrument on a

---

[313] W.J. Orvis, **1-2-3 for Scientists and Engineers**, San Francisco: Sybex, 1991.
[314] L.M. Mezei, **Laboratory Lotus**, Englewood Cliffs, N.J.: Prentice Hall, 1989.
[315] G.I. Ouchi, **Lotus in the Lab**, Redwood City, Calif.: Addison-Wesley, 1988
[316] L.M. Mezei, **Practical Laboratory Information Management for Scientists and Engineers**, Englewood Cliffs, N.J.: Prentice Hall, 1992.
[317] D.M. Etter, **Quattro Pro: A Software Tool for Engineers and Scientists**, Redwood City, Calif.: Benjamin/Cummings Pub. Co., 1993.
[318] R.G. Parks, **Quattro Pro for Scientific and Engineering Spreadsheets**, New York: Springer-Verlag, 1992.
[319] P-E Express, The Perkin-Elmer Corporation, 761 Main Ave., Norwalk, CT 06859-0156; 1-800-762-4002.

regular basis. It was necessary to build a rugged device that would consistently provide for reproducible placement of the samples to be analyzed. The optimum sample cell module required for this project had to allow for the mounting of samples immobilized on thin sheet-like materials and supports in the form of pellets as well. No permanent modifications to the LS-50 instrument itself were allowable.

The design plans for the framework of the sample cell module were based on the layout of the sample cell accessory originally packaged with the LS-50 instrument. Figure 20 illustrates the layout and dimensions of this platform. Following the construction of this framework, it was then necessary to design and construct the sample enclosure itself. Square tubular aluminum stock was chosen for the four walls of the chamber and windows were machined into two adjoining surfaces of this material. Figure 21 shows the dimensions and placement of the windows within the resulting component. Two fused silica (*Suprasil*) plates were selected as the excitation and emission windows.[320] The two windows measure one inch square and are 0.0625 inches thick. The transmission characteristics of the Suprasil windows were measured using a Perkin-Elmer λ3 UV-VIS spectrophotometer and the resulting spectra are illustrated in figure 22. In order to provide an airtight seal, the Suprasil windows were mounted inside the square tubular aluminum enclosure using black RTV (**R**oom **T**emperature **V**ulcanization) silicone rubber.[321]

The next portion of the design process involved selecting a suitable base plate and a removable top for the enclosure. A 0.20-inch thick piece of aluminum stock was selected as the starting material for the bottom plate. This piece was milled down to 2.50 inches square so that it would serve as a base plate for the enclosure. It was then affixed to the walls of the enclosure by utilizing four short sections of 0.0625-inch thick aluminum angle stock (90º) and sixteen small machine screws. The outer walls of the enclosure and the base plate were drilled and tapped to accept the machine screws. Prior to attaching the enclosure to the base plate, a small quantity of black RTV silicone rubber was placed around the bottom edge of the enclosure in order to insure an airtight seal between the two components. The enclosure was then mounted onto the custom built framework using two small machine screws.

The top of the enclosure was more difficult to design. It was necessary to manufacture this portion of the enclosure so that it could be easily removed and replaced during a series of consecutive SSRTP analyses. Additionally, an airtight seal was essential in order to minimize the entry of oxygen and moisture into the sample chamber. A 2.50-inch square top plate was machined from 0.10-inch thick aluminum stock. A 0.125-inch thick layer of soft rubber gasket material was then affixed to one side of this plate using RTV silicone rubber. Similar to the attachment of the base plate, the upper outer walls of the enclosure were drilled and tapped in order to accommodate four short sections of 0.0625-inch thick aluminum angle stock (90º). These four pieces were attached to the enclosure via eight small machine screws. Four studs were set vertically in the aluminum angle stock in order to serve as mounting points for the top plate. In order to facilitate the ease of removal and replacement of the top plate, four wing nuts were fitted to the studs. This design allows the operator to adjust the wing nuts to a sufficient tightness

---

[320] Amersil Inc., Hillside, NJ 07205

[321] General Electric Company, Silicone Products Division, RTV Products Department, Waterford, New York, 12188

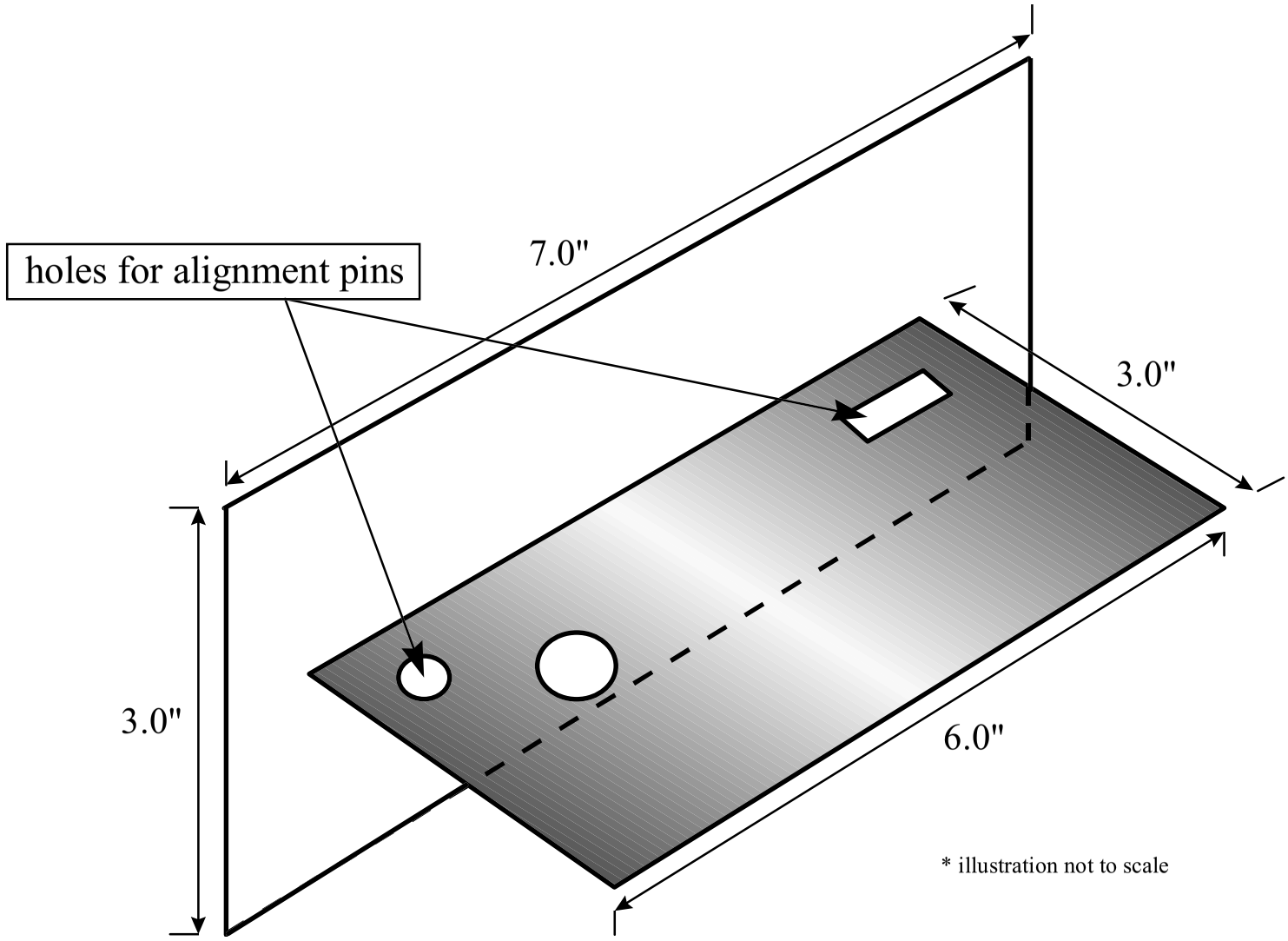

Figure 20. LS-50 sample holder platform

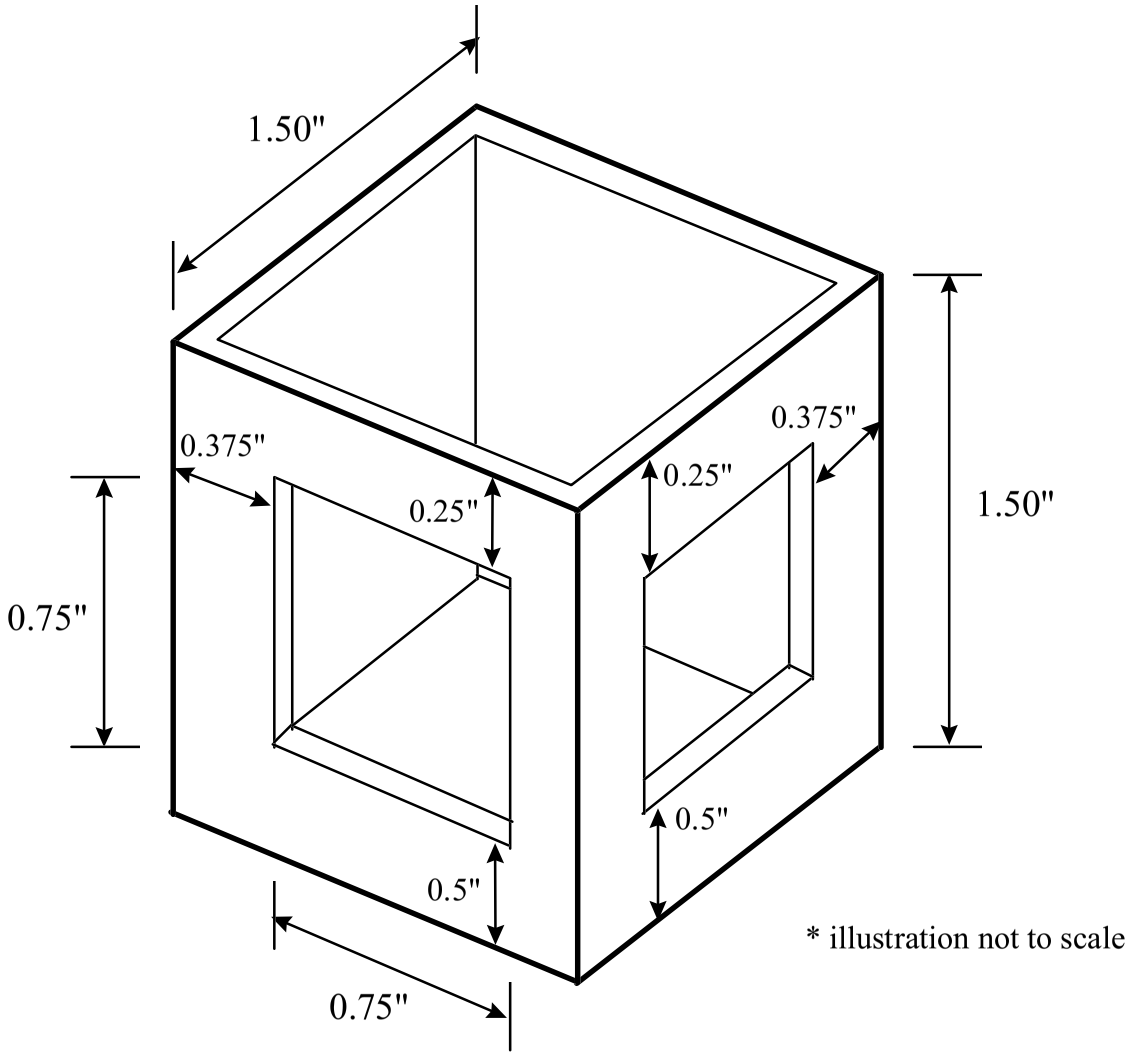

Figure 21. Enclosure dimensions and window locations

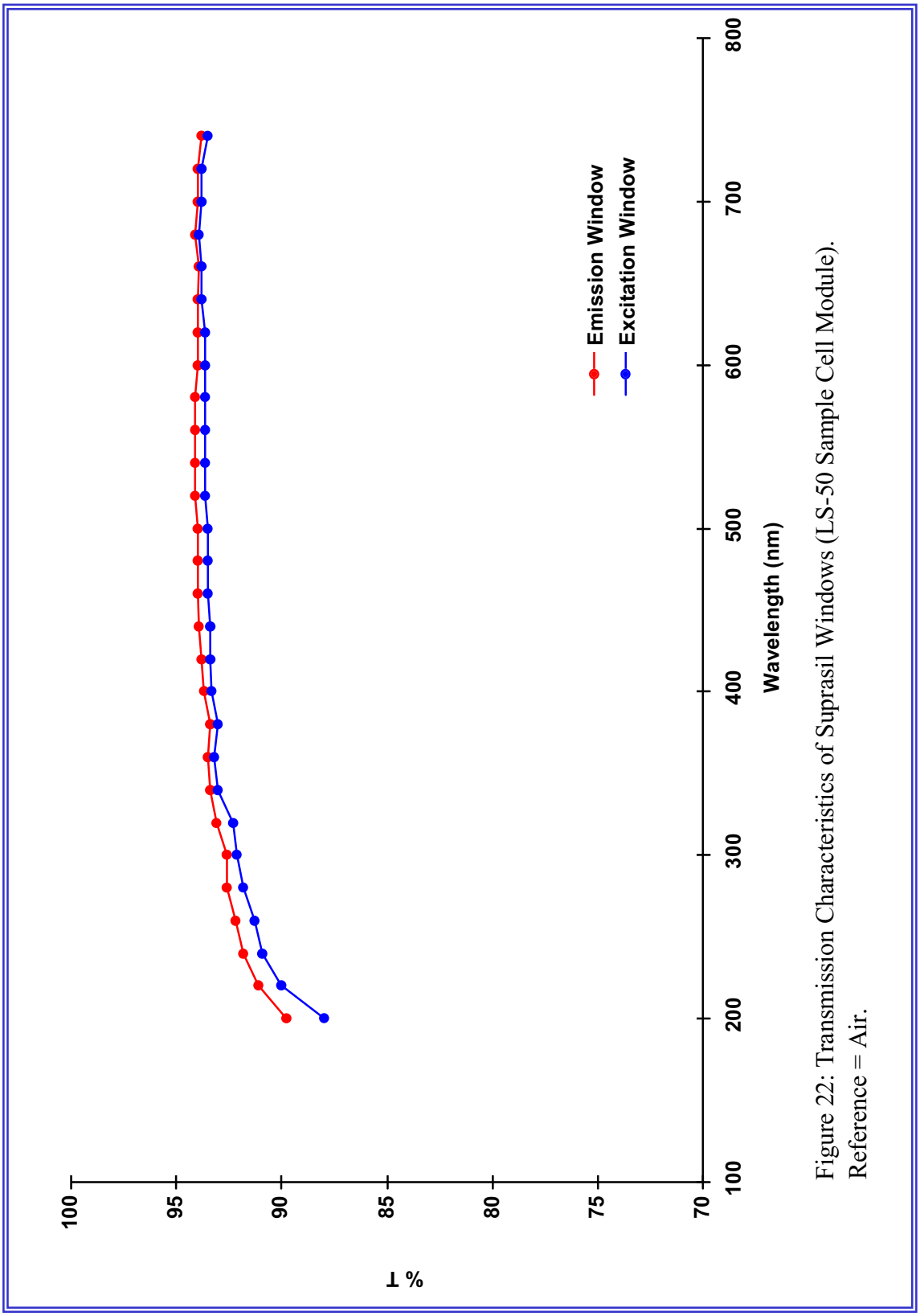

Figure 22: Transmission Characteristics of Suprasil Windows (LS-50 Sample Cell Module).
Reference = Air.

to compress the rubber gasket material. The compression of the top seal is sufficient to allow for the exclusion of ambient oxygen and moisture under purge conditions.

5.2.4 Dry Gas Purge System

Having completed the sample enclosure, the next step was to design and install a suitable dry gas purge system. A hole was drilled and tapped into the base plate of the enclosure that would accept a standard 90° brass Swagelok™ fitting.[322] A 0.25-inch diameter hole was drilled through the vertical portion of the mounting framework in order to allow a six foot length of 0.25-inch O.D. plastic tubing to pass through and mate with the 90° fitting found beneath the sample enclosure. A standard Swagelok™ connector was used at this junction. At the free end of the plastic tubing, a Swagelok™ 0.25-inch stem quick-connect was attached. This quick-connect feature insures the portability of the sample cell module.

In order to allow for the dry gas to flow through the sample cell module, a small NUPRO™ purge valve was added to the system.[322] The valve was adjustable so that the gas flow through the sample enclosure could be easily regulated. The valve's entrance and exit ports were manufactured to accommodate 0.0625-inch O.D. tubing. Using standard stainless steel Swagelok™ fittings, a short section of 0.0625-inch flexible tubing was inserted between the purge valve and the body of the sample enclosure. In order to attach the tubing to the sample chamber, a male Swagelok™ fitting was mounted on one of the rear-facing walls of the enclosure. The interior face and threads of this fitting were sealed to the interior wall of the enclosure using black RTV silicone rubber. Finally, the purge valve was installed *beneath* the sample enclosure with the adjustment control protruding through the vertical wall of the accessory platform. By carefully selecting the position of the valve's regulator (and the aforementioned plastic tubing that passes through the vertical plate), there remained just enough clearance to allow the sample compartment cover at the front of the LS-50 to swing down and open. This allows for a quick and easy substitution of samples by the operator during a series of multiple analyses.

[322] Dibert Valve and Fitting Company, Inc., Roanoke, Va., 1-540-366-0555.

5.2.5 Sample Holder

Due to the limited workspace available within the LS-50 sample compartment and the strict design requirements set forth, the manufacture of the sample enclosure was a non-trivial task. However, the design of a suitable sample holder still remained. It was necessary to construct the sample holder in a manner that would allow it to be placed reproducibly within the sample enclosure. It would offer the capability of mounting both sheet-like support materials (such as filter paper) and solid supports in the form of pellets (such as HPMC). In order to facilitate the exchange of support materials, the holder must be easily removable from the sample enclosure. Additionally, the SSRTP support materials would need to be positioned so that they were in exact alignment with the excitation beam entering the sample compartment.

Figure 23 illustrates the resulting sample holder that was designed and manufactured for these purposes. The holder was machined from 0.375-inch thick aluminum stock. The front surface of the holder is 1.75 inches wide. The rear face of the holder is one inch wide. The sides are beveled at 45°. For this work, 0.5-inch diameter filter paper discs and 13mm diameter HPMC pellets were used as the solid substrates. These substrates were readily accommodated by using an end-mill to create a 13 mm-wide circular depression in the front surface of the sample holder. All original design criteria were sufficiently met during construction of the sample cell module. Figure 24 is a photograph of the sample cell module.

The commercially available Perkin-Elmer front surface accessory lists at $2,120.00.[323] The sample cell module constructed for this project could be duplicated by SSRTP researchers at a materials cost of approximately $282.00. In addition to its use as a research tool, the simplicity of design and overall durability of this sample cell module should make it particularly attractive to educators. It would allow for the RTP technique to be readily introduced to those undergraduate teaching laboratories that have access to the Perkin-Elmer LS-50 (or comparable) luminescence spectrometer. Table 14 lists the raw materials used for this design and their representative costs if purchased separately.

[323] Perkin Elmer, **Supplies and Accessories for UV/Visible and Fluorescence Spectrometry**, 1994/1995 catalog. The Perkin-Elmer Corporation, 761 Main Avenue, Norwalk, CT 06859-0156, Order No. PEX-UV2.

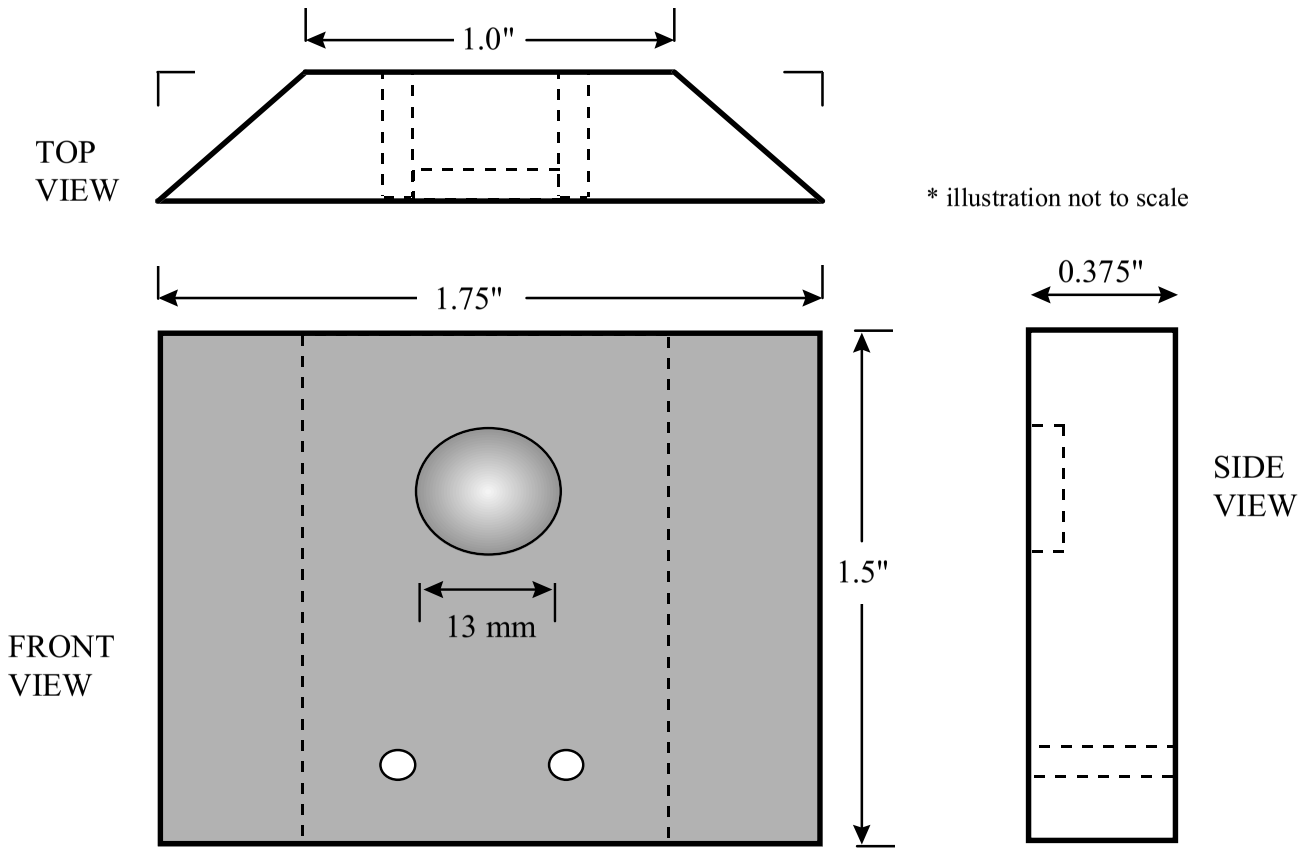

Figure 23. Sample holder layout and dimensions.

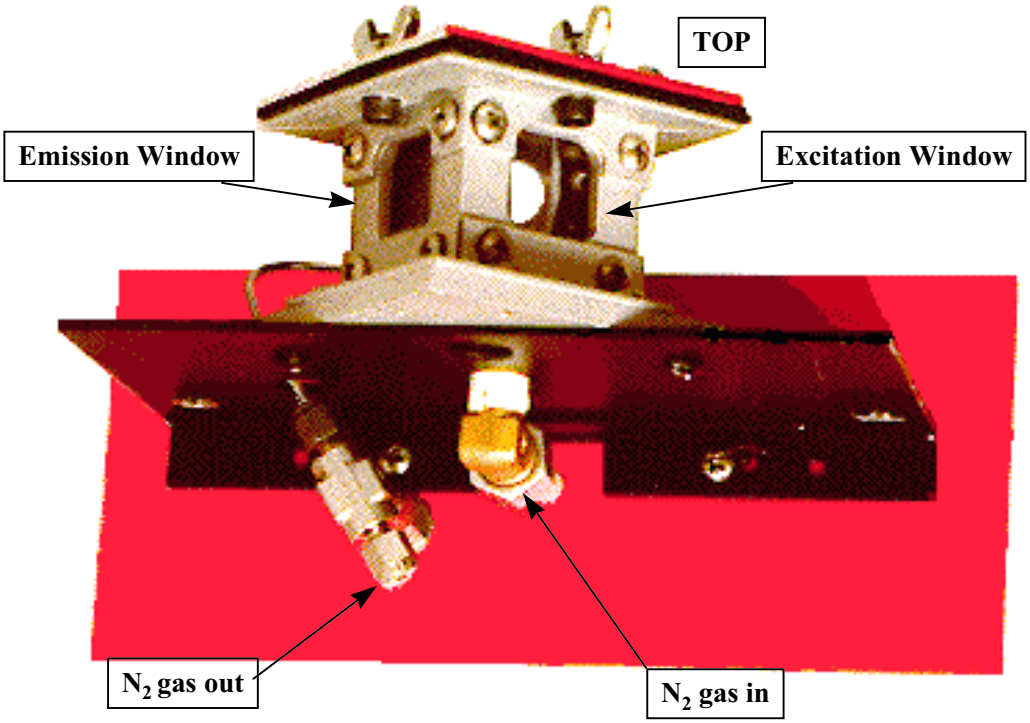

Figure 24. Photograph of the custom-built LS-50 SSRTP sample cell module

Table 14. Sample Cell Module Raw Materials and Estimated Costs

Material:	**Estimated Cost:**
two fused silica windows (one inch square)	≈ $100
Swagelok™ fittings and regulator valve	≈ $100
aluminum stock materials	≈ $50
flexible tubing	≈ $10
thirty-five machine screws	≈ $4
black RTV silicone rubber	≈ $4
teflon tape	≈ $4
rubber gasket material	≈ $6
flat-black spray paint	≈ $4
	TOTAL: ≈ $282

During the final stages of the project, an LS-50 front surface accessory was loaned by Dr. Pam Perrone of Perkin-Elmer. The device was not suitable for RTP studies in its standard configuration. However, following careful examination, it was determined that the accessory could be modified to incorporate a necessary dry gas purge system. The process was initiated by removing the sample mounting bracket and powder holder assembly. Measurements were taken from the original accessories and then detailed plans were drafted prior to the manufacture of modified components. The basic structure of the sample mounting bracket was retained; however, a solid top was added to the improved version. All open seams and joints were sealed with RTV sealant. Plastic tubing connectors were fitted to the housing using epoxy. One connector served as the purge gas inlet and the other as an outlet port. The excitation and emission windows were covered with two fused silica (*Suprasil*) plates[320] using RTV sealant. The transmission characteristics of these excitation and emission windows are shown in Figure 25. A photograph of the modified P-E front surface accessory is found in Figure 26.

The standard P-E powder holder assembly served as a model while preparing a sample holder for the HPMC pellets and filter paper discs. The original powder holder is a two-piece unit with a circular Suprasil window covering the front surface. A powder is introduced to the front portion of the assembly by the user and the two pieces are then fitted together. In this manner, it is possible to trap a thin layer of powdered or crystalline material behind the window. Since the HPMC pellets and filter paper discs used for this project are solid disc-like supports, the Suprasil window could be disregarded. Plans for a similar unit capable of accepting 13 mm diameter discs were designed on paper and submitted to the Physics Department machine shop. Mr. Fred Blair provided the subsequent expertise and craftsmanship necessary to construct this particular assembly.

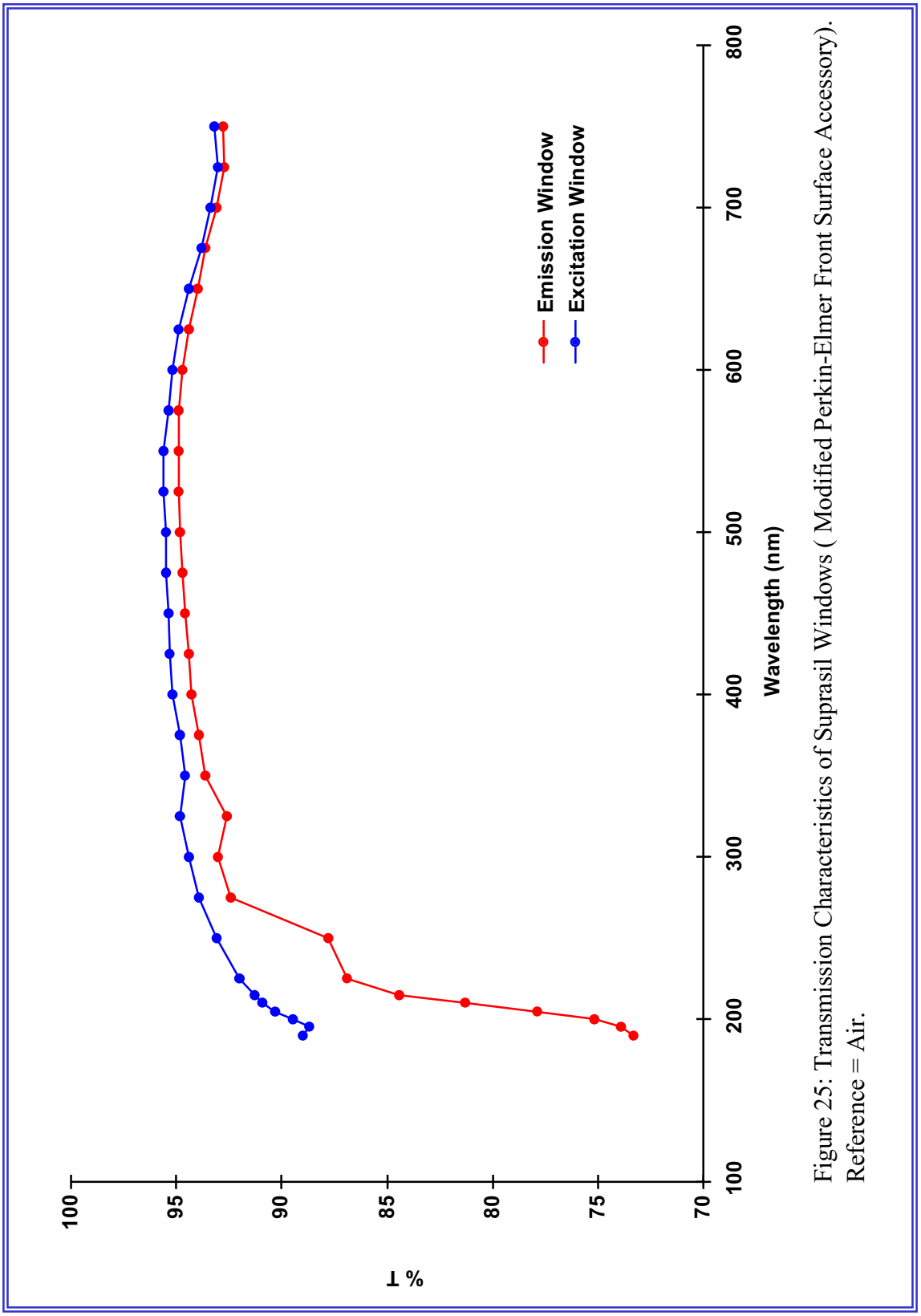

Figure 25: Transmission Characteristics of Suprasil Windows (Modified Perkin-Elmer Front Surface Accessory). Reference = Air.

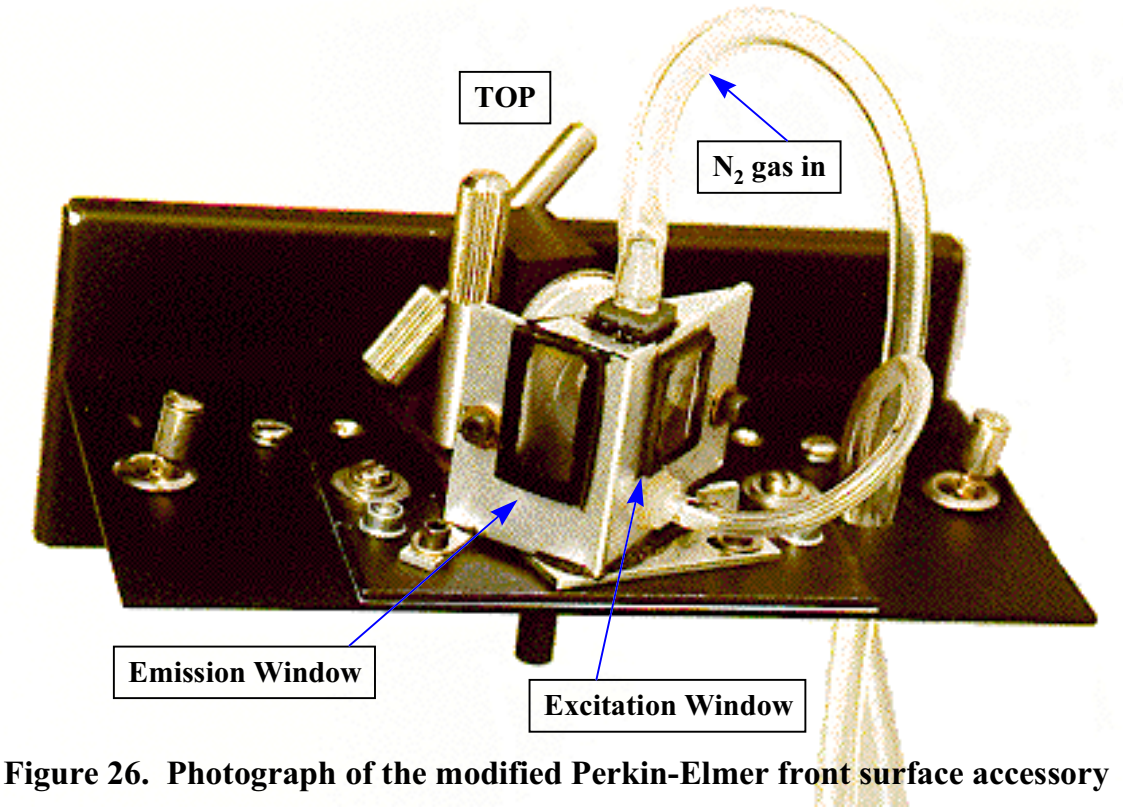

Figure 26. Photograph of the modified Perkin-Elmer front surface accessory

5.3 Sample Drying Equipment

Figure 27 illustrates the layout of the dry nitrogen gas purge system utilized. Bottled nitrogen gas is initially metered by a pressure regulator at the cylinder. It then passes through a column of Drierite™ desiccant[324] and finally into the sample enclosure itself. The regulator valve found at the sample cell module ultimately controls the flow rate of the nitrogen gas through the system. After passing through the sample chamber, the purge gas is vented to the ambient atmosphere surrounding the sample cell module. The purge gas flow rate was measured with a soap bubble flow-meter and maintained within 200 to 250 mL/min during the project.

Solid support materials were pre-dried in a manner described earlier by Schulman and Walling,[38] Winefordner, et al.,[325] Niday and Seybold,[41] Malmstadt, et al.,[287] and Vo-Dinh and colleagues.[326] A 110 volt, red-filtered, infrared heatlamp was utilized (G-E Order Code 250R40/10).[327] The drying temperature is regulated simply by adjusting the distance between the sample and the lamp. Vo-Dinh has reported that "Many investigators have used the drying method with heating lamps because it is rapid, convenient, and generally nondestructive.".[12]

5.4 Procedures

5.4.1 Preparation of Solid Substrates

A laboratory pellet press (13 mm die) was used to prepare the HPMC pellets required for this study.[328] The die was rated at a maximum load of 10 tons and was used in conjunction with a Carver hydraulic lab press.[329] Prior to pressing, a small quantity of HPMC was massed on an analytical balance.[330] The starting material for each individual pellet consisted of 0.0650 to 0.0700 grams of HPMC. The compression force utilized in the manufacture of each pellet was 17K PSI. Following removal from the pellet press die, a Vernier caliper was used to determine the thickness of each pellet. Based on this range of masses and force of compression, the thickness of each pellet ranged from 0.048 cm to 0.056 cm. Those pellets not of uniform thickness were discarded if the variation was found to be larger than ±0.005 cm. Each pellet was coded on one side using a pencil. This allowed the pellets to be individually catalogued according to their weight, thickness, and date of manufacture. This procedure was carefully followed for each individual pellet. The manufacture of a single pellet via this method requires an approximate preparation time of two to three minutes.

---

[324] Drierite™ consists of 97% anhydrous $CaSO_4$ & 3% $CoCl_2$. It is manufactured by the W.A. Hammond Drierite Company, Xenia, Ohio. 1-513-376-2927. Stock #23001. Size: 8 mesh.

[325] T. Vo-Dinh, E. Lue Yen, and J.D. Winefordner, *Talanta*, 1977, V. 24, p. 146.

[326] T. Vo-Dinh, G.W. Suter, A.J. Kallir, and U.P. Wild, *J. Phys. Chem.*, 1985, V. 89, p. 3026.

[327] General Electric Company, Nela Park, Cleveland, Ohio, 44112.

[328] Part #3000. Graseby-Specac Ltd., 301 Commerce Dr., Fairfield, CT 06430. 1-800-447-2558.

[329] Model C. Fred S. Carver, Inc., A subsidiary of Sterling, Inc., W142 N9050, Fountain Blvd., Menomonee Falls, WI 53051.

[330] Model #A-200DS; S.N. 0059775, Denver Instrument Company, 6542 Fig St., Arvada, CO 8004-1042. 1-800-321-1135.

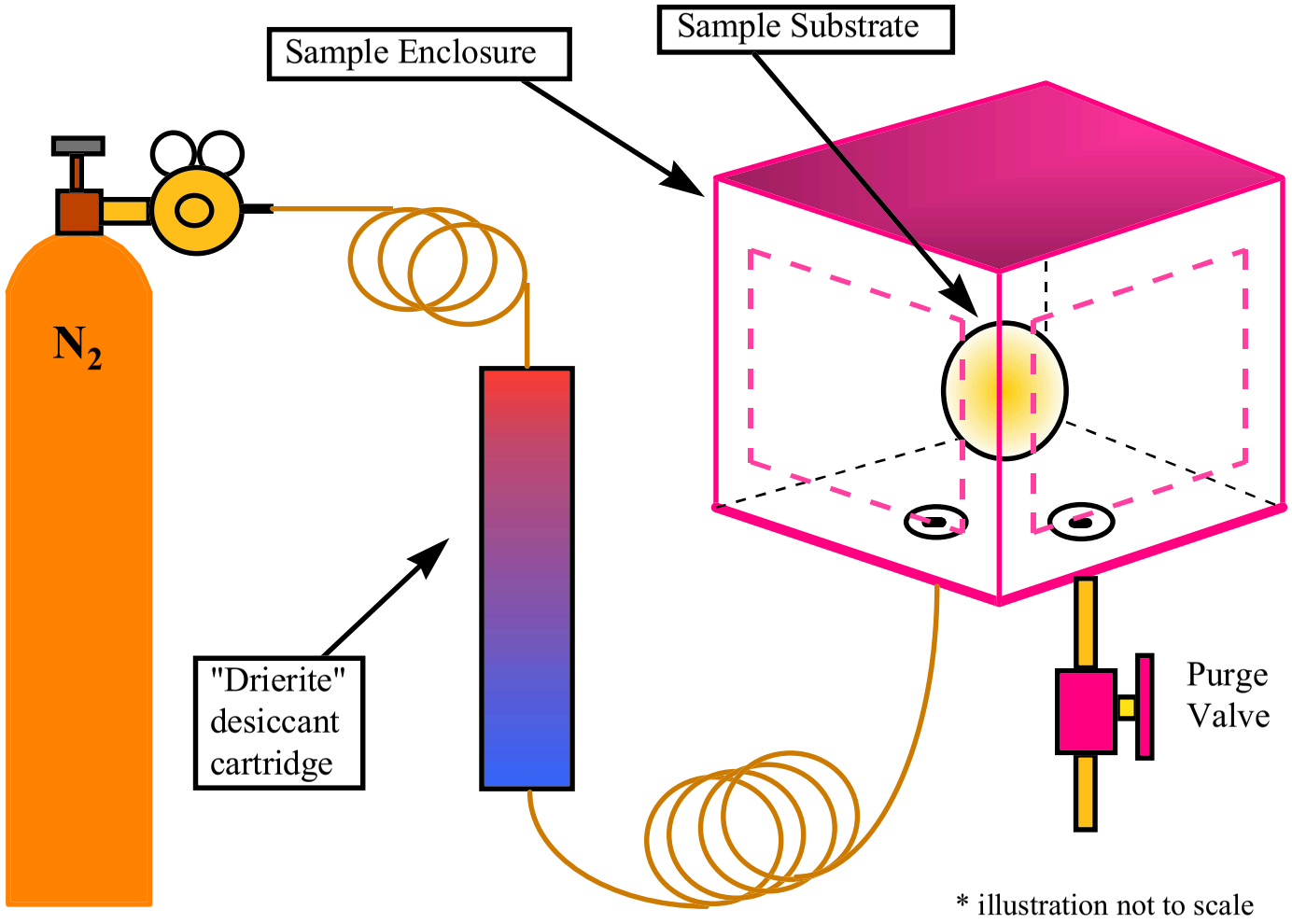

Figure 27. Dry Gas Purge System

Half-inch diameter filter paper discs were prepared using a 0.5-inch diameter cylindrical punch and the hydraulic laboratory press. Other laboratories have reported the use of paper hole-punching devices to prepare small diameter filter paper discs for use in conjunction with RTP studies.[12,331,332] In order to provide for a direct comparison of the support materials, multiple layers of filter paper were compressed in order to approximate the thickness and processing conditions of the HPMC pellets. Essentially, *filter paper pellets* were formed. By using 8 layers of filter paper and 17K PSI of compression force, the resulting pellets ranged from a thickness of 0.053 cm to 0.058 cm. Each filter paper pellet was coded on one side using a pencil. This allowed the pellets to be individually catalogued according to their thickness and date of manufacture.

Figure 28 provides a microscopic comparison (200X) of the surface features of a *K4M PREM* HPMC pellet and a P2 FisherBrand™ filter paper pellet. The samples were analyzed in the Chemistry Department Surface Analysis Laboratory at Virginia Tech on an I.S.I. SX40 scanning electron microscope by Mr. Frank Cromer.

[331] C.R. Englund, *J. Chem. Educ.*, 1992, p. A314.
[332] R.D. Huisman, *J. Chem. Educ.*, 1994, V. 71, p. A147.

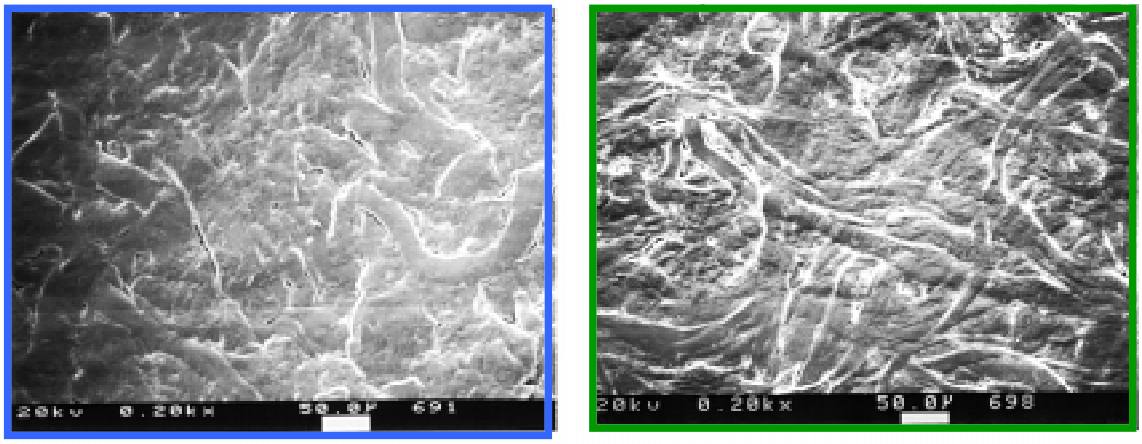

K4M PREM HPMC Pellet Filter Paper Pellet (FisherBrand P2)

Figure 28. A microscopic comparison of the surface features of a *K4M PREM* HPMC pellet and a filter paper pellet. (S.E.M. 200X)

5.4.2 Sample Delivery

In accordance with the techniques customarily practiced by other RTP researchers, the heavy-atom salt and phosphor solutions were spotted onto the surfaces of the solid substrates using 10 μL laboratory syringes.[333,334] Mastery of the sample spotting procedure is perhaps one of the most difficult steps in an RTP analysis. Slight variations in spotting technique can significantly affect the ultimate reproducibility and accuracy of the analytical results. For instance, creep-back and capillation effects are sometimes a problem when very small volumes of solution are delivered slowly to the support material.[335] A 1 μL drop can actually "climb" the syringe needle instead of dropping onto the pellet. This situation can occur even if the tip of a syringe needle is in direct contact with the substrate. Vo-Dinh has discussed many of the potential problems associated with consistent sample delivery.[12]

For the following series of studies, the diameter of a sample spot was measured with respect to volume of solution delivered for a variety of solid substrates. A solution of quinaldine red[336] in ethanol (25mg/100mL) was prepared as a suitable marking dye. A 10 μL syringe was used to deliver varying volumes of the dye and the diameter of the subsequent spot was measured at its widest point using a Vernier caliper to ±0.002 cm. There were two participants involved in the initial study so that variations in sample delivery technique between users could be compared. Table 15 lists the results of the spotting study for normal P2 FisherBrand filter paper. The 95% confidence intervals were calculated from the following equation:

$$\mu = \bar{x} \pm \frac{ts}{\sqrt{n}}$$

where $\bar{x}$ is the measured mean, s is the measured standard deviation, n is the number of observations, and t is the tabulated value of Student's t. Here, t=4.303 for two degrees of freedom at 95% confidence.[16] Percent relative standard deviation (%RSD) values are calculated by the following equation:

$$\%RSD = \frac{s}{\bar{x}} \times 100$$

The raw data obtained during the study is found in Appendix B.

---

[333] Hamilton Company, 4970 Energy Way, Reno, Nevada, 89502-4718, USA. 1-800-648-5950.
[334] Unimetrics, 501 Earl Road, Shorewood, IL 60436.
[335] A.D. Campiglia, D.M. Hueber, and T. Vo-Dinh, *Appl. Spectr.*, 1996, V. 50, p. 252.
[336] *Quinaldine Red* is 2-[2-[4-(dimethylamino)phenyl]ethenyl]-1-ethylquinolinium iodide.

Table 15. Relationship between delivery volume (1 μL - 8 μL) and reagent spot diameter for normal P2 FisherBrand filter paper (uncompressed, single layer).

Volume (**μL**) ±0.1 μL	User #1 Avg. spot diameter (**cm**) @ 95% confidence	User #1 Std. Dev.	User #1 %RSD	User #2 Avg. spot diameter (**cm**) @ 95% confidence	User #2 Std. Dev.	User #2 %RSD
1	0.592 ±0.0602	0.0242	4.09	0.566 ±0.0476	0.0192	3.39
2	0.777 ±0.0219	0.00880	1.13	0.796 ±0.0203	0.00816	1.03
3	0.914 ±0.103	0.0413	4.52	0.953 ±0.0285	0.0115	1.20
4	1.038 ±0.0474	0.0191	1.84	1.068 ±0.00364	0.00147	0.14
5	1.154 ±0.0291	0.0117	1.02	1.173 ±0.0328	0.0132	1.12
6	1.295 ±0.0289	0.0116	0.90	1.260 ±0.0414	0.0167	1.32
7	1.389 ±0.0482	0.0194	1.40	1.375 ±0.104	0.0419	3.05
8	1.459 ±0.0861	0.0347	2.38	1.451 ±0.0731	0.0294	2.03

Figure 29 graphically illustrates the relationship between sample spot size vs. delivery volume for the filter paper substrate. For normal P2 FisherBrand filter paper, the maximum sample volume that could be delivered to a half-inch (=1.27 cm) diameter substrate was 5 μL. Based on this study (using normal filter paper as the solid substrate), it was determined that sample spot size is relatively independent of variations in the sample delivery technique that may be employed by different analysts. Additionally, it is apparent from the plot that there is an approximate linear increase in sample spot diameter with respect to increasing delivery volume for normal filter paper ($R^2 = 0.988$; $y = 0.125x + 0.525$; range = 1 μL to 8 μL).

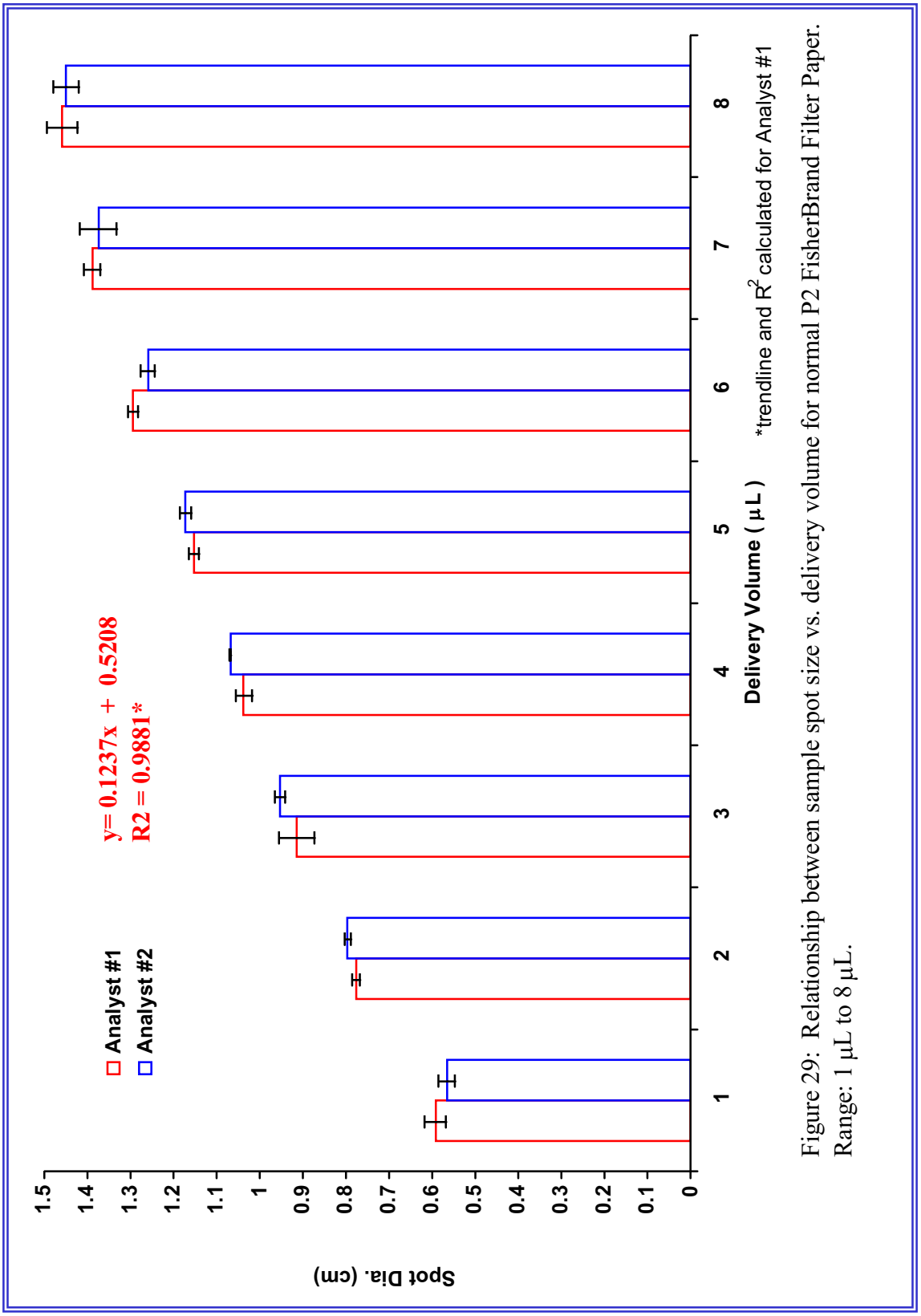

Figure 29: Relationship between sample spot size vs. delivery volume for normal P2 FisherBrand Filter Paper. Range: 1 µL to 8 µL.

HPMC pellets exhibit reagent sorption characteristics that differ considerably from normal, uncompressed filter paper. The rate of reagent transport through the surface of the filter paper is much higher compared to the rate of transport of solution through compressed HPMC pellets. This difference can largely be attributed to the extensive porosity of the filter paper in its natural state. Regardless of the rate at which the analyte is delivered to the substrate surface, a 3 μL volume will yield a spot diameter on normal FisherBrand P2 filter paper that is within the range of 0.85 to 1.0 cm. Table 16 illustrates this variation in spot diameter for 3 μL sample volumes on P2 filter paper. Samples were delivered at a variety of rates (range≅ 0.1 to 13 sec/μL), yet no apparent relationship between reagent delivery speed and spot diameter was evident.

Table 16. Variation of reagent spot diameter on normal P2 FisherBrand filter paper (uncompressed, single layer) with respect to constant delivery volume (3 μL). Random rates of sample delivery (≈0.1 to 13 sec/μL). The average is given at the 95% confidence interval.

Trial #	Spot Diameter (**cm**)
1	0.959
2	0.931
3	0.877
4	0.974
5	0.951
6	0.962
7	0.897
8	0.944
9	0.874
10	0.931
11	1.000
12	0.962
13	0.938
14	0.846
15	0.987
16	0.897
17	0.949
18	0.900
19	0.923
20	0.936
average	**0.932 ±0.0186**
%RSD	**4.27**

Table 17 illustrates the potential for spot size variation on a series of *K4M PREM* HPMC pellets. This study was initiated in order to determine the smallest spot diameter that could be achieved for a sample delivery of 1 μL using a microsyringe. The range of diameters for 16 trials was 0.244 to 0.564 cm. The 1 μL volumes were delivered over an approximate time period of 13 seconds. Although these spot sizes are likely atypical for most analyses (due to the extremely slow sample delivery rate), they nevertheless serve to illustrate the importance of careful syringe-handling technique when using manual sample delivery methods.

Table 17. Variation of reagent spot diameter on *K4M PREM* HPMC pellets with respect to constant delivery volume (1 μL). Slow sample delivery rate (≈13 sec/μL). The average is given at the 95% confidence interval.

HPMC pellet #	Spot Diameter (**cm**)
1	0.559
2	0.531
3	0.521
4	0.353
5	0.483
6	0.399
7	0.386
8	0.330
9	0.427
10	0.422
11	0.348
12	0.305
13	0.285
14	0.241
15	0.343
16	0.285
average	**0.389 ±0.0514**
%RSD	**24.6**

In order to measure the reproducibility of sample spot diameter with respect to delivery volume, further studies were carried out using *K4M PREM* HPMC, *E3 PREM* HPMC, *E15LV PREM* HPMC, and compressed *filter paper pellets*. Table 18 lists typical spot diameters for a sample delivery range of 1 to 3 μL on *K4M PREM* HPMC pellets. Table 19 lists typical spot diameters for a sample delivery range of 1 to 3 μL on *E3 PREM* HPMC pellets. Table 20 lists typical spot diameters for a sample delivery range of 1 to 3 μL on *E15LV PREM* HPMC pellets. Table 21 lists typical spot diameters for a sample delivery range of 1 to 3 μL on P2 FisherBrand filter paper pellets. The measured mean (spot diameter) associated with each delivery volume is calculated using the results of three individual trials. The surface area of a 13 mm dia. HPMC pellet is calculated to be 1.33 cm^2. The surface area of a half-inch dia. filter paper pellet is calculated to be 1.27 cm^2. Figure 30 provides a graphical comparison of the sample delivery characteristics of these four solid support materials. The raw data associated with each study is found in Appendix B.

Table 18. Representative reagent spot diameters for typical sample delivery on *K4M PREM* HPMC pellets (delivery volumes: 1 μL, 2μL, and 3μL).

Delivery Volume (**μL**) ± 0.1 μL	Avg. Spot Diameter (**cm**) @95% confidence	%RSD	surface area coverage %
1	**0.776 ±0.0410**	**2.13**	**35.6**
2	**0.915 ±0.147**	**6.46**	**49.5**
3	**1.084 ±0.159**	**5.90**	**69.4**

Table 19. Representative reagent spot diameters for typical sample delivery on *E3 PREM* HPMC pellets (delivery volumes: 1 μL, 2μL, and 3μL).

Delivery Volume (**μL**) ± 0.1 μL	Avg. Spot Diameter (**cm**) @95% confidence	%RSD	surface area coverage %
1	**0.306 ±0.0310**	**4.09**	**5.55**
2	**0.411 ±0.0182**	**1.79**	**9.96**
3	**0.516 ±0.0621**	**4.85**	**15.7**

Table 20. Representative reagent spot diameters for typical sample delivery on E15LV PREM HPMC pellets (delivery volumes: 1 μL, 2μL, and 3μL).

Delivery Volume (**μL**) ± 0.1 μL	Avg. Spot Diameter (**cm**) @95% confidence	%RSD	surface area coverage %
1	**0.316 ±0.00364**	**0.464**	**5.89**
2	**0.405 ±0.00964**	**0.959**	**9.67**
3	**0.490 ±0.0109**	**0.897**	**14.2**

Table 21. Representative reagent spot diameters for typical sample delivery on P2 FisherBrand filter paper pellets (delivery volumes: 1 μL, 2μL, and 3μL).

Delivery Volume (**μL**) ± 0.1 μL	Avg. Spot Diameter (**cm**) @95% confidence	%RSD	surface area coverage %
1	**0.839 ±0.282**	**13.5**	**43.5**
2	**0.951 ±0.224**	**9.50**	**55.9**
3	**1.011 ±0.130**	**5.19**	**63.2**

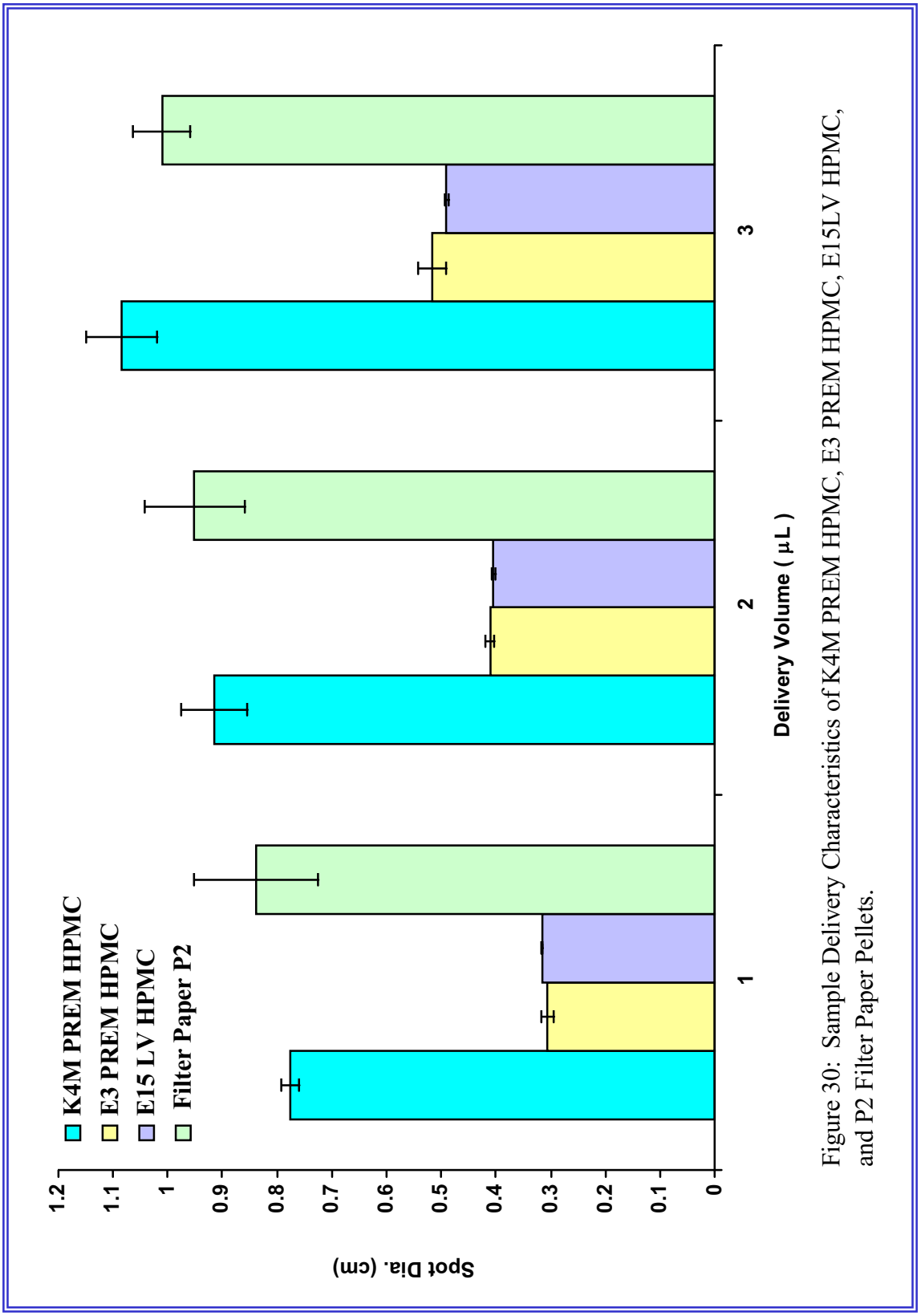

Figure 30: Sample Delivery Characteristics of K4M PREM HPMC, E3 PREM HPMC, E15LV HPMC, and P2 Filter Paper Pellets.

In summary, the RTP sample delivery studies reported here confirm the following:

a). For normal, uncompressed filter paper, reagent spot size may vary slightly between individuals as a result of differences in syringe-handling technique and physical non-uniformity of the matrix material. Nevertheless, the variations are not statistically significant as illustrated by the data.

b). For normal, uncompressed filter paper, the final diameter of the reagent spot is largely independent of the sample delivery rate.

c). For HPMC pellets, the diameter of the reagent spot can vary dramatically with adjustments in sample delivery rate. However, preliminary results indicate that automated sample delivery instrumentation will allow for significantly reduced spot diameters on HPMC supports in comparison to the corresponding sample volumes delivered onto filter paper supports. For 1 μL delivery volumes, it should be possible to achieve spot diameters approximating 0.3 cm using HPMC substrates compared to spot diameters approximating 0.6 cm for normal filter paper. Effectively, the sample will be concentrated in a smaller surface area on an HPMC support. Limits of detection should be improved for HPMC pellets as the size of the analyte spot more closely approximates the dimensions of the excitation radiation beam that strikes the sample.

d). As indicated by tables 18 and 21, compressed filter paper pellets exhibit sorption characteristics that are comparable to *K4M PREM* HPMC pellets. The surface area percent-coverage calculations yield similar results for these two support materials. On the other hand, for a 1 μL sample delivery, reproducibility appears to be favored for the HPMC matrix (2.13 %RSD vs. 13.5 %RSD). This result was unexpected since a series of 1 μL trials using uncompressed filter paper provided a %RSD of 4.05 (table 15).

e). As indicated by tables 19 and 20, the sample solutions delivered to E3 PREM and E15LV PREM HPMC yield small spot diameters of similar size for the two substrates. The sorption characteristics of the two materials are comparable. The surface area percent-coverage calculations support visual laboratory observations that these two types of Methocel™ (in pellet form) do not readily sorb ethanol-based solutions.

f). The reproducibility associated with the sample delivery step is excellent for E15LV PREM HPMC. The calculations for 1 to 3 μL sample volumes each yielded %RSD values of less than 1.0%.

5.4.3 Optimization of Experimental Parameters

Prior to initiating RTP investigations, it is necessary to optimize a number of procedural variables and instrumental variables. Table 22 provides a representative listing of the RTP parameters that must be addressed by the analyst prior to operating the LS-50 luminescence spectrometer.

Table 22. RTP parameters to be considered by the analyst prior to sample analysis

variable	limits	increment
sample volume	0 μL to 100 μL	n/a
sample drying time	0 min to ??? min	1 min
sample purge time	0 min to ??? min	1 min
excitation wavelength	200 nm to 800 nm	1 nm
emission range	200 nm to 650 nm	1 nm
scan speed	10 nm/min to 1500 nm/min	1 nm/min
excitation slit width	2.5 nm to 15 nm	0.1 nm
emission slit width	2.5 nm to 20 nm	0.1 nm
gate time (t_g)	0.01 ms to 500 ms	0.01 ms
delay time (t_d)	0 ms to 9490 ms	0.01 ms
PMT voltage	600 V to 900 V	1 V
digital signal filtering	binomial vs. Savitzky-Golay	n/a

For this particular study, the sample volumes delivered to the solid substrates were limited by four primary concerns:

a). concentration of the analyte,
b). concentration of the heavy-atom enhancer,
c). sensitivity of the instrument, and
d). sorption capacity of the support material.

The selection of a suitable delivery volume usually requires a few trial runs in order to determine the optimum conditions. For instance, if the initial RTP intensity is off-scale, then reagents can be diluted or the PMT operating voltage can be reduced.

Sample drying time depends largely on the volatility of the solvent used. For this project, ethanol was the solvent of choice (B.P. = 78.5 °C). Due to ethanol's moderate boiling point, only mild heating was required for solvent removal. As a result, sample drying times were very short (< 3 minutes per sample). Ethanol is a polar solvent that is capable of penetrating and swelling both filter paper and HPMC substrates.

The relationship between sample purge duration and RTP intensity was investigated during this project. Studies of this nature have been published in the literature for other support materials, but the reader is advised that results often vary significantly between laboratories. For

the HPMC substrates studied here, it was discovered that nearly 25 minutes of purge time will be required before RTP emission intensities begin to stabilize. Typically, there is a significant rate of growth in phosphorescence intensity for analytes during the time period between 0 to 15 minutes. It is important for the analyst to carefully record the duration of sample purge so that the reproducibility between runs can be optimized.

The optimum excitation wavelength and emission ranges vary from analyte to analyte. The LS-50 *prescan* utility is sometimes useful for determining approximate excitation and emission maxima. Nevertheless, spurious phosphorescence prescan results are not uncommon. As an alternative to relying solely upon prescan results, phosphorescence excitation and emission maxima have been suggested in the literature for a wide variety of potential analytes.[2,12,104]

For trace amounts of analyte, the PMT voltage can be manually increased by the analyst. For each analysis during this research, the working PMT voltage was noted and recorded. Although the PMT voltage was set to 900V for most runs, it was sometimes necessary to reduce the PMT voltage for concentrated samples in order to prevent the resulting phosphorescence intensities from venturing off-scale.

During this project, phosphorescence spectra were acquired using a delay time (t_d) of 2 ms and a gate time (t_g) of 5 ms. The delay time allowed for fluorescence emissions to sufficiently decay; whereas the gate time allowed for the PMT to be adequately exposed to the phosphorescence emissions prior to the next excitation pulse. The binomial digital filtering algorithm was applied to all spectra. It offers sufficient noise reduction in the experimental excitation and emission spectra with a minimum of phosphorescence peak distortion.

5.4.4 Detection of Outliers

An *outlier* is any observation that differs markedly from the majority of the other observations in a data set.[337] Many outlier tests have been developed for the determination of discordant observations.[338] However, a significant number of outlier detection schemes suffer from *masking effects*.[339,340] Such techniques cannot be relied upon to detect multiple outliers in a data set. In order to overcome this limitation, robust methods for outlier detection have been developed.[341,342]

Robust statistical methods rely on the use of various *estimators of location*. By generating sample influence curves, statisticians have developed a number of useful categories of estimators. Two of these categories are the "L-estimators" and "M-estimators". Briefly, L-estimators rely on sample influence curves derived either from the mean or median of a set of observations. The influence curve of the mean is generally considered to be non-robust since it

---

[337] P.L. Davies, *Fres. Z. Anal. Chem.*, 1988, Vol. 331, p. 513.

[338] B. Iglewicz and D.C. Hoaglin, **How to Detect and Handle Outliers**, Vol. 16 in *The ASQC Basic References in Quality Control: Statistical Techniques* (E.F. Mykytka, Ed.), Milwaukee, WI: ASQC Quality Press, 1993.

[339] R.B. Dean and W.J. Dixon, *Anal. Chem.*, 1951, Vol. 23, p. 636.

[340] M.K. Park, J.H. Cho, N.Y. Kim, and J.H. Park, *Anal. Chim. Acta*, 1993, Vol. 284, p. 73.

[341] Analytical Methods Committee, *Analyst*, 1989, Vol. 114, p. 1693. (Software discussed in this report is available on the internet. **URL**: http://lib.stat.cmu.edu/).

[342] J.E. Maisel, *Personal Engineering & Instrumentation News (PE&IN)*, April 1995, p. 66.

assigns equal weights to all observations (figure 31a).[343] On the other hand, the influence curve of the median represents the other extreme (figure 31b). It assigns a weighting of zero to all observations except the middle order statistics (or middle two, if n is even). The compromise between the two extremes is the "trimmed mean" (figure 31c). The trimmed mean influence curve is created by omitting a fixed proportion of the lowest and highest sample values and calculating the mean of the remaining observations. If the same proportion of observations are trimmed from both ends of the distribution, then a family of estimators known as "the α-trimmed means" is generated (where α is the percentage of trim). Trimmed means give equal weights to all observations in the middle 1-2α percent of the data and zero weight to the rest.

Since they are relatively easy to calculate, L-estimators have traditionally been the most widely used robust estimators. However, the disadvantage of the trimmed mean is that it down-weights the highest and lowest order statistics regardless of whether or not all of the observations are reliable. M-estimators (or maximum likelihood estimates) are those in which the influence associated with an observation changes gradually with the distance of the observation from the middle. Given an equation of the form

$$\sum \psi\left(x_i - T\right) / s = 0$$

M-estimates are solutions for "T", where s is a robust measure of spread. Although statisticians have proposed many different ψ functions, they may be grouped into two primary classes. The first class proposed by Huber is similar to the trimmed mean estimator discussed earlier (figure 32a).[344] The second type of M-estimator is a "redescending estimator". For this class of estimator, the influence curve increases and then decreases with increasing distance from the center of the distribution. The influence assigned to an extreme observation is eventually zero in every case. Three common M-estimators are the Hampel, the sine function, and the Tukey biweight (figure 32b-d).[343] Note that each of the influence curves is symmetric around the center. Therefore, they can only be legitimately used on normal sets of observations. The best robust estimators will comply with seven individual benchmarks that have been defined by Hampel.[345] Each of the three-part redescending M-estimators successfully address Hampel's requirements.

During the preliminary stages of the project, it was suspected that the SSRTP data sets might include multiple outlying observations due to: a). inconsistencies in sample delivery or b). physical non-uniformity of the RTP support materials utilized or c). both of these concerns simultaneously. Dr. Jeff Birch, professor of statistics at Virginia Tech[346], shared two useful Minitab® programs that utilize the Tukey Biweight M-estimate for outlier detection (Appendix A).[347]

---

[343] P.R. Jackson, *Robust Methods in Statistics* in **New Developments in Statistics for Psychology and the Social Sciences** (A.D. Lovie, Ed.), New York: The British Psychological Society and Methuen, 1986.

[344] P.J. Huber, *Ann. Math. Stat.*, 1964, V. 35, p. 73.

[345] F.R. Hampel, *J. Am. Stat. Assoc.*, 1974, V. 69, p. 383.

[346] Dr. Jeffrey B. Birch. Statistics Department, 406-A Hutcheson Hall, Virginia Tech, Blacksburg, VA 24061-0439. phone: (540) 231-7934. E-mail: jbbirch@vtvm1.cc.vt.edu.

[347] Minitab® is an easy-to-use, general purpose software package for statistical computing. Minitab, Inc., 3081 Enterprise Drive, State College, PA 16801. Phone: 1-814-238-3280. FAX: 1-814-238-4383.

a). mean

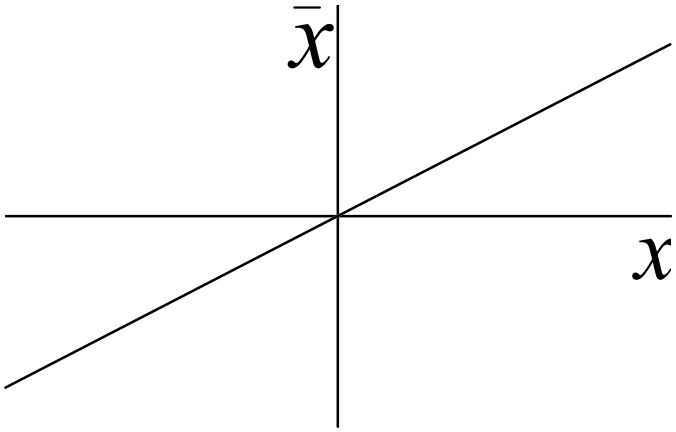

b). median

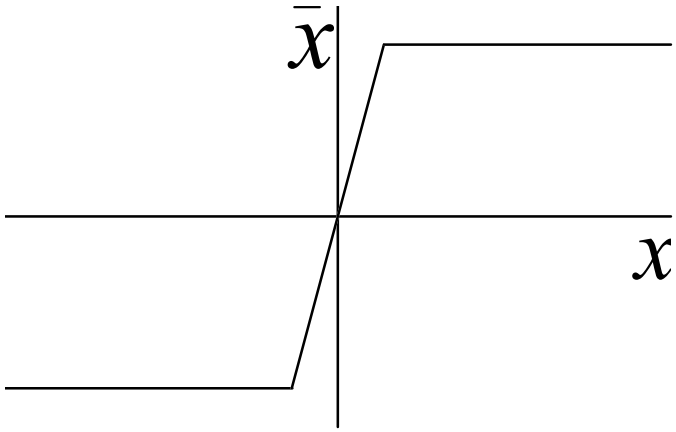

c). trimmed mean

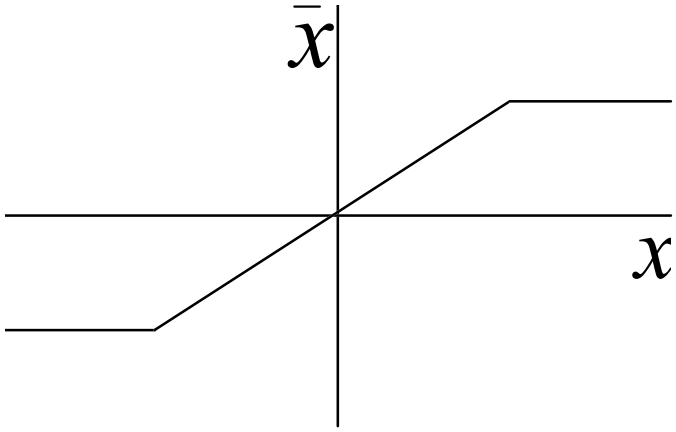

Figure 31. Influence Curves for L-estimators
(adapted from P.R. Jackson *Robust Methods in Statistics* in **New Developments in Statistics for Psychology and the Social Sciences**, (A.D. Lovie, Ed.), New York: The British Psychological Society and Methuen, 1986.)

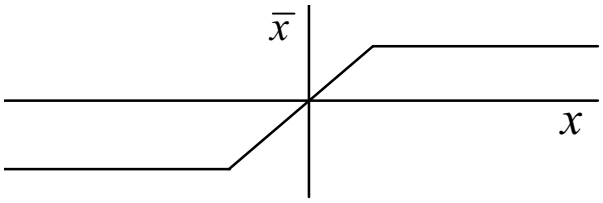

a). Huber M-estimate

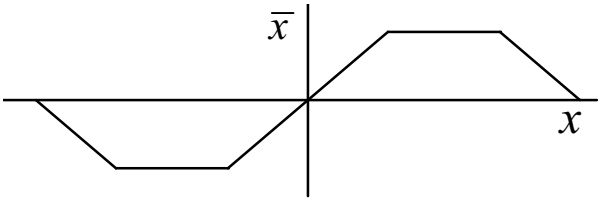

b). Hampel M-estimate

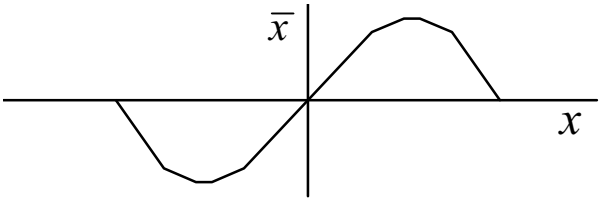

c). Sine function M-estimate

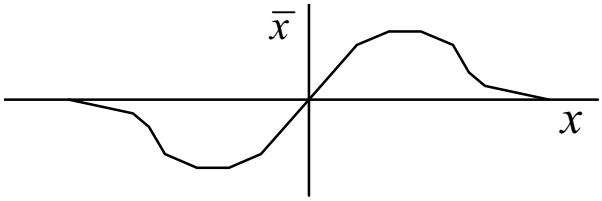

d). Tukey's Biweight M-estimate

Figure 32. Influence Curves for M-estimators
(adapted from P.R. Jackson *Robust Methods in Statistics* in **New Developments in Statistics for Psychology and the Social Sciences**, (A.D. Lovie, Ed.), New York: The British Psychological Society and Methuen, 1986.)

Although computer programs can readily calculate M-estimators, it is usually necessary to begin with simple robust measurements such as the median as an estimate of location and the median of the absolute deviations from the median (or "MAD") as an estimate of spread. The primary task of program STARTIRLS is to find the median of a data set and to determine the MAD. The median of a large data set is useful since it tends to be more resistant to the effects of outliers than the calculated average of the same set of observations. The calculated MAD is a robust estimator of spread that can be used as a substitute for the standard deviation of a set of observations. In fact, dividing the MAD by 0.6745 gives an approximately unbiased estimate of σ for normally distributed data.[343] Program variable **k4** is known as the *bisquare constant*. If the data is normal, a bisquare constant of 4.5 results in a *M-estimator* with 95% efficiency with respect to the sample mean. If the data is non-normal, then the m-estimators are resistant to the outliers.

A common feature of all M-estimators is that they require iteration. The influence function relies on estimates of both location and spread which in turn depend on the influence function and so on. For a given data set, program IRLSB computes a Tukey biweight M-estimator which is then used to assign robust weights to the individual data points on a scale of 0.0 to 1.0.[343] Tukey's biweight is defined as

$$\psi(x) = \begin{cases} x\left(1-x^2\right)^2, & |x| \le 1, \\ 0, & \textit{otherwise.} \end{cases}$$

"Good" data points are those that are weighted close to 1.0. Questionable data points receive small weights relative to the other weightings. Since aberrant data is sometimes more easily identified in graphical form as opposed to numerical lists, it may be advantageous to plot the $\text{weight}_{(i)}$ vs. i (where i is the observation number). Unfortunately, most statistics authorities recommend that outlying observations be retained or discarded solely at the discretion of the analyst. In this manner, the selection of the outliers is entirely subjective. One goal associated with the adoption of robust techniques is to make this process as objective as possible. Perhaps the best way to avoid analyst bias between related data sets is to choose and hold constant a robust weight threshold (identified here as "$\text{weight}_{(o)}$"). If $\text{weight}_{(i)}$ is less than $\text{weight}_{(o)}$, then an outlier is positively identified and the data point is discarded. Data points are retained when $\text{weight}_{(i)}$ is greater than $\text{weight}_{(o)}$. Although the selection of $\text{weight}_{(o)}$ remains subjective, the introduction of analyst bias is thereby avoided. Further details regarding the detection and

handling of outliers are found elsewhere.[348,349,350,351,352,353,354,355]

A demonstration of the usefulness of this robust statistical method is provided in the following example. Table 23 lists fifteen actual experimental SSRTP observations[356] and their corresponding robust weights as calculated using the programs STARTIRLS and IRLSB. Note that trial number five has received a weighting of zero and trial number twelve has been assigned an extremely low weighting. Two suspicious observations are positively identified.[357] In this particular example, the analyst chooses to remove the questionable results and then reanalyze the data set statistically.

As shown by table 24, the data set now yields significantly improved mean, standard deviation, and %RSD figures. The analyst's suspicions are confirmed: the disregarded observations were indeed outliers. Figure 33 provides a graphical illustration of the phosphorescence data set prior to the elimination of the outlying observations. The classical$\pm 1s$, $\pm 2s$, and $\pm 3s$ cutoff values are depicted by vertical bars. Figure 34 shows the updated phosphorescence data set after the outliers have been discarded. Note that the$\pm 1s$, $\pm 2s$, and $\pm 3s$ values are now much closer to the mean than before. During this project, all RTP data sets were analyzed for potential outlying observations using Tukey's biweight ψ function. However, these robust methods were not applied to the results of the sample delivery studies cited in section 5.4.2 and Appendix B.

---

[348] B. Barnett and T. Lewis, **Outliers in Statistical Data, 2nd Ed**, New York: John Wiley & Sons, 1984.

[349] J.C. Miller and J.N. Miller, **Statistics for Analytical Chemistry, 2nd Ed**, New York: John Wiley & Sons, 1988.

[350] P.C. Meier and R.E. Zünd, **Statistical Methods in Analytical Chemistry**, Vol. 123 in *Chemical Analysis: A Series of Monographs on Analytical Chemistry and Its Applications* (J.D. Winefordner, Series Ed.; I.M. Kolthoff, Editor Emeritus), New York: John Wiley & Sons, 1993.

[351] J.N. Miller, *Analyst*, 1993, Vol. 188, p. 455.

[352] M. Thompson, *Anal. Chem.*, 1989, Vol 61, p. 1942.

[353] D.B. Rorabacher, *Anal. Chem.*, 1991, V. 63, p. 139.

[354] F.R. Hampel, *Technometrics*, 1985, Vol. 27, p. 95.

[355] S. Bolton, **Pharmaceutical Statistics, 3rd Ed.**, New York: Marcel Dekker Inc., 1997.

[356] The analytical sample for this particular study was 1 µL of naphthalene in ethanol (410 ppm). 8.0 µL of 0.50% (wt/wt) NaI was added as the heavy atom enhancer. The duration of dry nitrogen gas purge was 3 minutes.

[357] For this particular data set, the Dixon's Q test would have identified only a single questionable observation (the data point at 494.6 intensity units) due to the masking effect. Likewise, if the analyst had simply chosen to discard all observations ouside the 95% confidence interval ($< \overline{x} - 2s$ or $> \overline{x} + 2s$), only a single aberrant data point could be discarded in this manner (once again, the observation at 494.6 intensity units). This robust method identifies both outlying observations simultaneously at an efficiency of 95% with respect to the sample mean.

Table 23. Detection of outlying SSRTP observations using robust weights.

Trial #	Phosphorescence Intensity	Tukey weighting
1	333.50	0.97375
2	301.10	0.98564
3	338.00	0.95968
4	348.90	0.91379
5	494.60	0.00000
6	325.90	0.99075
7	334.10	0.97204
8	293.40	0.96525
9	354.10	0.88629
10	319.00	0.99870
11	290.40	0.95498
12	207.30	0.31337
13	294.70	0.96930
14	315.30	0.99999
15	282.90	0.92377

Table 24. Statistical calculations associated with the SSRTP data used for the Tukey biweights method of outlier identification.

statistical function	SSRTP data set original observations	SSRTP data set outliers removed
average	322.21	317.79
median	319.00	319.00
std. deviation	59.66	23.55
%RSD	18.52	7.41

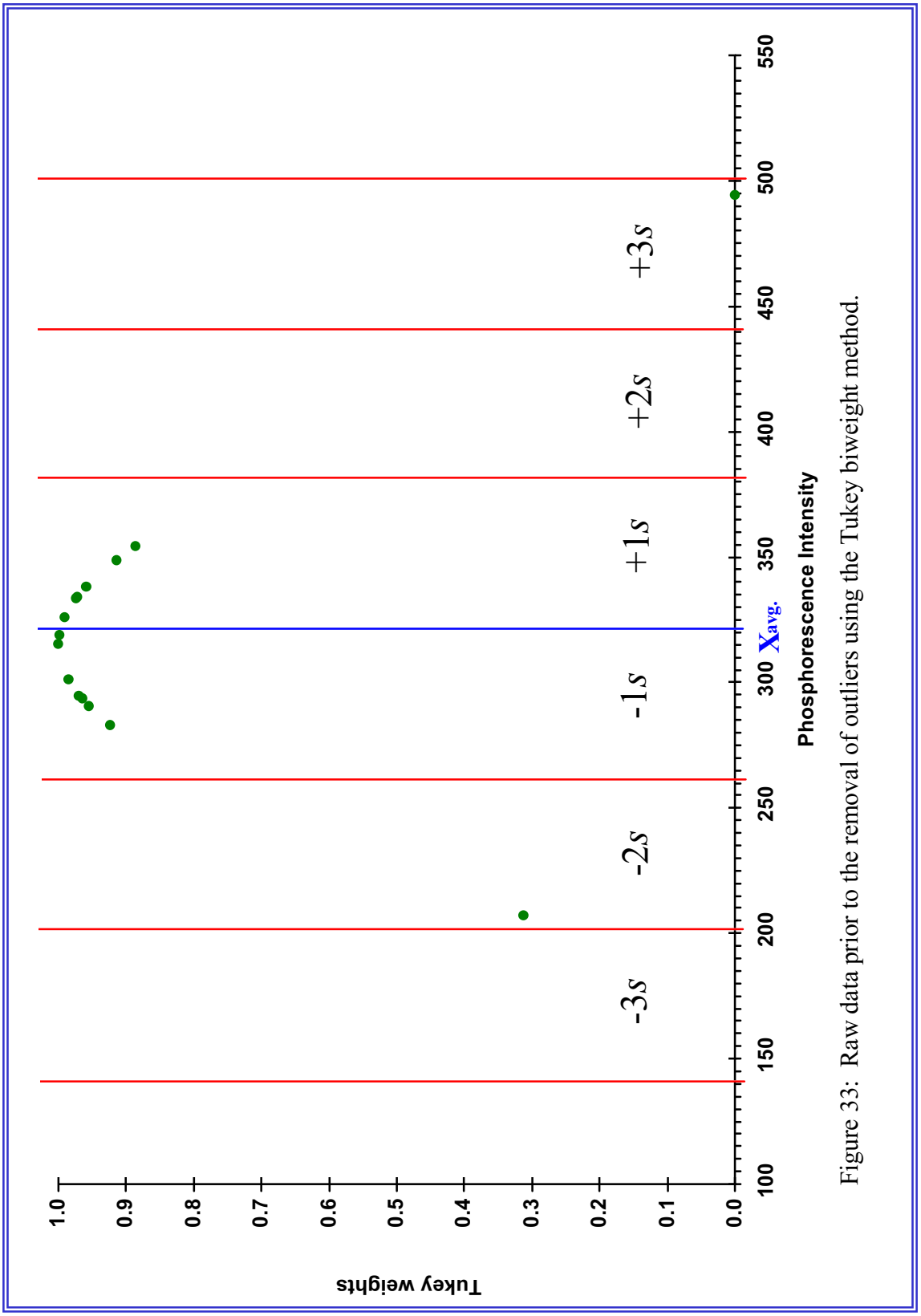

Figure 33: Raw data prior to the removal of outliers using the Tukey biweight method.

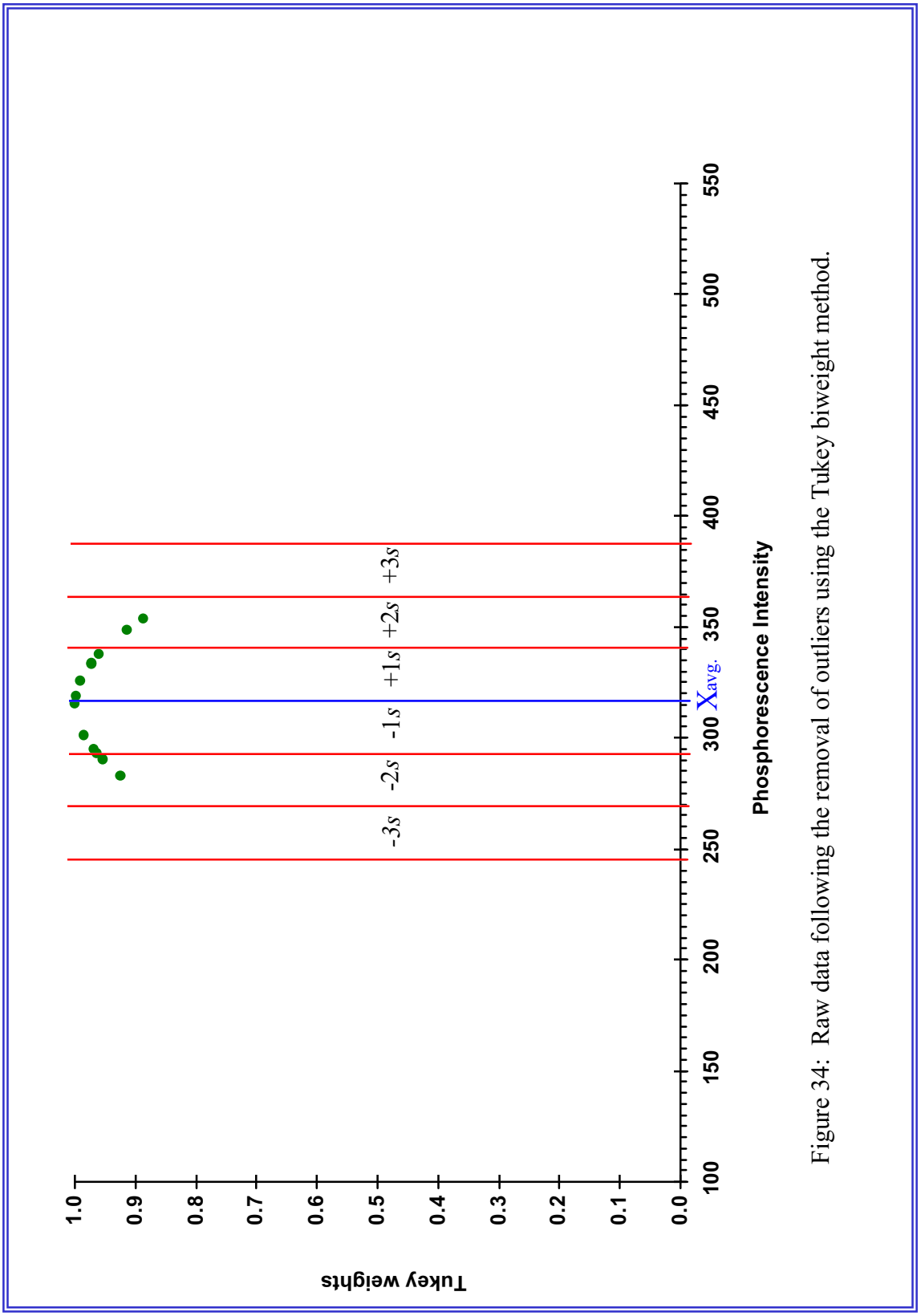

Figure 34: Raw data following the removal of outliers using the Tukey biweight method.

5.5 SSRTP Investigations

A study of the effects of sample purge time and substrate storage conditions

Contradictory reports discussing the effects of purge gases and sample storage conditions on RTP intensities are often found in the literature. A study was devised in the early stages of this project to determine if it would be possible to observe a statistically significant increase in RTP signal by storing the HPMC support materials overnight (≈ 15 hours) in a dry nitrogen-purged vessel versus overnight storage in a sealed container filled with Drierite™ desiccant. Several trials were carried out by spotting naphthalene and NaI solutions on *K4M PREM* HPMC pellets that had been stored overnight under dry N_2 purge conditions. Additional trials were carried out by spotting the same naphthalene and NaI solutions on HPMC pellets that were stored overnight in a desiccant-filled container. Following phosphor and heavy-atom salt spotting, all substrates were dried for three minutes. Each of these samples were analyzed in the custom-built sample cell module while exposed to a constant flow of dry N_2 purge gas. The last HPMC substrate in the series was prepared in the same manner as the preceding ones and stored overnight under desiccant. However, this particular sample was analyzed under ambient conditions with no dry N_2 purge gas present. The results of these trials are shown in figure 35.

The data obtained during this study shows that the specific storage conditions of the HPMC pellets prior to their use are not a major factor in the enhancement of RTP intensities so long as they are maintained in a dry atmosphere. The pellets stored within a desiccated environment yielded phosphorescence λ_{max} emission intensities that were only slightly higher than those of their counterparts stored under dry nitrogen purge conditions. This improvement in emission intensity was only evident after ≈ 10 minutes of dry N_2 gas purging and, if the standard deviations associated with each measurement are considered, the results are not statistically different from the substrates stored under nitrogen-purge conditions. Nevertheless, dry substrates are always important for maximizing SSRTP intensities regardless of the chosen drying technique. For the remainder of the project, all RTP substrates were stored within a sealed Drierite™-filled container prior to their use.

The overall trends shown by the graph in figure 35 are typical for SSRTP analyses carried out under purged and non-purged conditions. Note that the phosphorescence intensities yielded by the non-purged sample are significantly lower than those of the nitrogen-purged samples. Early in the trials, a signal improvement of approximately eighteen-fold is evident. Later in the trials, the gap in signal narrows to a factor of approximately three. This significant improvement in RTP intensity for the non-purged sample can likely be attributed to a small amount of residual ethanol within the HPMC pellet following the drying step. Since the substrate remains at room temperature in the sample cell module, the ethanol within the HPMC matrix can diffuse to the surface of the pellet and enter the vapor phase. This would reduce the probability of intermolecular collisional quenching between the solvent and the phosphor. The LS-50 itself may contribute to this process since it is possible that a portion of the heat lost from the interior of the instrument might be transferred to the sample cell module.

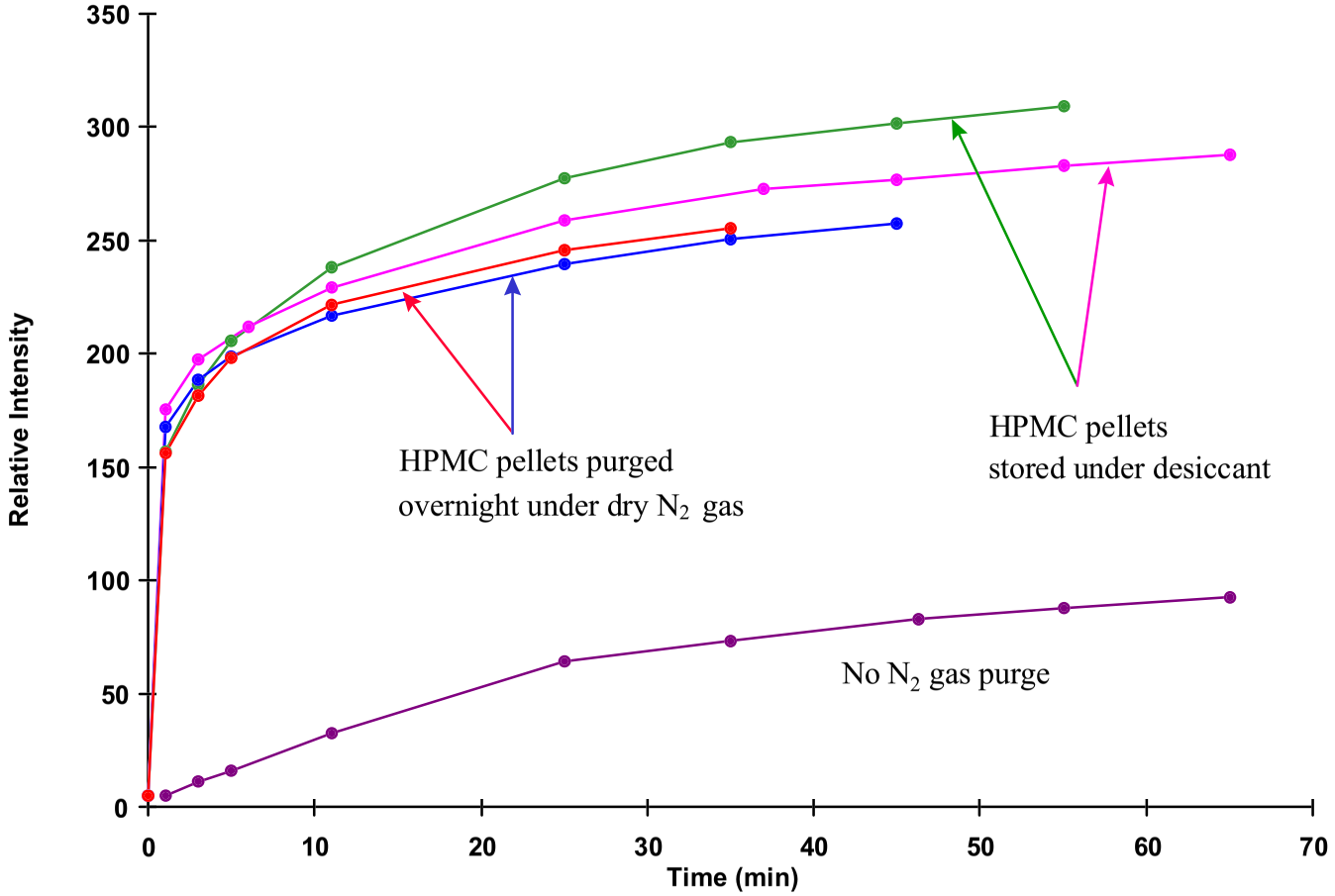

Figure 35: Growth of Phosphorescence Signal with Time for Naphthalene on HPMC Matrix. Pellets Stored Under N_2 Gas Purge vs. Pellets Stored Under Desiccant.

For the nitrogen-purged samples, a significant improvement in RTP intensity occurs within the first few minutes of the trial. This signal enhancement can be attributed to the removal of two noted phosphorescence quenching agents from the enclosed sample cell module: moisture and O_2. Approximately 20 minutes after the initiation of each of the trials, it becomes apparent that the RTP signals begin to plateau. Nevertheless, there continues to be a small improvement in RTP intensities for each sample as the dry N_2 gas purge continues. Once again, this signal improvement with time can likely be attributed to residual ethanol that remains within the HPMC matrix following the initial substrate drying step. As the solvent diffuses to the surface of the substrate and escapes into the surroundings, the probability of collisional quenching with the phosphor is significantly reduced.

Similar trends are observed for normal filter paper substrates. However, maximum RTP intensities are reached sooner for filter paper substrates than HPMC substrates (≈10 minutes vs. ≈20 minutes). This can be attributed to both the thickness and macroscopic porosity of the filter paper disc compared to the HPMC pellet. Figure 36 provides a comparison of the surface features of a typical P2 FisherBrand filter paper disc and the surface of a *K4M PREM* HPMC pellet. Residual ethanol should be more easily removed from the filter paper disc than the HPMC pellet during the dry gas purge step.

Following this study, it was decided that all future analyses be recorded at multiple intervals during the gas purging process. Thus, phosphorescence λ_{max} emission intensities during the project have typically been recorded at exactly three, six, fifteen, and twenty-five minute intervals during each trial. This standard operating procedure was essential for the collection of valid quantitative RTP data since the phosphorescence intensity of each trial can vary significantly in accord with either the duration of dry gas purge or residence time of the sample in the instrument. This discovery can be summarized in the form of a recommendation for future SSRTP investigators: whenever quantitative studies are launched, the collection of RTP data should be initiated at regular timed intervals in order to improve the reproducibility between trials.

The decision to cease data collection at a maximum purge time of twenty-five minutes certainly involves a trade-off. Figure 35 indicates that phosphorescence intensities will continue to steadily increase even after a purge time of forty minutes. Judging by the trends shown within the graph, it is likely that these phosphorescence signals will continue to be improved well past the one-hour mark. On the other hand, the time of analysis is an important concern. It is difficult to justify a one-hour (or longer) analysis time for a single sample when a 15-minute analysis will suffice. Therefore, subsequent RTP trials were terminated after spectra had been recorded at either fifteen or twenty-five minute intervals.

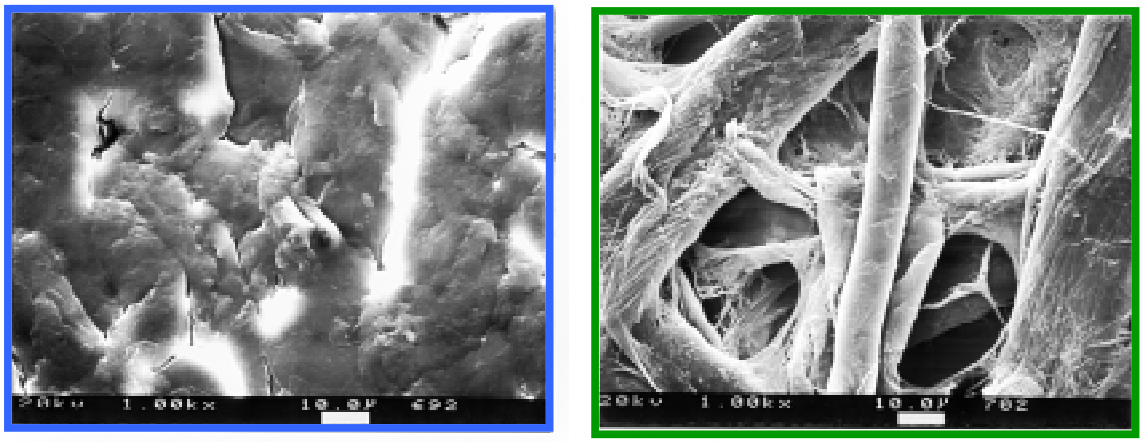

K4M PREM HPMC Pellet

Normal Filter Paper (FisherBrand P2)

Figure 36. A microscopic comparison of the surface features of a *K4M PREM* HPMC pellet and normal filter paper. (S.E.M. 1000X)

A study of the effects of different types of Methocel™ HPMC on RTP intensity

Three types of DOW Methocel™ were investigated in order to determine if there were significant differences in their performance as potential SSRTP matrix materials. The Methocel™ types selected were *K4M PREM, E3 PREM, and E15LV PREM.* Table 25 summarizes the pertinent RTP parameters associated with this series of investigations.

Table 25. Analytical conditions utilized for the Methocel™ HPMC study.

HPMC substrates	*K4M PREM / E3 PREM / E15LV PREM*
analyte	1.0 μL of 100 ppm naphthalene in ethanol
heavy-atom salt	8.0 μL of NaI in ethanol (16.5% wt/wt).
drying time	3 minutes
purge gas	dry N_2
$\lambda_{ex.}$	273 nm
PMT	900 V
t_d	2 ms
t_g	5 ms
ex. slit	5 nm
em. slit	15 nm

Figure 37 illustrates the RTP intensities achieved for a phosphor immobilized on each of these substrates. The substrates were analyzed individually using the custom-built SSRTP sample cell module. Each data point shown on the graph is representative of a minimum of five trials. Note that the *K4M PREM* HPMC pellets were responsible for an RTP λ_{max} emission approximately three times greater than the corresponding intensities obtained using the*E3 PREM* and *E15LV PREM* HPMC pellets. This is possibly due in part to the analyte sorption characteristics of the *E*-types of Methocel™. As indicated by tables 19 and 20, the sample solutions delivered to *E3 PREM* and *E15LV* PREM HPMC yield small spot diameters of similar size for the two substrates. The ethanol sorption characteristics of these two materials are comparable.

According to DOW, the primary feature that distinguishes the physical and chemical characteristics of *E*-type HPMC from *K*-type HPMC rests with the % methoxyl substitution. Both *E*- and *K*-types have 7-12% hydroxypropyl substitution; whereas the *E*-type has 28-30% methoxyl substitution and the *K*-type has 19-24% methoxyl substitution. The surface area percent-coverage calculations provided in tables 19 and 20 support laboratory observations that these two E-types of Methocel™ (in pellet form) do not readily sorb ethanol-based solutions. Although the proposal presented here is a speculative one, it is likely that the*E*-types of Methocel™ are poor SSRTP substrates simply because they are unable to trap the phosphors and/or heavy-atom salt during the sample delivery and substrate drying process. On the other hand, it seems unlikely that the percent-methoxyl substitution is solely responsible for the poor

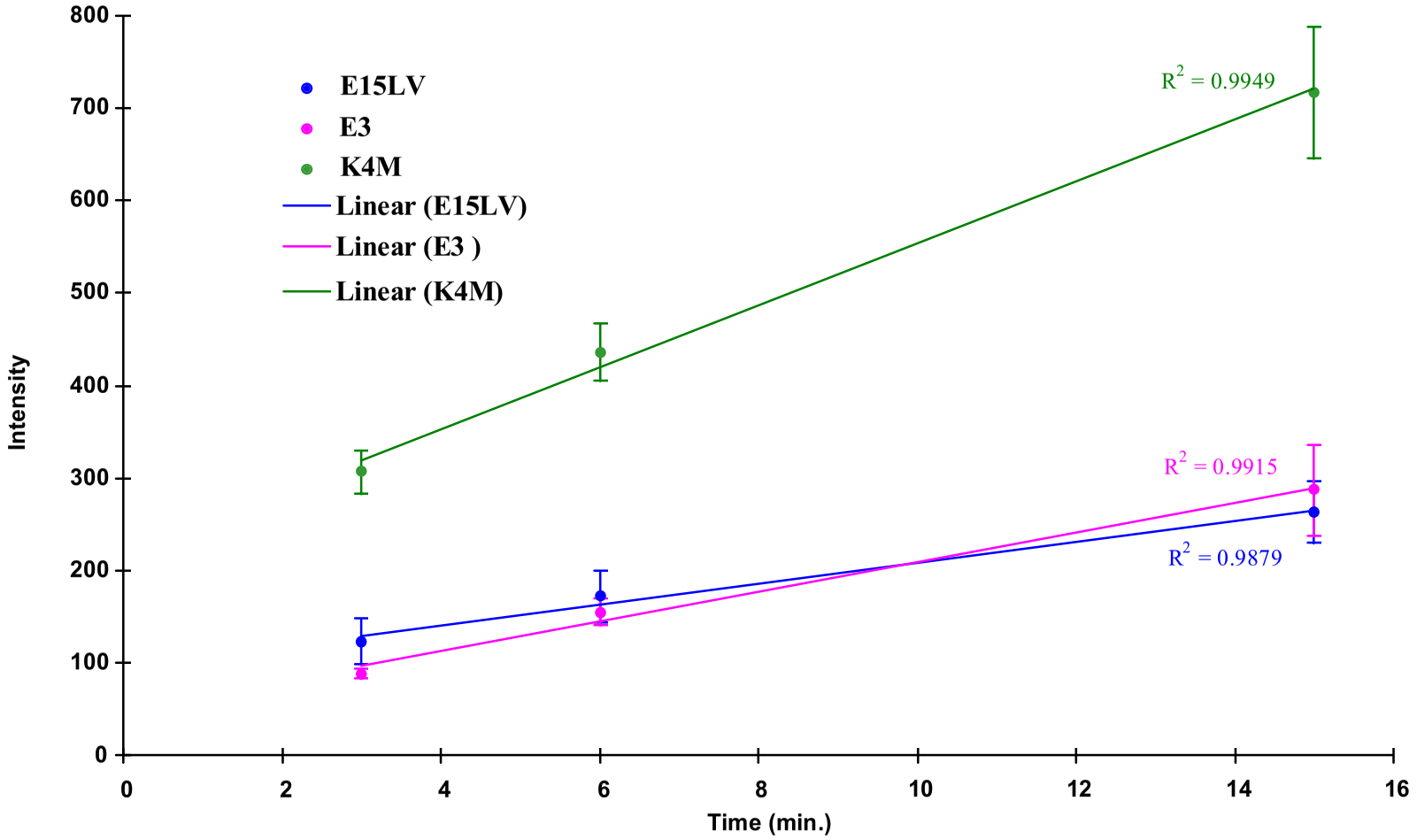

Figure 37: RTP Intensities for Naphthalene on Different Types of Dow Methocel HPMC pellets. Phosphor: 1.0 µL of 100 ppm Naphthalene in Ethanol. Heavy Atom: 8.0 µL of 16.5 % NaI. in Ethanol.

sample sorption characteristics of the *E*-type material. *E*-type vs. *K*-type particle sizes may play a role. For instance, Mitchell and colleagues have used B.E.T. surface area determinations (via nitrogen adsorption) to confirm that particle size is an important HPMC characteristic that is partially responsible for controlling the extent of solvent penetration into a tablet surface.[252] Since small particle sizes allow the HPMC granules to pack more tightly, it is possible to prepare HPMC substrates that are unlikely to have porous surfaces and correspondingly low levels of interparticulate porosity. Based on this information and the results of these investigations,*K4M PREM* hydroxypropylmethylcellulose was chosen as the HPMC substrate material for use during the remainder of the project.

A study of the influence of moisture and oxygen on phosphorescence λ_{max} emission intensities

Contradictory reports discussing the effects of moisture and oxygen on RTP intensities are often found in the literature. Schulman and Walling claimed that their early SSRTP measurements were oxygen insensitive.[38,89] In 1977, Vo-Dinh et al. reported that RTP intensities were lower when samples on paper substrates were dried in pure oxygen instead of pure nitrogen.[274] Bower and Winefordner found that their study regarding the influence of different gaseous environments on RTP provided anomalous results.[358]

Citta and Hurtubise have studied the abilities of water, oxygen, and air to quench RTP of certain phosphors immobilized on filter paper.[359] They reported that water was found to be a more potent quencher of RTP than oxygen. The mechanistic aspects of moisture quenching of RTP on filter-paper adsorbed phosphors were studied by Purdy and Hurtubise.[360] The humidity effects were examined for samples in a nitrogen atmosphere. It was found that the phosphorescence *lifetimes* were not affected much by relative humidity. A prior report by Batten and Nissan indicated that changes in phosphorescence intensities were attributed to a change of modulus in the three-dimensional filter paper matrix as the humidity increased.[361]

Two separate experiments were devised in order to investigate the influence of these noted quenching agents on the phosphorescence obtained from a model phosphor immobilized on *K4M PREM* HPMC. The analytical conditions associated with the moisture study are provided in Table 26. Spectra were acquired at three, six, fifteen, and twenty-five minute intervals.

Table 26. Analytical conditions utilized for the moisture studies.

substrate	*K4M PREM* HPMC
analyte	1.0 μL of either 200, 600, 1000, 1500, and 3310 ppm naphthalene in ethanol
heavy-atom salt	8.0 μL of NaI in ethanol (16.5% wt/wt).
drying time (NaI)	3 minutes
drying time (naph.)	2 minutes
purge gas	N_2 gas saturated with H_2O
$\lambda_{ex.}$	273 nm
PMT	900 V
t_d	2 ms
t_g	5 ms
ex. slit	5 nm
em. slit	15 nm

[358] E.L. Bower and J.D. Winefordner, *Anal. Chim. Acta*, 1978, V. 102, p. 1.
[359] L.A. Citta and R.J. Hurtubise, *Appl. Spectr.*, 1991, V. 45, p. 1547.
[360] B.B. Purdy and R.J. Hurtubise, *Anal. Chem.*, 1992, V. 64, p. 1400.
[361] G.L. Batten and A.H. Nissan, *Tappi J.*, 1987, V. 70, p. 119.

Prior to beginning the moisture study, it was necessary to select a method that would be suitable for saturating the nitrogen carrier gas with water. Numerous methods have been cited in the literature such as bubbling the carrier gas through a large volume of water, flowing the gas through a column containing wet granulated solids (such as clean quartz sand or glass beads), passing the gas over a container of water or ice, flowing the carrier gas across the surface of wet cloth tape, passing the gas through moistened layers of sponge, and even a vortex system of contact that involves a centrifugal action of the carrier gas over water in a cylindrical container.[362]

Techniques that involve the use of saturated salt solutions in order to maintain suitable relative humidity levels have also been mentioned.[363] Although the use of a salt solution is a simple method that allows for the attainment of accurate relative humidity conditions at room temperature, the time required for the gas in the test chamber to reach equilibrium with the solution can be extensive. Additionally, the equilibrium is lost whenever the investigator opens the chamber to insert a new sample. For this study, saturated salt solutions were not feasible due to the small dimensions of the sample cell module and the necessity that the housing be opened on a regular basis in order to exchange samples. Additionally a flowing stream of moisture-saturated carrier gas was preferred to a static, humidified environment.

A simple bubbling technique was chosen as the method for preparing humidified N_2 gas. The compressed gas was bubbled through three 1000 mL Erlenmeyer flasks connected in series using quarter-inch o.d. copper tubing and rubber stoppers. As an added safeguard, a fourth Erlenmeyer flask (500 mL) served as a trap between the water-filled flasks and the custom-built sample cell module. It was assumed here that the room-temperature nitrogen purge gas would be well saturated with moisture after passing through the saturator assembly. The design of the saturator assembly is essentially a simplification of an elegant instrument described and tested by P.R. Smith in the paper *A New Apparatus for the Study of Moisture Sorption by Starches and other Foodstuffs in Humidified Atmospheres*.[363]

Figure 38 provides a graphical illustration of the effect of moisture on SSRTP intensities. Each data point represented therein is the average of a minimum of four trials. For each individual trial, RTP intensities were obtained by recording the phosphorescence emission at λ_{max} for each spectrum. Note that the maximum average RTP signal recorded during the study was 39.4 for the 600 ppm sample that had been purged for fifteen minutes. This result approximates the typical RTP *blank* signal obtained under dry N_2 purge conditions. Furthermore, the qualitative appearance of many of the spectra obtained under these conditions was poor. Finally, for purposes of comparison, figure 38 includes a graphical representation of typical data acquired for an RTP analysis of 100 ppm naphthalene under dry nitrogen purge conditions. Except for the removal of the saturator apparatus, the analytical conditions selected for the 100 ppm measurements were consistent with those utilized during the moisture study.

---

[362] R.E. Ruskin, Ed., **Humidity and Moisture: Measurement and Control in Science and Industry, Vol. 1**, A. Wexler, Editor-in-Chief, New York: Reinhold Publishing Corp., p. 39.

[363] P.R. Smith, **Humidity and Moisture: Measurement and Control in Science and Industry, Vol. 3**, A. Wexler, Editor-in-Chief, New York: Reinhold Publishing Corp., p. 487.

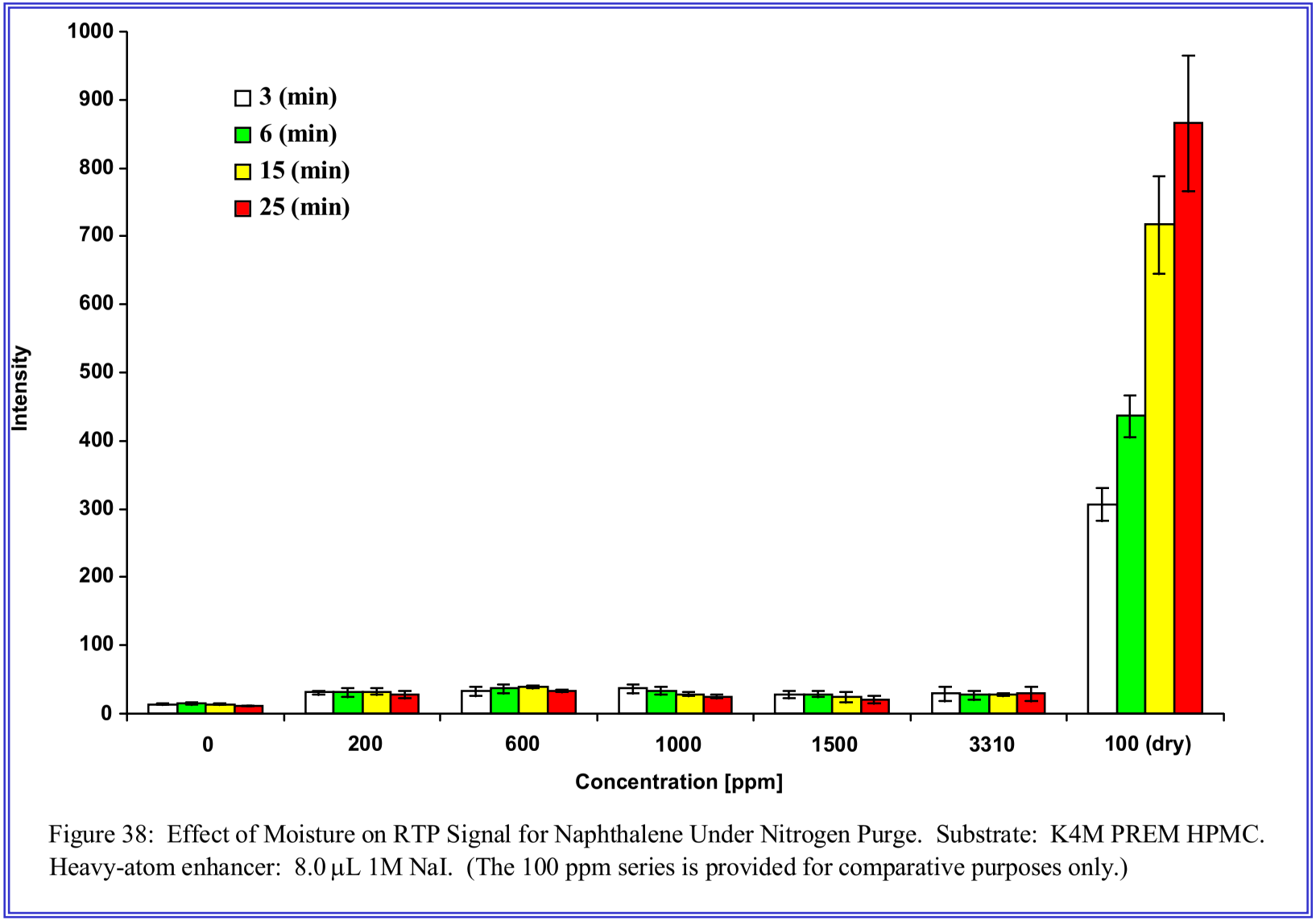

Figure 38: Effect of Moisture on RTP Signal for Naphthalene Under Nitrogen Purge. Substrate: K4M PREM HPMC. Heavy-atom enhancer: 8.0 µL 1M NaI. (The 100 ppm series is provided for comparative purposes only.)

For this series of investigations involving *K4M PREM* HPMC, it is proposed that the water molecules will compete with the naphthalene for guest sites on the surface of the host substrate and within the three-dimensional pellet matrix. This would have the effect of reversing the phosphor-support adsorption process and yielding an increased probability of collisional and vibrational quenching. It is also likely that the reduction in RTP intensity due to the adsorption of moisture is caused to an extent by the breakdown of the hydrogen-bonding network within the dry HPMC substrate. Since water is known to be an efficient swelling agent for cellulose-based materials, it is possible that the reduced RTP intensities can be attributed in part to a change in modulus of the three-dimensional HPMC matrix. In fact, for this study, the quenching of SSRTP by moisture may best be explained by considering the combined influence of each of these three individual proposals.

A separate study was carried out in order to determine the effect of dry oxygen gas on the magnitude of SSRTP intensities. Table 27 summarizes the analytical conditions used for this series of studies. Spectra were acquired at three, six, fifteen, and twenty-five minute intervals. Prior to their arrival at the sample cell module, each purge gas was passed through a cartridge of Drierite™ desiccant in order to remove trace levels of H_2O; thereby minimizing the possibility of signal quenching due to moisture.

Table 27. Analytical conditions utilized for the dry purge gas study.

substrate	*K4M PREM* HPMC
analyte	1.0 μL of 100 ppm naphthalene in ethanol
heavy-atom salt	8.0 μL of NaI in ethanol (16.5% wt/wt).
drying time	3 minutes
purge gases	dry nitrogen/dry oxygen/dry air
$\lambda_{ex.}$	273 nm
PMT	900 V
t_d	2 ms
t_g	5 ms
ex. slit	5 nm
em. slit	15 nm

Figure 39 provides a graphical representation of the results obtained from this study. Note that no SSRTP signals were evident for samples analyzed under an atmosphere of pure oxygen regardless of the duration of the dry gas purge. These results are consistent with those of RTP investigators elsewhere. Oxygen has consistently been reported to be one of the most efficient phosphorescence quenching agents.

Extremely weak RTP signals were recorded for those samples analyzed using dry U.S.P. medical air as the purge gas (21% O_2; 79% N_2). For this series of investigations, pure N_2 purge conditions yielded the strongest RTP signals. Following a twenty-five minute purge interval, the

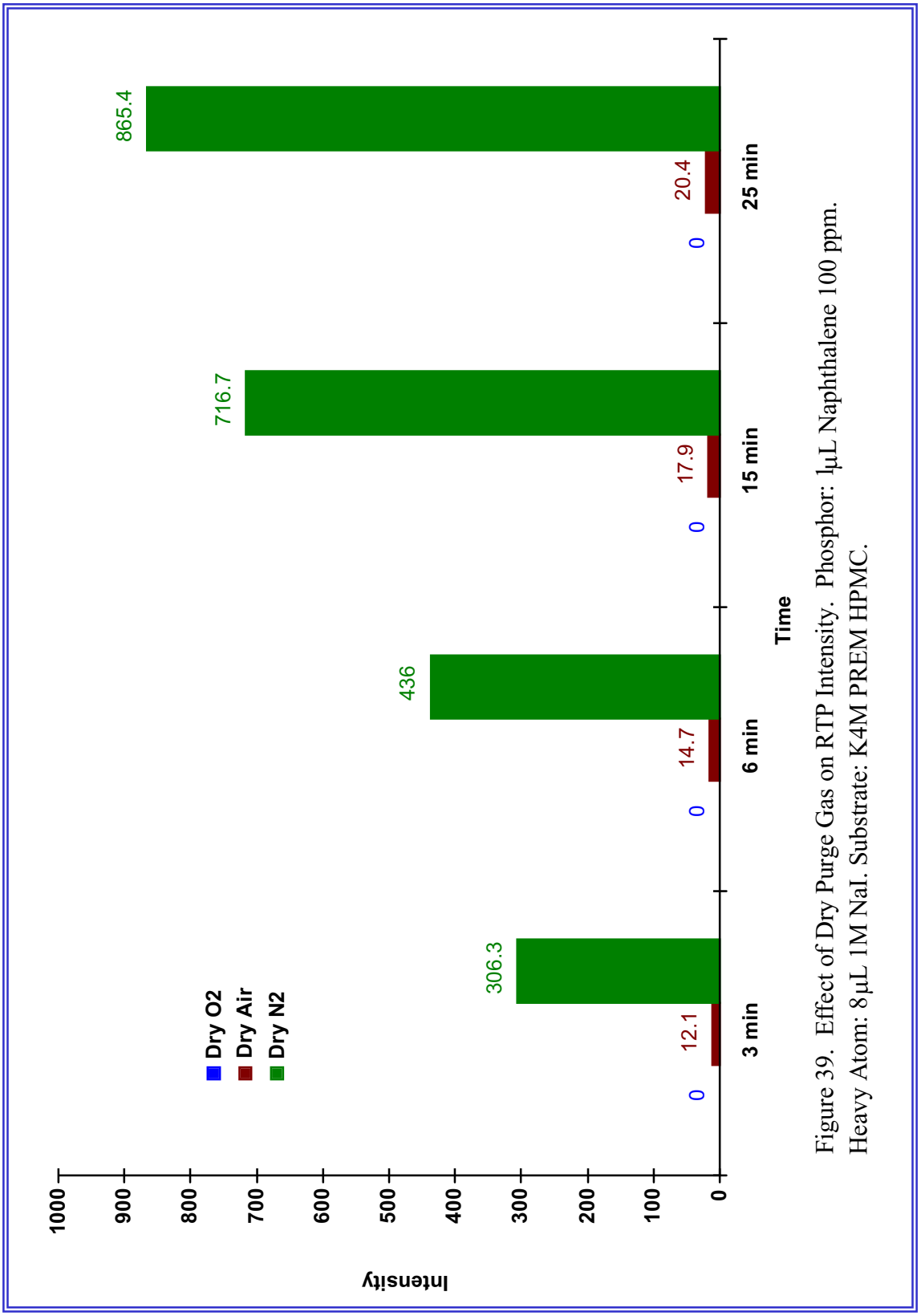

Figure 39. Effect of Dry Purge Gas on RTP Intensity. Phosphor: 1µL Naphthalene 100 ppm. Heavy Atom: 8µL 1M NaI. Substrate: K4M PREM HPMC.

RTP intensity for the dry nitrogen-purged sample was greater than the intensity of the corresponding dry air-purged sample by a factor of 42 (865.5 : 20.4).

Citta and Hurtubise have reported that moisture is a more potent quencher of RTP than oxygen for certain phosphors immobilized on filter paper.[359] This is contrary to the findings presented here for HPMC. It can be seen from figure 39 that no RTP signals were evident for those samples surrounded by pure oxygen; whereas in figure 38 weak RTP signals were observed for those samples analyzed in a moisture-laden atmosphere of nitrogen.

These studies serve to illustrate the importance of protecting RTP samples from the quenching effects of oxygen and moisture. Perhaps the simplest technique to overcome these effects is to analyze every sample under an atmosphere of dry N_2 gas. Although the sample preparation step is slightly extended by the required purge time of the system, the analyst is assured that oxygen and moisture will not interfere with the desired RTP measurements. For the remainder of the project, all RTP analyses were performed under dry nitrogen-purged conditions.

A study of the effect of different methods of heavy-atom delivery on RTP intensity.

At this time there is no general agreement within the SSRTP field regarding an optimal method of delivering the heavy-atom enhancer to the solid support material prior to performing an RTP analysis. One particular investigation has focused on four different methods.[284] However, the researchers observed no specific trends in their data that would preferentially support the selection of one procedure over any of the others. During this project, two particular methods were examined. The first involved a combined delivery of the heavy-atom and analyte. This technique required that the two components be pre-mixed in ethanol prior to their delivery. The second method relied on the individual delivery of heavy-atom and analyte solutions.

Table 28 summarizes the analytical conditions selected for this study. For the individual reagent deliveries, 1.2 mg of heavy-atom enhancer was delivered in the form of 8 μL of 1 M NaI. For the phosphor, 19.8, 39.5, or 79.0 ng was delivered in the form of 1 μL of either 25, 50, or 100 ppm naphthalene. In order to prepare pre-mixed standards of heavy-atom and phosphor, it was necessary to consider the 9 μL combined delivery volume of the two reagents. Thus, eight-ninths of the pre-mixed reagent effectively consists of 1 M NaI. The remaining one-ninth of the pre-mixed solution effectively includes naphthalene at either the 25, 50, or 100 ppm levels. The absolute quantity of heavy-atom delivered would once again be 1.2 mg; whereas the absolute quantity of phosphor would be either 19.8, 39.5, or 79.0 ng depending on which of the three standards was selected.

Table 28. Analytical conditions utilized for the heavy-atom sample delivery study.

substrate	*K4M PREM* HPMC
analyte	naphthalene (19.8 ng / 39.5 ng / 79.0 ng)
heavy-atom salt	NaI (1.2 mg)
solvent	ethanol
drying time	3 minutes
purge gas	dry N_2
$\lambda_{ex.}$	273 nm
PMT	900 V
t_d	2 ms
t_g	5 ms
ex. slit	5 nm
em. slit	15 nm

Figure 40 graphically illustrates the results obtained during the investigation. Each data point represented therein is the average of a minimum of three individual trials. Spectra were collected at three, six, and fifteen minute intervals. As noted in the figure, RTP intensities were greatest for those samples in which the heavy-atom and phosphor were delivered to the solid matrix individually. In each case, the RTP signals were greater than their counterparts by at least a factor of 2.

Effectively, when the phosphor is delivered in a large volume of solvent, it diffuses farther into, and across, the surface of the HPMC substrate. For instance, a 9 μL delivery volume will easily yield a 100% surface area coverage on a 13 mm diameter pellet; whereas a 1 μL delivery volume typically gives an approximate surface area coverage of 35.6%. These statistics become especially important when considering that the LS50 excitation beam covers only a small portion of the front surface of the pellet. The width and height of the beam as it strikes the substrate are approximately 3 mm and 7 mm, respectively. This yields an excitation beam that covers only ≈15% of the substrate surface. Thus, as the phosphor spot sizes more closely approximate dimensions of the excitation beam, it is expected that RTP intensities will be improved.

The results of this study confirm that it is advantageous to deliver the heavy-atom and phosphor to the RTP substrate individually. Since the heavy-atom is delivered prior to the analyte, the application of a relatively large volume of heavy-atom solution to the HPMC pellet surface is justified. On the other hand, relatively small volumes of analyte solution are recommended since this will minimize the diffusion of the phosphor across the surface of the pellet.

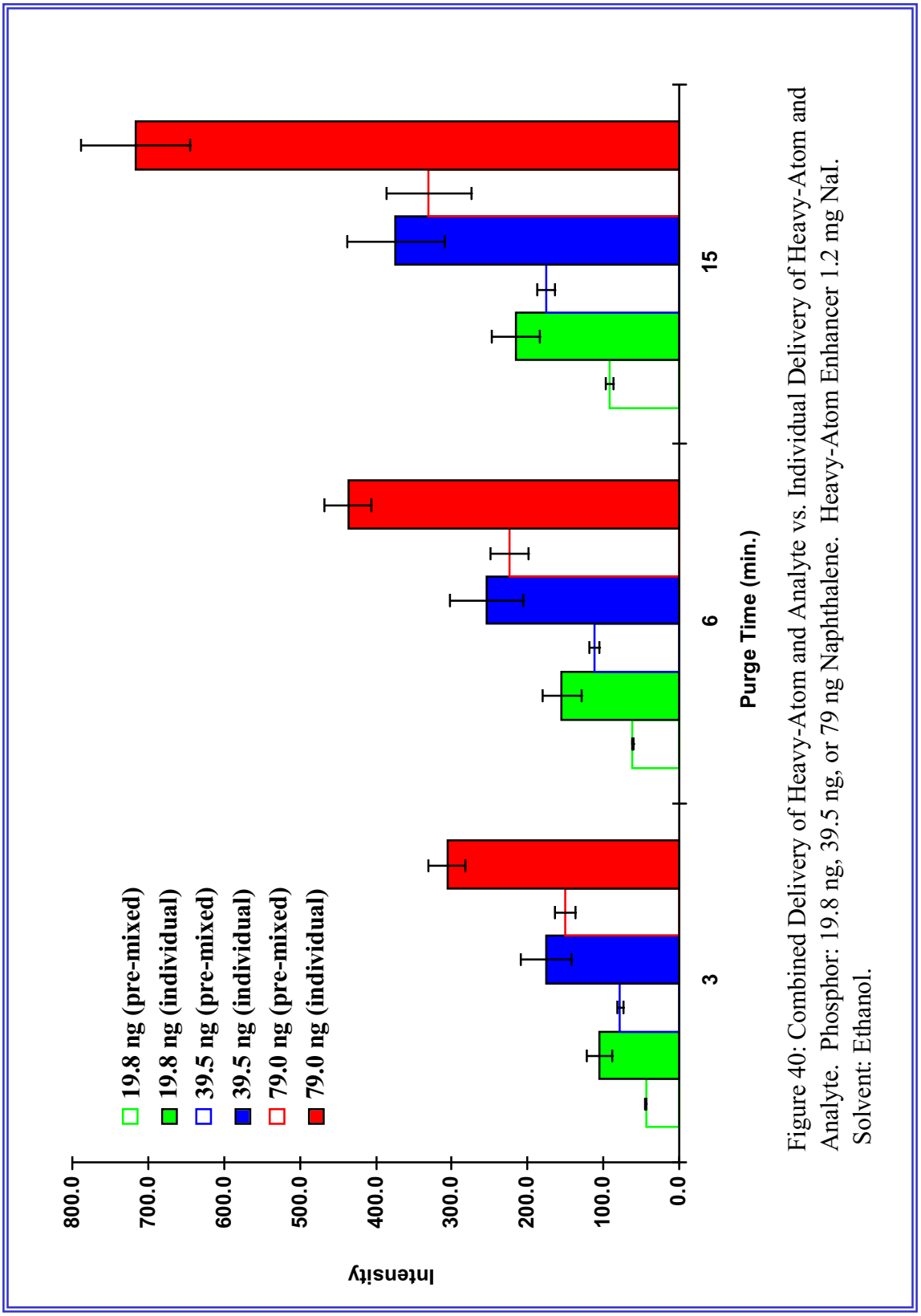

Figure 40: Combined Delivery of Heavy-Atom and Analyte vs. Individual Delivery of Heavy-Atom and Analyte. Phosphor: 19.8 ng, 39.5 ng, or 79 ng Naphthalene. Heavy-Atom Enhancer 1.2 mg NaI. Solvent: Ethanol.

A comparison of sensitivity and limit of detection for HPMC and filter paper pellets

The goal of this study was to determine which matrix material, HPMC or filter paper, would allow for the highest level of sensitivity and the lowest limit of detection (L.O.D.) for an SSRTP analysis. Naphthalene was chosen as the model phosphor. Both support materials were analyzed using the same experimental conditions as described in Table 29 in order to provide for a true comparison of results. A range of phosphor concentrations (5 ppm to 1500 ppm) was prepared volumetrically by dilution from a stock solution of naphthalene in ethanol.

Table 29. Analytical conditions utilized for the sensitivity and limit of detection study.

substrates	*K4M PREM* HPMC and P2 FisherBrand paper
analyte	1.0 μL of naphthalene in ethanol (various conc.)
heavy-atom salt	8.0 μL of NaI in ethanol (16.5% wt/wt).
drying time	3 minutes
purge gas	dry N_2
$\lambda_{ex.}$	273 nm
PMT	900 V
t_d	2 ms
t_g	5 ms
ex. slit	5 nm
em. slit	15 nm

The HPMC pellets were prepared using a pellet press and compression force of 17K PSI. The thickness of each HPMC pellet ranged from 0.048 cm to 0.056 cm. Those pellets not of uniform thickness were discarded if the variation was found to be larger than±0.005 cm. Since a direct comparison of the support materials was desired, multiple layers of filter paper were compressed in order to approximate the thickness and processing conditions of the HPMC pellets. By using 8 layers of filter paper and 17K PSI of compression force, filter paper pellets were formed having a range of thickness from 0.053 cm to 0.058 cm.

Six data points were used to prepare each calibration curve. For HPMC, these points included a background signal using heavy-atom salt only and five analyte determinations using concentrations of 5, 10, 25, 50, and 100 ppm. RTP intensities for naphthalene concentrations greater than 100 ppm were off-scale following a twenty-five minute sample purge time. For the filter paper substrate, the calibration curve included a background signal using heavy-atom salt only and five analyte determinations using concentrations of 200, 300, 600, 1000, and 1500 ppm.

Each naphthalene data point that appears within the two calibration curves is based on the calculated average of a minimum of ten experimental trials. The data point associated with the *blank* determination is based on the calculated average of a minimum of twenty experimental trials. The calibration curve derived from the HPMC study is shown in figure 41 and the calibration curve derived from the filter paper study is shown in figure 42. Both support materials

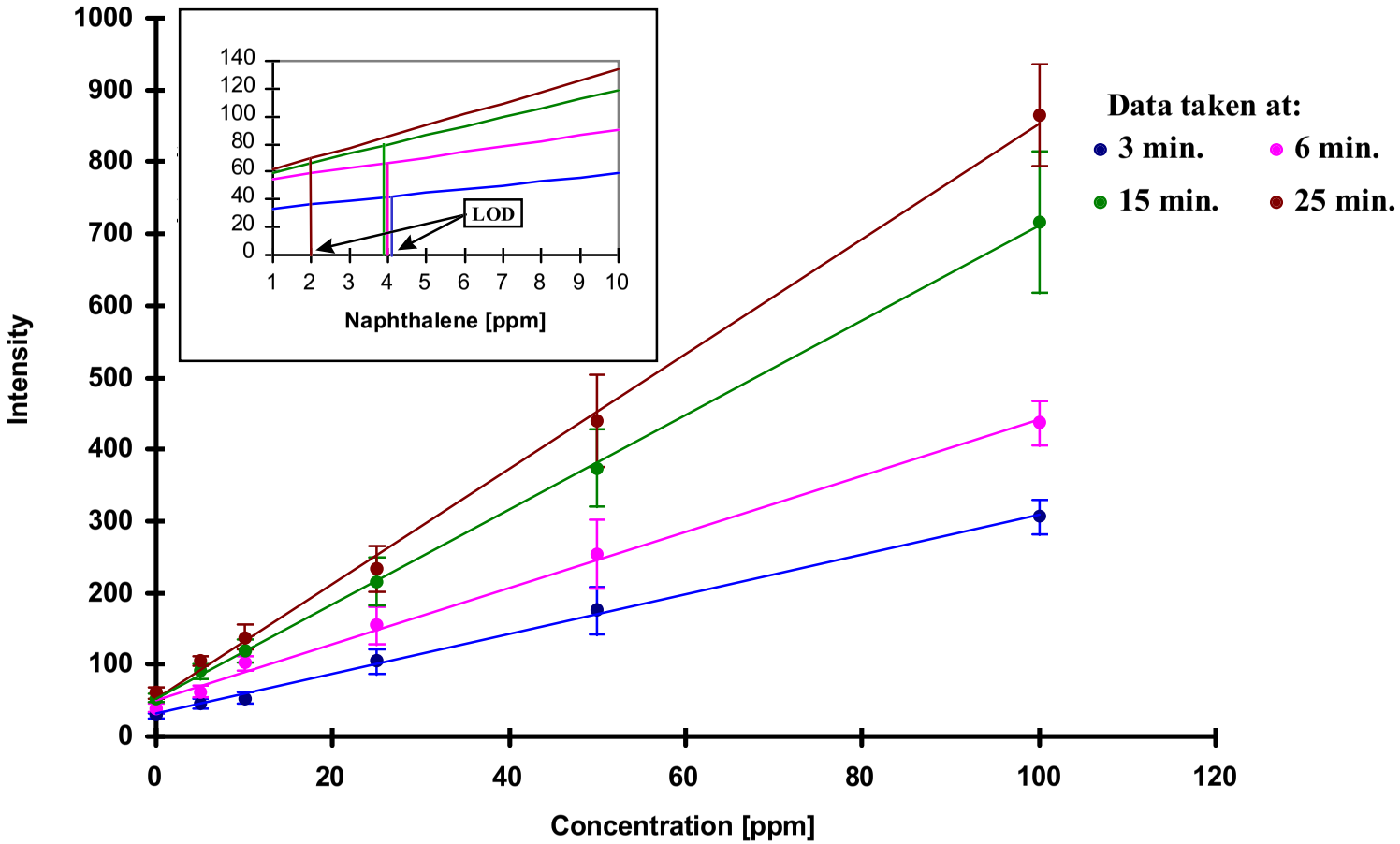

Figure 41: Limit of Detection for Naphthalene on K4M PREM HPMC. Phosphor: Naphthalene in Ethanol (Delivery Volume 1.0 μL). Heavy Atom: 8.0 μL 16.5% NaI in Ethanol.

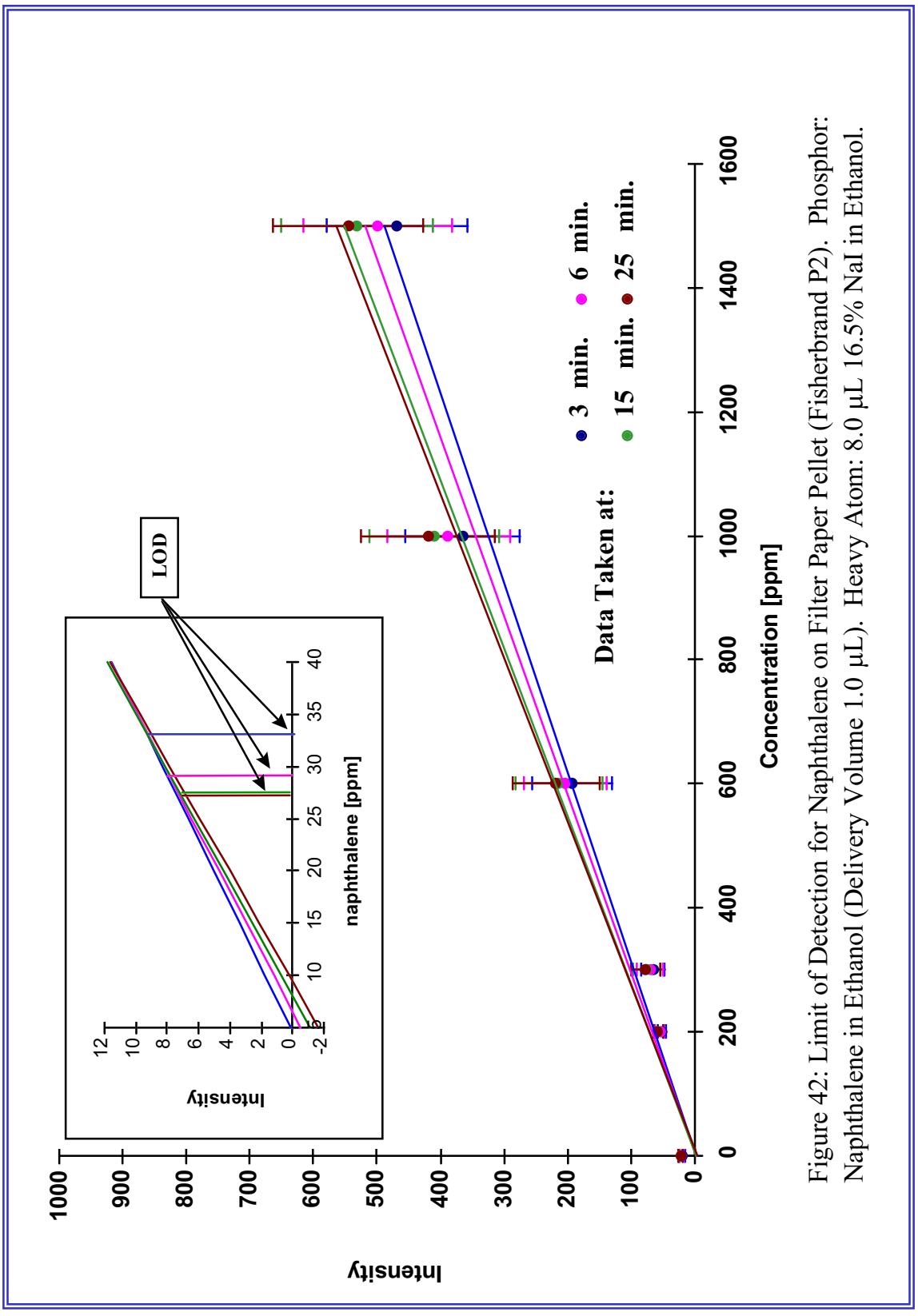

Figure 42: Limit of Detection for Naphthalene on Filter Paper Pellet (Fisherbrand P2). Phosphor: Naphthalene in Ethanol (Delivery Volume 1.0 µL). Heavy Atom: 8.0 µL 16.5% NaI in Ethanol.

yielded linear calibration curves within their respective concentration ranges. A nested graph in the upper left corner provides an enlargement of the L.O.D. region associated with each. All results are presented at the 95% confidence level.

Limits of detection were calculated using the *IUPAC approach* as described by Long and Winefordner[364] and a *propagation of errors approach* as described by Miller and Miller.[349] The IUPAC approach can only be considered to be valid if the major source of error associated with the calibration curve is in the blank determinations. Because of this limitation, the IUPAC approach will often give artificially low L.O.D. values since a measure of error is commonly associated with both the slope and y-intercept of an experimental calibration curve. Additionally, the IUPAC approach requires that the analyst perform a minimum of twenty trials in order to calculate an average that is representative of the blank signal. A disadvantage of this approach is that the determination of these blanks can often be very time-consuming. For this method, twenty such trials require an investment of ten hours of combined sample preparation and analysis time (assuming a sample drying time of three minutes and a purge time of twenty-five minutes per substrate).

The propagation of errors approach assumes that each point on the calibration curve (including the blank) has a normally distributed variation in the y-direction with a standard deviation that can be estimated by:

$$s_{y/x} = \left\{ \frac{\sum_i \left(y_i - \ddot{y}_i \right)^2}{n-2} \right\}^{\frac{1}{2}}$$

where y_i are the experimentally derived y-values and $\ddot{y}_i$ represents the fitted points on the calculated regression line corresponding to the individual x-values. The difference (y_i - $\ddot{y}_i$) is known as the *y-residual*. The number of experimental observations is represented by *n*. The degree of freedom is (n-2) for the linear regression calculation since only one straight line can be drawn through two points.[349]

Miller and Miller acknowledge that the experimental determination of s_B can be time-consuming and suggest that the use of $s_{y/x}$ in place of s_B when estimating limits of detection is valid. For this method, the calculated y-intercept is used as an estimate of y_B (the blank signal). The propagation of errors approach yields L.O.D. values that are consistent not only with the reliability of the blank determinations, but the reliability of the standards determinations as well. The results of both approaches are presented in tables 30 and 31 in accordance with recommendations given by Long and Winefordner.[364] Based on these figures of merit, it can be concluded that the *K4M PREM* HPMC is superior to the filter paper substrate when considering the sensitivity and limits of detection that can be achieved for an SSRTP analysis.

The sensitivity of an instrument measures its ability to discriminate between small differences in analyte concentration. Two factors define sensitivity: the slope of the calibration

[364] G.L. Long and J.D. Winefordner, *Anal. Chem.*, 1983, V. 55, p. 512A. Unfortunate typographical errors associated with a few mathematical expressions appear in this report. Corrections are available from the authors.

Table 30. Analytical figures of merit for *K4M PREM* HPMC pellets.

duration of dry N_2 purge	3.0 min.	6.0 min.	15.0 min.	25.0 min.
L.O.D. IUPAC approach (k=3) **standard deviation** ($\pm s_B$)	4 ppm ±4 ppm	4 ppm ±5 ppm	4 ppm ±8 ppm	2 ppm ±5 ppm
L.O.D. by propagation of errors **standard deviation** ($\pm s_{y/x}$)	4 ppm ±5 ppm	5 ppm ±11 ppm	3 ppm ±6 ppm	7 ppm ±16 ppm
correlation (R^2)	0.999	0.996	0.999	0.998
calibration sensitivity (*m*)	2.79	3.91	6.59	8.00
analytical sensitivity (γ) *5 ppm standard*	0.457	0.523	0.981	0.794
analytical sensitivity (γ) *100 ppm standard*	0.118	0.127	0.0920	0.0809
y-intercept (y_B)	30.91	51.02	53.21	53.69
limit of quantitation; L.O.Q.= $y_B + 10s_B$	(71) 14 ppm	(102) 13 ppm	(130) 12 ppm	(103) 6 ppm

Table 31. Analytical figures of merit for P2 FisherBrand filter paper pellets.

duration of dry N_2 purge	3.0 min.	6.0 min.	15.0 min.	25.0 min.
L.O.D. IUPAC approach (k=3) **standard deviation** ($\pm s_B$)	33 ppm ± 4 ppm	29 ppm ± 3 ppm	27 ppm ± 3 ppm	27 ppm ± 3 ppm
L.O.D. by propagation of errors **standard deviation** ($\pm s_{y/x}$)	342 ppm ± 30 ppm	340 ppm ± 31 ppm	334 ppm ± 32 ppm	334 ppm ± 33 ppm
correlation (R^2)	0.980	0.990	0.991	0.991
calibration sensitivity (*m*)	0.326	0.347	0.369	0.379
analytical sensitivity (γ) *200 ppm standard*	0.0460	0.0493	0.0507	0.0498
analytical sensitivity (γ) *1500 ppm standard*	0.00294	0.00299	0.00310	0.00318
y-intercept (y_B)	-1.52	-2.24	-2.97	-3.54
limit of quantitation; L.O.Q.= $y_B + 10s_B$ (assuming here that $y_B = 0$)	(35.6) 109 ppm	(33.2) 96 ppm	(33.7) 91 ppm	(33.5) 88 ppm

curve and the precision (or reproducibility) of the analysis. For two methods that have equal precision, the one with the steeper calibration curve will be more sensitive. The IUPAC definition of sensitivity is referred to as *calibration sensitivity*.[365] Given a linear calibration curve, calibration sensitivity is independent of analyte concentration and is determined by the slope (*m*) of the straight line. It can be argued that this definition is incomplete since it fails to address the precision associated with each of the observations within the data set.

As illustrated by the calibration curves (figures 41 and 42) and the statistical data (tables 30 and 31), the calibration sensitivity (*m*) varies significantly for the HPMC investigations. On the other hand, the calibration sensitivity (*m*) varies minimally for the filter paper pellets. Obviously, the HPMC substrates are much more sensitive to the duration of dry gas purge than the filter paper substrates. Figure 43 provides a comparison of the HPMC calibration sensitivities corresponding to the four different analysis times. At extended purge times, RTP intensities are much improved for the HPMC supports ($m = 8.00$ vs. $m = 2.79$); whereas the filter paper substrates show only marginal improvement ($m = 0.379$ vs. $m = 0.326$).

An alternative definition of sensitivity is given by the *analytical sensitivity* (γ) as proposed by Mandel and Stiehler.[366] The analytical sensitivity is the slope of the calibration curve (*m*) divided by the standard deviation of the signals. An advantage associated with the analytical sensitivity is that it is relatively insensitive to amplification factors. Although analytical sensitivity is independent of the units of the measured signal, it is often concentration dependent since the standard deviation of the signals can vary with concentration.

The limit of quantitation[367] (L.O.Q.) is defined as the lowest concentration at which quantitative measurements can be made using a particular analytical method. Although this figure of merit has not yet been widely adopted by the analytical community, it nevertheless serves as a useful benchmark for the investigator when considering the lowest limit of precise *quantitative* measurement that can be achieved as opposed to the *qualitative* detection limit described by the L.O.D. For each of the L.O.Q. determinations found in Table 30, the associated values denoted within parenthesis are the corresponding RTP intensities.

---

[365] D.A. Skoog and J.J. Leary, **Principles of Instrumental Analysis, 4th Ed**, New York: Saunders College Publishing, 1992.

[366] J. Mandel and R.D. Stiehler, *J. Res., Natl., Bur. Std.*, 1964, V. A53, p. 155.

[367] "Guidelines for Data Acquisition and Data Quality Evaluation in Environmental Chemistry", *Anal. Chem.*, 1980, V. 52, p. 2242.

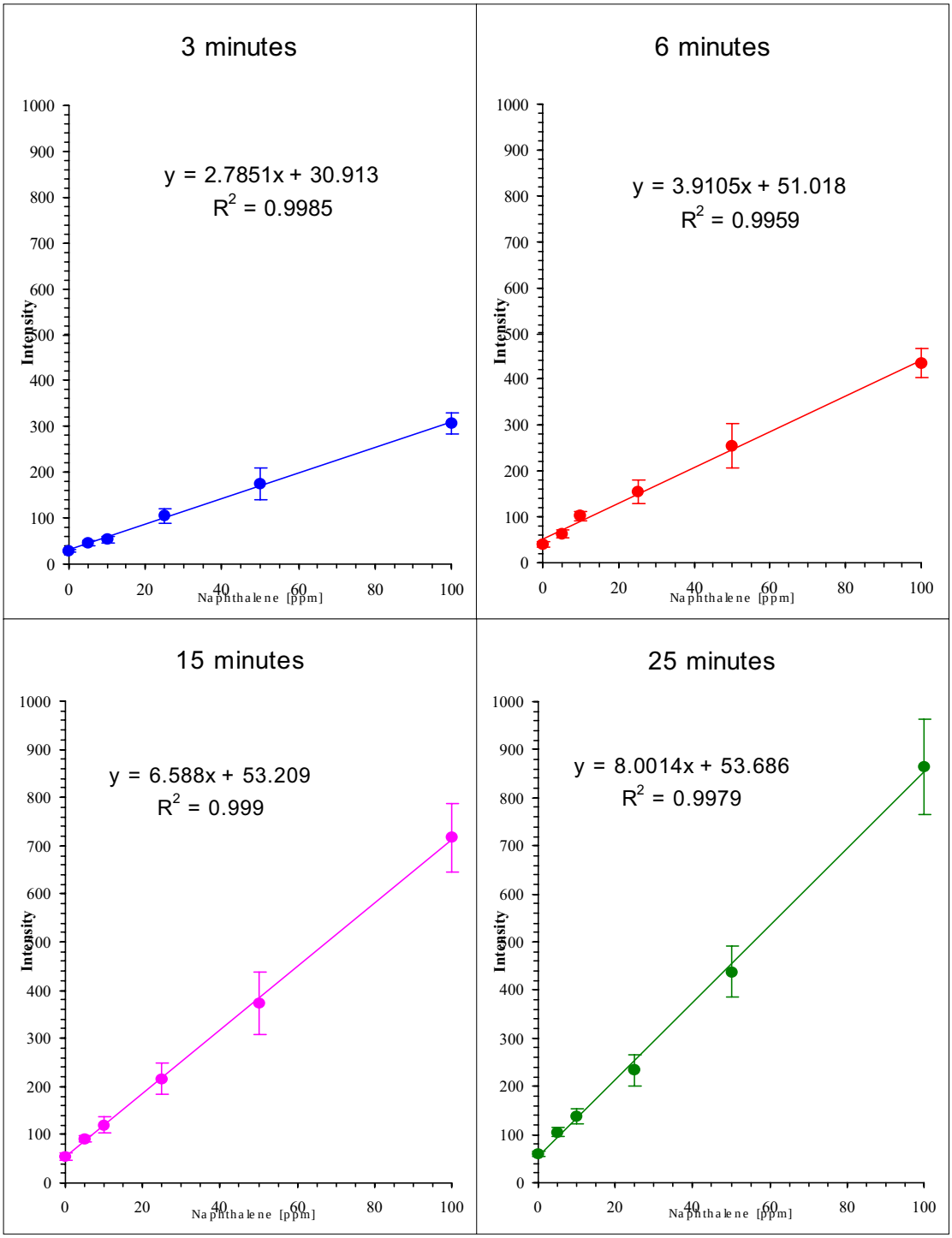

Figure 43: Calibration curves prepared for naphthalene on *K4M PREM* HPMC pellets at four different analysis times.

A study of the relationship between external heavy-atom salt concentration and SSRTP intensity

Although most SSRTP investigators regularly exploit the external heavy-atom effect in order to improve experimental phosphorescence intensities, few detailed studies regarding this enhancement effect have been published.[27,284,368,369] Vo-Dinh has proposed that there are three distinguishable heavy-atom concentration ranges for studies carried out on filter paper matrices.[284] For heavy-atom concentrations less than 0.01 M, there is an insufficient amount of heavy-atom present in the sample spot to induce significant phosphorescence enhancement. At moderate concentrations greater than 0.01 M, RTP intensities increase as the heavy-atom concentration increases. At high concentrations, saturation effects are evident. An increase in heavy-atom concentration yields either minimal RTP intensity improvement or no signal enhancement at all. Winefordner and colleagues propose that the heavy-atom might compete with the phosphor for binding sites on the filter paper or that the heavy-atom decreases the interaction of the analyte with the filter paper by forming a layer between them.[368]

During this project, two heavy-atom investigations were completed. For the first study, the initial concentration range of NaI in ethanol was 0 to 0.05 M. The analyte was naphthalene at a concentration of 415 ppm (2.56×10^{-3} M) in ethanol. RTP spectra were recorded at three, six, and fifteen minute intervals for each individual sample. The specific analytical conditions relating to this study are described in Table 32. Figure 44 graphically illustrates the results of the first series of investigations. Each data point found within the graph is the average of at least nine individual trials.

Table 32. Analytical conditions utilized for the heavy-atom enhancer study.

substrate	*K4M PREM* HPMC
analyte	1.0 μL of naphthalene in ethanol (100 ppm or 415 ppm)
heavy-atom salt	8.0 μL of NaI in ethanol 0.25% to 16.5% (wt/wt)
drying time	3 minutes
purge gas	dry N_2
$\lambda_{ex.}$	273 nm
PMT	900 V
t_d	2 ms
t_g	5 ms
ex. slit	5 nm
em. slit	15 nm

[368] I.M. Khasawneh, M. Chamsaz, and J.D. Winefordner,*Anal. Lett.*, 1988, V. 21, p. 125.
[369] I.M. Jakovljevic, *Anal. Chem.*, 1977, V. 49, p. 2048.

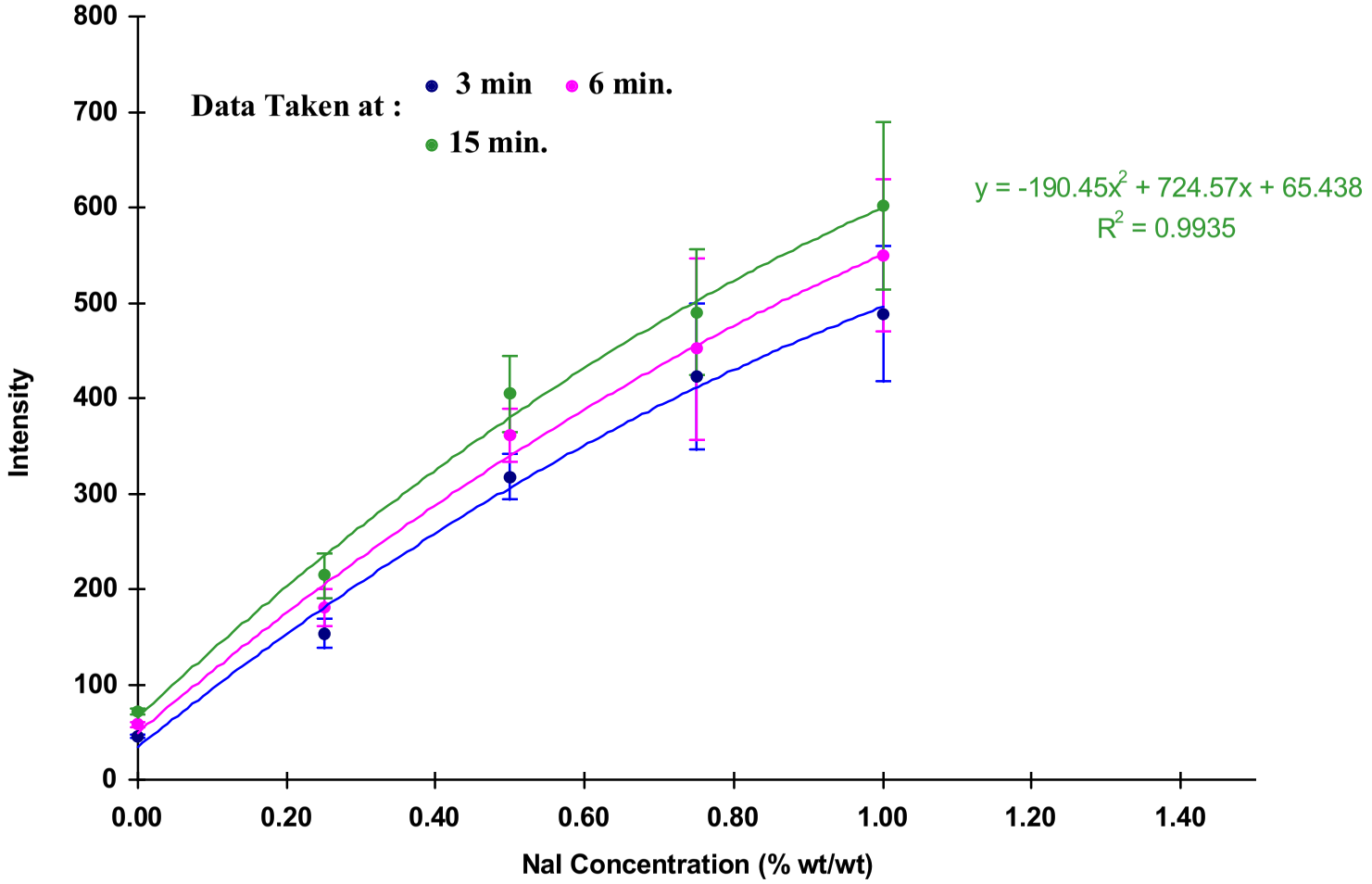

Figure 44: Effect of Heavy Atom Salt on RTP Intensity Using K4M PREM HPMC Substrates. Phosphor: 1.0 µL of 415.0 ppm Naphthalene in Ethanol. Heavy Atom: 8.0 µL of 0 to 1.0% NaI in Ethanol.

A statistical analysis tool bundled with Microsoft Excel™ spreadsheet software was used to identify direct relationships between heavy-atom concentration and RTP intensities. For this series of observations, the relationship between heavy-atom and RTP signal was best described by a polynomial curve. The resulting equation that most closely approximates the 15-minute data series is found in figure 44 ($R^2 = 0.994$).

A subsequent study was devised to examine the effect of higher NaI concentrations on RTP intensity. For this series, the concentration range of NaI in ethanol was 0 to 1 M. The analyte was naphthalene at a concentration of 100 ppm (6.17×10^{-4} M)in ethanol. RTP spectra were recorded at three, six, and fifteen minute intervals for each individual sample. The specific analytical conditions relating to this study are described in Table 32. Figure 45 provides a graphical illustration of the results of this series of investigations. Each data point found within the graph is the average of at least nine individual trials. An attempt was also made to identify a direct relationship between heavy-atom concentration and corresponding RTP intensity for these data sets. In contrast to the low concentration heavy-atom results using 415 ppm phosphor, it was discovered that linear curve-fits were the best approximations of the analytical data obtained for the expanded NaI concentration range. These discoveries for the HPMC/naphthalene/NaI system agree with similar findings for a filter paper/10^{-3} M phenanthrene/NaI system as reported by Vo-Dinh.[284]

Vo-Dinh has noted that "Saturation does not depend solely upon the absolute concentration of heavy-atoms but also upon the relative ratio between heavy-atoms and analytes."[284] Table 33 provides a comparison of the relative ratios of NaI to naphthalene for this study. Figure 46 is based on the calculations obtained in Table 33. It confirms that the concentration of NaI (% wt/wt) is not directly proportional to the relative ratio of NaI molecules to naphthalene molecules.

Vo-Dinh has also reported that "Since most heavy-atoms are near their solubility limits at 0.5-2M concentration range, the analyte concentrations should also be equal to or less than 10^{-3} in order to satisfy the requirement for saturation.".[284] Nevertheless, for these investigations, saturation effects were not positively identified for NaI at the 1 M (16% wt/wt) concentration level with 79 ng of naphthalene present.[368] However, the existence of a saturation peak might be possible at higher NaI concentrations and lower concentrations of naphthalene. Unfortunately, the preparation of standard NaI/ethanol solutions at concentrations much greater than 16.5 % wt/wt (approximately 1 M) is not possible due to the solubility limitations encountered for this particular system.

Table 33. Relative ratios of NaI in 8 μL sample volume to naphthalene in 1 μL sample volume (molecules NaI : molecules naphthalene).*

%NaI (wt/wt)	NaI (mol/L)	NaI (mg)	NaI molecules	naph. molecules	NaI **:** naph.
0	0	0	0	3.72×10^{14}	0 : 1
0.25	0.013	0.0158	6.36×10^{16}	3.72×10^{14}	171 : 1
0.50	0.026	0.0318	1.28×10^{17}	3.72×10^{14}	343 : 1
0.75	0.040	0.0478	1.92×10^{17}	3.72×10^{14}	515 : 1
1.0	0.053	0.0636	2.55×10^{17}	3.72×10^{14}	686 : 1
4.0	0.219	0.263	1.05×10^{18}	3.72×10^{14}	2,830 : 1
8.0	0.458	0.550	2.20×10^{18}	3.72×10^{14}	5,920 : 1
12.0	0.718	0.862	3.46×10^{18}	3.72×10^{14}	9,310 : 1
16.0	1.00	1.20	4.82×10^{18}	3.72×10^{14}	13,000 : 1

*(Naphthalene = 100 ppm = 6.17×10^{-4} M = 79 ng = 3.72×10^{14} molecules).

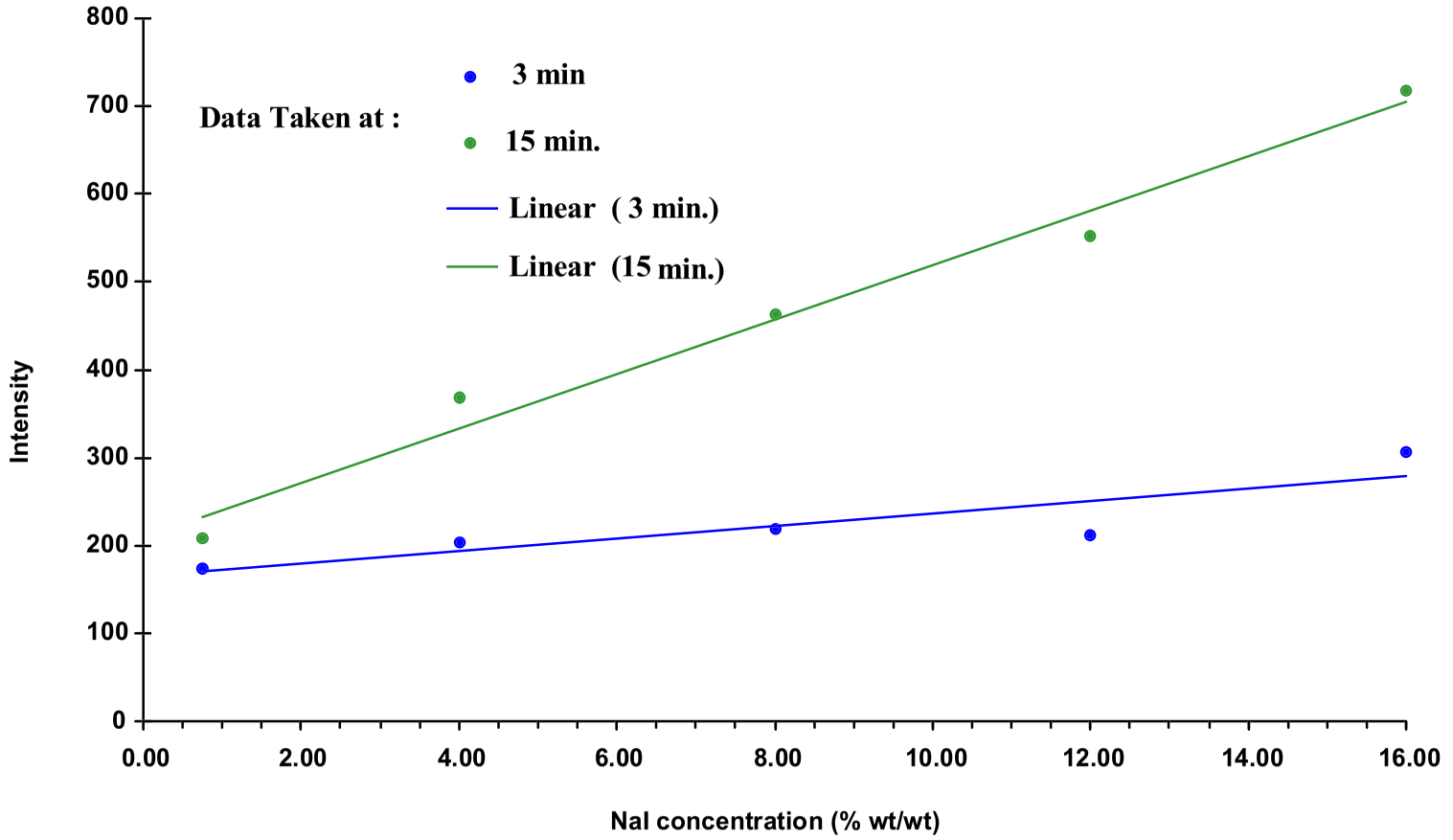

Figure 45: Effect of External Heavy Atom Salt on RTP Intensity using *K4M PREM* HPMC Substrates.
Phosphor: 1.0 µL of 100 ppm Naphthalene in Ethanol. Heavy Atom: 8.0 µL of NaI in Ethanol (0.75% to 16.5% wt/wt).

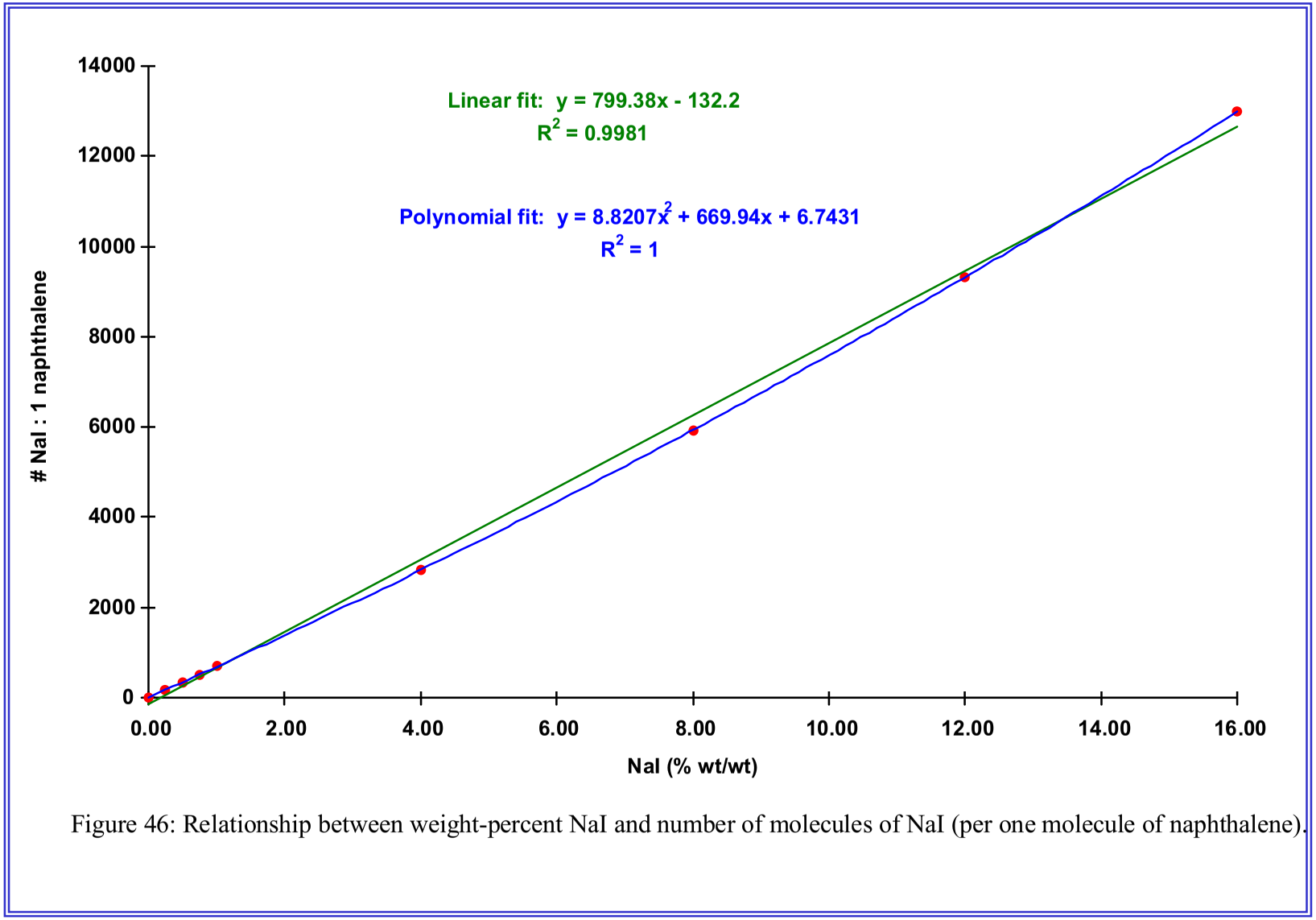

Figure 46: Relationship between weight-percent NaI and number of molecules of NaI (per one molecule of naphthalene).

A study to examine potential relationships between HPMC pellet thickness and SSRTP intensity

Modifications to the Perkin-Elmer front surface accessory allowed for the initiation of an investigation to determine if RTP intensities are dependent upon the thickness of the HPMC substrate. Prior to this study, all HPMC pellets were prepared to have a thickness of 0.048 cm to 0.056 cm.

Four sets of HPMC pellets were produced for this study. These four sets included pellets having the following thickness: 0.046 cm, 0.056 cm, 0.066 cm, and 0.084 cm. Following removal from the pellet press die, a Vernier caliper was used to determine the thickness of each pellet. Those pellets not of uniform thickness were discarded if the variation was found to be larger than ±0.005 cm. Each pellet was coded on one side using a pencil so that they could be individually catalogued according to their thickness.

It was not possible to prepare substrates having a thickness of less than 0.046 cm on a regular basis. Pellets thinner than 0.046 cm require less than 0.05g of starting material. Often, this small amount of starting material does not uniformly cover the faces of the polished dies. This results in the manufacture of pellets that do not have a uniform, reproducible thickness. Additionally, as HPMC pellets become thinner, they also become increasingly fragile and more difficult to remove from the pellet press die.

The design of the Perkin-Elmer front-surface accessory allows for the *front surface* of each solid support material to be reproducibly positioned with respect to the distance from the LS50 excitation slit. This is advantageous since the custom-built sample cell module only allows for the *rear surface* of the substrate to be reproducibly positioned with respect to the distance from the excitation slit.

Prior to using the front-surface accessory, the sample holder was aligned according to a standard procedure recommended by Perkin-Elmer. The LS50 was operated in **READ** mode in order to monitor the effect of accessory adjustments on RTP signal. In **READ** mode, the LS50 provides continuous RTP signal intensity updates at regular intervals rather than full spectral scans. Table 34 summarizes the analytical conditions selected for this investigation.

Table 34. Analytical conditions utilized for the pellet thickness study.

substrate	*K4M PREM* HPMC (thickness = 0.046, 0.056, 0.066, or 0.084 cm)
analyte	1.0 μL of naphthalene in ethanol (10 ppm)
heavy-atom salt	8.0 μL of NaI in ethanol (1 M)
drying time (NaI)	3 minutes
drying time (naph.)	2 minutes
purge gas	dry N_2
$\lambda_{ex.}$	273 nm
PMT	900 V
t_d	2 ms
t_g	5 ms
ex. slit	5 nm
em. slit	15 nm

Figure 47 is a graphical representation of the experimental data collected during this study. As illustrated by the graph, RTP intensity appears to be independent of HPMC pellet thickness within the range of 0.046 cm to 0.084 cm. For a given duration of dry N_2 purge, the RTP signal yielded by a single substrate is within the calculated experimental error of each of the others regardless of substrate thickness.

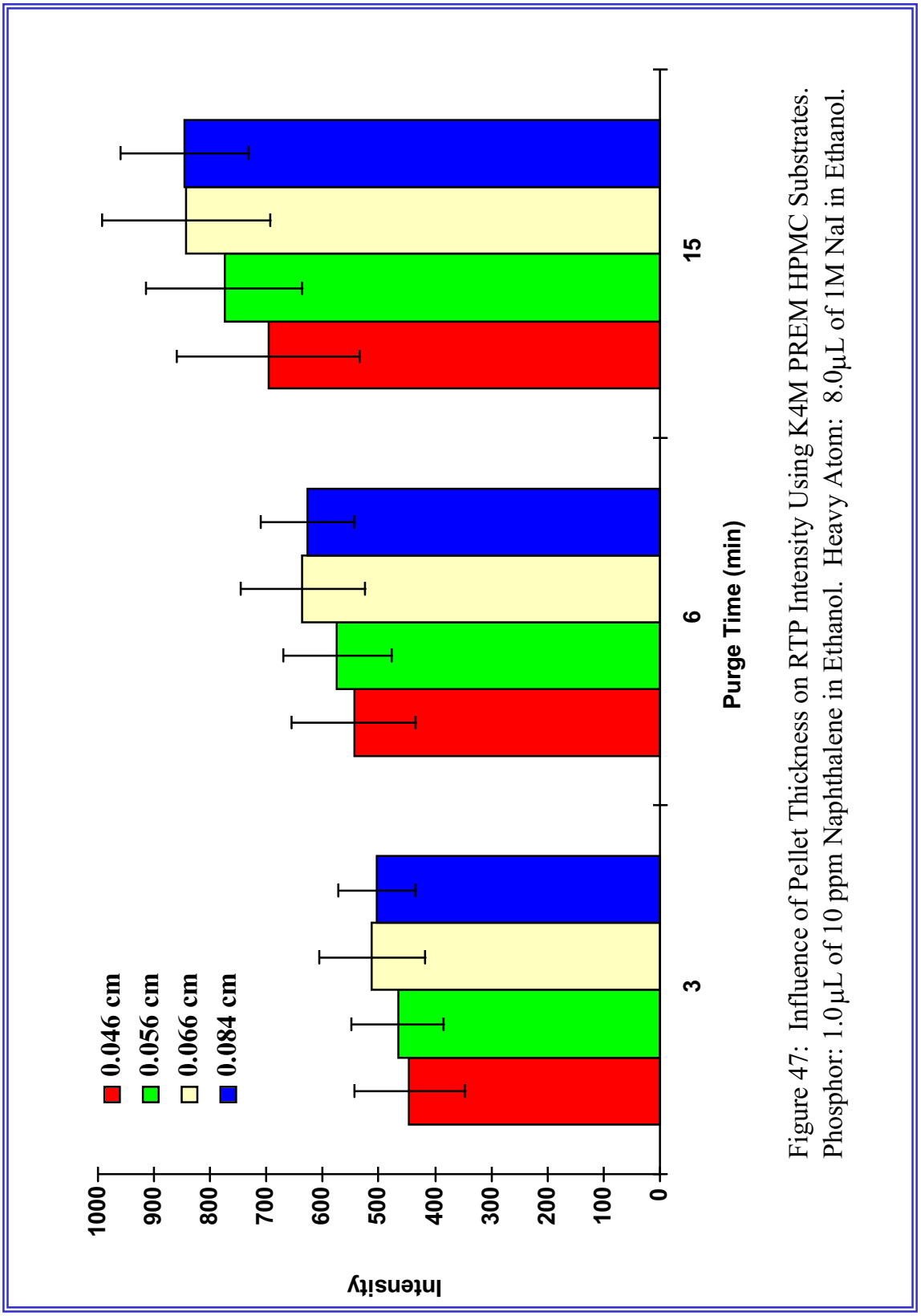

Figure 47: Influence of Pellet Thickness on RTP Intensity Using K4M PREM HPMC Substrates. Phosphor: 1.0 µL of 10 ppm Naphthalene in Ethanol. Heavy Atom: 8.0µL of 1M NaI in Ethanol.

Studies involving the modified Perkin-Elmer front-surface luminescence accessory

Early comparisons of the HPMC and filter paper support materials necessitated that *filter paper pellets* be prepared in order to maintain a constant substrate thickness. These pellets were merely multiple layers of P2 FisherBrand™ filter paper fused together in a die at 17K PSI using a hydraulic pellet press. This allowed for direct comparisons of the HPMC and filter paper substrates using the custom-built sample cell module. However, during the final phases of the project, a Perkin-Elmer (P-E) front-surface accessory was acquired on loan. Following substantial modification, the front-surface accessory allowed for substrates of any thickness to be utilized as solid supports for SSRTP analyses. Thus, a study was initiated in order to determine if uncompressed, single-layer filter paper discs yield improved RTP intensities compared to the *K4M PREM* HPMC pellets. A summary of the analytical conditions selected for this study is found in Table 35.

Table 35. Analytical conditions utilized for the single-layer filter paper substrate study.

substrate	normal P2 FisherBrand filter paper
analyte	1.0 μL of naphthalene in ethanol (10 ppm or 25 ppm)
heavy-atom salt	8.0 μL of NaI in ethanol (1 M)
drying time (NaI)	3 minutes
drying time (naph.)	2 minutes
purge gas	dry N_2
$\lambda_{ex.}$	273 nm
PMT	900 V
t_d	2 ms
t_g	5 ms
ex. slit	5 nm
em. slit	15 nm

Figure 48 provides a graphical representation of the results of this study. Two observations warrant discussion. First, the background (or *blank*) RTP signal associated with normal filter paper is quite high when using the modified Perkin-Elmer accessory. On the other hand, suitable qualitative naphthalene spectra are readily obtained at the 10 and 25 ppm levels when using this accessory. Next, note that the RTP intensities associated with each series are nearly independent of the duration of dry N_2 purge. The RTP signals obtained following a 15-minute interval of N_2 purge are only minimally greater in intensity than the RTP signals associated with those spectra acquired at the three minute mark. This can be attributed to the macroscopic porosity of the filter paper substrate. Residual solvent, moisture, and oxygen are more quickly

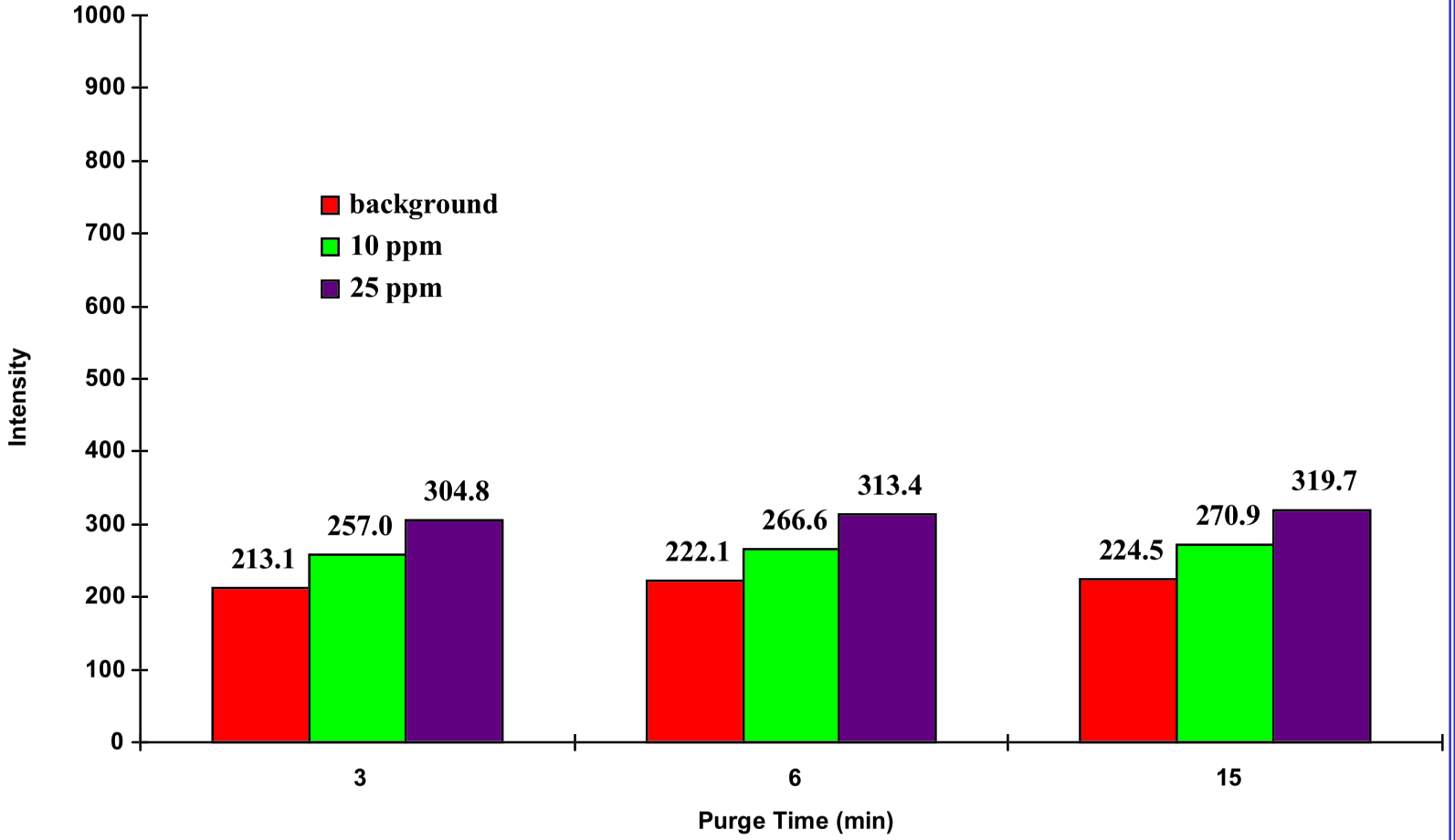

Figure 48: Single-Layer Filter Paper Substrate Study (Perkin-Elmer Accessory) .
Phosphor: 1.0 µL of Naphthalene in Ethanol (10 ppm or 25 ppm). Heavy Atom: 8.0 µL of NaI in Ethanol (1 M).

purged from within the filter paper matrix. Thus, when using normal filter paper discs as SSRTP substrates, the duration of dry N_2 purge could be minimized in order to allow the spectroscopist to collect a greater number of SSRTP spectra in a shorter period of time. This would be especially advantageous for laboratories that might be faced with heavy sample loads (for example, quality control or environmental analysis).

For purposes of comparison, the next series of investigations utilize the same analytical conditions as summarized in Table 35. However, in this instance, *K4M PREM* HPMC pellets are substituted for the filter paper discs. Figure 49 provides a graphical representation of the results of this study. Two observations warrant further discussion. First, the background (or blank) RTP signal associated with the compressed HPMC pellet is quite high in comparison to experimental background intensities obtained when using the custom-built sample cell module. The background signal is greater than 200 at a purge time of three minutes. When using the custom-built sample cell module, background signals for *K4M PREM* HPMC barely exceed an RTP intensity of 50 regardless of the duration of dry N_2 purge.

Furthermore, note that the RTP intensities associated with each series are not independent of the duration of dry N_2 purge. In fact, the RTP signal produced by the 25 ppm naphthalene sample following a 15-minute N_2 purge is off-scale. In addition to the 10 and 25 ppm samples discussed here, it was also possible to obtain qualitative RTP emission spectra for naphthalene at the 5 ppm level using *K4M PREM* HPMC pellets. However, naphthalene phosphorescence at the 2.5 ppm level could not be distinguished from background phosphorescence derived from the analytical blank.

In addition to these particular naphthalene determinations, the P-E accessory also allowed for the acquisition of qualitative RTP spectra for phenanthrene at the 1 ppm (0.8 ng) level using HPMC as the sample matrix. However, phenanthrene spectra at the 100 ppb (8 pg) level could not be qualitatively distinguished from the analytical blank.

Based on these preliminary results, it appears that the modified P-E front surface accessory will allow for moderately improved qualitative limits of detection in comparison to the custom-built RTP sample cell module. This minor improvement in sensitivity can be attributed to the enhanced alignment capabilities associated with the P-E device. An arrangement of tensioning springs and adjustment screws permits the operator to optimize the placement of the sample substrate with respect to the LS50 excitation beam. The custom-built SSRTP sample cell module and sample holder do not currently provide the investigator with these supplementary degrees of freedom.

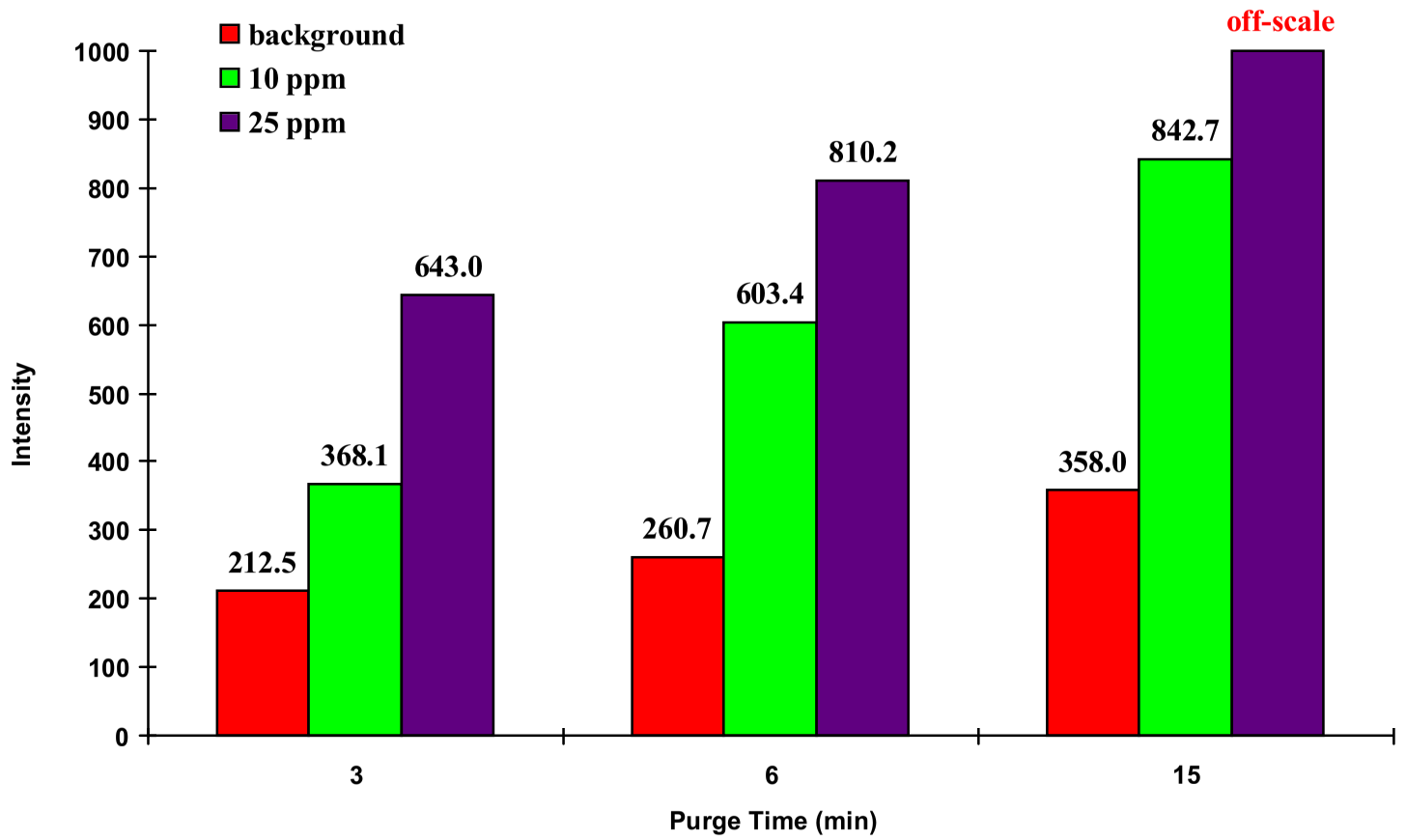

Figure 49: K4M PREM HPMC Substrate Study (Perkin-Elmer Accessory) .
Phosphor: 1.0 μL of Naphthalene in Ethanol (10 ppm or 25 ppm). Heavy Atom: 8.0 μL of NaI in Ethanol (1 M).

A modest library of SSRTP emission spectra acquired from an array of model phosphors trapped on *K4M PREM* HPMC substrates

The foremost advantage associated with the use of filter paper as an RTP support material rests with the ability of the media to provide emission spectra for nearly all phosphors. At this time, filter paper is considered to be a universally applicable matrix material for SSRTP investigations. In order to probe the potential of HPMC to serve as a universal SSRTP support material, a series of model phosphors were analyzed. SSRTP emission spectra were obtained for each analyte trapped on *K4M PREM* HPMC pellets. Table 36 summarizes the analytical conditions utilized for this series of investigations. Table 37 provides a catalogue of the model phosphors investigated. The emission spectra are plotted in figures 50 through 57. Background phosphorescence derived from the analytical blank is shown in blue; whereas the analyte RTP emission is plotted in red.

Table 36. Analytical conditions utilized for the preparation of a library of SSRTP emission spectra.

substrate	*K4M PREM* HPMC
analyte	1.0 μL of phosphor in ethanol
heavy-atom salt	8.0 μL of NaI in ethanol (1 M)
drying time (NaI)	3 minutes
drying time (phosphor)	2 minutes
purge gas	dry N_2
$\lambda_{ex.}$	varies according to phosphor
PMT	900 V
t_d	2 ms
t_g	5 ms
ex. slit	5 nm
em. slit	15 nm

Table 37. Catalogue of SSRTP emission spectra.

phosphor	concentration	$\lambda_{ex.}$	figure #
acenaphthene	200 ppm	296 nm	50
naphthalene	100 ppm	273 nm	51
2-naphthoic acid	200 ppm	280 nm	52
2-naphthol	400 ppm	290 nm	53
p-aminobenzoic acid (PABA)	50 ppm	284 nm	54
phenanthrene	5 ppm	260 nm	55
salicylic acid, sodium salt	200 ppm	297 nm	56
triphenylene	100 ppb	260 nm	57

Strong SSRTP emission spectra were acquired for each of these model phosphors using *K4M PREM* HPMC as the matrix material. Excellent spectral resolution is observed. Future SSRTP studies involving hundreds of phosphors will certainly be necessary in order to confirm or refute these preliminary findings. Nevertheless, this inaugural study illustrates the potential of *K4M PREM* HPMC to serve as a universal RTP matrix material.

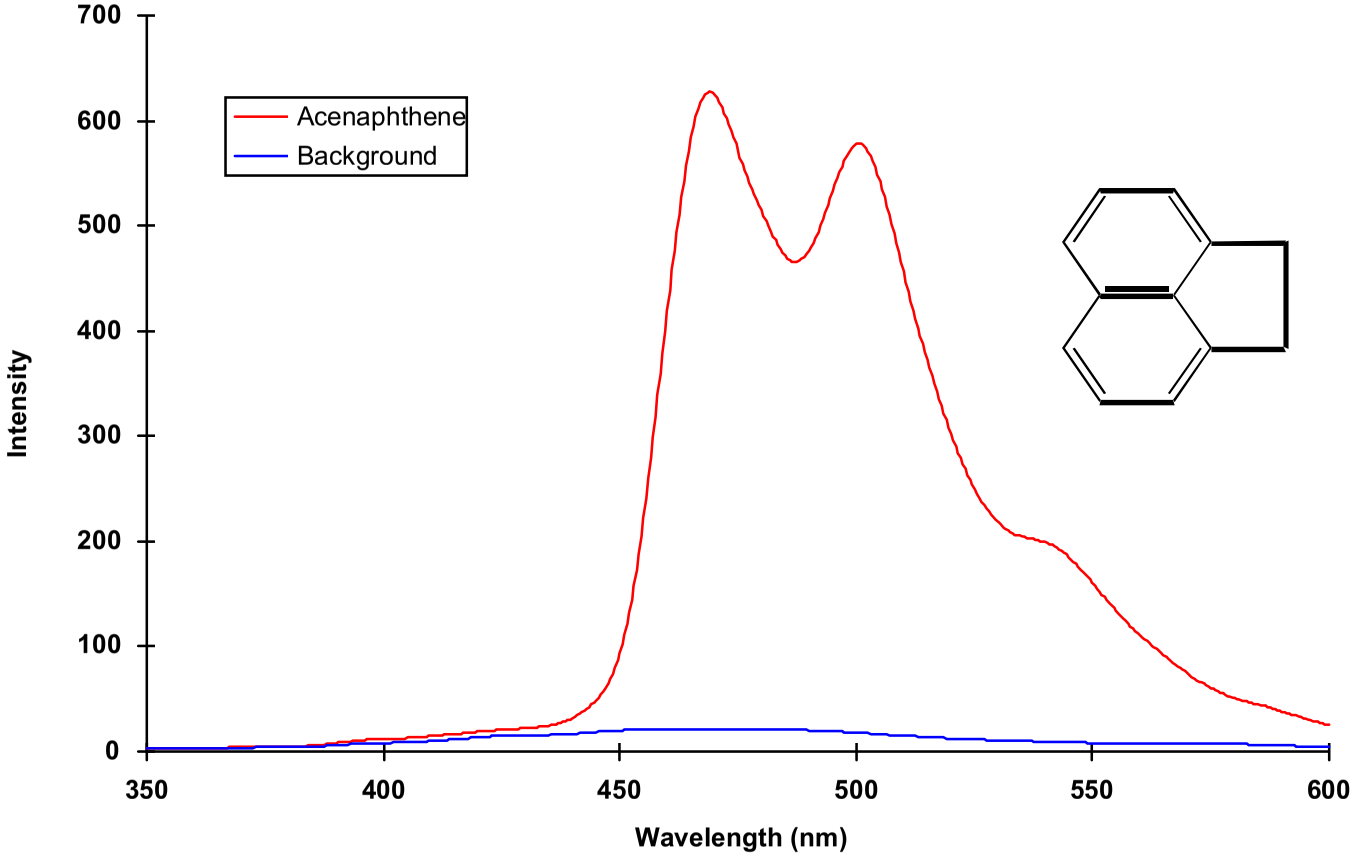

Figure 50: Representative Acenaphthene Emission Spectrum.
Phosphor: 1.0 μL of 200 ppm Acenaphthene in Ethanol. Substrate: K4M PREM HPMC.
Heavy Atom: 8.0μL of 16.5 % NaI in Ethanol. Excitation Wavelength: 296 nm.

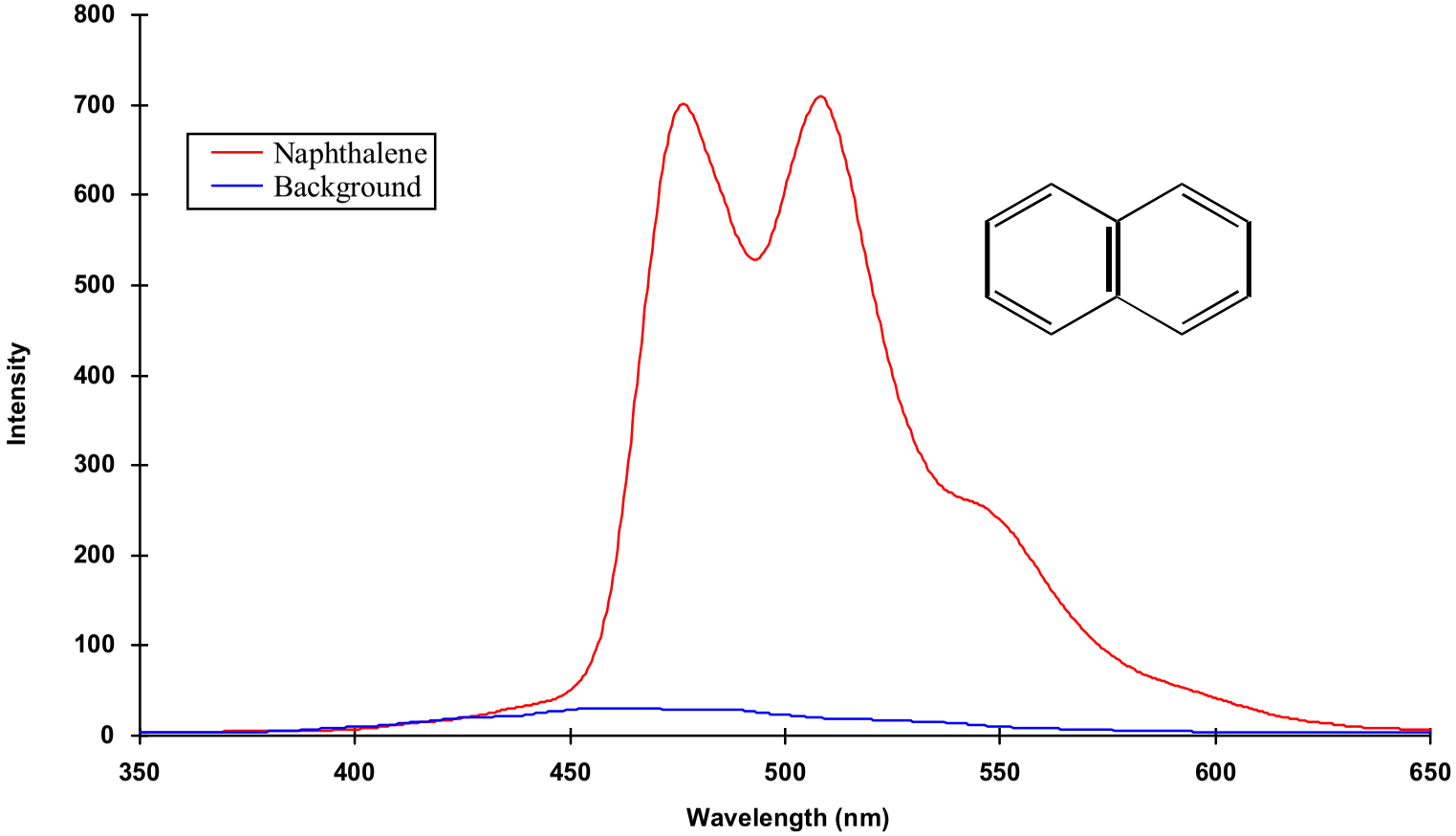

Figure 51: Representative Naphthalene Emission Spectrum.
Phosphor: 1.0 μL of 100 ppm Naphthalene in Ethanol. Substrate: K4M PREM HPMC.
Heavy Atom: 8.0μL of 16.5 % NaI in Ethanol. Excitation Wavelength: 273 nm.

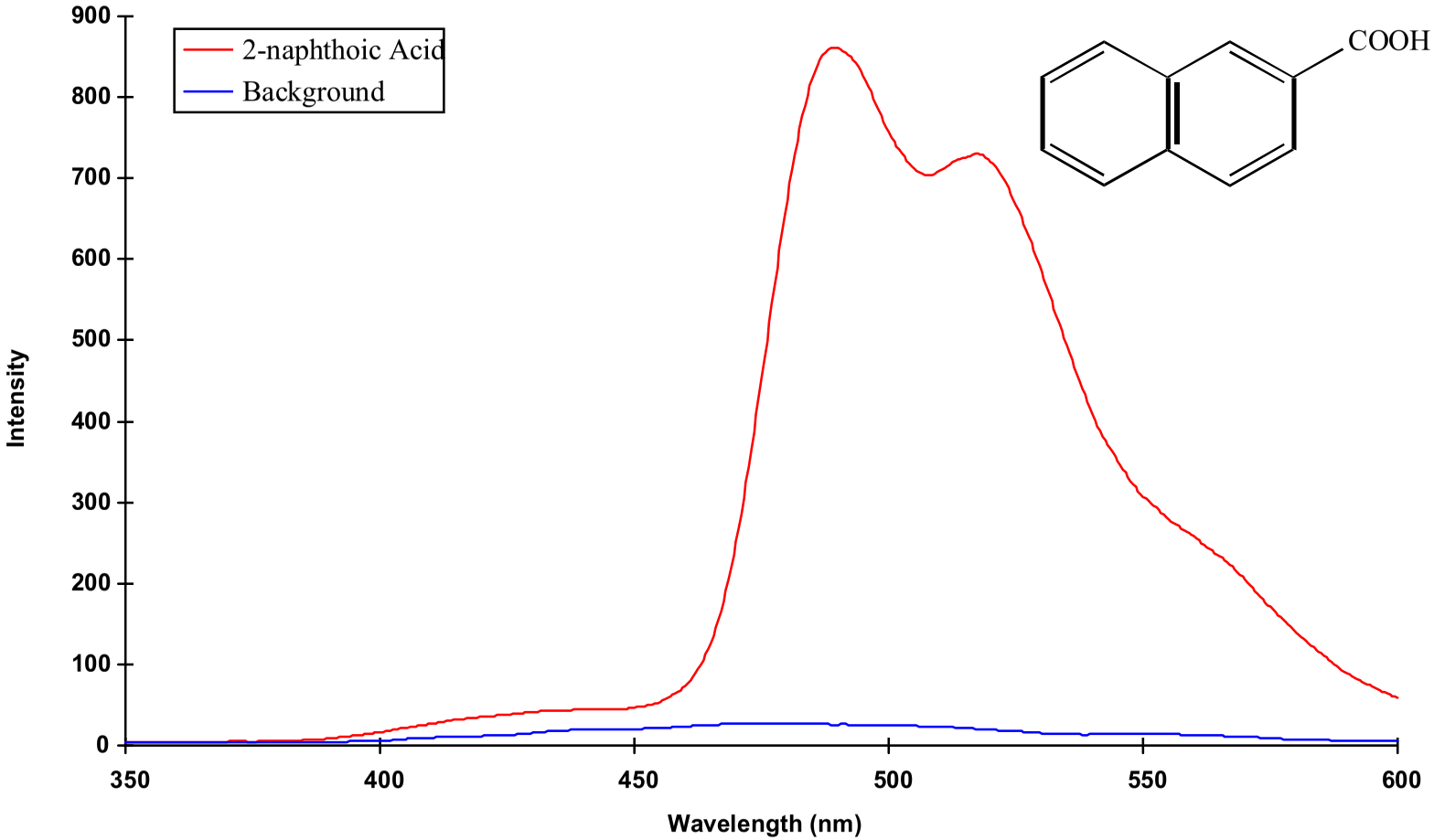

Figure 52: Representative 2-Naphthoic Acid Emission Spectrum.
Phosphor: 1.0 µL of 200 ppm 2-Naphthoic Acid in Ethanol. Substrate: K4M PREM HPMC
Heavy Atom: 8.0 µL of 16.5% NaI in Ethanol. Excitation Wavelength: 280 nm.

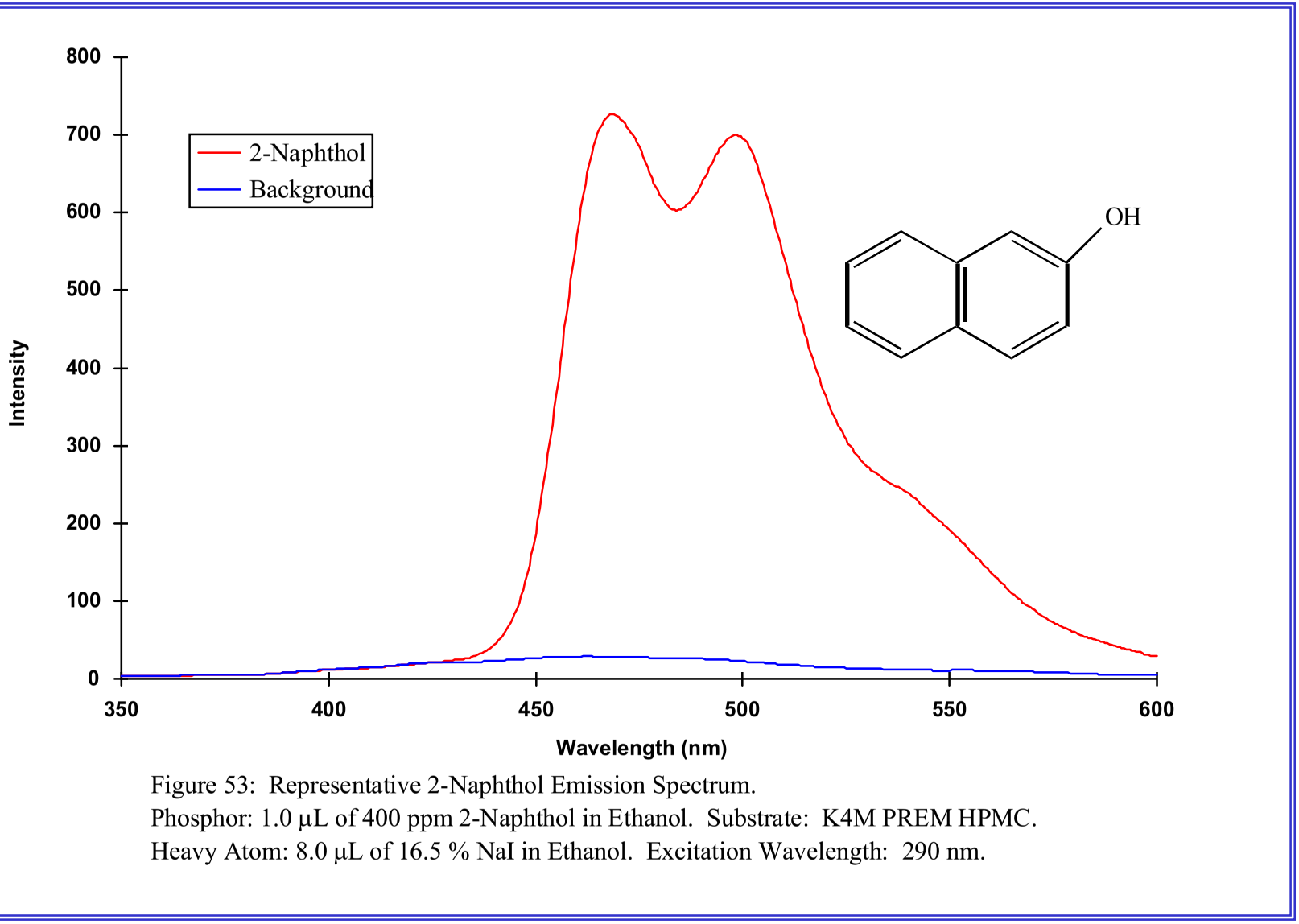

Figure 53: Representative 2-Naphthol Emission Spectrum.
Phosphor: 1.0 µL of 400 ppm 2-Naphthol in Ethanol. Substrate: K4M PREM HPMC.
Heavy Atom: 8.0 µL of 16.5 % NaI in Ethanol. Excitation Wavelength: 290 nm.

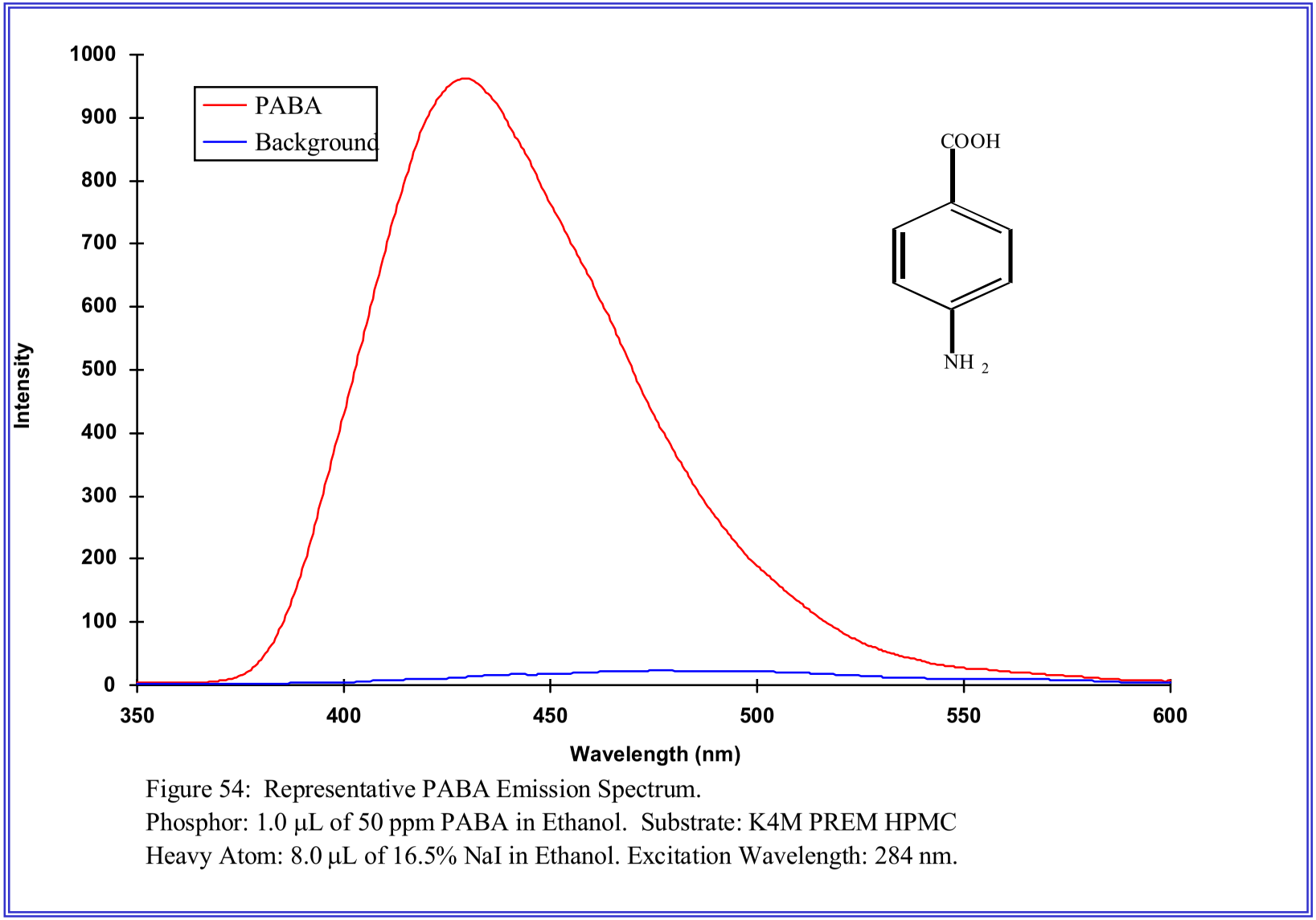

Figure 54: Representative PABA Emission Spectrum.
Phosphor: 1.0 µL of 50 ppm PABA in Ethanol. Substrate: K4M PREM HPMC
Heavy Atom: 8.0 µL of 16.5% NaI in Ethanol. Excitation Wavelength: 284 nm.

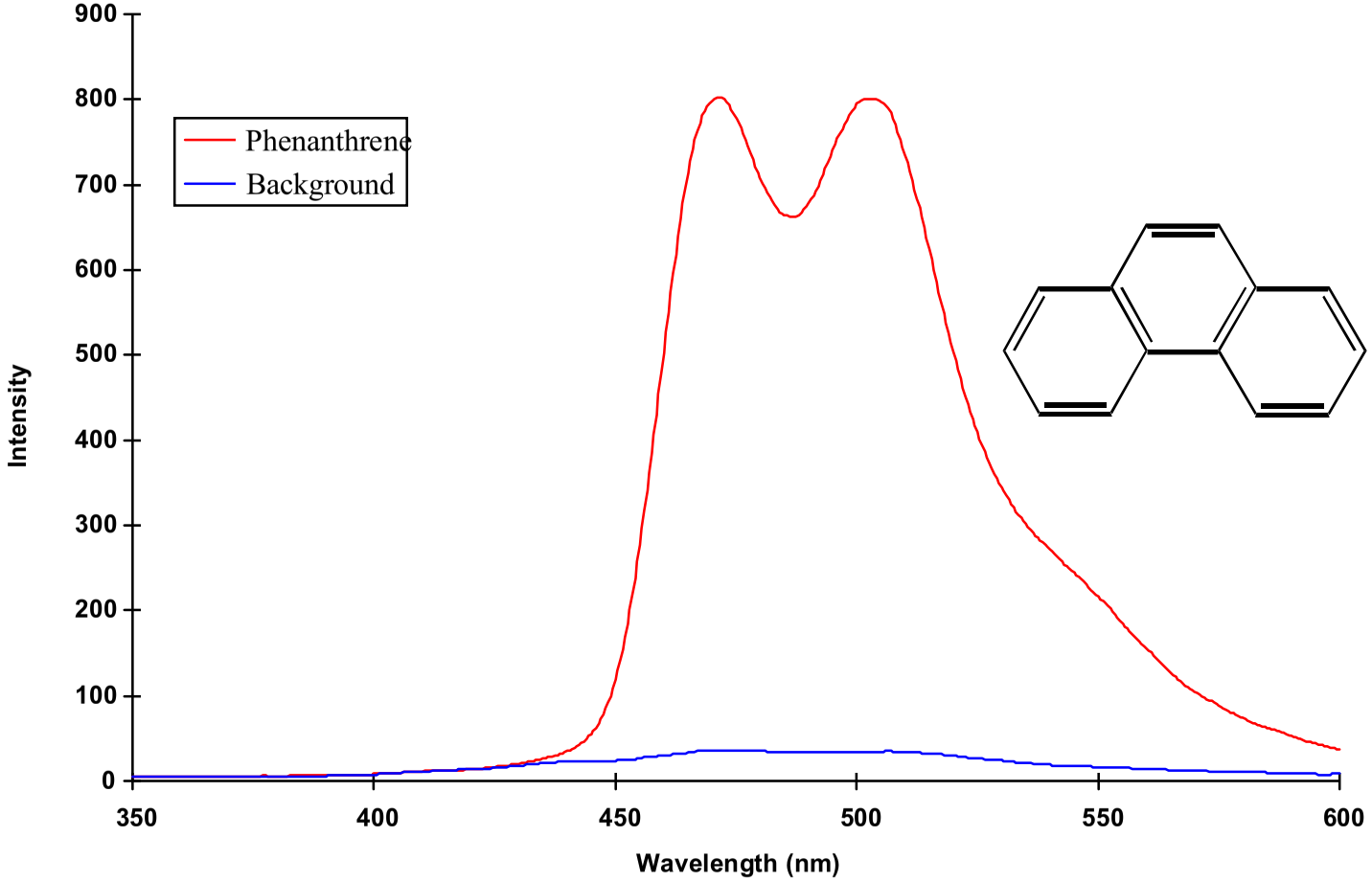

Figure 55: Representative Phenanthrene Emission Spectrum.
Phosphor: 1.0 μL of 5 ppm Phenanthrene in Ethanol. Substrate: K4M PREM HPMC.
Heavy Atom: 8.0μL of 16.5 % NaI in Ethanol. Excitation Wavelength: 260 nm.

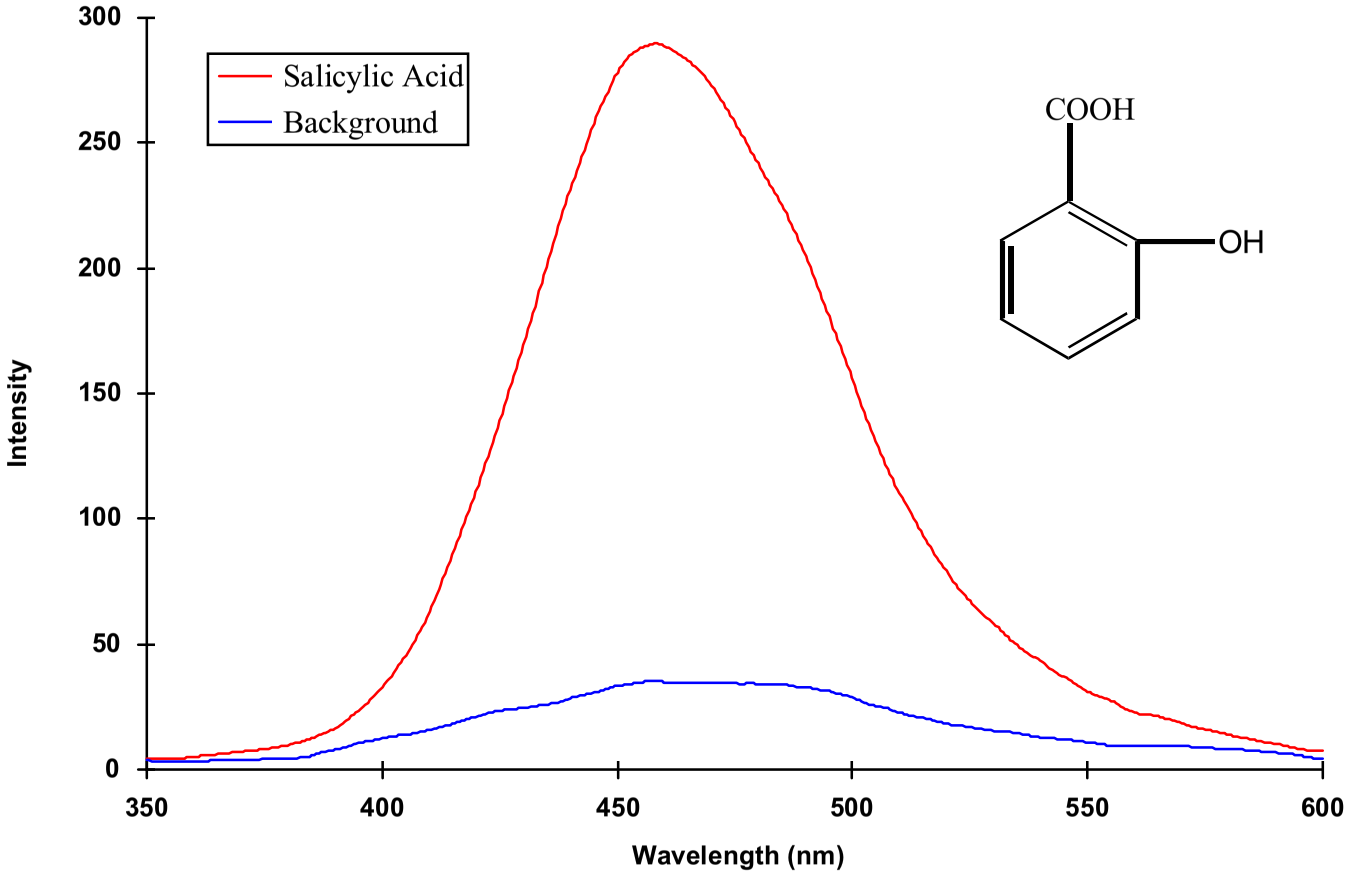

Figure 56: Representative Salicylic Acid (Sodium Salt) Emission Spectrum.
Phosphor: 1.0 µL of 200 ppm Salicylic Acid (Sodium Salt) in Ethanol.
Substrate: K4M PREM HPMC.
Heavy Atom: 8.0 µL of 16.5 % NaI in Ethanol. Excitation Wavelength: 297 nm.

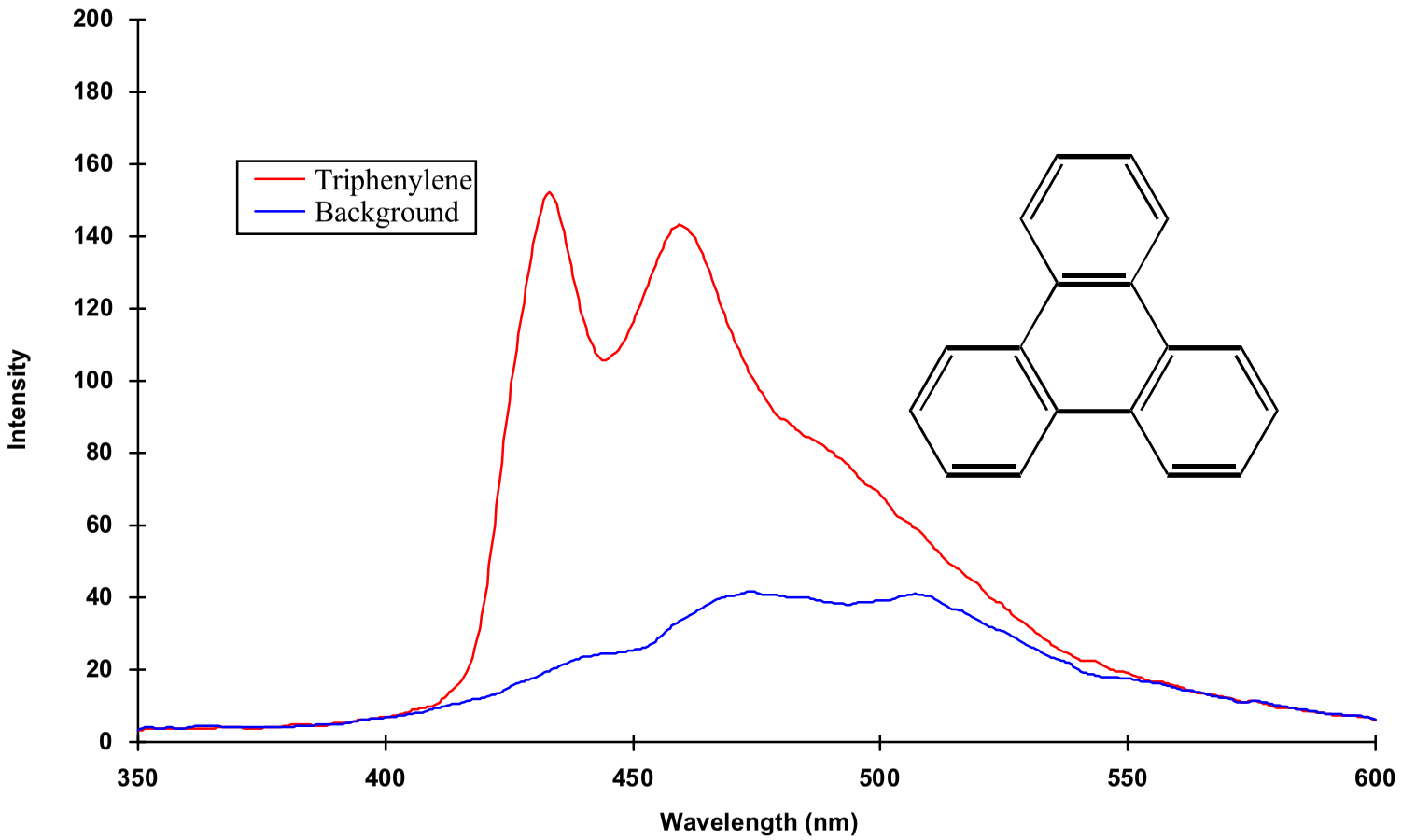

Figure 57: Representative Triphenylene Emission Spectrum.
Phosphor: 1.0 μL of 100 ppb Triphenylene in Ethanol. Substrate: K4M PREM HPMC
Heavy Atom: 8.0μL of 16.5% NaI in Ethanol. Excitation Wavelength: 260 nm.

6.0 Models

In this chapter, a series of models are developed that compare and contrast filter paper (i.e. cellulose) to HPMC in terms of their performance as SSRTP substrate materials.

6.1 Hydrophilic vs. Lipophilic Character

The question remains: "What specific characteristics of HPMC are responsible for its improved performance as an SSRTP matrix in comparison to conventional filter paper?". Obviously, the methoxyl and hydroxypropyl substituents present in HPMC are responsible for the fundamental differences between the two materials. *K4M PREM* HPMC has an approximate methoxyl substitution of 19-24% and a hydroxypropyl substitution of 7-12%. Figure 58 shows three rudimentary models that serve to illustrate the differences in substitution between native cellulose, 100% methylcellulose, and HPMC. Note that the polymeric chains have been shortened in length to merely 10 rings per chain. Also, considerable detail has been eliminated from the backbone of each chain for purposes of clarity.

The graphic in Figure 58 emphasizes the C2 and C6 functionality found on each polymeric backbone. Cellulose is fully hydroxylated. It would be expected to interact strongly with itself via internal hydrogen bonding and with other molecules that exhibit substantial polar or hydrogen-bonding character. As a result of the extensive hydroxylation, cellulose is extremely hydrophilic (or "water-loving"). Nevertheless, even though native cellulose exhibits such notable hydrophilicity, it isn't water-soluble. This is due to the high degree of crystallinity exhibited by cellulose in its native state. However, the Mercerization process that is initiated in order to convert native cellulose into a cellulose ether results in the destruction of a considerable degree of the cellulose crystallinity. As a result, the stereochemistry of the polymer is changed and the hydroxyl sites become "more visible" to other molecules. Substitution of the hydroxyls by large side-chain groups further prevents polymer crystallization.[370]

In contrast to native cellulose, 100% methylcellulose would be expected to be extremely lipophilic (or "fat-loving") due to its comprehensive methylation at sites C2 and C6. HPMC offers the best of both worlds. Even a small percentage of methyl and hydroxypropyl substitution gives HPMC both lipophilic character and hydrophilic character simultaneously. Based on its chemical structure, HPMC should be fully capable of interacting strongly with hydrophilic molecules *and* lipophilic molecules. In comparison to cellulose, HPMC should offer fewer hydrogen-bonding interactions and a greater number of dipole/induced-dipole or induced-dipole/induced-dipole interactions. This assumption is supported by the fact that HPMC is soluble in both water and a few organic solvents. Scheffel claims that it is the extent of

[370] F. Tanaka and M. Ishida, *J. Chem. Soc. Faraday Trans.*, 1995, V. 91, p. 2663.

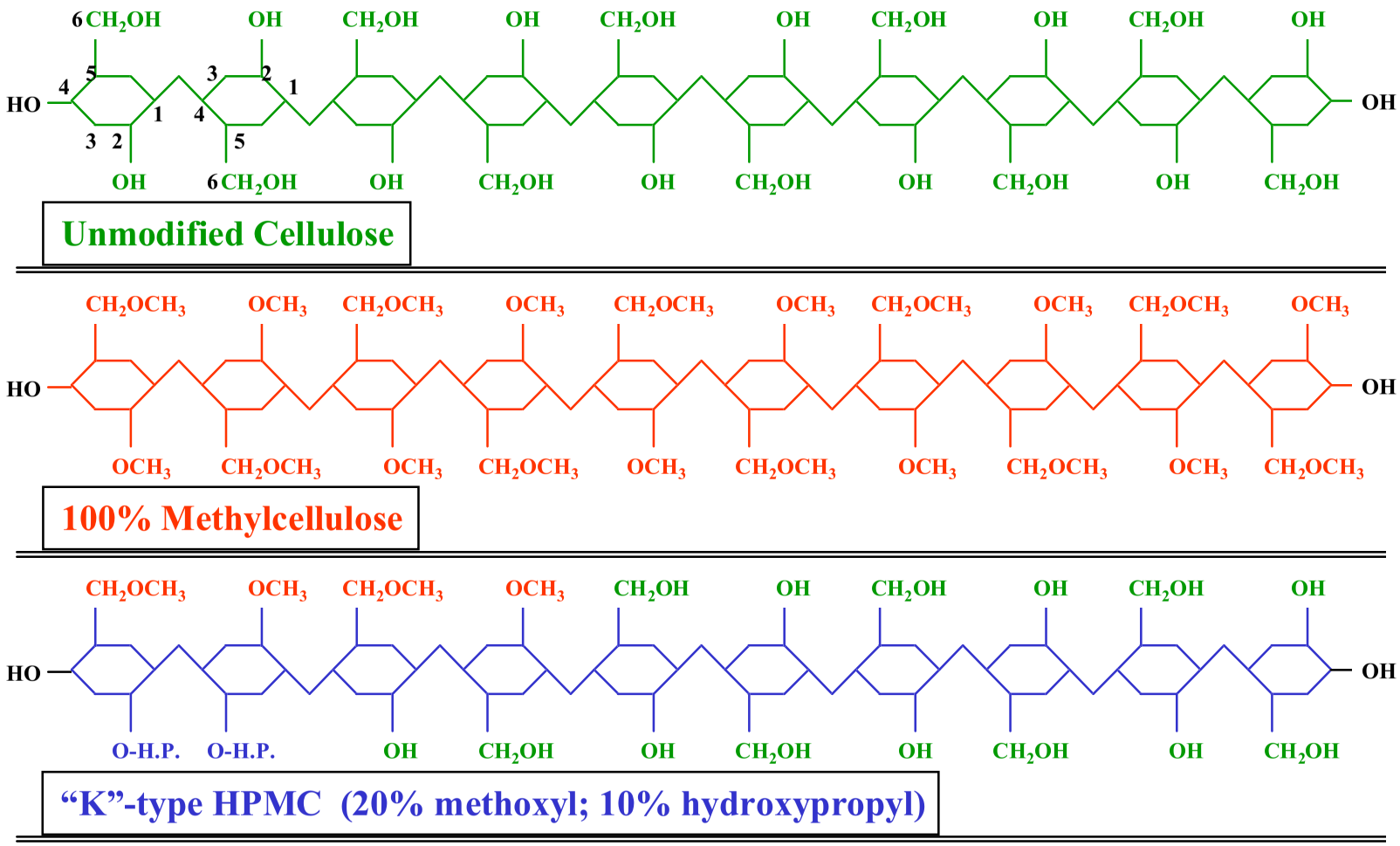

Figure 58. Cellulose, Methylcellulose, and HPMC polymeric chains.

(Note: to improve clarity and highlight the substitutions that occur at sites C2 and C6, considerable detail has been omitted from each polymer backbone.)

hydroxypropylation that is largely responsible for this enhanced solubility.[371] Mitchell and colleagues have proposed that the hydroxypropyl group is responsible for retarding the process of dehydration in HPMC.[256]

Figure 58 shows *K*-type HPMC as having 20% methoxyl substitution, 10% hydroxypropyl substitution, and 70% hydroxy functionality. Although the illustration is helpful for visualizing the extent of substitution found within the *K*-type HPMC polymer, the figure is unrealistic in many regards. First, it isn't possible for the manufacturer to control the degree of methoxyl and hydroxypropyl substitution so closely. Percentages of substitution are always cited as approximate *ranges*. Furthermore, with the exception of the relative reactivities of the primary C6 hydroxyl and the secondary C2 hydroxyl, the manufacturer has no control over the placement of individual substituents. The methoxyl and hydroxypropyl groups are distributed **randomly** along the cellulose backbone in the C2 and C6 sites. Thus, at present, the construction of a "true" molecular model that accurately represents the HPMC polymer is an exercise in futility.

6.2 Gelation of Cellulose Ethers

Unlike native cellulose, many cellulose derivatives such as HPMC are capable of producing a gel layer upon exposure to a solvent such as water. The pharmaceutical industry is especially interested in this feature since the rapid formation of a rubbery gel layer is considered to be an essential first step in achieving controlled drug release from HPMC matrices.[372] Upon contact with an aqueous solution, an HPMC tablet will begin to swell and its thickness will increase. As the polymer begins to dissolve in the solvent, chain disentanglement results in a slow erosion of the gel. Soluble drugs are released from within the tablet by diffusion through the gel layer. Insoluble drugs are released from the tablet as the gel erodes and fresh surfaces of the tablet become exposed.[256] If the matrix is solvated internally before a gel-layer has time to form, the resulting internal pressure may cause the tablet to disintegrate.[252]

A swollen polymer has three layers: a gel layer, a swollen, glassy layer, and a dry glassy core.[249] Figure 59 depicts these three layers at the surface of a wetted HPMC substrate. The polymer concentration decreases regularly beginning from the edge of the dry glassy core and ending with the surface of the gel layer. Within the dry glassy core, the polymer itself fills most of the space. In this region, the polymer chains are essentially frozen and unsolvated. In the swollen glassy layer, slight swelling produces higher solvent concentrations and allows for enhanced network mobility. In the gel layer, an even higher solvent concentration is expected and chain mobility is further increased. Nevertheless, chain entanglement is still quite strong within the gel layer and dissolution isn't expected to occur unless the substrate surface remains in contact with the bulk solution. If so, a gel layer-diffusion layer interface occurs and the chain entanglement within the matrix becomes so weak that the substrate can no longer hold the polymer chains together.

---

[371] K.G. Scheffel, Chapter 3 in **Water-Soluble Resins**, R.L. Davidson, Ed., New York: Reinhold, 1962.
[372] D.A. Alderman, *Int. J. Pharm. Tech. & Prod. Mfr.*, 1984, V. 5, p. 1.

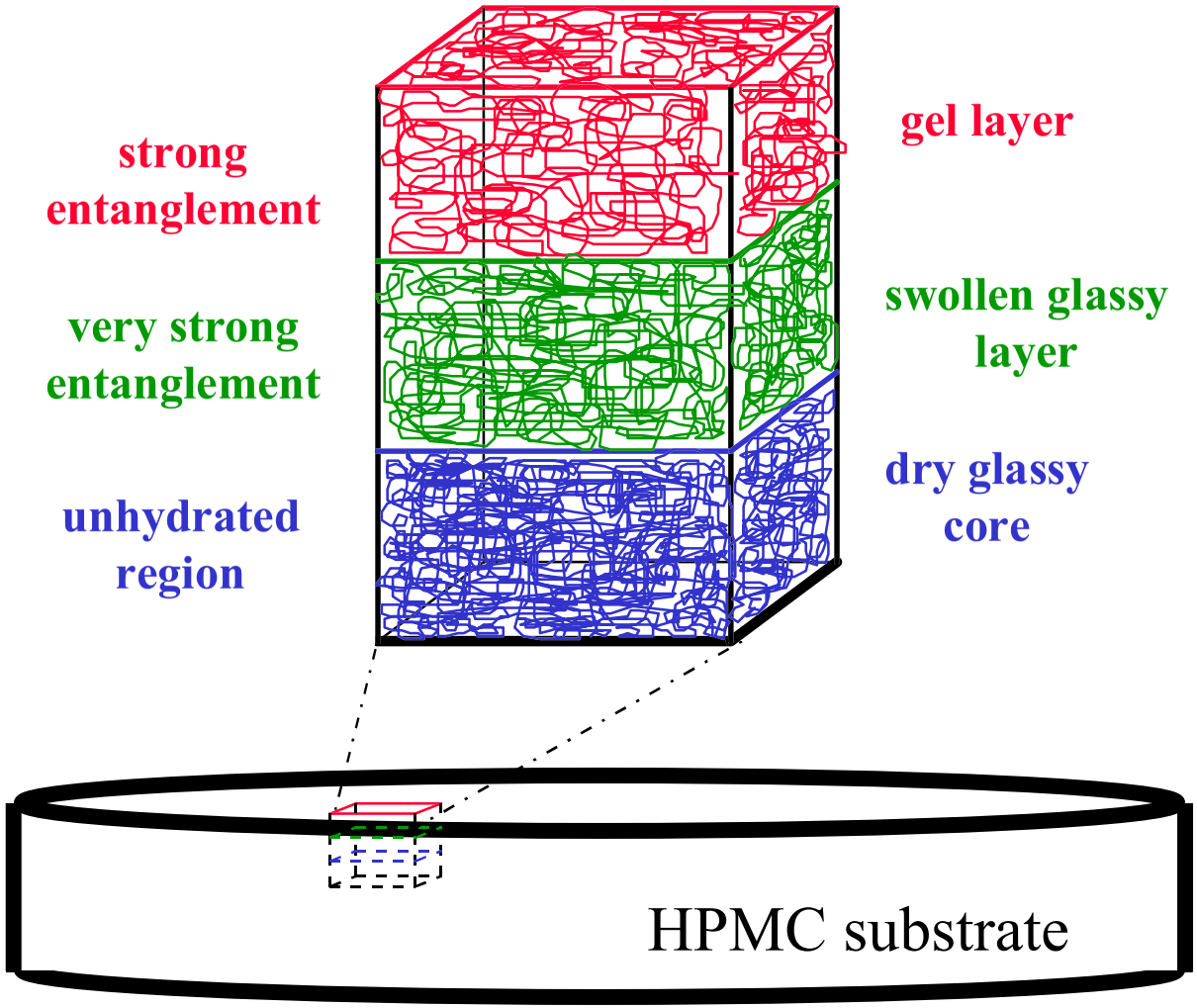

Figure 59. The three layers of a swollen HPMC pellet.

Pham and Lee have reported that the higher viscosity grades of HPMC (such as *K100M*) exhibit greater chain entanglement since their peak molecular weights are higher; whereas the lower viscosity grades (such as *K4M*) offer increased swelling rates.[254] Therefore, the *K4M* HPMC may be advantageous for use as an SSRTP substrate since it is possible that the solvent and analyte would be able to penetrate the matrix quicker than the polymer chains are able to disentangle. Mitchell et al. has discovered that *K4M* HPMC will swell in water to a greater extent than the *E4M* and *F4M* grades of HPMC since *K4M* is the most hydrophilic of the three cellulose ethers.[256] These findings are confirmed by Gerogiannis et al.[373]

During an SSRTP analysis, the RTP substrate doesn't come into contact with the bulk solution during the sample preparation step. Instead, a small volume of sample is delivered to the pellet surface and a drying step is initiated soon thereafter. Thus, a diffusion layer isn't expected. Nonetheless, it is possible for a sufficient volume of solvent to produce a thin gel layer at the surface of the substrate. Mitchell and colleagues have used a thermal mechanical analyzer in penetration mode to observe that *K4M* HPMC will yield a gel thickness of ≈1 mm following an exposure time to water of approximately thirty minutes.[256] Assuming a linear response, a gel thickness of ≈100 μm would be expected at approximately three minutes of exposure time. Following one minute of exposure to the hydrating solvent, a gel thickness of≈33 μm would be expected. Nevertheless, it is possible that the binding of water by a *K4M* HPMC substrate isn't linear over time. Therefore, the present assumption may not be valid.[374]

Although the solvent used for this project was ethanol instead of water, the formation of a thin gel-layer at the surface of the HPMC substrate is still quite possible. Even though the binding energy of the hydrogen bond with ethanol is weaker than with water, ethanol is fully capable of swelling the matrix and prohibiting direct association between the polymer chains. Given that a gel-layer would form at the surface of the HPMC substrate during heavy-atom and analyte delivery, what would become of the gel-layer during the application of heat energy necessitated by solvent removal? As the temperature is raised, the chains gradually lose the attached ethanol molecules and polymer-polymer association begins to take place. As desolvation proceeds, the amount of direct inter-chain association increases. This association continues until an infinite network of polymers is formed.

The author proposes that as the HPMC gel-layer collapses it forms a thin protective coating at the surface of the substrate. The Dow Chemical Company describes these HPMC coatings as "high-strength, water-soluble films".[247] Methocel™ films offer low oxygen and moisture vapor transmission rates and excellent stability to ultraviolet light. Dr. Colin Keary, of the Dow Chemical Company, has suggested that the film may act as a protective "skin" that can improve RTP intensities.[375] Conversely, the Dow Chemical Company has indicated that a film of 2 mil thickness (≈51 μm) may significantly reduce UV transmission.[247] Since UV light is expected to penetrate cellulosic materials no deeper than ≈100 μm, a thin Methocel™ film may

---

[373] V.S. Gerogiannis, D.M. Rekkas, P.P. Dallas, and N. Choulis, *Drug Dev. Ind. Pharm.*, 1993, V. 19, p. 1061.

[374] The same study also showed that a *K4M* HPMC disc will bind ≈ 2 mg of water in one minute and ≈ 3 mg of water in three minutes. The trend plateaus at ≈ 6 mg of water following an exposure time of approximately 30 minutes.

[375] Dr. Colin Keary, Dow Chemical Company, Midland, Michigan, 48674, personal communication, 1997.

in fact be disadvantageous for SSRTP analyses. Any gain in RTP signal that is enhanced by moisture and oxygen protection might possibly be negated by the reduction in quantity of UV light that is able to reach the phosphor during the excitation step. Hopefully, future studies by other researchers will shed more light on this tentative proposal.

6.3 Internal Energy, Cohesive Energy Density (CED), and the Cohesion Parameters

Given that HPMC has a lipophilic character and cellulose has a hydrophilic character, would it be possible to somehow quantify those qualitative descriptions? For many years, chemists have relied on the expression "like dissolves like" as a rule-of-thumb when considering the solubilities of solutes in various solvents. "Like dissolves like" calls to mind the ability of non-polar solvents to dissolve non-polar solutes and, conversely, points to the ability of polar solvents to dissolve polar solutes as well. In order for the components within a solution to mix uniformly, the chemical interactions between the individual constituents must be favorable. Miscibility is enhanced when solute and solvent are strongly attracted to one another. When solute and solvent strongly repel one another, uniform mixing is generally not achieved. Possible interactions between solute and solvent include: ion-ion, ion-dipole, ion-induced dipole, dipole-dipole, dipole-induced dipole, induced dipole-induced dipole, and hydrogen bonding. This work is concerned with the latter four types. Further details regarding each of the ionic and molecular interactions are found elsewhere.[376]

If the electron density within a molecule isn't uniform, regions of partial positive (δ+) and partial negative (δ-) charge will exist. Even though the molecule as a whole is neutral, the local charge imbalances cause portions of the molecule to behave as *dipoles*. Although a simple molecule such as H-Cl may have a single dipole, more complicated molecules can have multiple dipoles simultaneously. Some dipoles will be strong, while others may be weak. Some dipoles reinforce one another and others may exhibit a canceling effect. Nevertheless, the sum of all the dipoles is known as the *dipole moment* of the molecule. Molecules that have permanent dipole moments are said to be *polar*. If a molecule's dipoles perfectly cancel one another, then the molecule is said to be *non-polar*.

The electron clouds within non-polar molecules are in continuous, random motion. These random changes result in the creation of regions of variable electron density across the surface of the molecule. Such polar fluctuations occur regularly as electrons flow throughout the molecule. When two non-polar molecules are brought into close proximity, the random polar fluctuations in each molecule tend to induce corresponding polarities in the another. The molecules may begin to fluctuate together. This allows the temporary δ+ and δ- regions of the molecules to favorably interact. These induced attractions are referred to as *induced dipole-induced dipole forces* (or *London dispersion* forces). Dispersion forces are present to some degree in all molecules.

The polarity of a molecule is related to its atomic composition, its geometry, and its size. Polar molecules tend to arrange themselves in an orientation that favors the interaction of δ+ and δ- regions of the molecules (and vice-versa). Unlike charges will attract and the like charges will

[376] J.N. Israelachvili, **Intermolecular and Surface Forces**, 2nd Ed., New York: Academic Press, 1992.

repel. These intermolecular attractions are referred to as *dipole-dipole forces* (or *Keesom* interactions). It is still possible for a non-polar molecule to interact favorably with a polar molecule if the polar molecule is capable of inducing a temporary dipole in the non-polar molecule. The induced dipole within the non-polar molecule and the permanent dipole within the polar molecule will allow for the two molecules to be mutually attracted to one another. These interactions are known as *dipole-induced dipole forces* (or *Debye* interactions).[377]

A particularly strong intermolecular attraction occurs between molecules where a hydrogen atom is bonded to an electronegative atom such as fluorine, oxygen, or nitrogen. These electronegative atoms are able to attract the hydrogen's electron so tenaciously that the hydrogen is left with a strong $\delta+$ character while the electronegative atom assumes a strong $\delta-$ character. In this manner, the $\delta+$ hydrogen of one molecule is capable of forming a protonic bridge with the electronegative atom found within a neighboring molecule. Although polar in nature, the attraction is so strong that it is considered to be a *hydrogen bond* rather than merely a polar force.

When solvent and solute exhibit favorable intermolecular attractions, solubility is enhanced. In 1916, Hildebrand proposed that solubility is related to the corresponding internal energies associated with solvents and solutes.[378] According to Hildebrand, molecules will attract and interact with one another most effectively when the magnitudes of their internal energies are comparable. The *molar internal energy* of a pure, condensed material is its potential energy compared to that of the ideal vapor at the same temperature. Since strong attractive (or *cohesive*) forces exist between molecules in the condensed phases, each molecule is considered to have a significant negative potential energy relative to a corresponding molecule in the vapor phase. Internal energy is described by equation #1 (at pressures below atmospheric pressure).[379]

$$-U = \Delta H_{vap} - RT \tag{1}$$

where U is the molar internal energy (J mol^{-1}), ΔH_{vap} is the molar enthalpy of vaporization (J mol^{-1}), R is the gas constant (8.314 J K^{-1} mol^{-1}), and T is temperature (K).

The cohesive effect in condensed phases can be expressed in terms of the cohesive energy density (*CED*). The *CED* of a pure substance (described by equation #2) is a measure of the energy associated with the attractive forces between the molecules.

$$CED = \frac{-U}{V} \tag{2}$$

where V is the *molar volume* of the substance (cm^3 mol^{-1}). Molar volume can be calculated using equation #3.

$$V = \frac{MW}{\rho} \tag{3}$$

---

[377] J. Burke, *Solubility Parameters: Theory and Application* in the **AIC Book and Paper Group Annual**, C. Jensen, Ed., 1984, V. 3, p. 13. Also available online:
URL: http://sul-server-2.stanford.edu/byauth/burke/solpar/

[378] J.H. Hildebrand and R.L. Scott, **The Solubility of Non-Electrolytes**, New York: Dover, 1964.

[379] A.F.M. Barton, **CRC Handbook of Solubility Parameters and Other Cohesion Parameters**, Boca Raton, FL: CRC Press, Inc., 1983.

where *MW* is the molecular weight of the substance (g mol^{-1}) and ρ is its density (g cm^{-3}). Traditionally, *CED* values have been reported in units of calories per cubic centimeter (cal cm^{-3}). The appropriate SI unit is the megapascal (MPa) where 1 cal cm^{-3} is equivalent to 4.184 MPa (or 4.184 J cm^{-3}). Since the intermolecular forces involved in the vaporization of a substance are the same as those to be overcome when dissolving it, solubility theory predicts that dissolution will occur when a solute and solvent have similar *CED* values. As an extension of the concept "like dissolves like", Robertson and Luce have proposed that "like absorbs like" in instances where the basis of similarity is taken to be the *CED* of the components.[380] Following their study of the sorption of polymers on cellulose, it was suggested that the competition by solvent for sorption sites on the cellulose increases as the *CED* of the solvent approached the *CED* of the cellulose.[380]

In 1936, Hildebrand proposed that the square root of the *CED* should serve as a numerical value indicating the solvency behavior of a specific solvent. In 1950, he described this value as a *solubility parameter* and assigned the symbol δ to represent it (equation #4).[378]

$$\delta = \sqrt{CED} = \left[\frac{-U}{V}\right]^{1/2} = \left[\frac{\Delta H - RT}{V}\right]^{1/2} \qquad (4)$$

Traditionally, the units of δ have been reported as $cal^{1/2}$ $cm^{-3/2}$ and a number of authors have suggested naming the unit the "hildebrand" in honor of J.H. Hildebrand. Nevertheless, current usage favors the SI unit of $MPa^{1/2}$ (where 1 $cal^{1/2}$ $cm^{-3/2}$ = 2.045 $MPa^{1/2}$) and δ has become widely known as the "Hildebrand solubility parameter". Although the Hildebrand parameter is primarily a liquid state property, gases may be treated as hypothetical "liquid" solutes at atmospheric pressure and substances which are conventionally solids at ambient temperatures are treated as "subcooled liquids". In such cases, δ values calculated for non-liquid substances (such as polymers) should be referred to as *cohesion parameters*.

The Hildebrand parameter was originally developed from a theory of *regular solutions*.[381] A regular solution is one that has an ideal entropy of formation (i.e. a random molecular distribution) despite the existence of interactions which result in a non-ideal enthalpy of formation. By this definition, regular solutions are only those that involve dispersion forces since the orientation effects of polar molecules will cause nonrandom molecular distributions. In spite of this original definition, numerous researchers were successfully able to show that the Hildebrand parameter could be applied to non-regular solutions as well.[379] Nonetheless, the obvious weakness of the Hildebrand parameter is that it is a single parameter which attempts to incorporate a complex set of solvent-solute interactions: London dispersion forces, dipole-dipole forces, dipole-induced dipole forces, and hydrogen bonding interactions. Since the Hildebrand parameter is a single quantity that must reflect all of these effects, it is quite possible that two materials may have similar solubility parameters for very different reasons. Thus, two substances

[380] J.E. Luce and A.A. Robertson, *J. Polym. Sci.*, 1961, V. 51, p. 317.
[381] J.H. Hildebrand and R.L. Scott, **Regular Solutions**, Englewood Cliffs, NJ: Prentice-Hall, 1962.

may be immiscible despite the similarity of their solubility parameters.[382] Obviously, this limitation also applies to the calculated *CED* value as well.[383]

Hansen originally introduced a three-component solubility parameter system that extended the concept to polar and hydrogen bonding interactions as well as dispersion forces.[384,385,386] The three-component system can be used to interpret relations involved in liquid miscibility, polymer solubility, polymer compatibility, adsorption on solid surfaces, dispersion phenomena, and solubility of inorganic and organic solutes in organic solvents. The three-component solubility parameter is rationalized by assuming that the cohesive energy density depends on a non-polar dispersion interaction ($-U_d/V$), a polar interaction ($-U_p/V$) and a hydrogen bonding component
($-U_h/V$) as shown in equation #5.

$$-\frac{U}{V} = -\frac{Ud}{V} - \frac{Up}{V} - \frac{Uh}{V} \tag{5}$$

Alternatively, equation #5 can be rewritten as equation #6:

$$\delta_t^2 = \delta_d^2 + \delta_p^2 + \delta_h^2 \tag{6}$$

where δ_t refers to the *total solubility parameter*, δ_d is the *dispersion solubility parameter*, δ_p is the *polar solubility parameter*, and δ_h is the *hydrogen bonding solubility parameter*. As might be expected, the total solubility parameter is usually similar in magnitude to the Hildebrand solubility parameter; however, the two are rarely identical.[387] Sometimes it may be helpful to reduce this three-component system to two components by collecting the association interactions, δ_p and δ_h, as described in equation #7.

$$\delta_a = \left(\delta_p^2 + \delta_h^2\right)^{1/2} \tag{7}$$

In this manner, two-dimensional graphs may be prepared in order to illustrate trends involving the association interactions (δ_a) and the dispersion interactions (δ_d).

Although other two-component and three-component systems have been proposed, the three parameter system developed by Hansen is the most widely accepted to date.[377,379,387] In fact, the three parameters (δ_d, δ_p, and δ_h) are often referred to as *Hansen solubility parameters* in honor of C.M. Hansen. The three Hansen parameters may be determined empirically[379] or experimentally.[388,389,390] Hildebrand and Hansen parameters obtained by both means have been collected and published for a number of common solutes, solvents, polymers, pigments, and

---

[382] K.C. James, **Solubility and Related Properties**, Vol. 28 in the series *Drugs and the Pharmaceutical Sciences*, New York: Marcel Dekker, Inc., 1986.
[383] M.E. McDonnell and E.K. Walsh in **A Guide to Materials Characterization and Chemical Analysis**, J.P. Sibilia, Ed., New York: VCH, 1988.
[384] C.M. Hansen, *J. Paint Technol.*, 1967, V. 39, p. 104.
[385] C.M. Hansen, *J. Paint Technol.*, 1967, V. 39, p. 505.
[386] C.M. Hansen, *J. Paint Technol.*, 1967, V. 39, p. 511.
[387] A.F.M. Barton, *Chem. Rev.*, 1975, V. 75, p. 731.
[388] C.M. Hansen, *Ind. Eng. Chem. Prod. Res. Develop.*, 1969, V. 8, p. 2.
[389] K.M.A. Shareef, M. Yaseen, M.M. Ali, and P.J. Reddy, *J. Coatings Technol.*, 1986, V. 58, p. 35.
[390] W.L. Archer, *Drug Dev. Ind. Pharm.*, 1992, V. 18, p. 599.

elements. At present, the most comprehensive source is Allan Barton's superb **Handbook of Solubility Parameters and Other Cohesion Parameters** which cites nearly 2000 references. Barton has cautioned that the researcher must always remain aware of the history and derivation of solubility parameter collections since considerable variation may exist between empirically- and experimentally-derived values. Nonetheless, it has been proven that both methods are acceptable and calculated parameters are sometimes more accurate than experimental ones.[379]

For this study, Hansen parameters weren't readily available in the literature for most of the analytes studied. Therefore, it was decided that the cohesion parameters should be calculated for each chemical species in order to insure that the results were internally consistent. The total cohesion parameter (δ_t) was calculated by first obtaining the enthalpy of vaporization (ΔH_{vap}) associated with each substance. Since ΔH_{vap} values weren't readily available for all species, the Clausius-Clapeyron equation (equation #8) was used in conjunction with data found in vapor pressure tables to calculate molar enthalpies of vaporization.[391,392,393]

$$\ln P = \left(\frac{-\Delta H_{vap}}{R} \right) \frac{1}{T} + C \qquad (8)$$

where P is the vapor pressure, ΔH_{vap} is the molar enthalpy of vaporization (kJ mol^{-1}), R is the gas constant (8.314×10^{-3} kJ K^{-1} mol^{-1}), T is the temperature corresponding to the given vapor pressure (K), and C is a constant equivalent to the y-intercept. Using equation #8, values of ln P vs. 1/T were plotted using the Microsoft Excel spreadsheet. The slope of the resulting line multiplied by the gas constant provided suitable values of ΔH_{vap}. Table 38 is a collection of ΔH_{vap} values (via equation #8), U values (via equation #1), CED values (via equation #2), and δ_t values (via equation #4) for each substance. Also provided are their R^2 results calculated for the best-fit straight lines that describe $-\Delta H_{vap}/R$, densities (ρ in units of g/cm^3), molecular weights (MW in units of g mol^{-1}), calculated molar volumes according to equation #3 (V in units of cm^3 mol^{-1}), and CAS registry numbers. Since vapor pressure data was unavailable for triphenylene, this analyte was not included in the data set.[394] Also, a limited number of vapor pressure data points were available for p-aminobenzoic acid. Therefore, for PABA, ΔH_{vap} (and all calculated results based on ΔH_{vap}) should be considered to be approximate and inexact. Ethanol was included in this series of calculations since it was the solvent in which all analytes were dissolved prior to SSRTP analysis.

---

[391] D.R. Stull, *Ind. Eng. Chem.*, 1947, V. 39, p. 517.

[392] R.C. Weast, Ed., **CRC Handbook of Chemistry and Physics, 65th Ed.**, Boca Raton, FL: CRC Press, Inc., 1983.

[393] R. Sabbah, R. Chastel, and M. Laffitte, *Can. J. Chem.*, 1974, V. 52, p. 2201

[394] White has reported that ΔH_{vap} can be predicted for planar polycyclic aromatic hydrocarbons using Trouton's rule. However, the predictions reported are not in close agreement with the values calculated here using experimentally-derived vapor pressure tables (C.M. White, *J. Chem. Eng. Data*, 1986, V. 31, p. 198.).

Table 38. ΔH_{vap}, U, CED, δ_t, MW, ρ, and V for ethanol and analytes.

substance	ethanol	naphthalene	2-naphthol	2-naphthoic acid	salicylic acid	phenanthrene	PABA	acenaphthene
CAS registry #	[64-17-5]	[91-20-3]	[135-19-3]	[93-09-4]	[69-72-7]	[85-01-8]	[150-13-0]	[83-32-9]
$\lvert\Delta H_{vap}\rvert$ (kJ mol^{-1})	42.69	52.08	59.25	94.38	79.19	59.46	81.01	54.63
R^2	1.000	0.994	1.000	1.000	0.993	1.000	n/a	1.000
$\lvert U\rvert$ (J mol^{-1})	40207.49	49600.38	56772.83	91902.79	76707.65	56986.51	78532.43	52155.25
CED (J cm^{-3})	688.60	449.72	503.98	746.11	801.40	376.99	786.81	402.13
δ_t (MPa$^{1/2}$)	26.24	21.21	22.45	27.32	28.31	19.42	28.05	20.05
MW (g mol^{-1})	46.07	128.16	144.19	172.20	138.12	178.22	137.14	154.21
ρ (g cm^{-3})	0.789	1.162	1.28	1.398	1.443	1.179	1.374	1.189
V (cm^3 mol^{-1})	58.39	110.29	112.65	123.18	95.72	151.16	99.81	129.70

Koenhen and Smolders have reported an empirical correlation between refractive index (n_D) and the dispersion cohesion parameter (δ_d).[395] If experimental refractive index data is available, then δ_d can be calculated according to equation #9.

$$\delta_d = 19.5\, n_D - 1.4 \tag{9}$$

Unfortunately, experimentally-derived values of the refractive index obtained at the sodium "D" line were not readily available in the literature for each chemical species. In order to maintain consistency within the data set, it was decided that n_D should be approximated using the Lorentz-Lorenz equation (equation 10).

$$R_D = \left(\frac{n_D^2 - 1}{n_D^2 + 2}\right)\frac{1}{\rho} \tag{10}$$

where n_D is the refractive index of the substance, ρ is the density of the material (g cm^{-3}), and R_D is the specific refraction (cm^3 g^{-1}). Solving for refractive index, equation #10 is rearranged into the form shown by equation #11.

$$n_D = \sqrt{\frac{2R_D\rho + 1}{1 - R_D\rho}} \tag{11}$$

The specific refraction, R_D, is obtained by using equation #12.

$$R_D = \frac{Mr_D}{MW} \tag{12}$$

where MW is the molecular weight of the substance (g mol^{-1})and Mr_D is the material's molar refraction (cm^3 mol^{-1}). In instances where molar refraction values aren't tabulated, they may be

[395] D.M. Koenhen and C.A. Smolders,*J. Appl. Polym. Sci.*, 1975, V. 19, p. 1163.

computed via the use of tables of atomic and group refractions as found in numerous handbooks.[392,396] For this work, Mr_D was calculated in this manner. The results of calculations for Mr_D and n_D are collected in table 39. When compared to a few experimentally determined values of n_D for this particular set of substances, refractive indices determined by the Lorentz-Lorenz equation tended to be high by approximately 6%. Therefore, the n_D values obtained via the Lorentz-Lorenz method were all adjusted downward equally by 6% in order to more closely approximate real-world values. For example, the experimental value of n_D cited for naphthalene is 1.5823. The adjusted Lorentz-Lorenz n_D for naphthalene is 1.58. For this particular set of data, the exception is ethanol (experimental n_D = 1.3614; calculated n_D = 1.36). However, the adjustment is still a reasonable one since the Lorentz-Lorenz approach may fail to adequately compensate for the aromaticity of each of the other species. It is the adjusted n_D value, also reported in table 39, that is used to calculate δ_d for each substance. Although a slight amount of error is certainly introduced into the determination of δ_d for ethanol[397], it is the overall trend in cohesion parameters that is considered to be of the most significance for this work. The calculated value of δ_d for naphthalene (19.4 $MPa^{1/2}$) agrees well with the experimentally-derived δ_d of 19.2 $MPa^{1/2}$.[379] For each of the other phosphors, values of δ_d measured by experiment were unavailable in the literature.

Table 39. Mr_D, R_D, Lorentz-Lorenz n_D, adjusted Lorentz-Lorenz n_D, and δ_d.

substance	ethanol	naphthalene	2-naphthol	2-naphthoic acid	salicylic acid	phenanthrene	PABA	acenaphthene
Mr_D ($cm^3\ mol^{-1}$)	12.96	41.65	43.17	47.80	33.99	56.98	31.57	48.68
R_D ($cm^3\ g^{-1}$)	0.28	0.32	0.30	0.28	0.25	0.32	0.23	0.32
n_D	1.36	1.68	1.69	1.70	1.63	1.68	1.55	1.69
adjusted n_D	1.28	1.58	1.59	1.60	1.53	1.58	1.45	1.57
δ_d ($MPa^{1/2}$)	13.6	19.4	19.6	19.8	18.4	19.4	16.9	19.3

Multiple authors have reported empirical correlations between the dipole moment of a substance (μ) and its polar cohesion parameter (δ_p).[395,398,399] If experimental dipole moments are available, then δ_p can be calculated according to equation #13 or equation #14.

$$\delta_p = A\mu V^{-1/2} \tag{13}$$

[396] J.A. Dean, **Lange's Handbook of Chemistry, 14th Ed.**, NY: McGraw-Hill, 1992.
[397] The experimentally-determined value of δ_d for ethanol has been reported as 15.8 $MPa^{1/2}$. A.F.M. Barton, **CRC Handbook of Solubility Parameters and Other Cohesion Parameters**, Boca Raton, FL: CRC Press, Inc., 1983.
[398] C.M. Hansen and A. Beerbower in **Kirk-Othmer Encyclopedia of Chemical Technology Suppl. Vol., 2nd Ed.**, A. Standen, Ed., New York: Interscience, 1971, p. 889.
[399] K.A. Karim and D.C. Bonner, *Polym. Eng. Sci.*, 1979, V. 19, p. 1174.

where μ is the dipole moment (Debye), V is the molar volume ($cm^3\ mol^{-1}$), A is a constant equivalent to 18.3 ($cal^{1/2}\ mol^{-1/2}\ D^{-1}$), and δ_p is the polar cohesion parameter ($cal^{1/2}\ cm^{-3/2}$).

$$\delta_p = B\mu V^{-3/4} \tag{14}$$

where μ is the dipole moment (Debye), V is the molar volume ($cm^3\ mol^{-1}$), B is a constant equivalent to 50.1 ($cal^{1/2}\ cm^{3/4}\ mol^{-3/4}\ D^{-1}$), and δ_p is the polar cohesion parameter ($cal^{1/2}\ cm^{-3/2}$). Values are readily converted to S.I. units given 1 Debye = 3.336×10^{-30} C·m, 1 cal = 4.184 J, and1 $cal^{1/2}\ cm^{-3/2}$ = 2.045 $MPa^{1/2}$. Although equations #13 and #14 rarely yield identical δ_p results, the values tend to be comparable in magnitude. For this study, all polar cohesion parameters were calculated using equation #13. Table 40 provides the average experimental dipole moments that were applied to these calculations and the resulting values of δ_p.[400]

Table 40. μ and δ_p.

substance	ethanol	naphthalene	2-naphthol	2-naphthoic acid	salicylic acid	phenanthrene	PABA	acenaphthene
μ (Debye)	1.713	0	2.01	1.95	2.65	0	3.54	0.89
δ_p ($MPa^{1/2}$)	8.4	0.0	7.1	6.6	10.1	0.0	13.3	2.9

Given δ_t, δ_d, and δ_p, it is possible to calculate δ_h by rearranging equation #6 into the following form:

$$\delta_h = \sqrt{\delta_t^2 - \left(\delta_d^2 + \delta_p^2\right)} \tag{15}$$

Table 41 provides a collection of these calculated values and includes the association cohesion parameter as calculated by equation #7.

Unfortunately, a number of researchers have discovered that compounds such as salicylic acid apparently behave like polar molecules in polar environments and non-polar molecules in non-polar environments.[401,402] Thus, multiple sets of cohesion parameters may exist for molecules that are close analogues of salicylic acid (such as those in the benzoic acid family). Based on the ability of the chameleon to change its coloration in an effort to adapt to its immediate surroundings, Hoy has termed this behavior "chameleonic".[403]

[400] A.L. McClellan, **Tables of Experimental Dipole Moments**, San Francisco: W.H. Freeman and Company, 1963.
[401] K.B. Sloan, K.G. Siver, S.A.M. Koch, *J. Pharm. Sci.*, 1986, V. 75, p. 744.
[402] M.A.F. Gadalla, G.M. Ghaly, and M.W. Samaha, *Int. J. Pharm.*, 1987, V. 38, p. 71.
[403] K. Hoy, *J. Paint Technol.*, 1970, V. 42, p. 76.

Table 41. δ_t, δ_d, δ_p, δ_h, and δ_a.

cohesion parameter	δ_t (MPa$^{1/2}$)	δ_d (MPa$^{1/2}$)	δ_p (MPa$^{1/2}$)	δ_h (MPa$^{1/2}$)	δ_a (MPa$^{1/2}$)
source	ΔH_{vap}	n_D	μ	δ_t, δ_d, δ_p	δ_t, δ_d
ethanol	26.24	13.6	8.4	20.8	22.4
naphthalene	21.21	19.4	0.0	8.6	8.6
2-naphthol	22.45	19.6	7.1	8.3	10.9
2-naphthoic acid	27.32	19.8	6.6	17.6	18.8
salicylic acid	28.31	18.4	10.1	19.0	21.5
phenanthrene	19.42	19.4	0.0	0.8	0.8
PABA	28.05	16.9	13.3	18.0	22.4
acenaphthene	20.05	19.2	2.9	5.0	5.8

Comprehensive values of δ_t, δ_d, δ_p, and δ_h have been determined by experiment for ethanol and naphthalene only.[379] Table 42 provides a comparison of these calculated results with those determined by experiment. The assumption that the experimentally-derived cohesion parameter is the "true" value is a tenuous one. Therefore, statistical comparisons are pointless for this limited data set.

Table 42. A comparison of calculated cohesion parameters with those determined by experiment for ethanol and naphthalene.

cohesion parameter	δ_t (MPa$^{1/2}$)	δ_d (MPa$^{1/2}$)	δ_p (MPa$^{1/2}$)	δ_h (MPa$^{1/2}$)	δ_a (MPa$^{1/2}$)
ethanol (calc.)	26.24	13.6	8.4	20.8	22.4
ethanol (expmtl.)	26.5	15.8	8.8	19.4	21.3
naphthalene (calc.)	21.21	19.4	0.0	8.6	8.6
naphthalene (expmtl.)	20.3	19.2	2.0	5.9	6.2

Given representative values of δ_d, δ_p, δ_h, and δ_a, it is no longer necessary for one to represent chemical substances loosely in terms of their "philic" or "phobic" characters. Cohesion parameters allow for the careful quantitation of what have traditionally been qualitative descriptors. If asked to pick three non-polar phosphors from within table 41, one would quickly recognize that naphthalene, phenanthrene, and acenaphthene were the top three choices based on the value of δ_p alone. Which of the substances are likely to be the best hydrogen-bonders? Obviously, ethanol, salicylic acid, PABA, and 2-naphthoic acid… *in that order*.

In order to provide for meaningful comparisons between phosphor and SSRTP substrate, the next step is to calculate the full set of cohesion parameters for cellulose and HPMC. Fortunately, others have already accomplished this task. E. Doelker has reported semi-empirically-derived values of the Hansen cohesion parameters for *K*-type HPMC and cellulose.[404] These calculations were performed using the group contribution method of Van Krevelen.[405] The first step in the application of Van Krevelen's method involves the disassembly of a molecule into structural groups. A table of molar attraction constants (*F*) are consulted in order to derive F_{di} (the group contributions to the dispersion component) and F_{pi}^2 (the group contributions to the polar component). This method is not applicable to the calculation of δ_h and the hydrogen bonding energy (E_{hi}) per structural group must be utilized instead. Values of E_{hi} for the various structural groups are also readily available in tables.[406] Following summation of the individual group contributions, the cohesion parameters (δ_d, δ_p, and δ_h) are determined according to equations #16, #17, and #18.

$$\delta_d = \frac{\sum F_{di}}{V} \tag{16}$$

$$\delta_p = \frac{\sqrt{\sum F_{pi}^2}}{V} \tag{17}$$

$$\delta_h = \sqrt{\frac{\sum E_{hi}}{V}} \tag{18}$$

where F_{di} is the molar attraction constant for the dispersion contributions ($J^{1/2}$ $cm^{3/2}$ mol^{-1}), F_{pi} is the molar attraction constant for the polar contributions ($J^{1/2}$ $cm^{3/2}$ mol^{-1}), E_{hi} is the hydrogen bonding energy per structural group (J mol^{-1}), and V is the molar volume (cm^3 mol^{-1}). Molar volumes can also be computed from group contributions.[407]

Since cellulose and HPMC are macromolecules, these calculations are based on single structural units within the repeating polymer chain following the assumption that end groups generally have minimal effect on the numerical result.[408] Table 43 contains the cohesion parameters for cellulose and *K*-type HPMC as reported by Doelker.[404] Experimentally-derived cohesion parameters are also included for cellulose[409] and *K4M* HPMC[410,411]. Once again,

---

[404] E. Doelker, *Swelling Behavior of Water-Soluble Cellulose Derivatives* in **Absorbent Polymer Technology**(L. Brannon-Peppas and R.S. Harland, Eds.), New York: Elsevier, 1990, p. 129.

[405] D.W. Van Krevelen and P.J. Hoftyzer, **Properties of Polymers: Their Estimation and Correlation with Chemical Structure**, New York: Elsevier, 1976, p. 152-153.

[406] D.W. Van Krevelen and P.J. Hoftyzer, **Properties of Polymers: Their Estimation and Correlation with Chemical Structure**, New York: Elsevier, 1976, p. 154.

[407] D.W. Van Krevelen and P.J. Hoftyzer, **Properties of Polymers: Their Estimation and Correlation with Chemical Structure**, New York: Elsevier, 1976, p. 59-60.

[408] D.W. Van Krevelen and P.J. Hoftyzer, **Properties of Polymers: Their Estimation and Correlation with Chemical Structure**, New York: Elsevier, 1976, p. 43.

[409] H.L. Lee and P. Luner, *J. Wood Chem. Technol.*, 1991, V. 11, p. 247.

statistical comparisons are not provided since it is unknown if the experimental results are reliable enough to treat as "true" values.

Table 43. A comparison of calculated cohesion parameters with those determined by experiment for cellulose and *K*-type HPMC.

cohesion parameter	δ_t ($MPa^{1/2}$)	δ_d ($MPa^{1/2}$)	δ_p ($MPa^{1/2}$)	δ_h ($MPa^{1/2}$)	δ_a ($MPa^{1/2}$)
cellulose (calc.) E. Doelker	29.4	13.4	9.3	24.4	26.1
cellulose (expmtl.) H.L. Lee & P. Luner	36.9	17.0	16.4	28.4	32.8
hpmc (calc.) E. Doelker	22.7	13.7	7.0	16.7	18.1
hpmc (expmtl.) W.L. Archer	30.6	18.0	15.3	19.4	24.7

It is interesting to note that each of the experimentally-derived cohesion parameters for cellulose and *K*-type HPMC are consistently higher than those calculated by group contribution methods.[412] The experimental polar cohesion parameter determined for HPMC is questionably high in comparison to the value obtained by semi-empirical methods. This trend is also evident for the cellulose polymer. A personal communication from Dr. Raymond Rowe, an expert in the field of pharmaceutical excipient materials, advised "I am also a little skeptical regarding the experimental values for the polar component. A problem with HPMC is the very limited number of primary solvents in which it is soluble.".[413,414] On the other hand, it would be quite challenging for a researcher to define the repeating structural unit for the *K*-type HPMC polymer given that the methoxyl (≈20%) and hydroxypropyl (≈10%) substitutions are effectively located at random along the length of the polymer back-bone. It is paradoxical, but indeed possible, that neither the calculated nor the experimental cohesion parameters are realistic for cellulose and HPMC. The "true" values may fall somewhere in the middle ground. Regardless, in order to maintain consistency with earlier calculations of δ_d, δ_p, and δ_h, the semi-empirical cohesion parameters provided by Doelker were chosen for purposes of further comparison within this study. Additionally, the legitimacy of Doelker's cohesion parameters has been verified since

---

[410] W.L. Archer, *Drug. Dev. Ind. Pharm*., 1992, V. 18, p. 614.
[411] W.L. Archer, *Ind. Eng. Chem. Res*., 1991, V. 30, p. 2292.
[412] P. Sakellariou, R.C. Rowe, and E.F.T. White, *Int. J. Pharm.*, 1986, V. 31, p. 175.
[413] Dr. Raymond C. Rowe, Zeneca Pharmacueticals, Alderley Park, Macclesfield, Cheshire SK10 2TG, U.K, e-mail: ray.rowe@alderley.zeneca.com, *personal communication*, 1998.
[414] Multiple attempts to contact Dr. Wesley L. Archer by U.S. mail were unsuccessful (Specialty Chemicals TS&D, Larkin Laboratory, Dow Chemical USA, Midland, MI, 48674). There are apparent anomalies involving the results for the experimentally-derived cohesion parameters for *K4M* HPMC (and other HPMC types) as reported in *Drug Dev. Ind. Pharm.* 1992, V. 18, p. 599-616.

they are in close agreement with those reported earlier by R.C. Rowe for a "generic" HPMC binder.[415]

Given a full set of cohesion parameters for phosphors, solvent, and SSRTP substrates, one can now make meaningful comparisons between each. Since RTP intensities depend primarily on the ability of a matrix material to interact favorably with the phosphor, it is expected that analytes having cohesion parameters similar to those of HPMC will give rise to enhanced RTP when trapped by an HPMC substrate. Alternatively, analytes having cohesion parameters similar to those of cellulose will yield a greater RTP signal when trapped by a cellulose substrate. Figure 60 provides a graphical comparison of the cohesion parameters for naphthalene, *K4M* HPMC, ethanol, and cellulose. For purposes of comparison, water is included as well (δ_d = 15.6, δ_p = 16.0, and δ_h = 42.3).[379] Because of its extensive hydrogen-bonding, Barton has noted that the solubility parameter values for water are uncertain and that numerous variations exist in the literature.[379] The graph is plotted in the "bubble chart" form as described by the Microsoft Excel spreadsheet software. Essentially, the "bubbles" provide the third dimension of data with δ_d being equivalent to the *area of the bubble*. Observed graphically, differences in the magnitude of δ_d for each of the substances is minor. However, significant differences are observed with respect to the δ_p and δ_h components for each chemical species. The graph proves quantitatively that naphthalene is more *HPMC-like* than *cellulose-like*. Cellulose, on the other hand, is more similar to water with respect to its polar and hydrogen-bonding character than is *K4M* HPMC. This is in agreement with prior studies that have proven that water is more strongly bound to cellulose than HPMC. Since cellulose loves water with a greater passion than does HPMC, it is possible that RTP quenching will occur with a higher probability for those analytes that are trapped in normal cellulose substrates. For SSRTP analyses using normal cellulose substrates (such as unadulterated filter papers), a dry gas purge is always critical for achieving maximum RTP intensities. Furthermore, based on Figure 60, it is reasonable to assume that phosphors with $\delta_p \geq \approx 9$ and $\delta_h \geq \approx 24$ will be more strongly attracted to a cellulose matrix; whereas, phosphors with $\delta_p \leq \approx 7$ and $\delta_h \leq \approx 17$ will be more strongly attracted to a *K4M* HPMC matrix. It's certainly no accident that ethanol has intermediate polar and hydrogen-bonding characteristics compared to HPMC and cellulose. Better swelling is observed when the solubility parameters of the solvent and cohesion parameters of the polymer are as close as possible.[404]

Obviously, for large sets of data, the bubble chart approach has its limitations. A variety of other creative graphical approaches for representing the three Hansen parameters have been described in the literature. The Teas Graph is a reasonable choice which relies on the calculation of fractional parameters and the subsequent plotting of the adjusted parameters using triangular coordinates. Such methods are outside the scope of this project and details may be found elsewhere.[377] Rather than dealing with three-dimensions of data, the association parameter (δ_a) allows one to reduce three parameters into two components by combining the polar and hydrogen-bonding interactions mathematically as described in equation #7. This is an especially useful tool for quantitatively visualizing the intermolecular interactions that are possible for large

[415] R.C. Rowe, *Acta. Pharm. Technol.*, 1988, V. 34, p. 144.

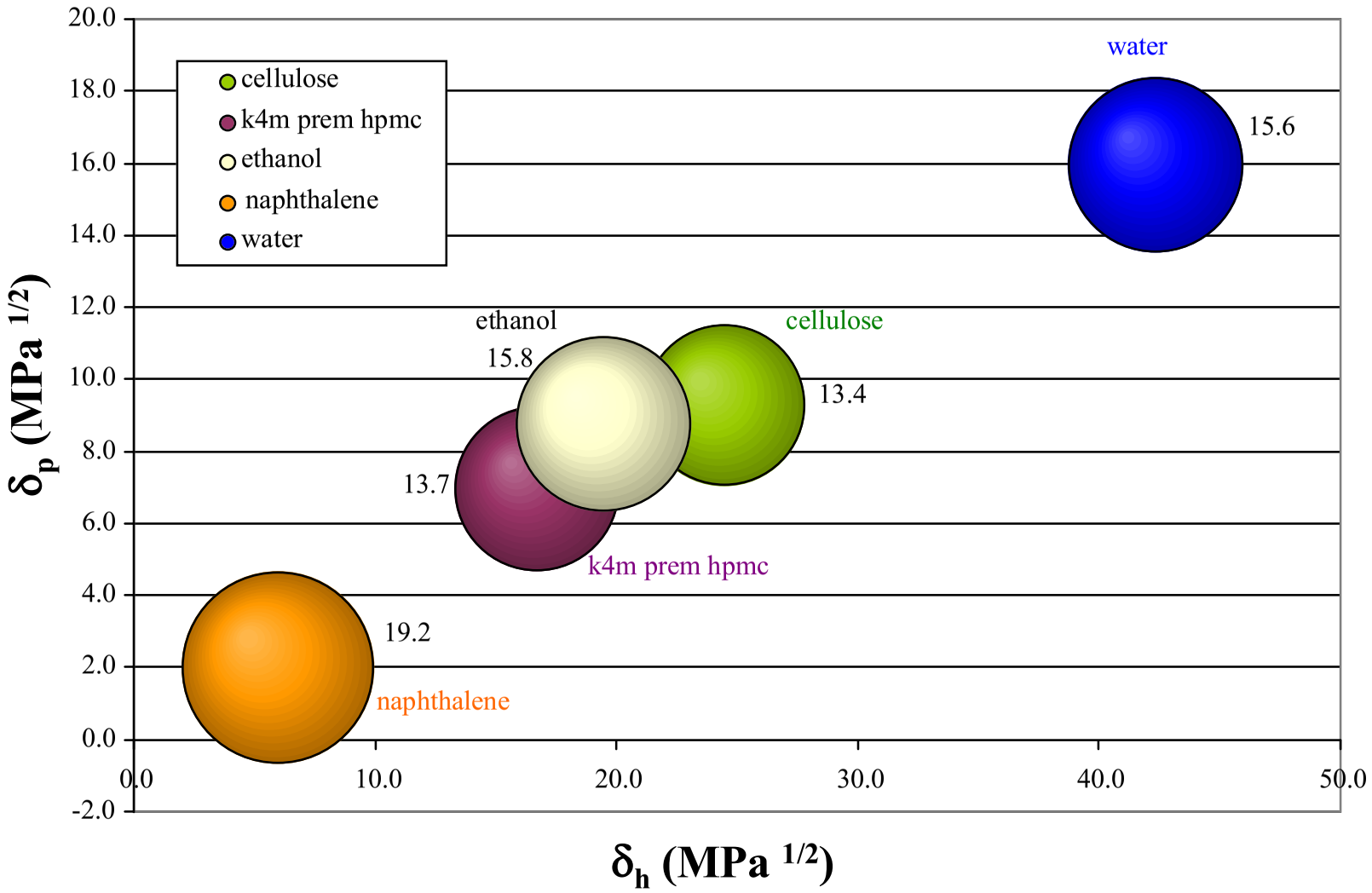

Figure 60. 3-D Bubble Plot of the Cohesion Parameters of Naphthalene, *K4M* HPMC, Ethanol, Cellulose, and Water.

numbers of substances. Figure 61 provides a graphical comparison of the dispersion and association parameters for cellulose, *K4M* HPMC, ethanol, and each of the phosphors studied during this project (not including triphenylene).

Figure 61 shows a number of interesting trends connected with the data set. First, the dispersion parameters are similar for cellulose, ethanol, and *K4M* HPMC. For the phosphors, variation in δ_d is small with the exception of PABA and salicylic acid which are intermediate between the other analytes and the RTP substrates. The distribution of association parameters is considerably wider than that of the dispersion parameters. 2-naphthol, naphthalene, acenaphthene, and phenanthrene all have small δ_a components. Based on this plot, each of the four would interact more favorably with HPMC than with cellulose. PABA, salicylic acid, and 2-naphthoic acid reveal δ_a parameters that are intermediate between cellulose and *K4M* HPMC. A quick visual estimation indicates that 2-naphthoic acid might find HPMC a more suitable host than cellulose. However, PABA and salicylic acid should interact favorably with either RTP substrate. According to Hansen, "When the energy properties of a material are similar to those of a given solvent, it will dissolve, swell, or adsorb on the material, as the case may be.".[388] This statement is expected to hold true for organic phosphors and SSRTP substrates as well.

The final step in this progression is to consider whether or not it is possible to quantify and predict more accurately the strength of the interactions between substrate and phosphor. R.C. Rowe has attempted to quantify the works of cohesion and adhesion between: a). drugs and polymeric binders (i.e. HPMC and others)[416,417,418] and b). film coatings and tablet surfaces.[419] One particular theoretical approach relies on the use of δ_t and δ_d for the prediction of the relative strengths of interaction for drug-drug, binder-binder, and drug-binder binary systems.[415] Unfortunately, the proposed model fails to adequately account for hydrogen bonding interactions.[420] Furthermore, it is yet unknown whether the magnitude of the surface free energy of a single molecule (or single macromolecule) will agree well with the magnitude of the surface free energy of a bulk, planar interface. Sinanoglu has suggested that the effective surface energies of isolated molecules will compare favorably with that of the corresponding planar macroscopic surface.[421,422] Regardless, this proposal will not hold true for compounds that exhibit metallic,
ionic, or hydrogen bonding interactions.[376]

At present, the best method for quantifying the interaction strength between two substances relies on the calculation of a parameter that represents the distance (D_{ij}), in three-dimensional space, between two total cohesion parameters.[388] The total cohesion parameter of a material is a point in three-dimensional space where the three vectors of the partial cohesion

---

[416] R.C. Rowe, *Int. J. Pharm.*, 1989, V. 52, p. 149.
[417] R.C. Rowe, *Int. J. Pharm.*, 1989, V. 53, p. 75.
[418] R.C. Rowe, *Int. J. Pharm.*, 1989, V. 56, p. 117.
[419] R.C. Rowe, *Int. J. Pharm.*, 1988, V. 41, p. 219.
[420] D.W. Van Krevelen and P.J. Hoftyzer, **Properties of Polymers: Their Estimation and Correlation with Chemical Structure**, New York: Elsevier, 1976, p. 162.
[421] O. Sinanoglu, *J. Chem. Phys.*, 1981, V. 75, p. 463.
[422] O. Sinanoglu, *Chem. Phys. Lett.*, 1981, V. 81, p. 188.

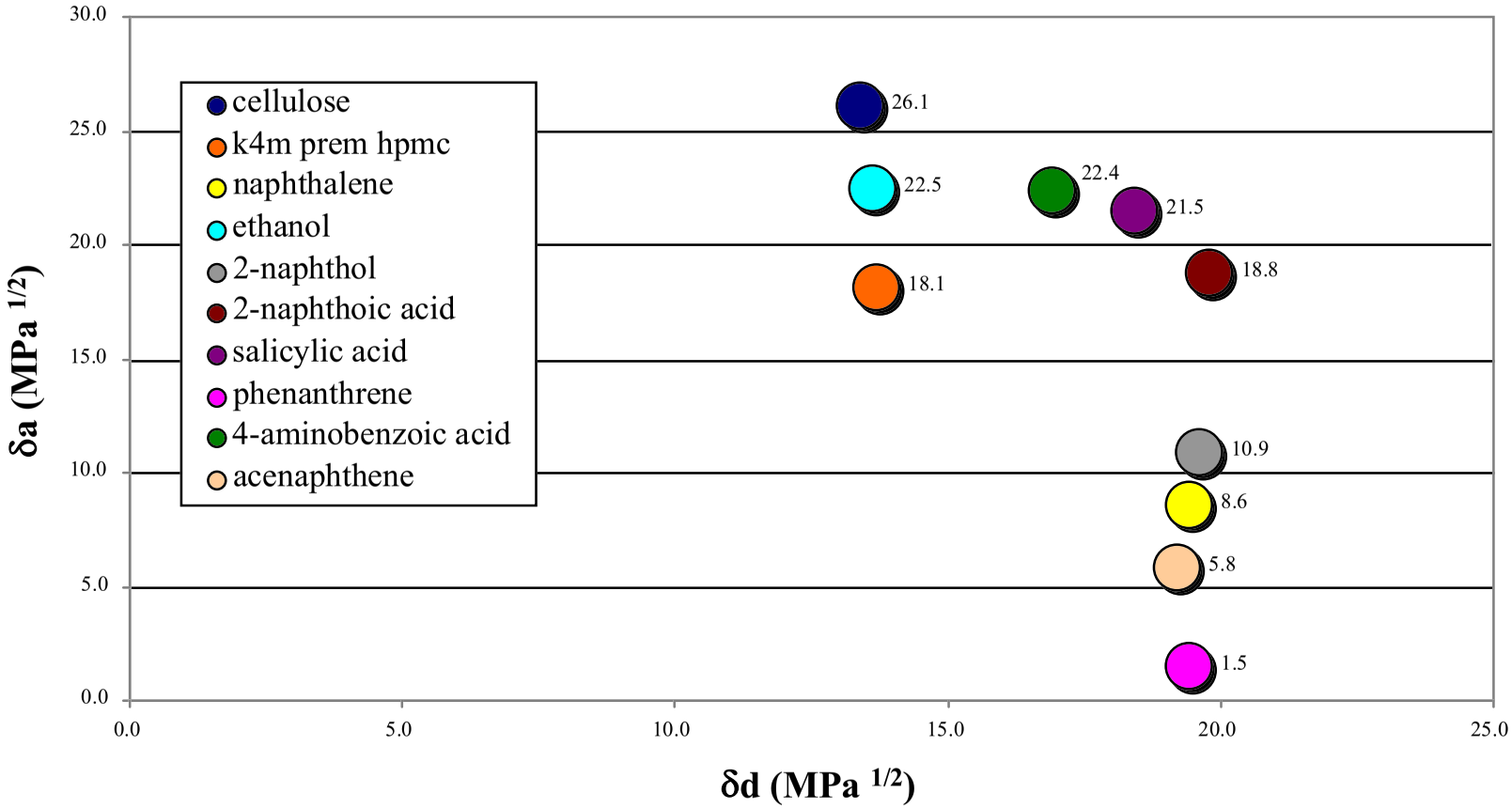

Figure 61. 2-D scatter plot that compares the dispersion and association parameters of cellulose, *K4M* HPMC, ethanol, and each of the model phosphors.

parameters meet as shown in Figure 62.[410,411] D_{ij} is determined by using equation # 19.

$$D_{ij} = \sqrt{\left((\delta_d^i - \delta_d^j\right)^2 + \left(\delta_p^i - \delta_p^j\right)^2 + \left(\delta_h^i - \delta_h^j\right)^2} \qquad (19)$$

where i and j represent the two respective materials.[389] Stronger interactions are expected between two substances as the magnitude of D_{ij} decreases. Hence, in comparing D_{ij} values between materials, it is profitable to search for the system having the shortest distance between the two total cohesion parameters. Table 44 includes the calculated D_{ij} values for both of the SSRTP substrates and each of the phosphors chosen for this project. The RTP solvent, ethanol, is also included in these calculations.

Table 44. Interaction strengths (D_{ij}) between SSRTP substrate and phosphor (or solvent).

phosphor (or solvent)	δ_d ($MPa^{1/2}$)	δ_p ($MPa^{1/2}$)	δ_h ($MPa^{1/2}$)	cellulose D_{ij} ($MPa^{1/2}$)	*K4M* HPMC D_{ij} ($MPa^{1/2}$)	ΔD_{ij}	preferred substrate
naphthalene	19.4	0.0	8.6	19.3	12.1	+7.2	hpmc
2-naphthol	19.6	7.1	8.3	17.4	10.3	+7.1	hpmc
2-naphthoic acid	19.8	6.6	17.6	9.7	6.2	+3.5	hpmc
salicylic acid	18.4	10.1	19.0	7.4	6.1	+1.3	hpmc
phenanthrene	19.4	0.0	0.8	26.1	18.3	+7.8	hpmc
PABA	16.9	13.3	18.0	8.3	7.2	+1.1	hpmc
acenaphthene	19.2	2.9	5.0	21.2	13.6	+7.6	hpmc
ethanol	13.6	8.4	20.8	3.7	4.3	-0.6	cellulose

The parameter ΔD_{ij} is calculated according to equation #20.

$$\Delta D_{ij} = D_{ij}^{cellulose} - D_{ij}^{hpmc} \qquad (20)$$

Positive values of ΔD_{ij} indicate that intermolecular interactions are favorable between a phosphor and the HPMC matrix. Alternatively, negative ΔD_{ij} values suggest favorable attractions between a phosphor and the cellulose matrix. The magnitude of ΔD_{ij} is indicative of the preference that a phosphor (or solvent) will have for one of the RTP substrates compared to the other. For instance, the low ΔD_{ij} values for PABA and salicylic acid imply that either RTP substrate should serve as a suitable matrix for these phosphors even though HPMC is the clear favorite. It is interesting to consider that ethanol has a slight preference for cellulose over HPMC. However, given the partial lipophilic character of HPMC, this result is not unexpected.

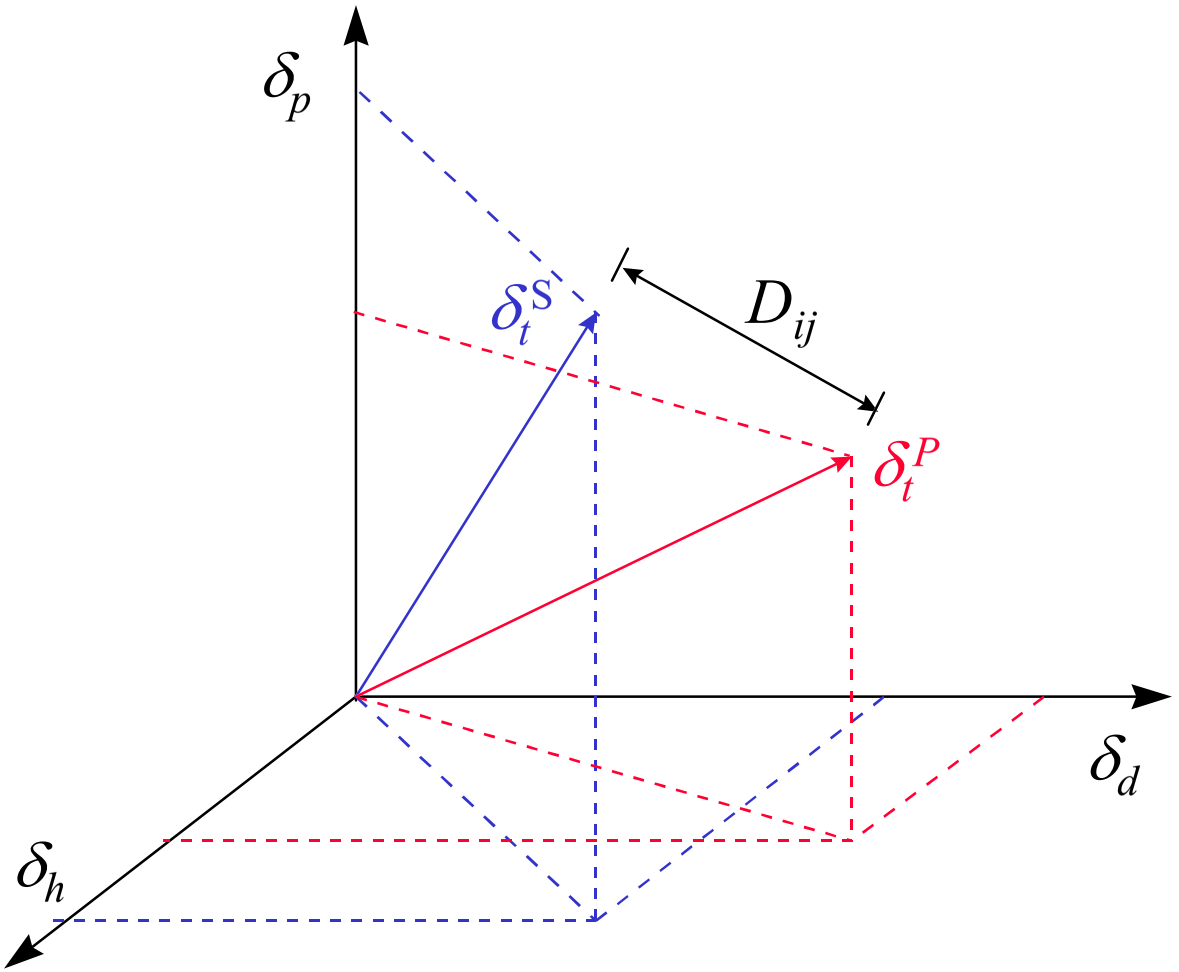

Figure 62. Cohesion parameters and D_{ij} in three-dimensional space (*S*= substrate=*i*; *P*=phosphor=*j*).

R.J. Hurtubise, an expert in the field of SSRTP, has theorized that it is the Young's modulus of a material that determines its suitability for use as an RTP substrate. Young's modulus (*E*) is a fundamental property of a solid material that is directly related to its interatomic or intermolecular binding energy. It is a measure of the *stiffness* of the material. Roberts and colleagues have discovered a linear relationship between the derived values of the CED of a substance and its Young's modulus.[423] Furthermore, they suggest that the Young's modulus of a material might be predicted from its Hansen cohesion parameters. Newton et al. have demonstrated a relationship between the Hansen parameters and the mechanical properties of a homologous series of benzoic acid esters.[424] Their results confirm that a calculation of Young's modulus from Hansen cohesion parameters is possible. It will now be possible to relate the proposals presented within this dissertation to the RTP theories that have been promoted by other researchers. The adoption of cohesion parameters for the quantification of substrate-phosphor interaction is certainly the next logical step in the advancement of the field of SSRTP spectroscopy.

Nevertheless, it should be noted that the models devised in section 6.3 are crude and oversimplified. These results are intended for the prediction of trends inherent to this research project only. In other words, it would be careless and professionally irresponsible to apply the numerical results published within this section to studies of paint formulations, drug transport through skin, or any other application without giving due consideration to their original source or nature of derivation. On the other hand, the empirical and semi-empirical data provided within section 6.3 clearly illustrate the potential of this approach toward the prediction of favorable RTP matrix-phosphor interactions. Unfortunately, before these models can be applied further, additional RTP studies will be necessary using new phosphors and SSRTP substrate materials. Furthermore, a comprehensive set of partial cohesion parameters will be needed for each of the phosphors and SSRTP substrates to be studied.

[423] R.J. Roberts, R.C. Rowe, and P. York, *Powder Technol.*, 1991, V. 65, p. 139.
[424] J.M. Newton, A.B. Mashadi, and F. Podczeck, *Eur. J. Pharm. Biopharm.*, 1993, V. 39, p. 153.

7.0 Interpretation of Results and Related Discussion

The two primary goals of the dissertation research were to i). determine whether the naphthalene/NaI/HPMC or naphthalene/NaI/filter paper system would allow for the greatest sensitivity, the lowest limit of detection (LOD), and the lowest limit of quantitation (LOQ) for an SSRTP analysis and ii). to gain whatever insights that the results might reveal about these two different SSRTP approaches. With the exception of changes to the concentration ranges of the phosphor, both support materials were analyzed using the same experimental conditions in order to provide for a true comparison of results. Both support materials yielded linear calibration curves within their respective concentration ranges. LOD's were calculated for both substrates using two recognized methods: the International Union of Pure and Applied Chemistry (IUPAC) approach and a propagation of errors approach.[364,349] The IUPAC recommends that the LOD be defined as the concentration of an analyte leading to a signal three times the standard deviation of 20 measurements.[425] Additionally, the IUPAC calibration sensitivity (unitless) was determined for both substrates by calculating the slopes of the linear calibration curves (*m*). Since the LOD only describes a qualitative limit of detection, a limit of quantitation (LOQ) was also calculated for each substrate. The determination of the analytical figures of merit for the naphthalene/NaI/HPMC combination resulted in a calibration sensitivity of 2.79, LOD of 4 ppm (3 ng), and LOQ of 14 ppm (11 ng). Investigations of the naphthalene/NaI/filter paper combination produced a calibration sensitivity of 0.326, LOD of 33 ppm (26 ng), and LOQ of 109 ppm (86 ng). Although analysis time increases significantly, extended purging with dry-nitrogen gas yields improved sensitivities, lower LOD's, and lower LOQ's for both support materials when LOD and LOQ are calculated according to the IUPAC guidelines. In each instance, HPMC yielded analytical figures of merit that were superior to those obtained using filter paper. Additionally, since RTP emission intensities are stronger for the HPMC-bound analyte, the possibility that background phosphorescence will interfere with the analysis is significantly reduced (Figure 63). Depending on the apolar, polar, and hydrogen-bonding character of the analyte, *K4M PREM* HPMC pellets have the potential to offer the SSRTP spectroscopist lower limits of detection, lower limits of quantitation, and greater sensitivity compared to filter paper pellets.

A modest library of SSRTP emission spectra was prepared by analyzing a collection of eight phosphors trapped on *K4M PREM* HPMC substrates. A variety of probe analytes were selected to attain diversity with regard to size, shape, chemical functionality, and apolar/polar character. The model phosphors chosen for this study were acenaphthene, naphthalene, 2-naphthoic acid, 2-naphthol, p-aminobenzoic acid, phenanthrene, salicylic acid (sodium salt), and triphenylene. Strong SSRTP emission spectra were acquired for each of these analytes. Future

[425] IUPAC, *Pure Appl. Chem.*, 1976, V. 45, p. 65.

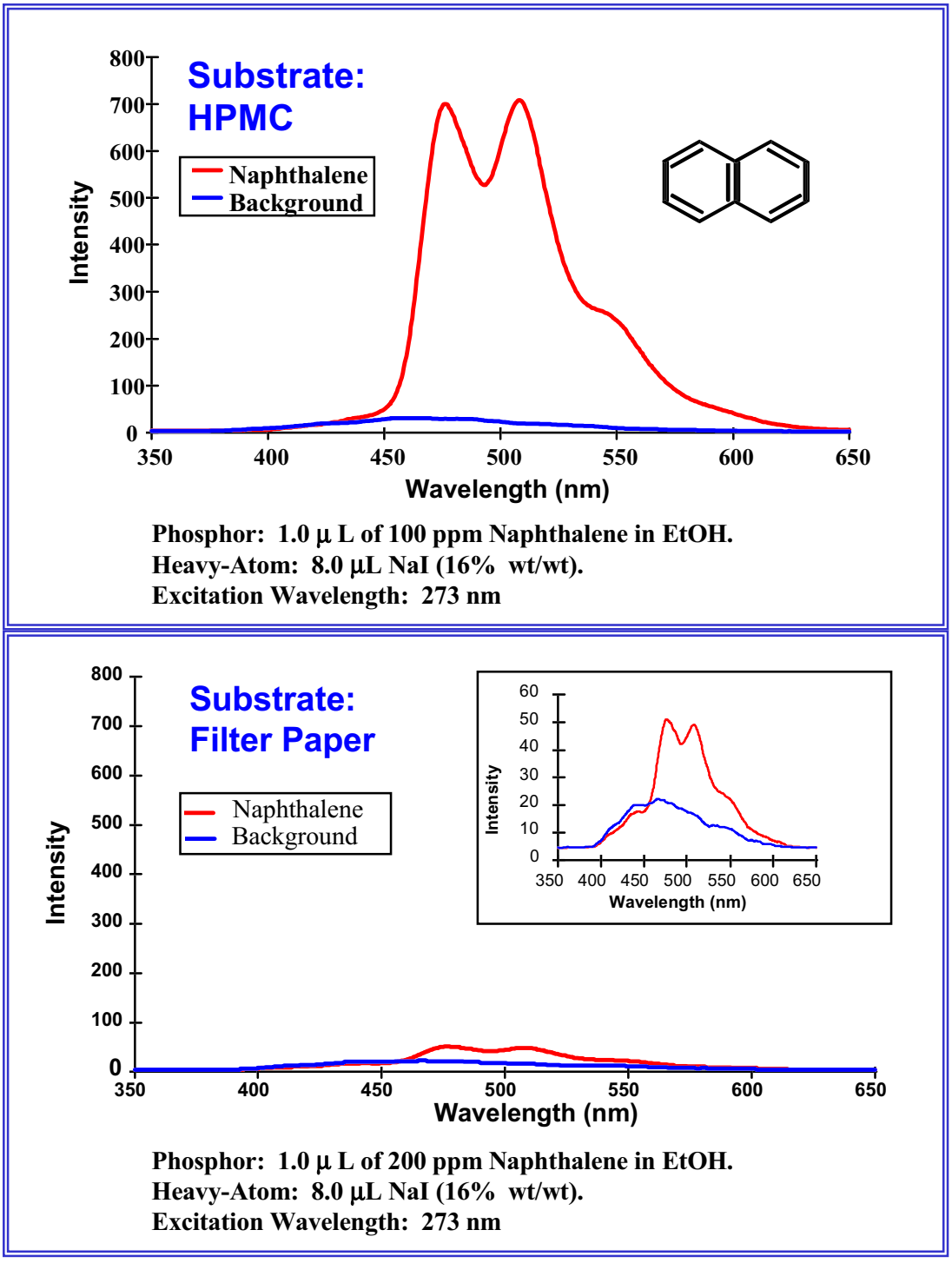

Figure 63. A comparison of Naphthalene SSRTP emission spectra for HPMC vs. filter paper supports. Background emission (NaI only) is shown in blue for both substrates.

SSRTP studies involving hundreds of phosphors will be necessary in order to support these preliminary findings. Nevertheless, this inaugural study illustrates the potential of *K4M PREM* HPMC to serve as a universal RTP matrix material.

7.1 A Comparison of HPMC and Cellulose Substrates

SSRTP requires that an analyte be rigidly immobilized upon and/or within a solid support material. At room temperature, physical trapping of the phosphor by the matrix and favorable substrate-phosphor intermolecular interactions contribute to the minimization of collisional deactivation and result in an increased phosphorescence quantum yield. For this research, solid HPMC pellets were produced by directly compressing the native HPMC powder in a die between two punches under a load of 17K psig. Filter paper "pellets" were also manufactured in this fashion so that the surface features and macroscopic porosity of both materials were as similar as possible. Unfortunately, native HPMC is a particulate material whereas sheets of filter paper are comprised of intertwined cellulose fibers. Therefore, the original physical structure of the support material introduces a variable that cannot be disregarded.

7.1.1 Mechanics of Substrate Compaction

What are the natures of the HPMC and cellulose microenvironments following the conversion of these materials into rigid pellets? To answer this question, it is first necessary to review the mechanics of compaction. Compaction is defined as the *compression* and *consolidation* of a two-phase system due to an applied force.[426] Compression involves a reduction in volume of a powder bed due to the application of a stress (i.e. pressure). Consolidation is an increase in the mechanical strength of a material resulting from particle-particle interactions. Compaction results in the transformation of a powder into a pellet of defined shape and size. Although new concepts such as percolation theory and fractal geometry have provided additional insights into the physics of tablet compaction, the classical models of excipient compaction are most pertinent to this project.[427]

During delivery of the HPMC to the pellet die, the individual particles flow readily. The fine particles fill voids between the larger ones and a close packing arrangement results. The packing characteristics of the HPMC are governed by the density, size, size distribution, shape and surface properties of the individual particles as well as variables such as the rate of particulate flow and the relationship between the die-cavity diameter and particle diameter. These characteristics define the number of contact points and potential bonding areas between the HPMC particles.

Initially, before the upper punch makes contact with the powder bed, there are only tiny points of contact between the HPMC particles. As the compression cycle begins, the particles flow with respect to each other and the finer particles enter the voids between the larger particles.

---

[426] I. Ghebre-Sellassie, **Multiparticulate Oral Drug Delivery**, New York: Marcel Dekker, Inc., 1994.
[427] H. Leuenberger, R. Leu, and J-D Bonny in **Pharmaceutical Powder Compaction Technology**, G. Alderborn and C. Nyström, Eds., New York: Marcel Dekker, Inc., 1996.

The density of the powder bed is increased. Since spherical particles initially assume a close packing arrangement, they undergo less particle rearrangement than do flaky or filamentous particles. As the punches continue to approach one another, forces are transmitted through the interparticulate points of contact and deformation of the material occurs. If the deformation disappears entirely upon release of the stress, then the deformation is said to be *elastic*.[428] If the particles do not completely recover following the removal of the stress, then the deformation is said to be *plastic*. The force required to initiate a plastic deformation is called the yield value. If the applied stress is released before the yield value is attained, the particles elastically regain their original shapes and rearrange to a closely packed state. Figure 64 diagrams the stages of compaction.

After the yield value is attained, either plastic deformation or fragmentation become the dominant mechanisms of compaction. Plastic deformation typically occurs for particulates in which the shear strength is less than the tensile strength. Fragmentation is most commonly encountered during the compaction of hard, brittle materials in which the shear strength is greater than the tensile strength. If fragmentation occurs, the surface area of the powder increases. As new surfaces are created, the potential bonding area between particles increases. Densification of the compact is further enhanced as the new, smaller fragments begin to fill the voids between the larger particles. Some materials, such as HPMC, sodium chloride, and starch, exhibit high plastic deformation. Others, exhibit high elastic deformation. Highly brittle materials, such as crystalline lactose and sucrose, exhibit extensive fragmentation. Nevertheless, there is no single excipient material that exhibits only one mechanism of deformation.

Bonding occurs between the new surfaces formed by deformation and/or fragmentation. The attraction between particles is inversely proportional to the distance between them. When the particles are in close proximity, a bond is created and they can become attached to each other. There are several mechanisms that contribute to the strength of a bond. *Mechanical interlocking* is due to the entanglement of the particles. Irregular particle shapes and rough particle surfaces promote interlocking. Mechanical interlocking is the only bonding mechanism that does not involve atomic forces and it is expected to contribute very little to the overall strength of the pellet. Asperitic bonding can also occur as a result of melting at the points of contact where the applied pressure is sufficiently high enough to liquefy the solid particles. In this manner, the contact area between particles increases significantly and solid bridges are formed. This mechanism is called *fusion or cold welding* since the overall temperature of the pellet remains cold. Finally, *intermolecular forces* promote molecular bonding. Hydrogen bonding, van der Waals forces, and ionic bonding are potential contributors. Since van der Waals forces can be significant at particle separations of up to 10 nm, the particles need not necessarily be in contact with each other. Water sorption layers at the surfaces of polar particles are also expected to participate in interparticulate attraction. Since plastic deformation produces an increased contact area between the particles, extensive hydrogen-bonded networks are facilitated by the water sorption layers.

---

[428] E.L. Parrott in **Pharmaceutical Dosage Forms - Tablets Vol. 2**, H.A. Lieberman and L. Lachman, Eds., New York: Marcel Dekker, Inc., 1981.

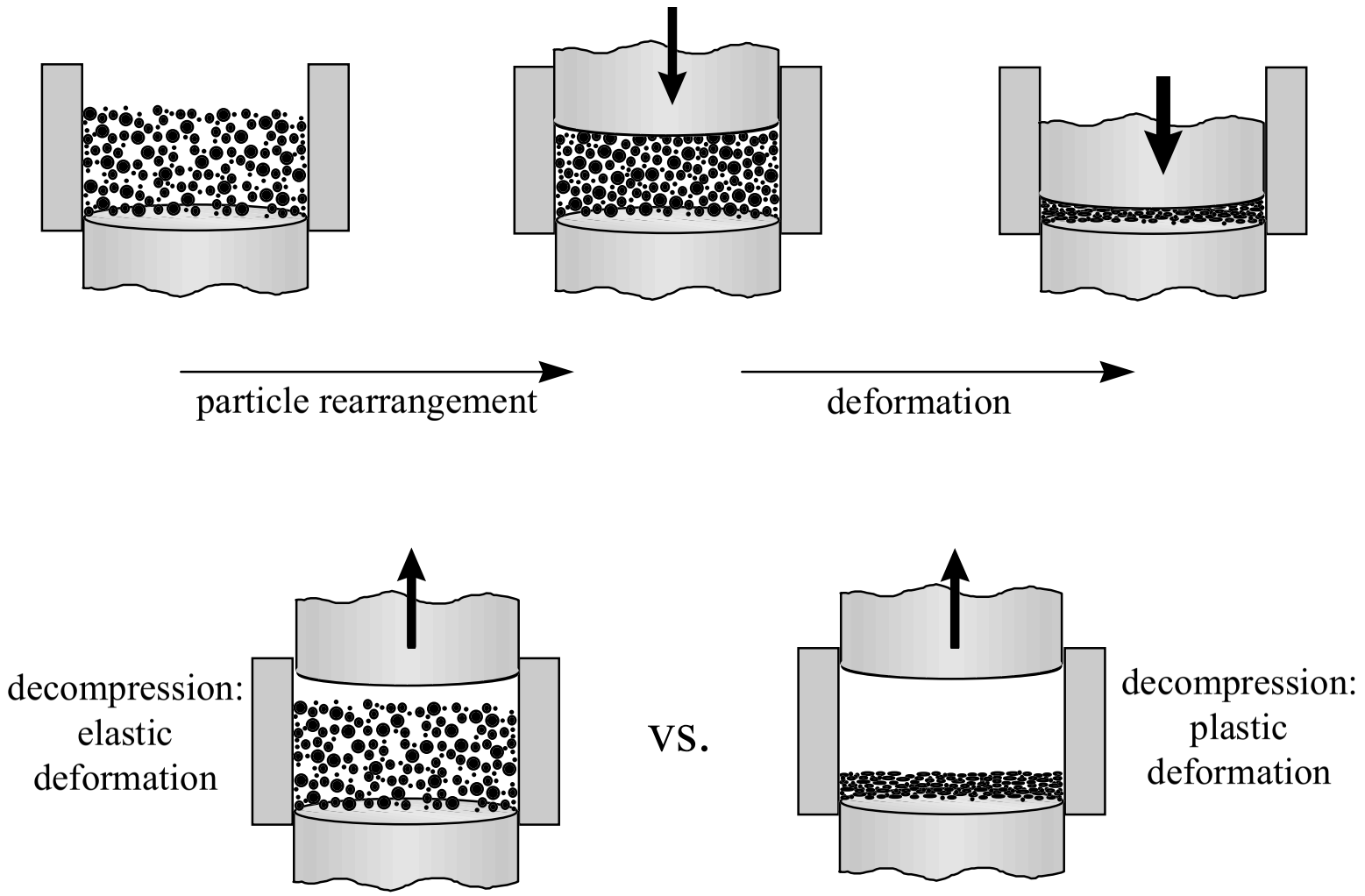

Figure 64. The Stages of Particulate Compaction

7.1.2 Theoretical Modes of Particulate Bonding for HPMC and Filter Paper Compacts

Nyström and Karehill have proposed that intermolecular forces are the dominating bond mechanism for pharmaceutical materials.[429] In principle, high strength pellets are attainable by utilizing materials that offer limited elastic deformation, extreme plastic deformation, and a large compact surface area. For HPMC, intermolecular forces are the primary modes of particulate bonding with mechanical interlocking playing a reduced role in the bonding process. For multiple layers of filter paper, intermolecular interactions are also expected to be the primary bonding mechanisms. Although the entanglement of cellulose fibers between individual sheets is possible, mechanical interlocking does not contribute significantly to the strength of these compacts. On the other hand, HPMC-HPMC and cellulose-cellulose hydrogen bonding is expected to be enhanced by the moisture sorption layers that are present within each material. Recent studies have confirmed this proposal. The effect of moisture on the tensile strength of tablets is a result of the balance between monolayer adsorbed moisture, internally absorbed moisture, and externally adsorbed moisture. By increasing the quantity of monolayer adsorbed moisture and internally absorbed moisture present for each HPMC particle, it is possible to significantly improve the
tensile strength of HPMC compacts.[258] Similar explanations account for the decrease in mean yield pressure and elastic recovery of HPMC tablets with increasing relative humidity. Figure 65 models the different states of moisture involved with HPMC.

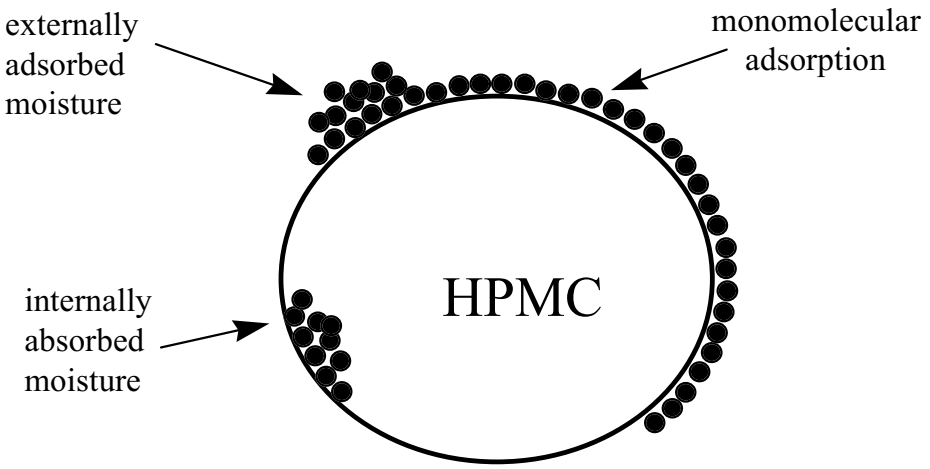

Figure 65. Representation of the three mechanisms by which water could be held in HPMC particles.
(adapted from Nokhodchi, et al., J. Pharm. Sci., V. 86, No. 5, May 1997)

[429] C. Nyström and P-G Karehill in **Pharmaceutical Powder Compaction Technology** G. Alderborn and C. Nyström, Eds., New York: Marcel Dekker, Inc., 1996.

Following compaction, macroscopic porosity is no longer evident for either the HPMC or cellulose pellets. However, each solid specimen will retain a certain level of microscopic porosity. For most pharmaceutical compacts, porosity typically ranges from 5% to 35%.[430] The gas phase in the compact can be described as a continuous phase consisting of a three-dimensional network of connected pores. Thus, the compact can be physically described by both the characteristics of the interparticulate pore system (e.g., porosity, pore surface area, and pore size distribution) and by the properties of the particles that constitute the matrix (e.g., particle size distribution, surface area, and the packing characteristics or relative locations of the particles). Figure 66 shows two rudimentary models of the packing that occurs within highly-compressed filter paper pellets and HPMC pellets. Both diagrams rely on a *jigsaw puzzle* approach. For filter paper, the "pieces" of the puzzle are long and thin as would be expected of cellulose fibers; whereas, the HPMC "pieces" are irregular in shape and show a greater degree of mechanical interlocking.

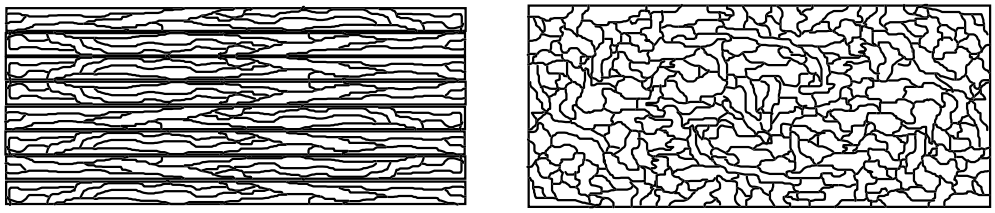

cross-sectional side view of an
eight-layer filter paper pellet*
compact thickness = 600 μm

cross-sectional side view of an
HPMC pellet*
compact thickness = 600 μm

Figure 66. A comparison of the expected packing arrangements adopted by cellulose fibers and HPMC particles within pellets.
*not drawn to scale

Models developed by the pharmaceutical sciences assist one in visualizing the complex physical structure of an HPMC pellet at the macro- and microscopic levels. However, the composition of a filter paper compact is more difficult to visualize since statistical and continuum models are both unsatisfactory for describing its physical structure. The surface structures of HPMC and filter paper substrates are neither uniform nor homogeneous.

7.2 A Comparison of the Supramolecular Structures of Cellulose and HPMC

HPMC and cellulose are both linear chain polymers. Although the biosynthetic machinery is complex and not fully understood, woody plants produce cellulose and arrange the chains to form densely packed microfibrils.[166] These cellulose microfibrils are arranged in distinct layers. Some layers are more rigid than others due to the addition of lignin and matrix polysaccharides. Complex, multi-layered structures such as wood fiber cells are built up in this

[430] G. Alderborn in **Pharmaceutical Powder Compaction Technology** G. Alderborn and C. Nyström, Eds., New York: Marcel Dekker, Inc., 1996.

fashion. The cellulose chains in each microfibril are probably synthesized together by enzyme complexes located on the cytoplasmic membrane. In this manner, they are extruded in organized form into the cell wall with their alignment and pattern of deposition determined by the cytoplasmic fibrillar protein system known as the microtubules. Figure 67 illustrates the manner in which cellulose chains, in the form of elementary fibrils, comprise cellulose microfibrils. Microfibrils are responsible for forming macrofibrils and the macrofibrils, in turn, are responsible for forming the fibers that comprise the layers of the plant cell wall. The cellulose fibers that comprise filter paper are readily observed by electron microscopy as shown in figure 36.

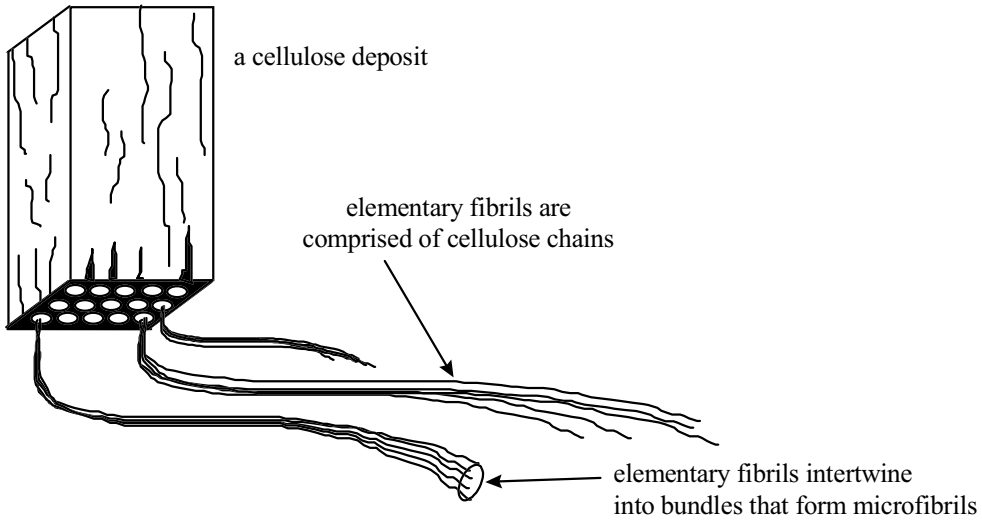

Figure 67. Relationship between cellulose chains and microfibrils
(adapted from D.A. Rees, **Polysaccharide Shapes**, New York: John Wiley & Sons, 1977)

In an effort to understand the interactions between HPMC and cellulose chains at the supramolecular level, one must rely on models proposed by the polymer sciences. Unfortunately, polymer researchers have conventionally studied well-defined systems of synthetic polymers instead of the naturally occurring biopolymers. Nevertheless, many of the theories that apply to the synthetic macromolecules also pertain equally well to HPMC and cellulose.

7.2.1 Molecular Weight Considerations

A knowledge of molecular weight and molecular weight distribution of polymers is important since there is a definite relationship between polymer molecular weight and the mechanical properties of the polymer. The average molecular weight of *K4M PREM* HPMC is 96,000 g/mol.[248,249] The average molecular weight of the cellulose chains that comprise Fisherbrand P2 filter paper is unknown. Nevertheless, Krässig has estimated that naturally occurring cellulose has a molecular weight close to 2,000,000 g/mol.[163] This high degree of polymerization is significantly reduced during physical and chemical treatment. Therefore, most processed cellulose substrates offer average molecular weights within the range of 130,000 to

500,000 g/mol. It should be noted that both HPMC and cellulose are polydisperse. Estimated average molecular weights are considered to be *number average molecular weights* as represented in figure 68.

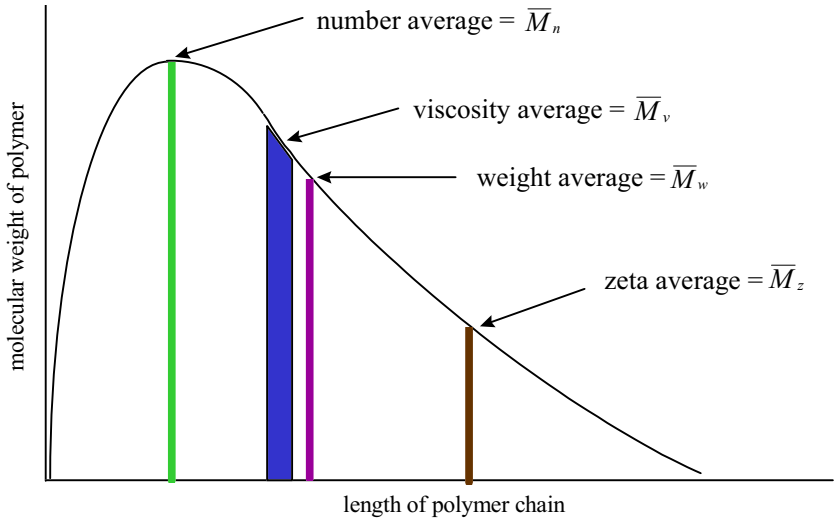

Figure 68. The relationship between molecular weight distribution and average molecular weights of a generic polymer.
(adapted from E. Sjöström, **Wood Chemistry: Fundamentals and Application, 2nd Ed** . New York: Academic Press, Inc., 1993..)

7.2.2 The Fibrillar Network Model of Cellulose

At present, the structure of cellulose fibers is best represented by a fibrillar network model. This simplified model depicts the fiber as being comprised of a network of elementary fibrils which intertwine randomly to form micro-and macrofibrils. The expected diameter of a microfibril is estimated to fall within the range of 10 to 30 nm. The elementary fibrils consist of strands of cellulose crystals (i.e. chains) and have an estimated diameter of 2 to 4 nm. The internal cohesion between the crystals within these strands is dictated by the length of the fiber-forming polymer molecules as they pass alternately through several elementary crystallites and the extent of less-ordered interlinking regions between the crystals. The coherence of the fibrils in their secondary aggregations is given either by hydrogen bonds at close contact points or by diverging molecules. Access into this structure is provided by i). large voids formed by imperfect axial orientation of the fibrillar aggregates, ii). interstices of nanometer dimensions between the fibrils, and iii). by the less-ordered (amorphous or paracrystalline) interlinking regions between the crystallites inside the elementary fibrils. Interfibrillar spaces within the plant cell wall range between 1.2 to 5 nm in the wet state and approximately 1 nm in the dry state. Although no single interpretation of cellulose fiber structure is universally accepted at present, the fibrillar network model is the current favorite. Figure 69 illustrates the three fundamental interpretations that have been proposed.

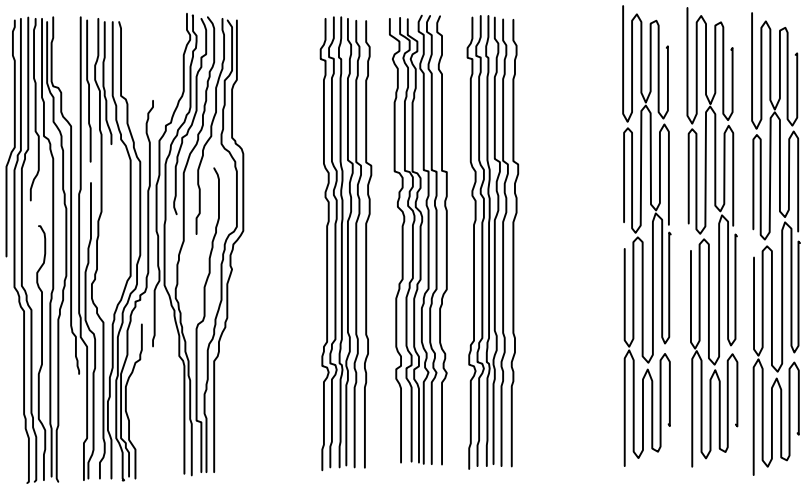

Figure 69. Three proposed models of cellulose fibril structure.
(adapted from D. Fengel & G. Wegener, **Wood: Chemistry, Ultrastructure, Reactions**, New York: Walter de Gruyter, 1989.)

7.2.3 The Behavior of Cellulose and HPMC during Full Dissolution

The fibrillar network model of cellulose fibril structure is considered to be a highly ordered system containing transitional chains. In comparison to cellulose, it seems likely that HPMC will exist as a less-ordered network containing both chain associations and entangled regions. Figure 70 illustrates two models that compare these proposed differences in supramolecular architecture. Even if cellulose is dissolved in a suitable solvent such as cadoxen, the individual chains are still expected to form entangled associations and isolated associations as illustrated in figure 71. Additionally, an ideal separation that allows individual cellulose ribbons to assume linear, random-coil geometries will only occur in very dilute solutions (i.e. cellulose < 0.05%). Chain associations and entangled regions are more likely in HPMC as a result of the Mercerization process that native cellulose is subjected to during the preparation of a suitable alkali cellulose. When exposed to a dissolving solvent, HPMC is expected to initially form an infinite network of molecules with numerous regions of elevated entanglement. As dissolution continues, the entangled regions are minimized and an ideal entangled network is formed. Finally, if the polymer disentanglement concentration is exceeded, then a uniform solution of linear, random coil geometries is achieved. Unlike cellulose, HPMC solutions can be prepared in high concentrations.

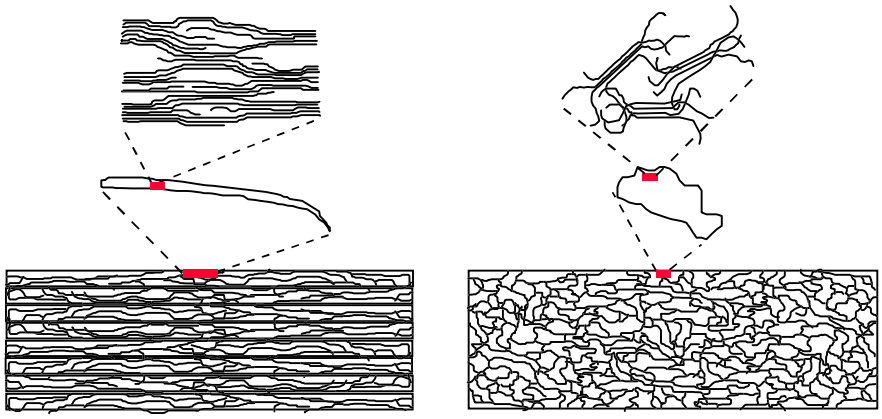

a). cross-sectional side view of an eight-layer filter paper pellet* approximate pellet thickness = 600 µm

b). cross-sectional side view of an HPMC pellet* approximate pellet thickness = 600 µm

Figure 70. Two models that compare the internal supramolecular structures of pellets produced from a). cellulose fibers and b). HPMC particles.
*not drawn to scale

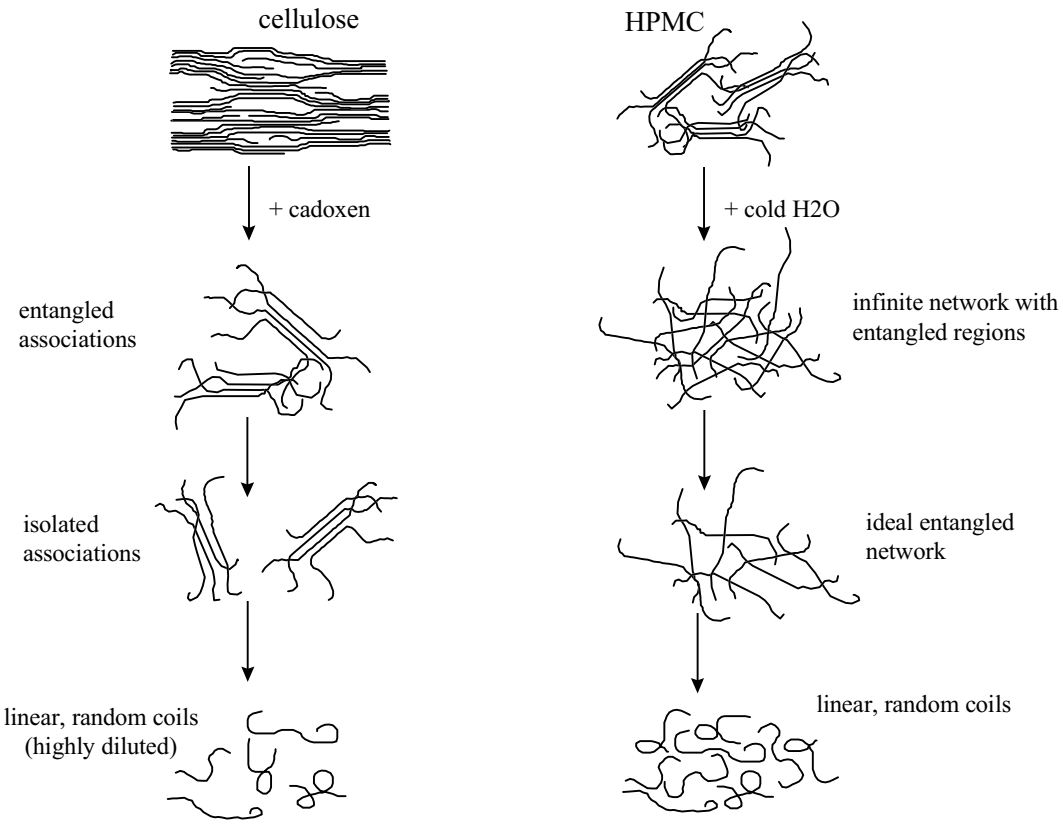

Figure 71. Behavior of cellulose and HPMC during full dissolution.
*not drawn to scale

7.2.4 The Effect of Ethanol on Cellulose and HPMC Matrices

Even though models of the dissolution behavior of cellulose and HPMC are useful for visualizing the intermolecular interactions between polymer chains, cadoxen and cold water were not the solvents utilized for these investigations. What are the effects of a swelling SSRTP solvent (i.e. ethanol) on these two substrates? There are three important parameters that govern the swelling of cellulose and HPMC by ethanol: i). the structure of the substrate, ii). the molar volume of the swelling agent, and iii). the similarities of the matrix δ_h and δ_p parameters to those of the ethanol. The initial stage of swelling depends on the interrelation between the magnitude, distribution, and interconnection of voids in the samples and the molar volume of the ethanol. The size distribution of the voids is, of course, highly dependent on the moisture content of the matrix. Since the δ_h parameter for ethanol ($\delta_h = 20.8$) is similar to the δ_h parameter of cellulose ($\delta_h = 24.4$), ethanol is able to disrupt the hydrogen bonds between the hydroxyl groups in the accessible regions of the cellulose network. Due to swelling, networks of interconnected pores and channels are expanded. This increases the accessible surfaces and opens the fibrillar interstices and other submicroscopic pores. Likewise, the δ_h parameters of ethanol ($\delta_h = 20.8$) and HPMC ($\delta_h = 16.7$) are sufficiently similar to allow for extensive hydrogen bond splitting.

Nevertheless, the swelling behavior of filter paper is unusual compared to other cellulose networks. Mantanis and colleagues have discovered that filter paper swells almost three times more than α-cellulose and to an extent nearly four times greater than *Avicel* microcrystalline cellulose.[197] A full interpretation of these observations has not been offered; however, the researchers have theorized that the enhanced swelling of filter paper is probably related to morphological factors. Gao and colleagues have reported that the swelling of *K4M* HPMC pellets is anisotropic with a preferential expansion in the axial direction.[253]

Figure 72 proposes that ethanol is capable of producing an infinite entangled network when delivered to a "dry" HPMC pellet. With the passage of time, an ideal entangled network forms at the surface of the pellet. When the ethanol is removed from the matrix by heating, the ideal entangled network collapses and a thin gel layer results at the pellet surface. Although ethanol is also capable of swelling the cellulose fibrillar network, an infinite entangled network of cellulose molecules is not expected. Furthermore, ethanol is neither capable of producing an ideal entangled cellulose network nor fully dissolving the highly ordered cellulose ribbons that comprise the elementary fibrils.

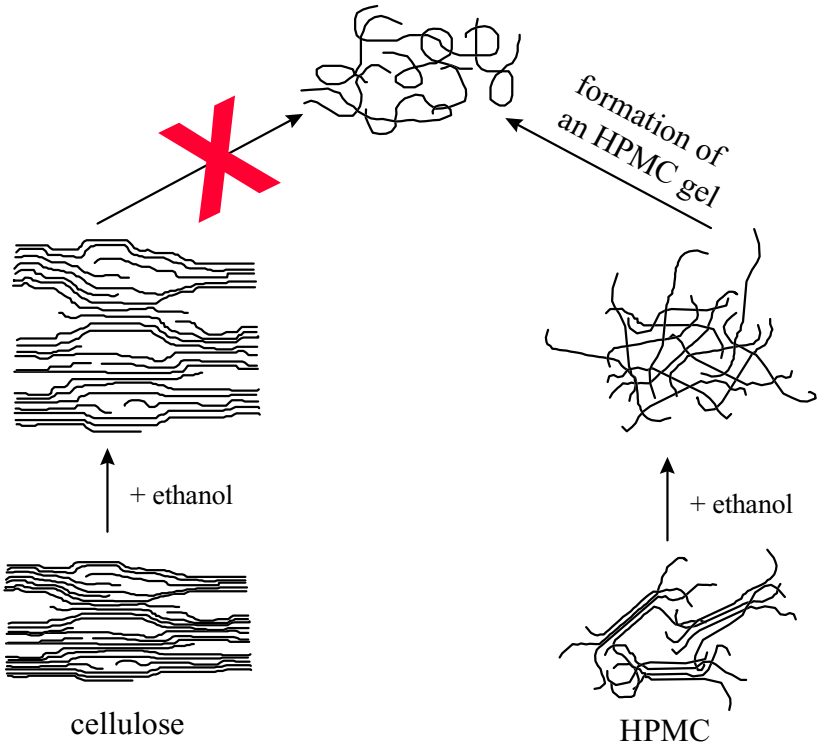

Figure 72. Solvent-induced swelling of cellulose and HPMC.
*not drawn to scale

7.2.5 Physical Interactions Involving Phosphor, Heavy Atom, and Substrate

What is the physical nature of the phosphor/heavy-atom/substrate interactions for each of these matrices? For filter paper, this is an important question that has not yet been adequately addressed by the SSRTP community. Even in the absence of heavy-atom perturbers, polar and ionic phosphors will yield strong RTP intensities when immobilized by filter paper. It has been proposed that strong adsorption interactions due to hydrogen bonding are responsible for the production of intense RTP emission from these analytes. For nonpolar phosphors analyzed under the same conditions, RTP signals are extremely low. Investigators have theorized that only weak dispersion interactions are present between nonpolar phosphors and the filter paper matrix. Thus, production of intense RTP emission from nonpolar aromatic compounds in filter paper is possible, but requires the utilization of the external heavy-atom effect.

The premier theory for describing the interaction of phosphor, heavy-atom, and filter paper is a matrix isolation model based on the extensive hydrogen bonding that exists between cellulose ribbons. Hurtubise has attempted to quantitate the relationship between hydrogen bonding in filter paper and multiple SSRTP parameters by comparing τ_p and ϕ_p to E, the Young's modulus of the paper.[117] Analytes and heavy-atoms are thought to be immobilized in the pores and voids between cellulose chains. Pores and voids, in general, provide hydroxyl-rich

surfaces.[431] Nishigaki and colleagues have further extended this model by proposing that trapping in filter paper is size specific.[118] They suggest that small phosphors such as vanillin will retain mobility within a cellulose cage; whereas, a large phosphor such as 9-anthracenemethanol will be perfectly trapped (Figure 73). Given vanillin's freedom of mobility, the probability is much greater that it will undergo collisional quenching in comparison to the 9-anthracenemethanol.

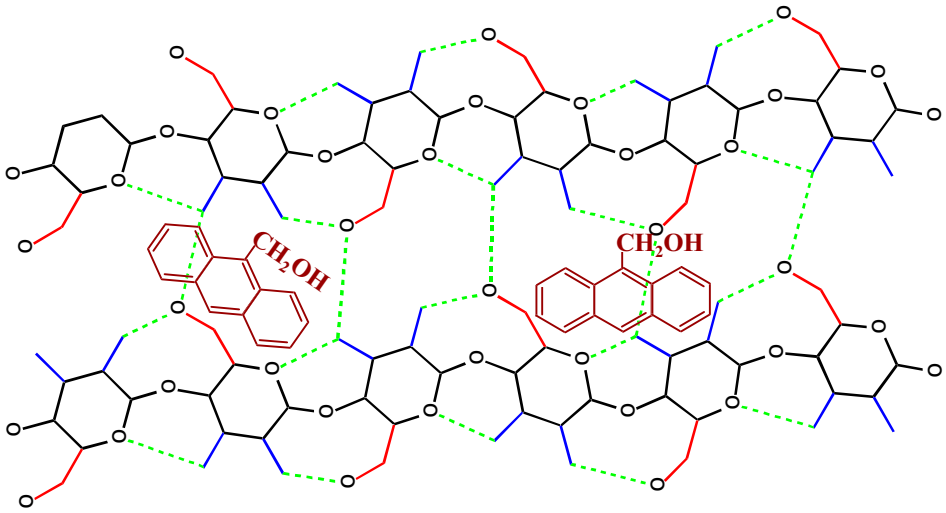

Figure 73. Size-specific trapping of a phosphor in the absence of extensive phosphor-substrate hydrogen bonding (according to Nishigaki, et al.)
*not drawn to scale

Figure 74 is an interaction model developed by the author to illustrate the physical trapping of phosphor and heavy-atom within filter paper and HPMC. Both support materials are shown in the swollen state even though the solvent molecules are not included. To improve clarity, only heavy-atoms in the vicinity of the phosphor are shown. As holds true for the filter paper, extensive hydrogen bonding between HPMC chains is also critical for the successful immobilization of analyte and heavy-atom. Although neither figure is drawn to scale, size-specific trapping should also be possible for the HPMC matrix. Unfortunately, these illustrations are two-dimensional; whereas, matrix isolation occurs in a three-dimensional world. If one were to visualize these materials in 3-D, it would be readily apparent that the intertwined elementary cellulose fibrils found in filter paper would form micro-capillary channels. Such capillaries exist at many levels for cellulose. This is no surprise to those who are familiar with plant biology since plant species such as trees rely on a mechanism of capillary action to draw water from the soil and transfer it to their upper- and outermost extremities. Thus, the proposed cage-like structure of filter paper that is considered to be partially responsible for immobilizing phosphors

[431] S.P. Rowland in **Textile and Paper Chemistry and Technology** ACS Symposium Series 49, J.C. Arthur, Jr., Ed., Washington D.C.: American Chemical Society, 1977.

can also be described in terms of a capillary arrangement. On the other hand, since HPMC chains are expected to be more disordered than the cellulose in filter paper, the HPMC should form an ideal entangled network. Ordered HPMC capillaries, if present at all, should be minimal. During the drying step, ethanol sorption layers are eliminated and direct inter-chain hydrogen bonding is reintroduced to both matrices. If ambient humidity is high, the existence of cellulose-water hydrogen bonding should not be ignored. Nevertheless, the filter paper structure effectively collapses inward as cellulose-ethanol bonds are replaced by cellulose-cellulose hydrogen bonds. Similarly, HPMC-ethanol bonds are replaced by HPMC-HPMC hydrogen bonds. In this manner, phosphor molecules and heavy-atoms become rigidly trapped within the substrates. Generally, k_P is less than 10^4 S^{-1} since the $T_1 \rightarrow S_0$ transition is spin-forbidden. This allows sufficient time for a nonradiative decay of T_1 (i.e. $k'_{nr} > k_P$). Since $k'_{nr} = k'_{ec} + k'_{isc}$ and $k'_{ec} >> k'_{isc}$, then dynamic collisional quenching (i.e. k'_{ec}) must be significantly reduced for phosphorescence to occur. Efficient phosphor immobilization by the filter paper and HPMC matrices ensures that k'_{ec} is substantially reduced.

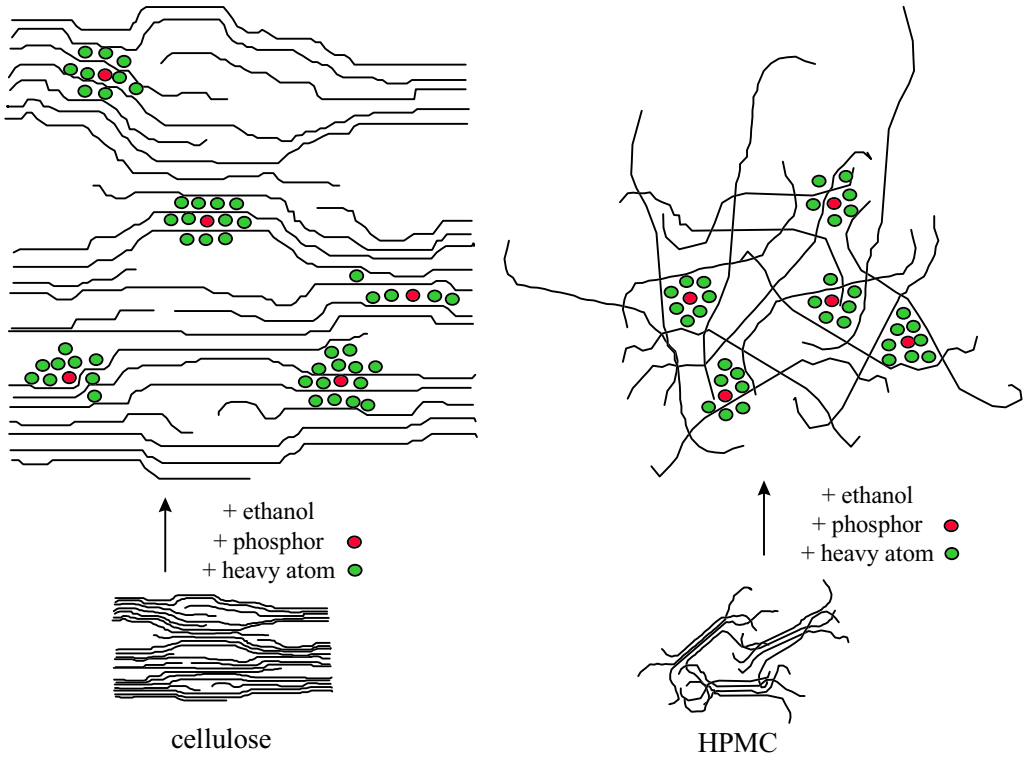

Figure 74. Physical interaction of phosphor, heavy atom, and substrate.
Limited quantity of heavy atom enhancers shown for purposes of clarity.
Solvent molecules not shown for purposes of clarity.
*not drawn to scale

HPMC yields substantial improvements in RTP intensity in comparison to filter paper when naphthalene is selected as the probe analyte. Since direct phosphor-substrate hydrogen

bonding is not permitted, the improvement in signal intensity can't be attributed to enhanced immobilization of the analyte due to direct hydrogen bond interactions. Although it is possible that the HPMC pores and voids more closely approximate the size of the naphthalene molecule than do the *cages* within the cellulose matrix, it seems unlikely that this explanation would account entirely for such a substantial enhancement in RTP intensity. According to Hurtubise's proposals that relate RTP emission to E, it is also possible that the structural rigidity (i.e. the *stiffness*) of the HPMC pellet can be a factor if E is considerably greater for HPMC compacts than for filter paper compacts. Nevertheless, these investigations were outside the scope of this research project. Is it possible that a simpler explanation might account for the improved RTP intensities?

7.3 Fluid Flow Dynamics, Substrate Permeability, and Molecular Diffusion

The capillary action of the solid support material is responsible for controlling the rate and extent of solvent and phosphor migration across the surface of the substrate. Although gravity may contribute to a small extent, it is expected that capillary action is primarily responsible for the penetration of the solution into the interior of the matrix. Traditional modes of planar chromatography also rely on capillary flow-controlled conditions. The velocity at which the solvent front moves is a function of the distance of the front from the solvent entry position. The velocity of the solvent front declines as the distance increases. Consequently, the mobile phase velocity is not constant throughout a planar chromatogram unless modern forced-flow techniques are adopted.[432]

The speed at which a mobile phase will move through a stationary phase by capillary action is described by

$$\left(Z_f\right)^2 = \kappa t$$

where Z_f is the distance moved by the mobile phase from the sample origin to the solvent front, κ is the velocity constant, and t is time. The velocity constant is given by

$$\kappa = 2 K_0 d_p \left(\frac{\gamma}{\eta}\right) \cos\theta$$

where K_0 is the permeability constant, d_p is the average particle diameter, γ is the surface tension of the mobile phase, η is the viscosity of the mobile phase, and θ is the contact angle.[433] The velocity constant increases with increasing average particle size. Therefore, coarse particle substrates offer greater solvent front velocities. The mobile-phase velocity for fine particle substrates declines rapidly with increasing migration distance until it becomes so slow that diffusion causes the spots to broaden at a rate faster than the spot centers are able to migrate through the stationary phase. The coarse particle stationary phase is more permeable than the fine particle stationary phase and solvent velocity will be higher at longer plate lengths. Although it is yet unknown if the relative permeabilities of the SSRTP support materials are a

[432] C.F. Poole and S.K. Poole, *Anal. Chem.*, 1994, V. 66, p. 27A.
[433] C.F. Poole and S.K. Poole, *Anal. Chem.*, 1989, V. 61, p. 1257A.

major concern during the sample delivery step, these intriguing similarities are worthy of future study. For "coarse particle" substrates such as those prepared from cellulose fibers, solvent (or solution) velocity and permeability are predicted to be greater than for a fine particle substrate such as HPMC. For an HPMC support, sample flow rates should decrease considerably with increasing migration distance since sample permeability is reduced.

Since the filter paper and HPMC pellets are non-uniform and heterogeneous, one might wonder if the RTP signal enhancement is merely due to a significant difference in the molecular diffusion of the phosphor/solvent system through the compact during the sample delivery step. According to tables 18 and 21, the approximate surface area coverage of 1 μL of marker dye (in ethanol) using an HPMC compact is 35.6%; whereas, under the same conditions, the approximate surface area coverage of a filter paper compact is 43.5%. For these limited data sets, HPMC is clearly a more favorable SSRTP environment. Since the sample spot doesn't spread so widely across the compact, the concentration of phosphor that is expected to interact with the fixed excitation beam from the spectrometer should be higher. Undoubtedly, this would result in improved RTP intensities.

On the other hand, the penetration depth of the phosphor is a variable that should not be overlooked. Figure 75 illustrates the results of a penetration depth study that were obtained using both filter paper and HPMC compacts. As before, 1 μL of marker dye[434] (in ethanol) was delivered to four compacts comprised of filter paper and four compacts consisting of HPMC. Each pellet was divided through the center using a single-edge razor blade. For the HPMC substrates, a Meiji optical microscope (reflection mode) with an eyepiece millimeter scale (0.1 mm gradations) was utilized to measure approximate penetration depths. For the filter paper substrates, penetration depth was estimated by simply disassembling the pellet (as one might peel away the layers of an onion skin). The calculated thickness of a single filter paper layer was then used to estimate the total penetration depth.

Penetration depth and marker dye profiles were consistent for all filter paper pellets examined. The maximum penetration depth for eight layers of filter paper compressed to 17K psig was 240 μm (±10 μm). The dye profiles for each pellet approximated the shape of a smooth concave lens (or watch glass) if viewed side-on. The maximum penetration depth for HPMC compressed to 17K psig was 300 μm (±10 μm). The dye profiles for each HPMC pellet were non-uniform. This non-uniformity is best explained by considering the irregularity of the original HPMC particles and the random mechanical interlocking that ties the individual particles into a coherent structure. In a filter paper pellet, the inter- and intra-sheet voids are somewhat oriented in comparison to the randomized paths of the interstices found between particles within an HPMC pellet. These results indicate that permeability is favored in the X and Y directions for multiple-layer filter paper pellets. For HPMC pellets, capillary movement of the solvent, albeit irregular, occurs to a slightly greater extent in the Z direction, thereby allowing a sample to penetrate deeper into the solid substrate. These results partially offset the surface area coverage results discussed earlier. Whereas, the surface area coverage is greater for a filter paper pellet in comparison to an HPMC pellet, the reverse is true when comparing penetration depths. Since the predicted penetration depth of the UV excitation beam (≈100 μm) is considerably less than the

[434] Methyl Violet B Base

predicted phosphor penetration depths for both materials, it is unlikely that the substantial RTP signal enhancement observed for the HPMC-naphthalene system can be attributed solely to the ability of the HPMC to trap a greater quantity of analyte within the fixed dimensions of the excitation beam.

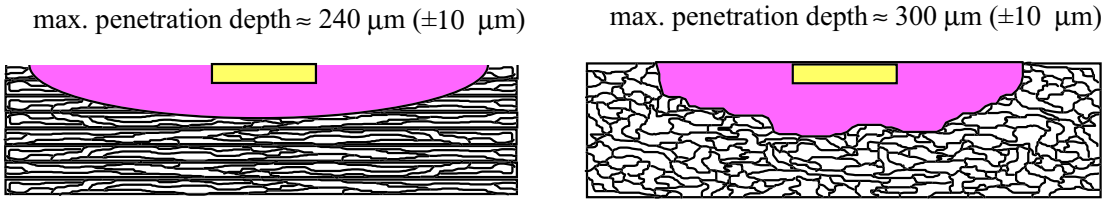

cross-sectional side view of an eight-layer filter paper pellet*
pellet thickness = 584 μm

cross-sectional side view of an HPMC pellet*
pellet thickness = 610 μm

The yellow bar represents the predicted maximum penetration depth of UV light into the pellet (≈100 μm)

Figure 75. The penetration depth and spot profile of 1 μL of marker dye when delivered to filter paper and HPMC pellets.
*not drawn to scale

7.3.1 Application of Partition and Adsorption Theories to Cellulose and HPMC Matrices

Is it possible that the naphthalene phosphor is effectively concentrated within the sample spot when delivered to the HPMC pellet according to interactions that are explained by theories developed within the field of paper chromatography? The SSRTP sample delivery process is similar to that of the sample introduction step required for paper chromatographic determinations. In paper chromatography (PC), the cellulose serves as an inert support for the stationary phase. If the paper is untreated during the manufacturing process, then the water adsorbed on the cellulose from the atmosphere serves as the stationary liquid phase.[435] PC theory proposes that the cellulose support material is not directly involved in the separation. Partitioning of the analyte between the stationary and mobile liquid phases is considered to be the mechanism by which the separation is accomplished. The separation of individual components in a mixture depends on the nature of the nonbonding intermolecular interactions that occur within the phases.

The analytical methods used for PC are nearly identical to those of thin-layer chromatography (TLC). The most common form of TLC is adsorption chromatography.[436] In

[435] J. Gasparic and J. Churácek, **Laboratory Handbook of Paper and Thin-Layer Chromatography** New York: John Wiley & Sons, 1978.
[436] J.C. Touchstone, **Practice of Thin Layer Chromatography 3rd Ed.**, New York: John Wiley & Sons, Inc., p.3.

TLC, the stationary phase is usually a solid such as alumina or silica gel. Silica gel and alumina are used primarily to separate lipophilic compounds. Separation occurs when one component in a mixture is more strongly adsorbed by the stationary phase than the other components. Since adsorption is primarily a surface phenomenon, the degree of separation is dependent on the surface area of the adsorbent available. Therefore, small particle sizes are advantageous when selecting a stationary phase. Native, fibrous cellulose or microcrystalline cellulose powder can also be used in TLC to separate hydrophilic compounds. The behavior of cellulose coated in a thin layer on a glass, plastic, or aluminum support is similar to that of a paper support used in PC. Additionally, as for PC, partitioning is mostly responsible for controlling the separation process since water molecules efficiently cover up the "active sites" on the cellulose particles by hydrogen-bonding. According to PC and TLC theory, the adsorbed water on the cellulose surface enhances the hydrophilic nature of the matrix and very little solute adsorption occurs.

When a 1 μL volume of naphthalene in absolute ethanol is delivered to filter paper, the water in the filter paper serves as a stationary liquid phase, the cellulose serves as an inert support, and the ethanol serves as a mobile liquid phase. As the naphthalene spreads across (and into) the filter paper, it partitions between the two phases. Considering only the magnitudes of the Hansen solubility parameters that represent the polar and hydrogen-bonding characters of these substances, naphthalene ($\delta_p = 0.0$,$\delta_h = 8.6$) is more ethanol-like ($\delta_p = 8.4$,$\delta_h = 20.8$) than water-like ($\delta_p = 16.0$,$\delta_h = 42.3$). Therefore, the naphthalene will reside mostly in the mobile phase as it spreads through the filter paper. The distribution coefficient of the naphthalene between the two phases will be small. As the ethanol is removed during the drying step, the magnitude of the distribution coefficient will increase as the amount of phosphor per unit of stationary phase grows.

This conclusion provokes yet another challenging thought problem. As the ethanol is vaporized, does the naphthalene prefer to interact with the liquid water phase or the solid cellulose phase? By comparing the Hansen parameters of naphthalene to those of water and cellulose, the cellulose-naphthalene system is favored. However, such attraction and interaction can no longer governed by the liquid phase solubility theories that explain partition chromatography. The intermolecular forces that govern adsorption chromatography are now more suitable for describing naphthalene's preference for cellulose instead of water. These interpretations agree well with the cohesion parameter models developed in Chapter 6. On the other hand, PC and TLC theory predicts that very little naphthalene will bind to cellulose fibers or particles by mechanisms of adsorption since the naphthalene is unable to compete effectively with ambient water molecules for the cellulose active sites. Thus, in the case of filter paper, naphthalene is rigidly trapped within an inimical environment that employs only limited, if any, direct phosphor-substrate intermolecular attraction as a mechanism of immobilization.

Since HPMC binds water in the same manner as cellulose, partitioning effects are also primarily responsible for governing the distribution of the phosphor between the water stationary phase and the ethanol mobile phase. Considering only partition theory, the distribution coefficients for these systems in both matrices should be equivalent. In terms of adsorption theory, the distribution coefficients for the cellulose-naphthalene system and the HPMC-naphthalene system are expected to be different. Unfortunately, in TLC, little emphasis is placed on quantitatively describing the apolar, polar, and hydrogen-bonding characteristics of the

sorbents used since their attributes tend to remain relatively constant in comparison to the variations in mobile phase that can be achieved. In comparison to PC/TLC sorbents, the strength of liquid mobile phases can be carefully tuned by consulting and applying solvent strength parameters (ϵ^0) and polarity indices (P′) during the preparation of binary mobile phases.[437,438] The field of planar chromatography does acknowledge that the surface activity of a sorbent is important and that the magnitude of surface activity can be directly related to the surface area of the substrate. However, at present, the only way to quantify sorbent activity in TLC is to provide an indication of the sorbent's water content (the activities of sorbents such as silica gel and alumina are primarily controlled by adjusting their water content).[436]

To answer the question stated earlier, it is indeed possible that lipophilic SSRTP substrates such as HPMC have the potential to effectively concentrate lipophilic phosphors in the center of the sample spot due to mechanisms of adsorption. Alternatively, it is also possible that certain hydrophilic matrices will allow for the concentration of strongly hydrophilic analytes in the center of the sample spot due to adsorption mechanisms. These theories are fully supported by the cohesion parameter model developed in chapter 6. To summarize, RTP intensities should be greater for the HPMC-naphthalene system than for the cellulose-naphthalene system as a result of favorable mechanisms of adsorption in the HPMC-naphthalene system that allow for more molecules of phosphor to interact with the LS-50 excitation beam. On the other hand, it is unlikely that this explanation accounts entirely for the significant improvements in RTP signal that are observed. Cohesion parameter theory suggests that the most important factor contributing to the enhanced RTP intensities is the magnitude of the adsorption strength that occurs between the naphthalene and HPMC since their polar and hydrogen bonding characters are more similar than those of naphthalene and cellulose (as illustrated in Figure 60).

7.3.2 Rationale for the Adoption of Cohesion Parameter Theory

Even though planar chromatography theories aren't presently suitable for quantitatively describing the natures of TLC sorbents, cohesion parameter theory is an alternate approach that has the potential to address this limitation. R.C. Rowe has utilized partial cohesion parameters to model binder-substrate interactions in tablets.[415] The model was useful for predicting trends in substrate-substrate, binder-binder, and substrate-binder interactions. The binary systems involved a number of powder substrates granulated with HPMC, methylcellulose, and polyvinyl pyrrolidone. Rowe has also used cohesion parameter theory to model the adhesion of film coatings to tablet surfaces.[419] Rowe's predicted trends for the adhesion of hydroxypropylcellulose to a series of low-energy polymer substrates were consistent with prior studies reported by Johnson and Zografi.[439] Johnson and Zografi measured the adhesion of hydroxypropylcellulose to polyethylene terephthalate, polymethylmethacrylate, and polyethylene by physically detaching the films normal to the substrate surface (a "butt adhesion test"). Furthermore, trends predicted for the adhesion of a series of cellulose derivatives to both

---

[437] L.R. Snyder, **Principles of Adsorption Chromatography**, New York: Marcel Dekker, 1968.
[438] L.R. Snyder, *J. Chromatogr. Sci.*, 1974, V. 92, p. 223.
[439] B.A. Johnson and G. Zografi, *J. Pharm. Sci.*, 1986, V. 75, p. 529.

microcrystalline cellulose and anhydrous lactose were consistent with prior laboratory observations.[440,441] In all cases, microcrystalline cellulose yielded higher predicted interaction parameters and higher ideal butt adhesive strengths than anhydrous lactose when films of cellulose acetate, hydroxypropylcellulose, and ethyl cellulose were coated onto each substrate.

Following his investigation of polar/non-polar interactions in the granulation of organic substrates with polymer binding agents, Rowe determined that a parabolic relationship exists between the reduced spreading coefficient and the fractional polarity of the substrate.[418] In this study, partial cohesion parameters were useful for calculating the thermodynamic works of cohesion and adhesion between the substrates (phenacetin, hydrocortisone, aspirin, ethinamate, etc.) and polymer binders (HPMC, methylcellulose, polyvinyl pyrrolidone, acacia, and starch). Finally, Rowe has used partial cohesion parameters to prepare two-dimensional solubility parameter maps that are useful for predicting the compatibility (or incompatibility) of blends of ethyl cellulose with HPMC or hydroxypropylcellulose.[442]

Podczeck and colleagues studied Hansen cohesion parameters during their investigation of the adhesion strength of particles of salmeterol base and a series of salmeterol salts to compacted lactose monohydrate surfaces.[443] They concluded that it was partially possible to predict the adhesion strength of a series of chemically related compounds to a defined surface using primary chemical structures. However, the model failed to account for differences in molecular configuration and surface structure since deformation characteristics such as ductility and brittleness cannot be predicted using cohesion parameters alone. Khalil and Martin have used salicylic acid as a model compound to study the relationships between total solubility parameters and drug transport through lipoidal membranes.[444] They concluded that the closer the δ_t value of the drug was to that of the membrane, the faster the rate of transport of the drug into the membrane. Using solubility parameters for salicylic acid, hairless mouse skin, and various polar and nonpolar vehicles, Sloan, et al. have studied the relationship between theoretical partition coefficients and experimentally determined permeability coefficients as they pertain to transdermal drug transport.[401] The rate of transfer of salicylic acid from one phase to a second phase was directly dependent on the difference between the values of the solubility parameters of the solute and the phases. The greater the difference between the solubility parameter of the solute and phase one, the faster the transfer to the second phase. Smaller δ_t differences between the solute and phase one resulted in slower transfer rates. The slowest rate of transport was observed when the magnitude of the salicylic acid δ_t was approximately the same as that of the vehicle δ_t (i.e. the solvent δ_t).

Cohesion parameter theory was useful for interpreting and quantifying the phosphor-substrate interactions observed during this project. Given the past history of the model in successfully quantifying solid-solid, solid-liquid, and liquid-liquid interactions, this approach should be equally beneficial for quantitatively describing interactions between TLC sorbents,

---

[440] R.C. Rowe, *J. Pharm. Pharmacol.*, 1977, V. 29, p. 723.
[441] R.C. Rowe, *J. Pharm. Pharmacol.*, 1978, V. 30, p. 669.
[442] R.C. Rowe, *J. Pharm. Pharmacol.*, 1986, V. 38, p. 214.
[443] F. Podczek, J.M. Newton, and M.B. James, *J. Adhesion Sci. Technol.*, 1995, V. 9, p. 1547.
[444] S.A. Khalil and A.N. Martin, *J. Pharm. Sci.*, 1967, V. 56, p. 1225.

stationary phases, mobile phases, and analytes. The combined study of sorbent cohesion parameters and mobile phase solubility parameters can offer new insight into fundamental PC/TLC interactions.

7.4 *K*-type HPMC vs. *E*-type HPMC

During this project, three high-purity grades of DOW HPMC were investigated as potential SSRTP substrate materials (*K4M PREM*, *E3 PREM*, and *E15LV PREM*). *K4M PREM* HPMC was found to yield substantially greater RTP intensities than the other two varieties. The primary difference between the *K*-type and *E*-type Methocel™ rests with the percent-methoxyl substitution. The *K*-type has approximately 19-24% methoxyl substitution; whereas the *E*-type has approximately 28-30% methoxyl substitution. The number that follows the letter designator (i.e. *K* or *E*) identifies the viscosity of the product in millipascal-seconds (mPa·s) measured at a 2% concentration in water at 20 °C. In designating viscosity, the letter "M" is used to represent 1000. The "LV" designator refers to special low viscosity products. Since polymer viscosity is directly related to polymer molecular weight, these *E*-type products have much lower molecular weights (i.e. shorter HPMC chain lengths) than the *K4M PREM* HPMC. Generally, the lower viscosity grades of HPMC permit faster swelling rates. This observation is consistent with the known molecular weight dependence of the rate of solvent penetration in glassy polymers. However, results reported here confirm that this model will not hold true when different types of HPMC are compared.

During the sample delivery step, the author has visually observed an interfacial tension effect between the ethanol-based standard solutions and the *E*-type pellets that appears to interfere with sample sorption. Sample droplets tend to "bead up" at the surface of the *E*-type pellet and are resistant to spreading across the surface of the substrates. This surface phenomenon appears to be similar to the minimization of contact area that will occur between substances such as water (a polar liquid) and waxy paper (a nonpolar solid). These visual observations are corroborated by the results of surface area percent-coverage calculations (tables 19 and 20) which further support the premise that *E*-type compacts do not readily sorb ethanol-based solutions. This finding can be explained in part by evaluating the δ_p and δ_h cohesion parameters of the *E*-type HPMC (δ_p=6.2 and δ_h=14.2) versus the *K*-type (δ_p=7.0 and δ_h=16.7).[404] Reports in the literature have indicated that *K*-type HPMC hydrates more quickly than the *E*-type in aqueous environments.[256,373] This finding has been confirmed by the manufacturer.[375] A reasonable prediction is that similar trends will be observed when ethanol (δ_p=8.4 and δ_h=20.8) is substituted for water (δ_p=16.0 and δ_h=42.3). Thus, for these investigations, it can be concluded that the *K*-type HPMC serves as a superior RTP support compared to the *E*-type HPMC simply because it interacts more favorably with the RTP solvent. This enhanced permeability offers a greater degree of compact swelling and allows the phosphor/heavy-atom system to be more easily transported into the interstices of the *K*-type pellet prior to the collapse of the HPMC matrix upon removal of the RTP solvent.

Nevertheless, cohesion parameter theory might only partly account for the enhanced permeation of phosphor/heavy-atom systems in *K*-type HPMC in comparison to *E*-type HPMC.

For instance, Mitchell and colleagues have used B.E.T. surface area determinations (via nitrogen adsorption) to confirm that particle size is an important HPMC characteristic that is partially responsible for controlling the extent of solvent penetration into a tablet surface.[252] Since small particle sizes allow the HPMC granules to pack more tightly, it is possible to prepare HPMC substrates that are unlikely to have porous surfaces and correspondingly low levels of interparticulate porosity. Unfortunately, particle size data was not readily available for the *K*- and *E*-type matrix materials utilized during these investigations. Even though this information wasn't necessary to achieve the goals of this research project, particle size measurements are promising candidates for future investigations since the data might provide additional insights into the nature of the HPMC-phosphor interaction.

7.5 The External Heavy Atom Effect and Spin-Orbit Coupling

Two detailed external heavy-atom investigations were completed. The addition of an external heavy-atom salt intensifies spin-orbit coupling and results in the enhancement of a molecule's phosphorescence emission. Although the external heavy-atom effect is generally useful for enhancing all phosphorescence measurements, the technique is especially beneficial for SSRTP analyses. For an LTP analysis, the heavy-atoms are randomly dispersed in the entire sample volumes being analyzed. However, for SSRTP, the heavy-atoms can be concentrated on a small sample spot following the evaporation of the solvent(s). Therefore, the effective concentration of the heavy-atoms will be much greater for a dried spot compared to a homogeneous solution. For a solid substrate such as paper, the heavy-atoms and the analyte molecules will be held in close proximity in the interstices between the cellulose fibers. This spatial constraint results in a more efficient heavy-atom effect. Matrix immobilization and trapping reduce collisional quenching (i.e. k'_{ec}). However, the heavy-atom effect primarily increases the rates of $S_1 \rightarrow T_1$ intersystem crossing (k_{isc}), $T_1 \rightarrow S_0$ phosphorescence (k_P), and $T_1 \rightarrow S_0$ intersystem crossing (k'_{isc}). The net effect is a decrease in τ_P, an increase in ϕ_P, and a decrease in ϕ_F. Although the nonradiative rate is enhanced as well, external heavy atoms generally increase k_P to a greater extent than k'_{nr}.

For the first heavy-atom study, the initial concentration range of NaI in ethanol was 0.00 to 0.05 M. Using 415 ppm naphthalene as the model phosphor and *K4M PREM* HPMC as the solid support, the dependence of RTP signal on heavy-atom concentration was found to obey a polynomial relationship ($y = -190.45x^2 + 724.57x + 65.44$; $R^2 = 0.994$). The second study examined the effect of higher NaI concentrations (0 to 1 M) on the RTP intensity of 100 ppm naphthalene. The upper concentration limit of NaI (1 M) was limited by its solubility. The results of the second set of investigations suggest a linear enhancement of RTP signal as heavy-atom concentration is increased. For the heavy-atom data acquired at 15 minutes of dry nitrogen purge, the equation that best describes the linear relationship between NaI concentration and RTP response is given by $y = 31.11x + 208.13$; $R^2 = 0.981$. However, this equation will not remain constant for all naphthalene/NaI/HPMC data sets since adjustments to purge time, changes in heavy atom concentration, and changes in phosphor concentration will each contribute to variation in RTP intensities. As illustrated in figures 44 and 45, saturation peaks were not

observed for either of these studies. On the other hand, the existence of a saturation peak would be expected for an SSRTP analysis utilizing higher NaI concentrations and lower naphthalene concentrations.

7.5.1 Supporting Results (Phosphor: Phenanthrene; Heavy-atom: Sodium Iodide)

Vo-Dinh and Hooyman studied the relationship between heavy-atom concentration and RTP intensity for a series of phenanthrene solutions (in ethanol) immobilized on filter paper using sodium iodide as the heavy-atom perturber.[284] The results of their study are shown graphically in figure 76. The graphs in figure 76 were prepared by estimating data points from a semi-log plot published by the investigators.[284] Microsoft Excel software was used to convert the X-axis from a log scale to normal coordinates. Note that the results of this study are similar to those illustrated in figures 44 and 45. It is possible for an approximate linear relationship to exist between phenanthrene RTP intensity and heavy-atom concentration over a wide range of NaI concentrations. For the data shown in figure 76, this appears to be especially true for 0.001 M phenanthrene at heavy-atom concentrations greater than 0.1 M. Saturation peaks are evident above NaI concentrations of 0.1 M. However, this is only true for the very dilute phenanthrene solutions (0.0001 M and 0.00001 M).

7.5.2 Supporting Results (Phosphor: Biphenyl; Heavy-atom: Sodium Bromide)

Winefordner and colleagues studied the relationship between heavy-atom concentration and RTP intensity for a 200 ppm biphenyl sample and a series of several different heavy-atom salts.[368] The results of their study are shown graphically in figure 77. The graphs in figure 77 were prepared by estimating data points from a semi-log plot published by the investigators.[368] Microsoft Excel software was used to convert the X-axis from a log scale to normal coordinates. Once again, note that it is possible for an approximate linear relationship to exist between biphenyl RTP intensity and heavy-atom concentration. For the data shown in figure 76, this appears to be especially true for phosphor RTP intensities measured with sodium bromide as the heavy-atom perturber (0.1 to 1.0 M NaBr). Again, as shown in figure 76, saturation peaks are evident above heavy-atom concentrations of 0.1 M. For the biphenyl/NaBr system, the saturation peak isn't evident until a heavy-atom concentration of 1.0 M is attained. For these results, it would be interesting to observe if the saturation peaks would be right-shifted or, in some cases, disappear by increasing the biphenyl concentration.

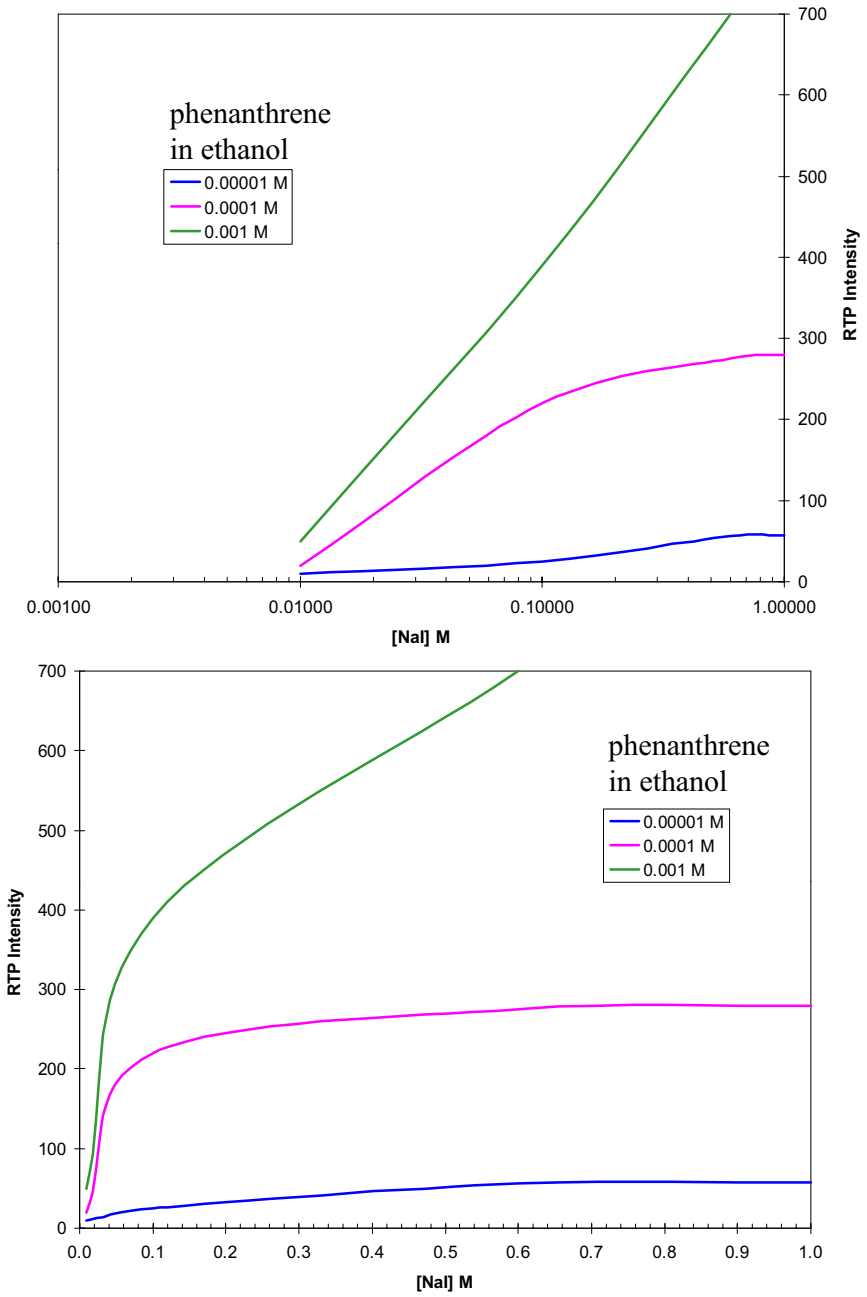

Figure 76. Effect of Heavy-Atom Concentration (NaI) on Phenanthrene RTP Intensity. Filter paper matrix.
(adapted from: T. Vo-Dinh and J.R. Hooyman, *Anal. Chem*., 1979, V. 51, p. 1915)

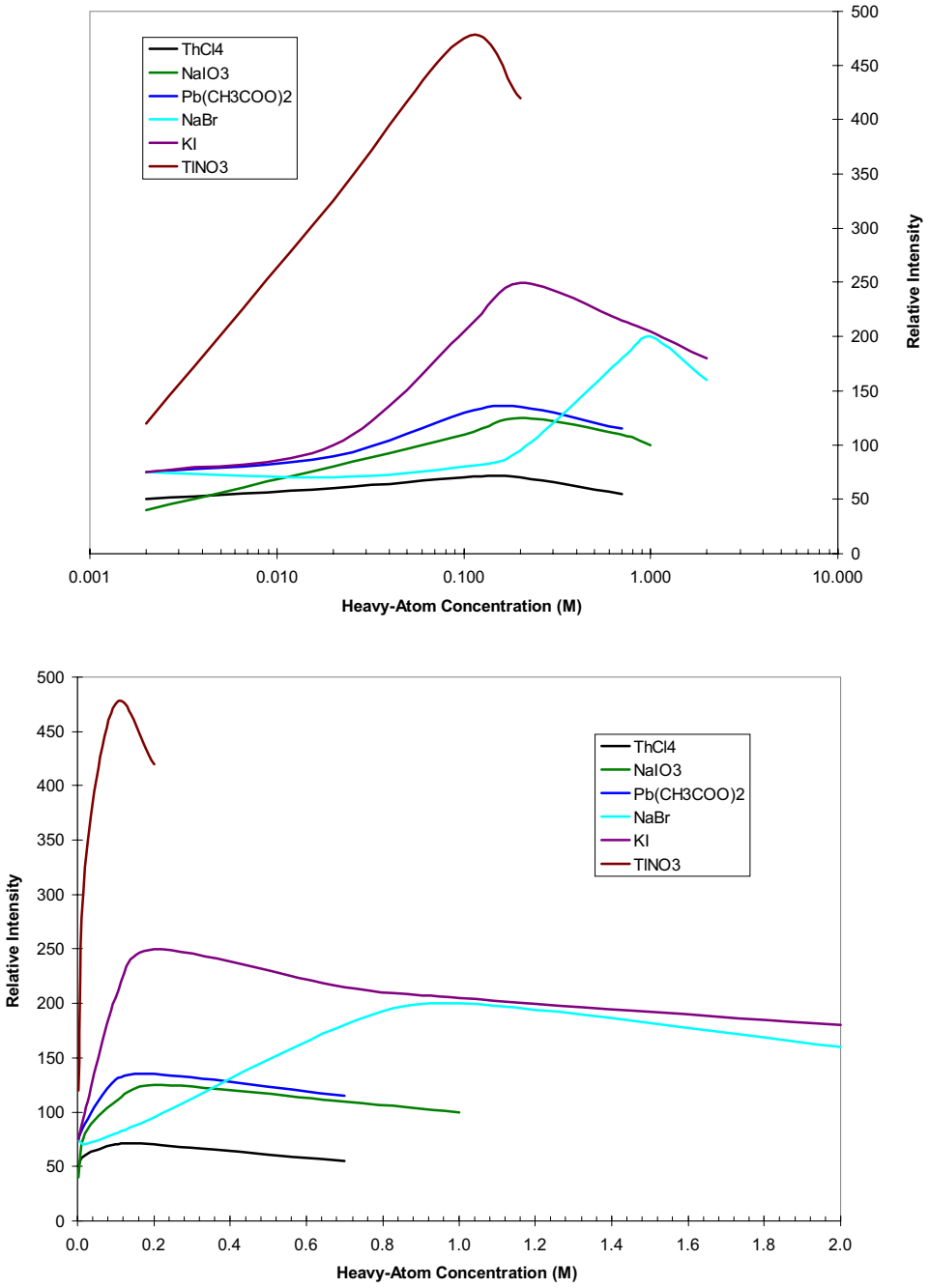

Figure 77. Effect of Heavy-Atom Concentrations on the RTP Intensity of Biphenyl. Filter Paper Matrix.
(adapted from: I.M. Khasawneh, M. Chamsaz, and J.D. Winefordner, *Anal. Lett.*, 1988, V. 21, p. 125)

7.5.3 Influence of Heavy-Atom Saturation on Analytical Calibration Curves

Dr. Brian Tissue, of Virginia Tech, has suggested that external heavy-atom saturation effects should influence the linearity of analytical working curves such as those shown in figure 41. However, since excellent linearity was observed for each of the naphthalene/1M NaI/HPMC working curves evaluated during this project (i.e. 0.999 @ 3 min. dry gas purge; 0.996 @ 6 min. dry gas purge; 0.999 @ 15 min. dry gas purge; and 0.998 @ 25 min. dry gas purge) and comprehensive heavy-atom studies weren't necessary to meet the original goals of the project, no specific attempts were made to test such a theory in the laboratory.

Vo-Dinh and Hooyman have studied the effect of an external heavy-atom perturber (NaI) on three different concentrations of phenanthrene.[284] Nevertheless, linearity cannot be suitably evaluated for an analytical working curve comprised of only three data points. In an attempt to address Dr. Tissue's theory, a model data set has been assembled by combining the pertinent results of this project with those reported by Vo-Dinh and Hooyman. The experimental results upon which this model is based have already been discussed earlier in the dissertation (figures 41, 45, and 76). The model relies on two key assumptions. It is assumed that the heavy-atom concentration vs. RTP intensity trends are similar for the phenanthrene/NaI and naphthalene/NaI pairs. Furthermore, it must be assumed that these trends will be similar for the RTP results obtained using both HPMC and filter paper matrices.

Figure 78 illustrates the model in graphical form. Five separate phosphor concentrations are evaluated. The 100 ppm results are taken directly from figure 45 (15 minute dry-gas purge). The 1M NaI data points for each curve are taken from figure 41. The 5, 10, 25, and 50 ppm trends are estimated from Vo-Dinh's results. According to the model, saturation effects, or the onset of saturation effects, are apparent for the lower concentrations of naphthalene (5 ppm, 10 ppm, and 25 ppm). Naturally, these trends are consistent with those observed by Vo-Dinh and Hooyman for the phenanthrene/NaI system.[284]

So that linearity can be properly evaluated, data points have been collected for each naphthalene sample within the model at heavy-atom concentrations of 0.1M NaI, 0.6M NaI, and 1M NaI. Each resulting data series is shown in figure 79. Trendlines and R^2 values for linear curve-fits are included as well. The 1M NaI data (shown in blue) is actual experimental data collected during this project (see figure 41). For the brown and green curves, the points at 5, 10, 25, and 50 ppm are derived from the model in figure 78. However, the points at the ends of the curves (i.e. those at 100 ppm naphthalene) are actual experimental results. Thus, in figure 79, eight points are estimated and seven data points are derived from experiment. Note that linearity begins to deteriorate at low concentrations of NaI (R^2=0.9998 for 1M NaI vs. R^2=0.9095 for 0.1M NaI). Granted, a significant change in heavy-atom concentration is required for the production of a large difference in R^2, but the trend is clear. This model supports Dr. Tissue's perceptive theory.

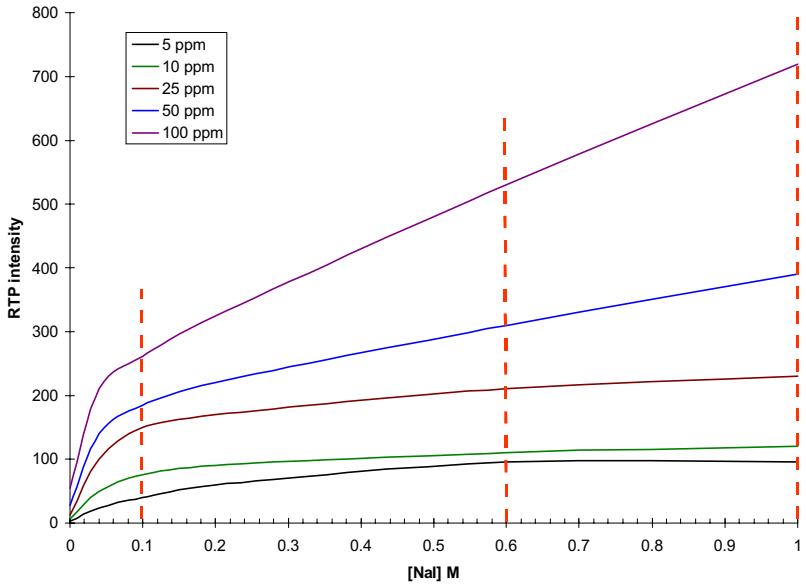

Figure 78. Effect of Heavy-Atom Concentration (NaI) on Naphthalene RTP Intensity. HPMC matrix. Simulated Data Sets.

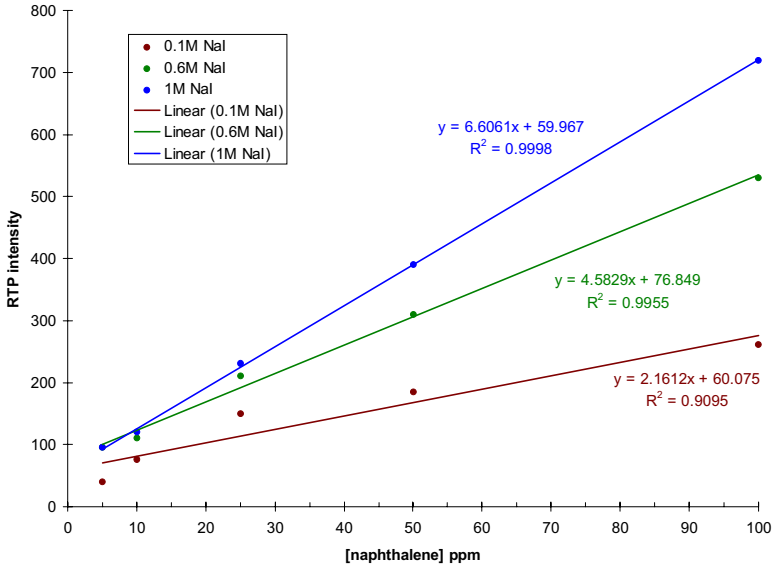

Figure 79. A Comparison of Analytical Working Curve Linearities Based on the Simulated SSRTP Data Set Shown in Figure 78 (the 1M NaI plot is derived from actual experimental data as shown in Figure 41).

Furthermore, as illustrated in figure 77, RTP intensity is at a maximum at the heavy-atom saturation point. At this point, heavy-atom enhancement is also maximized. RTP intensity begins to decrease as additional heavy-atom is added. Although not sufficiently addressed by this particular model, it seems possible that the continued addition of heavy-atom past the point of maximum enhancement will cause some analytical working curves to deviate from linearity at "high" heavy-atom concentrations as well. Unfortunately, the theoretical model presented here pertains only to the naphthalene/NaI pair and, as shown in figures 76 and 77, the overall trends exhibited by working curves of RTP intensity vs. heavy-atom concentration for different phosphor/heavy-atom combinations can vary significantly. Further experimental evidence will be necessary to confirm or refute these theories. Additionally, such investigations have the potential to provide an opportunity for the SSRTP spectroscopist to carefully evaluate saturation effects as a function of analyte-to-enhancer ratio. No such conclusions can be drawn from the data presented herein since nearly all spectra were obtained using only 1M NaI (or 16.5% wt/wt NaI) as the external heavy-atom enhancer.

Vo-Dinh has recommended that "Whenever comparisons between performance of different heavy atoms are given, the results at saturation conditions are the most meaningful because they correspond to the maximum enhancement that could be obtained with a given heavy atom.".[284] Based on the results of this study, an additional recommendation can be made. When confronted with non-linear analytical calibration curves, the SSRTP spectroscopist should attempt to optimize the linearity of the SSRTP calibration curves by carefully adjusting external heavy-atom enhancer concentration and/or heavy-atom type. Unfortunately, at present, such an optimization may only be possible via a trial-and-error approach.

7.5.4 Phosphor/Heavy-Atom Interaction According to an Influence Sphere Model

The observation that SSRTP intensity can be significantly enhanced by carefully selecting heavy-atom enhancers has been confirmed for numerous phosphor-substrate combinations including the naphthalene-HPMC system described here. Although the curves that characterize the direct relationship between the two factors aren't always perfectly linear, regular increases in heavy-atom concentration generally result in substantial increases in RTP intensity (at least until a saturation condition is reached). Phosphorescence enhancement by external perturbation is thought to depend on the spin-orbit coupling interaction that occurs between an excited phosphor and a nearby heavy-atom. Spin-orbit coupling effectively mixes some singlet character into triplet states and some triplet character into singlet states thus destroying their pure character and orthogonal nature. The quantum mechanical treatment of S-O coupling has been described in detail elsewhere.[17,20,445,446] Nevertheless, since a clear understanding of S-O coupling can provide insight into the phosphorescence process, a brief theoretical treatment of S-O coupling has been included in Appendix C.

---

[445] R. Eisberg and R. Resnick, **Quantum Physics of Atoms, Molecules, Solids, Nuclei, and Particles**, 2nd Edition, New York: John Wiley & Sons, Inc., 1985.

[446] P.W. Atkins and R.S. Friedman, **Molecular Quantum Mechanics**, 3rd Edition, New York: Oxford University Press, 1997.

Traditionally, researchers have assumed that phosphorescence enhancement by S-O coupling between a phosphor and a heavy-atom will not be effective unless contacts, collisions, or complexations occur between the two species.[28] Some investigators have proposed that S-O coupling enhances $S \leftrightarrow T$ transitions by the formation of charge-transfer complexes where the aromatic molecule (M) is an electron donor and the heavy-atom perturber (P) is an electron acceptor.[447] Others have proposed that exchange interactions are favored over charge-transfer complexes.[20] Nevertheless, it has been difficult for investigators to distinguish these two models experimentally and, after fifty years of scrutiny, there still isn't a unified theory of heavy-atom enhancement upon which all spectroscopists agree.[448]

For a given naphthalene molecule (approximate dimensions: 3 Å × 7 Å) in free space surrounded by an excess of NaI, it should only be possible to pack a maximum of ten iodine anions around the planar phosphor since the diameter of a spherical iodine anion is approximately 4.4 Å and its volume is approximately 44.6 $Å^3$. This ideal model neglects the presence of sodium cations, SSRTP matrix interference, and phosphor-iodide/iodide-iodide repulsion. In reality, fewer than ten iodine anions are expected to interact directly with the π-electron clouds that lie above and below the planar naphthalene molecule. Four or five iodine anions is a reasonable estimate.

On the other hand, for an 8 μL NaI delivery volume, table 33 suggests that an individual naphthalene molecule has the potential to be surrounded by thousands of heavy-atoms when relatively concentrated NaI solutions (i.e. > 0.2 M) are applied to the matrix.[449] The results presented in figure 45 indicate that hundreds or thousands of heavy-atoms are responsible for significantly enhancing the SSRTP of a given naphthalene molecule. If only a few heavy-atoms were solely responsible for RTP saturation, then phosphorescence intensities would peak (or plateau) at extremely low concentrations of NaI (i.e. < 0.01 M). Thus, how can it be that a single naphthalene molecule is able to interact simultaneously with hundreds or thousands of heavy-atom molecules by either contact, collision, or complexation while the phosphor remains immobilized in an SSRTP matrix?

---

[447] M. Zander, **Phosphorimetry** (translated from German by T.H. Goodwin), New York: Academic Press, 1968.

[448] After examining the pertinent literature, White and Seybold developed a strong argument for the exchange interaction model since i). absorption measurements in solution have failed to detect complexes between I^- ions and phosphors such as fluorene or triphenylene, ii). I^- ions shouldn't be effective electron acceptors in a charge-transfer complex with a neutral aromatic molecule, and iii). the isoelectronic species Xe and Cs^+ are considerably less effective heavy-atom perturbers than I^- even though they are expected to be better electron acceptors on the basis of their nuclear charges.[27] Nevertheless, this argument doesn't exclude the possibility that a charge-transfer complex might exist between an electron-accepting phosphor and an electron-donating I ion.

[449] Because the ratios in table 33 are relative ratios, it becomes necessary to consider the actual delivery volumes for both the 100 ppm naphthalene solution and each heavy-atom solution. Since a larger heavy-atom delivery volume (8 μL) will allow the individual sodium cations and iodine anions to spread farther across the HPMC substrate and penetrate deeper into the dry glassy core, true ratios of heavy-atom to phosphor will be somewhat less than those cited in table 33 if 1 μL volumes of phosphor are utilized. Nevertheless, under these conditions, an individual phosphor molecule should still be surrounded by thousands of heavy-atoms when 8μL of 1M NaI is utilized.

For a given naphthalene molecule, there must exist a three-dimensional *sphere of influence* that specifies the number of heavy-atom molecules that can interact with it. White and Seybold have used the Perrin equation to develop a "quenching sphere" model that is useful for explaining the degree of fluorescence quenching that occurs between a fluorophor and a surrounding alkali halide salt.[27] According to McGlynn, quantum mechanical models of S-O coupling satisfactorily explain both fluorescence quenching and phosphorescence enhancement by heavy-atoms.[20] Quenching by paramagnetic species is also attributed to S-O coupling interactions. Consequently, since perturbation theory describes photoluminescence quenching and enhancement interactions according to the same fundamental mechanisms, the Perrin sphere approach must also hold for heavy-atom enhancement in an SSRTP environment. Surprisingly, it appears that a heavy-atom *enhancement sphere* model has not yet been discussed in the relevant literature.

To apply this model, heavy-atom perturbation is assumed to be complete for all phosphor molecules within an influence sphere of radius, *R*, around the heavy-atom. According to White and Seybold, a suitable value of *R* for the iodide anion is 14 Å.[450] An ideal two-dimensional influence sphere is shown for the naphthalene/NaI system in figure 80. An individual heavy-atom is not expected to induce perturbation outside of the sphere. Given these conditions, the model implies that the phosphorescence enhancement of a particular phosphor will depend on a weighted summation of the individual perturbations of all of the surrounding heavy-atoms. In this manner, many heavy-atoms could induce the unpairing of electron spin by participating in the production of a field that would exert a long-range influence on a phosphor's excited electron. According to this model, direct contact between the phosphor and most of the surrounding heavy-atoms would be unnecessary.

In addition to being consistent with the findings reported herein, this model is also agreeable with those LTP experiments that suggest that the external heavy-atom effect merely increases the S-O coupling that is already present within a phosphor.[20] For the few heavy-atoms that directly contact the phosphor, short-range charge-transfer and/or exchange interactions are still viable mechanisms of RTP enhancement. Nevertheless, the enhancement sphere approach is complementary to these current theories since it provides a reasonable explanation of how a non-neighboring heavy-atom might influence the ϕ_P of an isolated phosphor. Although the proposal is a tentative one, it seems possible that the intriguing "knee" observed in many plots of RTP intensity vs. heavy-atom concentration (i.e. figures 76 and 78) is representative of a short-range contact mechanism of SSRTP enhancement; whereas, the remainder of the curve may be due to the long-range field effect discussed earlier.[451]

---

[450] *R*, the critical radius (in Å), is calculated using $F/F_0 = e^{-\upsilon[Q]}$ (the Perrin equation) where F and F_0 are fluorescence intensities with and without quencher respectively, $\upsilon \equiv 4\pi R_0^3 N/3$, $N=6.02 \times 10^{-4}$, and [Q] is the quencher concentration in mol/L. According to White and Seybold, υ is 6.5 L/mol for the iodine anion.

[451] Dr. Brian Tissue, of Virginia Tech, has suggested that although the "knee" in a typical RTP enhancement vs. heavy-atom concentration curve may be due to a physical phenomenon such as a change in enhancement mechanism, a chemical effect is more likely to be responsible for the decrease in RTP enhancement past a certain heavy-atom concentration as shown in figure 77. For instance, competing equilibria might prevent a single heavy-atom from interacting with the phosphor (e.g. $3I^- \leftrightarrow I_3^-$).

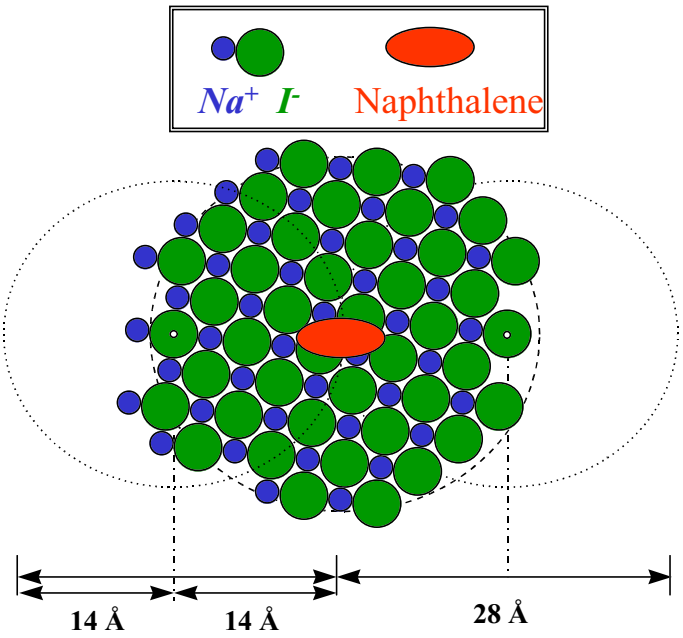

Figure 80. Two-dimensional Representation of a Perrin Sphere for Naphthalene surrounded by NaI. Approximate naphthalene dimensions: 3Å x 7Å. Na^+ ionic radius: 1.15Å. I^- ionic radius: 2.2Å. Radius of Perrin sphere from the center of an iodide ion: 14Å.
(Perrin sphere radius from: White & Seybold, *J. Phys. Chem.*, 1977, V. 81, p. 2035.)

Regardless, it should be noted that the Perrin model is unrealistic in some respects. For instance, it assumes a sharp cutoff in perturbation at a distance (*R*) from the center of the heavy-atom; whereas, a more gradual dependence must actually exist. Another potential limitation of this model involves the physical nature of the SSRTP matrix itself. Given pore and void diameters within the matrix of less than approximately 30 Å (3 nm), it wouldn't be physically possible to account for a full complement of iodine anions around an individual naphthalene molecule.[452] Nonetheless, given these conditions, the Perrin influence sphere approach does serve as a suitable interaction model for heavy-atom perturbation since more than 100 heavy-atoms can be included within a spherical volume surrounding the naphthalene molecule when *R* = 14 Å. Unfortunately, if *R* is truly on the order of 14 Å for I^-, then the model cannot account for naphthalene/NaI perturbation interactions involving thousands of heavy-atoms per phosphor.

A relatively new analytical technique referred to as Fluorescence Resonance Energy Transfer (FRET) spectroscopy may offer additional insight.[453] FRET involves the radiationless transfer of energy within a molecule, or between molecules, by resonance interaction between

[452] Based on the Perrin sphere model, one might expect that a pure heavy-atom salt pellet would allow for room-temperature phosphorescence intensities to be maximized and LOD's to be minimized. However, as discussed in section 7.5.6, such substrates are not ideal SSRTP matrices.
[453] Author unknown, *Fluorescence Resonance Energy Transfer(FRET) spectroscopy*, **URL:** http://www.anatomy.usyd.edu.au/mru/fret/abot.html

chromophores. The distances are considerably greater than interatomic and a physical contact (or kinetic collision) between the donor (dye) and acceptor (chromophore) isn't necessary.[454] FRET efficiency depends upon the linear distance in space between the donor and acceptor. The distance between the pair at which energy transfer is approximately 50% efficient is referred to as the *Förster distance*. For the FRET technique, the *Förster distance* has been determined to be 40 Å. However, transfer efficiency doesn't approach zero until the donor and acceptor are separated by a distance of at least 80 Å.

Given a Perrin sphere *R* value of approximately 80 Å, then thousands of heavy-atoms could be arranged inside the influence sphere with ease. For a variety of *R*, the approximate number of NaI molecules that might be found within a Perrin sphere are indicated in Table 45. Based on their ionic radii, the volume of the spherical sodium cation is calculated to be 6.4 $Å^3$ and the volume of the spherical iodine anion is determined to be 44.6 $Å^3$. By simple addition, the total NaI volume is estimated to be 51 $Å^3$. As one might expect, NaI molecules will not pack tightly enough within an influence sphere to fill all of the available space. Furthermore, the matrix itself may intrude upon the influence sphere. The likelihood that a portion of the matrix will lie inside an ideal Perrin sphere increases substantially as *R* increases. Since part of an influence sphere volume will be occupied by either voids due to irregular (and imperfect) NaI packing or encroachment of the SSRTP matrix, the results in Table 45 are approximated by applying estimated "packing efficiencies".

For the 1M NaI and 100 ppm naphthalene system discussed in section 5.5, it is estimated that there can be up to 13000 heavy-atoms per naphthalene molecule within a Perrin enhancement sphere (see table 33). Note that this relative ratio is ideal and it does not take into consideration any differences in heavy-atom and phosphor transport across, and into, the SSRTP matrix. Table 45 shows that an influence sphere radius of 70 Å would allow for the placement of more than 14000 NaI molecules around a phosphor even if only 50% of the volume of the influence sphere was occupied by the NaI. Although the proposal remains speculative at this time, such an approach would allow one to successfully model phosphor/heavy-atom perturbation interactions that involve thousands of heavy-atoms per phosphor molecule. Future studies of the external heavy-atom effect will hopefully shed further light on this tentative model.

[454] B.W. Van Der Meer, G. Coker III, and S.-Y. Chen, **Resonance Energy Transfer Theory and Data**, New York: VCH, 1994.

Table 45. Estimated external heavy-atom salt (NaI) packing within a variety of Perrin influence spheres (volumes calculated by $4/3\pi r^3$).

R (Å)	calculated Perrin sphere volume ($Å^3$)	Number of NaI's assuming 70% packing efficiency	Number of NaI's assuming 60% packing efficiency	Number of NaI's assuming 50% packing efficiency
14	11494	158	135	113
20	33510	460	394	329
30	113,097	1552	1331	1109
40	268,083	3680	3154	2628
50	523,599	7187	6160	5133
60	904,779	12419	10645	8870
70	1,436,755	19720	16903	14086
80	2,144,661	29437	25231	21026

7.5.5 Matrix Packing due to the Addition of a Heavy-Atom Salt

In addition to promoting S-O coupling, high heavy-atom concentrations are also expected to allow for an improved matrix effect. Phosphors will be held more rigidly within the solid support material as pores and voids are tightly packed by heavy-atom salts. The permeation of oxygen and moisture into the environment of the phosphor will also be hindered. Thus, nonradiative quenching (k'_{nr}) would be reduced. Based on these discussions, it becomes clear that a single mechanism isn't responsible for all heavy-atom enhancement effects. Since the overall improvement in RTP intensity is best explained by considering the contribution of each individual effect, the development of a unified theory of external heavy-atom enhancement should prove to be a challenging task.

7.5.6 An Attempt to Maximize Spin-Orbit Coupling via the use of Alkali Salt Substrates

It is worth noting here that Schutt and Li have recently detected RTP emission from several phosphors using a solid support composed entirely of alkali salts (CsI, KI, KBr, and KCl).[455] Two sample preparation techniques were investigated. The solid-solid method involved the preparation of a compact from a phosphor/heavy-atom mull. The second method relied on the preparation of a pure alkali halide compact upon which 0.2 μL of phosphor solution was delivered by syringe (sample spotting). RTP emission signals were more reproducible for the spotting technique than the solid-solid method. When using the alkali halide pellets, the LOD for naphthalene by the spotting technique was 100 ng. For these investigations using the LS-50 spectrometer, the IUPAC LOD for naphthalene trapped in an HPMC/NaI matrix was

[455] W. Schutt and Y. Li, *Anal. Lett.*, 1995, V. 28, p. 307.

calculated to be 3 ng following a dry nitrogen purge time of 3 minutes. Another laboratory, using different instrumentation, has reported an LOD of 1.2 ng for naphthalene immobilized in a filter paper/NaI matrix.[456] Unfortunately, one should always be wary of LOD comparisons between laboratories since SSRTP investigators have rarely specified the exact manner in which this figure of merit is calculated.

Considering the modified Perrin enhancement sphere model, it is initially surprising that the naphthalene limits of detection reported by Schutt and Li (using a pressed heavy-atom pellet) are approximately 33 times higher than those reported here using HPMC substrates. Although it is the external heavy-atom that principally enhances the rate of intersystem crossing, effective matrix trapping is primarily responsible for reducing the rate of nonradiative decay from the excited triplet to the singlet ground (k'_{nr}). Additionally, in accord with the modified Perrin model, there is a certain linear distance in space past which a single phosphor molecule will no longer experience the influence of extra heavy-atoms in its surrounding. Furthermore, heavy atoms tend to enhance k'_{nr}. Since an HPMC matrix reduces k'_{nr}, it is easy to imagine specific conditions where effective matrix trapping would surpass the heavy-atom effect in providing for strong RTP intensities.

For a compression range of 5000 psi to 13000 psi, Schutt and Li discovered that SSRTP intensities peaked when alkali halide pellets were compressed at 9000 psi. For the compression of most excipient materials (such as HPMC), transitional packing occurs for applied pressures up to 285 psi. Between 285 psi and 1150 psi, temporary columns can be formed within the powder bed. Plastic deformation or fragmentation occur between 1150 psi and 14200 psi. Bonding and densification occur between 14200 psi and 28500 psi. This information, combined with the observations of Schutt and Li, suggests a possible future experiment. HPMC pellets could be prepared at various pressure intervals within a range of 5000 to 20000 psi to determine if a certain compaction pressure would yield maximum RTP signals for specific phosphor/heavy-atom combinations. The lower pressure boundary would be limited only by the ability of the HPMC to maintain a nonfriable compact following the compression process and during solvent penetration after the sample delivery step. The upper limit would be restricted only by the mechanical strength of the hydraulic press and pellet die.

Figure 81 explains why the spotting technique is preferred over the solid-solid method for the analysis of phosphors using HPMC substrates. Precision is improved since the spotting technique allows for the phosphor and heavy-atom to be placed more reproducibly at the surface of the compact within the excitation beam. RTP intensities are also improved since a greater quantity of analyte and heavy-atom perturber will be immobilized within the fixed dimensions of the excitation beam.

[456] T. Vo-Dinh and R.B. Grammage, *Anal. Chim. Acta*, 1979, V. 107, p. 261.

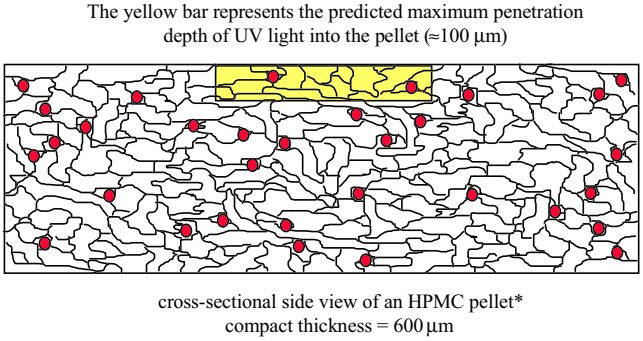

Figure 81. The disadvantage of preparing SSRTP substrates by the solid-solid (or mull) technique. Red circles = phosphor. "Jigsaw puzzle" pieces = HPMC particles.
*not drawn to scale

7.6 Potential Photochemical Interferences Considered

Electronically excited molecules are distinctly different from their ground state counterparts in terms of polarity and reactivity.[457] Photochemical reactions can compete with k_F and k_P. Even though the mean lifetime of fluorescence is short in comparison to the times required for most chemical reactions, isomerization, photoionization, photodissociation, and acid-base equilibrium can occur rapidly in the excited singlet state. The long lifetimes of excited triplet states offer an increased probability that phosphors will participate in photochemical reactions instead of returning to the ground state by phosphorescence. Therefore, for most photochemical reactions, the triplet state is more important than the singlet state. When phosphors are immobilized in rigid glasses, viscous media, or solid supports, photochemical reactions do not typically result in serious interference. The appearance of extra emission bands in an RTP spectrum is suggestive of photochemical reactions that occur in the excited triplet state. For these investigations, anomalous emission bands were not evident within the RTP spectra.

Photodecomposition of an analyte may provide unexpectedly low RTP intensities.[66] Dissociation occurs when photons of sufficient energy rupture bonds following their absorption. Predissociation occurs when a bond is ruptured after internal conversion. Both dissociation and predissociation are most likely in molecules that absorb at wavelengths shorter than 200 nm. The degree of photodecomposition is proportional to the power of the excitation beam and sample exposure time. Therefore, the rate of photodecomposition can be minimized by decreasing the intensity of an excitation source (smaller excitation slit width) and increasing the sensitivity of the detector. Alternatively, a shutter can be used to protect the phosphor from unnecessary exposure to the excitation beam between measurements.[14] Since the excitation wavelengths used for these investigations were each longer than 260 nm, dissociation and predissociation could not interfere with the SSRTP measurements.

---

[457] J.D. Winefordner, S.G. Schulman, and T.C. O'Haver, **Luminescence Spectrometry in Analytical Chemistry** New York: Wiley-Interscience, 1972.

7.7 Suggested Improvements Regarding the Custom-built Sample Cell Module

The commercially available Perkin-Elmer front surface luminescence accessory costs $2,120.[323] In its standard configuration, the device is not suitable for use in RTP studies. However, this project confirmed that the accessory will allow for the collection of suitable SSRTP emission spectra if it is modified to incorporate a dry gas purge system. Alternatively, the custom-built sample cell module constructed for this project could be duplicated by SSRTP researchers at a materials cost of approximately $300. In addition to its use as a research tool, the simplicity of design and durability of this sample cell module should make it particularly attractive to educators. It would allow for the RTP technique to be readily introduced to those teaching laboratories that have access to the Perkin-Elmer LS-50 luminescence spectrometer. The custom-built sample module was satisfactory for these investigations; however, it could be improved by i). adding adjustment points to provide additional degrees of freedom in positioning the solid substrate within the excitation beam, ii). modifying the sample holder to allow for reproducible positioning of the substrate with respect to the front surface of the support rather than the rear surface, and iii). including a shutter mechanism that could be used to prevent the excitation beam from irradiating the sample between trials.

7.8 The Modified Perkin-Elmer Front-Surface Luminescence Accessory

The modified Perkin-Elmer front-surface luminescence accessory allowed for uncompressed, single-layer filter paper discs to be examined and compared to the *K4M PREM* HPMC substrates. It was discovered that the RTP intensities obtained using filter paper discs are nearly independent of the duration of dry N_2 purge. The RTP signals obtained after a 15-minute interval of N_2 purge are only minimally greater in intensity than the RTP signals corresponding to those spectra acquired at the three minute mark. The macroscopic porosity of the filter paper allows for residual solvent, moisture, and oxygen to be quickly purged from the interstices of the matrix.

By using the same phosphor and heavy-atom solutions, it was possible to compare the RTP intensities yielded by the filter paper discs to those provided by the *K4M PREM* HPMC pellets. In each case, the HPMC compacts provided greater RTP intensities than the corresponding uncompressed filter paper discs. For future investigations, a full-scale LOD/LOQ study would be warranted for these two systems using the modified P-E accessory. Qualitative spectra were acquired at the 5 ppm (4 ng) level for naphthalene and 1 ppm (0.8 ng) level for phenanthrene. Based on these preliminary results, the modified P-E front surface accessory will allow for moderately improved LOD's in comparison to those obtained for the naphthalene/NaI system using the custom-built RTP sample cell module. It would also be instructive to compare the results of SSRTP trials for the naphthalene/NaI system using both uncompressed filter paper discs and compressed filter paper pellets. For all materials, there is a decrease in Young's

modulus with increasing porosity.[458] Therefore, a compressed filter paper pellet should have a greater Young's modulus (*E*) than does a single uncompressed filter paper substrate. According to Hurtubise, RTP intensities would be greater for the support material having the higher *E* value.

7.9 Production of an HPMC Gel Layer

Unlike native cellulose, many of the cellulose derivatives such as HPMC are capable of producing a gel layer upon exposure to certain solvents (see figure 72). Water penetration into materials of low crystallinity and high glass transition temperatures (such as HPMC) follows a Fickian mechanism of diffusion. Polymers with low glass transition temperatures exhibit anomalous water diffusion. Within the arena of pharmaceutical formulations, the effect of particle size on the hydration of HPMC is not fully understood. Coarse fractions of HPMC are thought to hydrate too slowly to allow sustained drug release. Matrices prepared with coarse particle sizes will disintegrate before the external layers are fully hydrated. The surrounding solution is able to penetrate the dry glassy interior of the compact at a rate that is greater than the rate at which chain disentanglement occurs. However, the production of an external gel layer maintains the integrity of the matrix and protects the active drug ingredient in the inner part of the matrix from dissolution. Small size fractions of HPMC allow uniform hydration into the matrix, thereby effectively retarding the release of the active.

Upon contact with a sufficient volume of ethanol, an HPMC tablet will begin to swell and its thickness will increase. The swelling of the matrix prohibits direct association between the polymer chains at the surface of the substrate and a thin gel layer is produced. Since the protective gel layer requires a finite time to form, the phosphor can continue to enter the inner layers of the matrix before the gel coat is completely formed. Theoretically, *K4M* HPMC will yield a gel thickness of ≈33 μm following one minute of exposure to the solvent. Phosphor molecules will penetrate the gel layer during this time. As the temperature of the HPMC is raised, the chains gradually lose the attached ethanol molecules and polymer-polymer association begins to take place. The matrix begins to immobilize phosphor molecules that have diffused across the gel layer into and into the surface layers of the substrate. As desolvation proceeds, the amount of direct inter-chain association increases. This association continues until an infinite network of polymers is formed. This author proposes that as the HPMC gel layer collapses it has the potential to form a thin protective film at the surface of the substrate. Dr. Colin Keary, of the Dow Chemical Company, has suggested that this thin film might act as a protective "skin" that can improve RTP intensities by shielding the phosphor molecules from ambient oxygen and moisture.[375]

7.10 Determination of Intermolecular Interaction Strengths between Phosphor and Matrix

The Hildebrand total cohesion parameter and three Hansen partial cohesion parameters have been used to quantify the strength of intermolecular interactions between solid substrate

---

[458] R.C. Rowe and R.J. Roberts, *Mechanical Properties* in **Pharmaceutical Powder Compaction Technology** G. Alderborn and C. Nyström, Eds., New York: Marcel-Dekker, Inc., p. 286.

materials and a series of seven model phosphors. Since HPMC has a lipophilic character compared to the hydrophilic cellulose that comprises filter paper, it is proposed that certain phosphors will be more strongly bound to an HPMC substrate than to a filter paper matrix. This is the first attempt within the field of phosphorescence spectroscopy to explain RTP signal enhancement in terms of the quantitative description of the apolar, polar, and hydrogen-bonding characteristics of analytical phosphors and their respective RTP substrates. Based on calculations of D_{ij} reported here for acenaphthene, naphthalene, 2-naphthoic acid, 2-naphthol, p-aminobenzoic acid, phenanthrene, and salicylic acid (sodium salt), HPMC is expected to be the preferred RTP matrix for each analyte. Calculations of D_{ij} for ethanol clearly indicate that the RTP solvent interacts equally well with both HPMC and cellulose as a result of its polarity and ability to hydrogen bond. Henceforth, the phosphorescence spectroscopist will have a new tool that will assist in the selection of optimal substrates for solid-surface room-temperature studies. Until now, the selection of suitable RTP matrix materials has mostly involved a trial-and-error approach. In many other instances, serendipity has played a key role in the discovery of new RTP substrates. Since the RTP investigator can now make reliable predictions regarding phosphor-substrate interactions prior to attempting an analysis, cohesion parameter theory should prove to be a major advancement in the field of SSRTP research.

7.11 Related Observations and Interpretations

Although the following observations are independent of the original hypothesis, their discussion here is nevertheless warranted since each offers additional insight into the nature of the SSRTP phenomenon.

- **Substrate Storage.** The specific storage conditions of HPMC substrates prior to their use are not a major factor in the enhancement of RTP intensities so long as the support materials are maintained in a dry atmosphere. Desiccants such as Drierite™ are attractive since they are low-in-cost, renewable with mild heating, and provide a self-indicating color change as moisture is absorbed.
- **Dry Nitrogen Gas Purge.** For phosphors trapped on HPMC and filter paper pellets, RTP intensities are extremely sensitive to the duration of dry nitrogen purge. Significant improvements in RTP intensity occur within the first few minutes of the analysis. This signal enhancement can be attributed to the removal of moisture, oxygen, and residual solvent from the substrate. Normal filter paper substrates appear to be relatively insensitive to the duration of dry gas purge. This can be attributed to the macroscopic porosity of the material. Moisture, oxygen, and residual solvent are more quickly purged from within the pores, voids, and interstices of the compressed filter paper matrix.
- **Moisture Quenching.** For *K4M PREM* HPMC substrates, the quenching of RTP by water vapor was studied using a humidified atmosphere of nitrogen gas. Phosphorescence intensities were significantly attenuated due to the quenching effects of moisture. It is proposed that the water molecules compete with the phosphor for guest sites within the host matrix. This would have the effect of reversing the phosphor-support adsorption process and yielding an increased probability of

collisional and vibrational quenching. It is also likely that the reduction in RTP intensity due to the adsorption of moisture is caused to an extent by the breakdown of the hydrogen-bonding network within the dry HPMC substrate. Since water is known to be an efficient swelling agent for cellulose-based materials, it is possible that the reduced RTP intensities can be attributed in part to polymer disentanglement (i.e. a change in modulus) of the three-dimensional matrix. For HPMC, the quenching of SSRTP by moisture may best be explained by considering the combined influence of these three rationales.

- **Oxygen Quenching.** For *K4M PREM* HPMC substrates, the quenching of RTP by oxygen was studied using dry O_2 gas and dry medical air (21% O_2; 79% N_2). For comparative purposes, samples were also analyzed within an atmosphere of dry nitrogen gas. Phosphorescence intensities were fully attenuated when samples were analyzed in the presence of pure oxygen and severely attenuated when analyzed in an atmosphere of 21% oxygen. For this series of investigations, pure N_2 purge conditions provided the strongest RTP signals. Following a twenty-five minute purge interval, the RTP intensity for the dry nitrogen-purged sample was greater than the intensity of the corresponding dry air-purged sample by a factor of 42. Although a definitive explanation has not yet been agreed upon, investigators have proposed that oxygen quenching may be due to intermolecular exchange interactions[20] or mechanisms of contact charge transfer.[36] Regardless, these studies substantiate the importance of protecting HPMC substrates from the quenching effects of oxygen.
- **Heavy-Atom Delivery.** Two methods of heavy-atom delivery were studied using *K4M PREM* HPMC substrates. The first technique involved the pre-mixing of heavy-atom and analyte in ethanol prior to their application. The second method relied on the individual delivery of heavy-atom and analyte solutions. The results associated with this study confirm that the second method is preferred. When heavy-atom and analyte are spotted onto the substrate individually (in that order), each component remains focused in the center of the pellet. However, when heavy-atom and analyte are pre-mixed and then delivered together, the large volume of solvent involved effectively allows the phosphor to diffuse farther into, and across, the surface of the HPMC substrate. Thus, the excitation beam interacts with a smaller quantity of analyte and SSRTP intensities are significantly reduced. These observations are consistent with the results obtained during the preliminary reagent delivery studies.
- **HPMC Substrate Thickness and RTP Intensity.** A Perkin-Elmer front-surface luminescence accessory was modified to allow for SSRTP investigations using substrates of varying thickness. Four sets of *K4M PREM* HPMC substrates were manufactured for this study. These four sets included pellets having the following thickness: 0.046 cm, 0.056 cm, 0.066 cm, and 0.084 cm. Using naphthalene as the model phosphor and NaI as the heavy-atom enhancer, RTP intensity was found to be independent of HPMC pellet thickness within the range of 0.046 to 0.084 cm. For a given interval of dry nitrogen gas purge, the RTP signal yielded by a single substrate is within the calculated experimental error of each of the others regardless of substrate thickness.

- **Reagent Delivery.** For HPMC pellets, the diameter of the reagent spot can vary significantly with adjustments in sample delivery rate. Results associated with these investigations (section 5.4.2) indicate that automated sample delivery equipment will allow for improved reproducibility and reduced reagent spot diameters. Compressed filter paper pellets exhibit sorption characteristics similar to HPMC; however, when using normal, uncompressed filter paper, the final diameter of the reagent spot is independent of sample delivery rate.
- **Detection of Outliers.** The SSRTP technique is prone to errors in phosphorescence intensity when analyzing multiple samples of the same concentration due to the physical non-uniformity of the sample substrates and inconsistencies in syringe handling by the analyst during the sample delivery step. Assuming that the sample delivery process is fully optimized, SSRTP reproducibility is still limited to between 10 and 15% when inhomogeneous sample matrices are utilized.[335] The robust Tukey biweights method of outlier detection assists the spectroscopist with the identification of discordant observations. If outlying observations are rejected, relative standard deviations are typically reduced to less than 10% for most SSRTP data sets. Additionally, the Tukey biweight weights function is superior to traditional methods since it is resistant to masking effects and will allow for the detection of multiple outliers in a data set. In the field of phosphorescence spectroscopy, this is the first report that discusses the application of robust statistical methods. Furthermore, it is conceivable that other spectroscopic methods of analysis would benefit by the adoption of robust statistical techniques in this manner.

8.0 Summary and Conclusions

The selection of an RTP matrix is an important consideration since the choice of support material can be critical to the successful observation of phosphorescence. These investigations confirm that *K4M PREM* HPMC is an effective SSRTP matrix material. Using sodium iodide as the heavy-atom perturber, strong RTP spectra were obtained for the following probe phosphors when immobilized on HPMC: acenaphthene, naphthalene, 2-naphthoic acid, 2-naphthol, p-aminobenzoic acid, phenanthrene, salicylic acid (sodium salt), and triphenylene. Sodium iodide was the heavy-atom of choice for all investigations since it favorably enhanced the RTP emission of each model phosphor.

Model phosphors and sodium iodide were delivered to the HPMC substrate using a two-step microsyringe spotting technique. Ethanol was a satisfactory SSRTP solvent for these investigations since it reliably i). dissolved each analyte and the heavy-atom salt, ii). promoted matrix swelling by splitting hydrogen-bonds within the HPMC network, and iii). swelled the HPMC compacts at a sufficiently slow rate to prevent pellet disintegration. Samples were carefully dried prior to analysis using an infrared heat lamp. This drying technique was rapid, convenient, and nondestructive.

The high background phosphorescence originating from filter paper substrates can interfere with the detection and quantitation of trace-level analytes. High-purity grades of HPMC were investigated as SSRTP substrates in an attempt to overcome this limitation. Unfortunately, SSRTP background emissions are comparable for the two materials. However, when compared directly to filter paper, *K4M PREM* HPMC allows the spectroscopist to achieve greater sensitivity, lower limits of detection (LOD), and lower limits of quantitation (LOQ) for certain phosphor/heavy-atom combinations since SSRTP signal intensities are stronger. For example, the determination of the analytical figures of merit for a naphthalene/sodium iodide/HPMC system provided a calibration sensitivity of 2.79, LOD of 4 ppm (3 ng), and LOQ of 14 ppm (11 ng). Investigations of a naphthalene/sodium iodide/filter paper system produced a calibration sensitivity of 0.326, LOD of 33 ppm (26 ng), and LOQ of 109 ppm (86 ng).

A matrix isolation effect is primarily responsible for the exceptional performance of both filter paper and *K4M PREM* HPMC as SSRTP support materials. Extensive hydrogen-bonding between the polymer chains allows for the formation of pores, interstices, and cages. The size of these voids are expected to be similar for both biopolymers. However, the cellulose macromolecules comprise a highly ordered, crystalline system that contains transitional chains. The paracrystalline HPMC exists as a less-ordered network containing both chain associations and entangled regions. When ethanol is delivered to filter paper, cellulose-cellulose hydrogen-bonding is reduced and the matrix swells. When ethanol is delivered to HPMC, a swollen glassy layer is formed by an infinite entangled network of HPMC chains. At the surface of the HPMC compact, an ideal entangled network produces a gel layer. As solvent is removed and the network collapses, the HPMC gel layer forms a thin protective coating at the surface of the substrate that reduces oxygen and moisture permeation.

On the other hand, a gel coating at the surface of the substrate will only partially account for the enhanced RTP intensities provided by the HPMC matrix. The individual apolar, polar, and hydrogen-bonding characters of each phosphor-substrate combination cannot be ignored. Intermolecular dispersion forces are especially important since they are universal. Dispersion interactions (i.e. induced dipole-induced dipole forces) are independent of the particular type of molecule and are present in all condensed matter systems. Although the interaction strengths are relatively weak, dispersion forces are long-range. For a lipophilic model phosphor such as naphthalene, the hydroxypropyl and methoxyl functional groups present in HPMC allow for an enhanced phosphor-substrate attraction. Since the cellulose backbone is fully hydroxylated, filter paper is more hydrophilic than HPMC. Therefore, filter paper will interact most strongly with analytes that exhibit substantial polar or hydrogen-bonding character. This interpretation is supported by a quantitative model of intermolecular attraction based on Hansen's cohesion parameter theory.

It is also possible that favorable substrate-phosphor interactions that occur during the sample delivery step might contribute to the production of greater RTP intensities. Partitioning and adsorption are important concepts in the field of planar chromatography. Since the SSRTP sample delivery process is similar to that of the sample introduction step required for paper chromatographic determinations, substrate-phosphor interactions can also be modeled in terms of partitioning and adsorption. Considering only partition theory, the distribution coefficients for the cellulose system and the HPMC system are expected to be equivalent. However, in terms of adsorption, the distribution coefficients should be different. As a result, a lipophilic SSRTP matrix will have the potential to effectively concentrate lipophilic phosphors in the center of the sample spot by mechanisms of adsorption. Hydrophilic substrates would do the same for hydrophilic analytes. If more phosphor is retained in the center of the RTP support, then a greater number of phosphor molecules will be available to interact with the spectrometer's excitation beam. These interpretations are fully supported by Hansen's cohesion parameter theory.

If phosphor trapping in filter paper is indeed size-specific, then it might be possible that the probe phosphor is retaining more mobility within the filter paper matrix than it does in the HPMC substrate. This explanation seems unlikely since the pores and voids within the matrix are packed tightly by the external heavy-atom salt when high NaI concentrations are utilized. Further studies will be necessary to either confirm or refute this theory. To summarize, enhanced SSRTP intensities for the naphthalene/HPMC system can best be explained by i). favorable van der Waals interactions between the analyte and support as described by cohesion parameter theory, ii). the formation of a thin, protective gel coating at the surface of the substrate, and iii). a greater retention of the phosphor in the center of the sample spot via mechanisms of adsorption (also accounted for by solubility/cohesion parameter theory).

The Perkin-Elmer LS-50 luminescence spectrometer was utilized for all of these studies. Since a suitable SSRTP accessory is not commercially available for use with the LS-50, a sample cell module was built in-house by the investigator. The sample chamber was designed to accommodate purge gas studies. Results have confirmed that both triplet oxygen and moisture quench the RTP originating from HPMC-trapped phosphors. For HPMC, oxygen quenches the RTP signal to a greater extent than moisture. No SSRTP signal was observed when the phosphor

was exposed to a dry oxygen gas atmosphere. Therefore, a dry nitrogen purge gas was used for all other investigations to ensure that strong SSRTP intensities were obtained. Although analysis time increases significantly, extended purging with dry-nitrogen gas yields improved sensitivities, lower LOD's, and lower LOQ's for both HPMC and filter paper support materials when LOD and LOQ are calculated according to the IUPAC guidelines.

The results of studies reported herein confirm that *K*-type HPMC is superior to *E*-type HPMC as an SSRTP sample support when the phosphor is naphthalene, the heavy-atom is NaI, and the RTP solvent is ethanol. Compacts prepared from the premium grades of *E*-type HPMC do not readily sorb ethanol-based samples. Since *K*-type HPMC interacts more favorably with this solvent, the phosphor/heavy-atom system is more easily transported into the pores and voids of the pellet. An interfacial tension effect between the ethanol-based samples and the *E*-type HPMC has been observed visually in the laboratory during the sample delivery step. Cohesion parameter theory partially accounts for these observations. However, the particle size of the *K*- and *E*-type matrix materials may also play a role.

Two detailed heavy-atom investigations were completed. For the first heavy-atom study, the initial concentration range of NaI in ethanol was 0.00 to 0.05 M. Using 415 ppm naphthalene as the model phosphor and *K4M PREM* HPMC as the solid support, the dependence of RTP signal on heavy-atom concentration was found to obey a polynomial relationship ($y = -190.45x^2 + 724.57x + 65.44$; $R^2 = 0.994$). The second study examined the effect of higher NaI concentrations (0 to 1 M) on the RTP intensity of 100 ppm naphthalene. The upper concentration limit of NaI (1 M) was limited by its solubility. The results of the second set of investigations suggest a linear enhancement of RTP signal as heavy-atom concentration is increased. Saturation peaks were not observed for either of these studies. However, the existence of a saturation peak is expected for SSRTP analyses utilizing higher NaI concentrations and lower naphthalene concentrations.

A three-dimensional enhancement sphere (i.e. Perrin sphere) was useful for specifying the number of heavy-atom molecules that can interact with the phosphor. Although the Perrin influence sphere serves as an adequate interaction model for more than 100 iodide anions surrounding a single naphthalene molecule when $R = 14$ Å, it cannot presently account for phosphor/heavy-atom interactions involving thousands of heavy-atoms per analyte unless $R >> 14$ Å. Although the development of such models was outside the scope of this project, the topic is worthy of future study and investigation.

A Perkin-Elmer front-surface luminescence accessory was modified so that uncompressed, single-layer filter paper discs could be used as SSRTP substrates. It was discovered that the RTP intensities obtained using filter paper discs are nearly independent of the duration of dry nitrogen purge. The RTP signals obtained after a 15-minute interval of N_2 purge are only minimally greater in intensity than the RTP signals corresponding to those spectra acquired at the three minute mark. The macroscopic porosity of the filter paper allows for residual solvent, moisture, and oxygen to be quickly purged from the interstices of the matrix.

The modified P-E accessory was also used to directly compare the RTP intensities produced by an uncompressed filter paper/naphthalene/NaI system to those acquired using a *K4M PREM* HPMC/naphthalene/NaI system. In each case, the HPMC compacts provided greater RTP intensities than the corresponding uncompressed filter paper discs. For future investigations, a

full-scale LOD/LOQ study would be warranted for these two systems using the modified P-E accessory. Qualitative spectra were acquired at the 5 ppm (4 ng) level for naphthalene and 1 ppm (0.8 ng) level for phenanthrene. Based on these preliminary results, the modified P-E front surface accessory will allow for moderately improved LOD's in comparison to those obtained for the naphthalene/NaI system using the custom-built RTP sample cell module.

Because human factors and matrix anisotropy both introduce error into SSRTP measurements, reproducibility between trials is generally limited to between 10 and 15%. Naturally, filter paper and HPMC substrates are non-heterogeneous media. Since this deficiency cannot be addressed experimentally, a robust statistical method was examined for the detection of questionable SSRTP data points and the deletion of outlying observations. If discordant observations are discarded, relative standard deviations are typically reduced to less than 10% for most SSRTP data sets. Robust techniques for outlier identification are superior to traditional methods since they operate at a high level of efficiency and are immune to masking effects.

The Hildebrand total cohesion parameter and three Hansen partial cohesion parameters have been used to quantify the strength of intermolecular interactions between solid substrate materials and a series of seven model phosphors. Since HPMC has a lipophilic character compared to the hydrophilic cellulose that comprises filter paper, it is proposed that certain phosphors will be more strongly bound to an HPMC substrate than to a filter paper matrix. This is the first attempt within the field of phosphorescence spectroscopy to explain RTP signal enhancement in terms of the quantitative description of the apolar, polar, and hydrogen-bonding characteristics of analytical phosphors and their respective RTP substrates. Based on calculations of D_{ij} reported here for acenaphthene, naphthalene, 2-naphthoic acid, 2-naphthol, p-aminobenzoic acid, phenanthrene, and salicylic acid (sodium salt), HPMC is expected to be the preferred RTP matrix for each analyte. Calculations of D_{ij} for ethanol clearly indicate that the RTP solvent interacts equally well with both HPMC and cellulose as a result of its polarity and ability to hydrogen bond. Henceforth, the phosphorescence spectroscopist will have a new tool that will assist in the selection of optimal substrates for solid-surface room-temperature studies. Until now, the selection of suitable RTP matrix materials has mostly involved a trial-and-error approach. In many other instances, serendipity has played a key role in the discovery of new RTP substrates. Since the RTP investigator can now make reliable predictions regarding phosphor-substrate interactions prior to attempting an analysis, cohesion parameter theory should prove to be a major advancement in the field of SSRTP research.

9.0 Suggested Future Work

A few potential avenues of future investigation that relate directly to this project include:

- the examination of other varieties of DOW Methocel™ (such as the *F*- and *J*-types),
- the use of HPMC from other excipient manufacturers,
- the determination of analytical figures of merit for additional model phosphors using *K4M PREM* HPMC as the RTP support material of choice,
- the investigation of additional external heavy-atom salts as phosphorescence enhancers, and
- the expansion of the phosphorescence emission spectra library in order to determine if *K4M PREM* HPMC will continue to serve as a universal matrix material.

Ideas relating to the broader domain of SSRTP research made themselves known from time to time during this extended research project. Since these notions are outside of the scope of the original project, they are presented here with the hope that they will provide a spark that will ignite the flame of future SSRTP investigations.

Industrial Gums as SSRTP Matrix Materials

Industrial gums are polysaccharides that are regularly used in both food and nonfood industries.[240] Generally, the term *gum* refers to a plant or microbial polysaccharide (or a derivative) that is dispersible in either hot or cold water to produce a viscous mixture or solution. In the food industry, gums are used as additives in order to improve or control the properties of a food product. Since they are widely available, low-in-cost, and nontoxic, they are especially attractive as modifiers in the food industry. Their use in nonfood applications largely depends on their unique properties and cost in comparison to similar synthetic polymers.

Although new polysaccharides are continually being studied, the gums commonly used in foods are starches, cellulose derivatives, guar gum, locust bean gum, pectin, algin, carrageenan, xanthan, and gum arabic. Agar and gums ghatti, karaya, and tragacanth are used to a much lesser extent. Each gum has unique properties that are related to its particular molecular structure. Because cellulose and hydroxypropylmethylcellulose have proven to be such useful RTP matrix materials, many of the industrial gums deserve further attention in order to determine if they have the potential to serve as solid supports for RTP research.

A Digital Syringe for Improved Manual Sample Delivery

The Hamilton Company has recently introduced a *digital syringe* that should be useful during the SSRTP sample preparation step. This hand-held, syringe-coupled device displays liquid volumes on a small digital LCD readout. Accuracy and precision (depending on syringe

series) is claimed by the Hamilton company to be better than ±0.5 %.[459] The digital syringes are calibrated by the Hamilton Company using N.I.S.T. traceable methods.[460]

Precision Syringe Drive Modules for Automated Sample Delivery

The Hamilton Company has also recently introduced precision syringe drive (PSD/2) modules that may be useful during the SSRTP sample preparation step. The PSD/2 module allows for a syringe to be computer controlled. Syringe sizes from 10 µL to 25 mL may be used. The user-specified speed range of the device, 2 to 60 seconds per stroke, would be especially useful when working with RTP substrates such as *K4M PREM* HPMC.[461]

Each PSD/2 module has a built-in RS-232 connection for communication with a controlling computer. Two communication protocols are available that allow the user to: position syringes using absolute or relative positions, select syringe speed, stop and restart syringe movements, and adjust the amount of backlash compensation needed for optimal accuracy and precision. Modules equipped with an optional EEPROM can have up to eight methods down-loaded into memory. Methods are then selected by TTL switch closure. Accuracy of the PSD/2 module is >99.5% @ 100% stroke and >98% @ 5% stroke. Precision is >99.7% @ 100% stroke and >98% @ 5% stroke. Full resolution of the device is 2000 steps per stroke. In other words, each step of the drive motor is responsible for delivering 0.05% of the total syringe volume.

Automated Tablet Manufacturing Equipment for Improved RTP Substrate Production

The manufacture of a single HPMC pellet during this project required an approximate preparation time of two to three minutes. With practice, this preparation time might be reduced. However, if large quantities of HPMC pellets are desired, the time invested in substrate preparation can become significant.

The pharmaceutical industry has overcome this processing limitation by adopting specialized tablet manufacturing equipment. The simplest device is the *single-punch tablet machine* that makes one tablet for each revolution of a hand-crank. These single punch tablet machines, when motorized, have an output of 60 to 150 tablets per minute. However, according to Sadlik, "when single-punch machines are operated at speeds in excess of 100 tablets per minute, the weight variations of the finished tablets can vary excessively (due to the short period of time devoted to die-filling and compression)".[260] Although too slow for commercial production, such a tablet press would be ideal for preparing HPMC pellets on a small scale within the laboratory.

---

[459] Marketing literature. Hamilton Company, 4970 Energy Way, Reno, Nevada, 89502-4178, USA. 1-800-648-5950.

[460] S. Mayes and W. McAuliffe, **Hamilton Company Technical Bulletin:** *Certification, Traceability, and Use of a Highly Accurate Digital Syringe Device*, Reprinted from the poster presented at Pittcon `96, Chicago, March 4, 1996.

[461] Marketing literature. Hamilton Company, 4970 Energy Way, Reno, Nevada, 89502-4178, USA. 1-800-648-5950.

Multiple-punch tablet machines are available that operate two to twelve punches simultaneously. Production is enhanced, but there is greater potential for lack of uniformity in the tablets due to irregular filling of the holes in the die. *Rotary tablet machines* are also commercially available.[260,261] These automated tablet machines offer better control of tablet weight and are less likely to entrap air during processing. A rotary tablet machine can contain multiple sets of punches and dies. According to Banker, as many as 12,000 tablets can be produced per minute using a rotary tablet machine.[261]

Flying-Spot Scanning and Laser Excitation Sources for SSRTP

R.W. Frei has described a technique that has proven useful for the analysis of thin-layer chromatography (TLC) substrates by diffuse reflectance spectroscopy.[462] The technique, known as *flying spot scanning*, involves the scanning of the chromatographic zones with a small spot of monochromatic light in a zigzag pattern.[463,464] The flying spot technique, as applied to SSRTP, would theoretically allow for the detection of inhomogeneities within a given sample spot on the surface of a solid substrate. Additionally, by averaging the phosphorescence intensities obtained as the spot traverses the surface, a more accurate and precise SSRTP analysis should be achieved. On the other hand, Hurtubise has theorized that the flying-spot technique will not be advantageous for solid-surface fluorescence measurements since the fluorescence received by the photodetector is a linear function of the amount of substance for analysis at small amounts of the substance.[104] New SSRTP instrumentation and experiments will be necessary in order to confirm or refute these theories.

Vo-Dinh and colleagues have described the use of laser-based instrumentation for synchronous luminescence spectroscopy.[465] More recently, they have constructed an instrument that allows the investigators to perform laser-induced SSRTP analyses of polycyclic aromatic hydrocarbons.[335] Phenanthrene, pyrene, benzo[*g,h,i*]perylene, chrysene, coronene, and 1,2-benzofluorene were the model phosphors used in this study. The heavy-atom salt was thallium(I)acetate. All solutions were delivered to filter paper substrates using 2 μL micropipettes. A nitrogen-pumped laser and a dye laser were used as the excitation sources.

By narrowly focusing the excitation beam, the researchers were able to achieve laser probe areas of approximately 6.4 mm^2.[466] Since the excitation beam was smaller than the sample spot size, it was possible for the investigators to position the substrate within the sample holder in order to obtain RTP emission spectra from six different regions of the sample spot. The relative standard deviations of the maximum emission intensities were calculated to be within the

---

[462] R.W. Frei, *Diffuse Reflectance Spectroscopy; Applications, Standards, and Calibration (With Special Reference to Chromatography)* in **Standardization in Spectrophotometry and Luminescence Measurements, NBS Special Publication 466**, (K.D. Mielenz, R.A. Velapoldi, and R. Mavrodineanu, Eds.), Washington D.C.: U.S. Government Printing Office, 1977.

[463] J. Goldman and R.R. Goodall, *J. Chromatog.*, 1969, V. 40, p. 345.

[464] L.R. Treiber, B. Oertegren, R. Lindsten, and I. Oertegren, *J. Chromatog.*, 1972, V. 73, p. 151.

[465] C.L. Stevenson and T. Vo-Dinh, *Appl. Spectr.*, 1993, V. 47, p. 430.

[466] According to the investigators, the laser probe area on the paper substrate was approximately 1/10 the area of the sample spot size (i.e. 0.9-cm diameter).

two- to five-percent range. The researchers attributed this excellent reproducibility to the nearly homogeneous deposition of the phosphors (and heavy-atom enhancer) on the filter paper substrate. When six different filter paper substrates were compared, the RSD was calculated to be 7.3% (pyrene) and 7.7% (phenanthrene).

On the other hand, there are a number of limitations associated with the use of lasers for SSRTP excitation. For this study, the investigators were limited to only two monochromatic excitation wavelengths (337 nm and 385 nm). Another limitation rests with the potential for photodecomposition of the analytes if they are excited at wavelengths that coincide with their absorption maxima.

Appendix A

The following Minitab® programs were contributed by Dr. Jeff Birch, professor of statistics at Virginia Tech.

Program STARTIRLS

```
noecho
#Program startirls.  Executed before irlslh or irlslb programs.
#Finds the median of c1, store in k1; puts mad in k2
let k1=medi(c1)
let k2=(medi(abso(c1-medi(c1))))/.6745
let k3=1.5
let k4=4.5
names c3='oldest', c4='newest', c5='relchg'
print k1, k2
end
echo
```

Program IRLSB

```
noecho
#This is the program irlslb-execute blank times to get Tukey biweight m-estimate
#of location using the IRLS method.
# Before execution of this program set k4 to bisquare constant,
# and execute "startirls' to set k1 and k2.
#The bisquare m is stored in k5
let c100=c1-k1      #obtain the new residuals for iteration
let c15=c100/k2      #c15 are rescaled residuals
let c6=c15 le k4      #determine those residuals le to constant
let c7=((1-(c15/k4)**2)**2)*c6      #c7 are the weights
let k5= sum(c7 * c1)/sum(c7)      #k5 is the weighted mean
let k7=abso(k5-k1)/k1      #k7 is the relative change
let c3=k1
let c4=k5
let c5=k7
print c3 c4 c5
let k1=k5      #let theta old=theta new
end
echo
```

Appendix B

Raw Data: Relationship between delivery volume (1 μL - 8 μL) and reagent spot diameter for normal P2 Fisherbrand filter paper (uncompressed, single layer). The average for each is given at the 95% confidence interval.

Delivery Volume (**μL**) ±0.1 μL	User #1 Spot diameter (**cm**)	User #2 Spot diameter (**cm**)
1	0.594	0.584
1	0.566	0.569
1	0.615	0.546
avg. for 1 μL	**0.592 ±0.0602**	**0.566 ±0.0476**
2	0.787	0.805
2	0.772	0.790
2	0.772	0.792
avg. for 2 μL	**0.777 ±0.0219**	**0.796 ±0.0203**
3	0.950	0.965
3	0.922	0.942
3	0.869	0.953
avg. for 3 μL	**0.914 ±0.103**	**0.953 ±0.0285**
4	1.016	1.067
4	1.049	1.069
4	1.049	1.069
avg. for 4 μL	**1.038 ±0.0474**	**1.068 ±0.00364**
5	1.161	1.158
5	1.140	1.181
5	1.161	1.181
avg. for 5 μL	**1.154 ±0.0291**	**1.173 ±0.0328**
6	1.285	1.275
6	1.308	1.242
6	1.3293	1.262
avg. for 6 μL	**1.295 ±0.0289**	**1.260 ±0.0414**
7	1.410	1.328
7	1.384	1.410
7	1.372	1.387
avg. for 7 μL	**1.389 ±0.0482**	**1.375 ±0.104**
8	1.443	1.478
8	1.499	1.420
8	1.435	1.455
avg. for 8 μL	**1.459 ±0.0861**	**1.451 ±0.0731**

Raw Data: Representative reagent spot diameters for typical sample delivery on *K4M PREM* HPMC pellets (delivery volumes: 1 μL, 2μL, and 3μL). The average for each is given at the 95% confidence interval.

HPMC pellet #	Delivery Volume (**μL**) ± 0.1 μL	Spot Diameter (**cm**)
1	1.0	0.777
2	1.0	0.759
3	1.0	0.792
	avg. for 1 μL	**0.776 ±0.0410**
4	2.0	0.874
5	2.0	0.983
6	2.0	0.889
	avg. for 2 μL	**0.915 ±0.147**
7	3.0	1.143
8	3.0	1.092
9	3.0	1.016
	avg. for 3 μL	**1.084 ±0.159**

Raw Data: Representative reagent spot diameters for typical sample delivery on *E3 PREM* HPMC pellets (delivery volumes: 1 μL, 2μL, and 3μL). The average for each is given at the 95% confidence interval.

HPMC pellet #	Delivery Volume (**μL**) ± 0.1 μL	Spot Diameter (**cm**)
1	1.0	0.312
2	1.0	0.292
3	1.0	0.315
	avg. for 1 μL	**0.306 ±0.0310**
4	2.0	0.406
5	2.0	0.419
6	2.0	0.406
	avg. for 2 μL	**0.411 ±0.0182**
7	3.0	0.544
8	3.0	0.495
9	3.0	0.508
	avg. for 3 μL	**0.516 ±0.0621**

Raw Data: Representative reagent spot diameters for typical sample delivery on E15LV PREM HPMC pellets (delivery volumes: 1 μL, 2μL, and 3μL). The average for each is given at the 95% confidence interval.

HPMC pellet #	Delivery Volume (**μL**) ± 0.1 μL	Spot Diameter (**cm**)
1	1.0	0.315
2	1.0	0.315
3	1.0	0.318
	avg. for 1 μL	**0.316 ±0.00364**
4	2.0	0.401
5	2.0	0.409
6	2.0	0.404
	avg. for 2 μL	**0.405 ±0.00964**
7	3.0	0.495
8	3.0	0.488
9	3.0	0.488
	avg. for 3 μL	**0.490 ±0.0109**

Raw Data: Representative reagent spot diameters for typical sample delivery on P2 FisherBrand filter paper pellets (delivery volumes: 1 μL, 2μL, and 3μL). The average for each is given at the 95% confidence interval.

filter paper pellet #	Delivery Volume (**μL**) ± 0.1 μL	Spot Diameter (**cm**)
1	1.0	0.815
2	1.0	0.739
3	1.0	0.963
	avg. for 1 μL	**0.839 ±0.282**
4	2.0	0.912
5	2.0	1.054
6	2.0	0.886
	avg. for 2 μL	**0.951 ±0.224**
7	3.0	1.069
8	3.0	0.968
9	3.0	0.996
	avg. for 3 μL	**1.011 ±0.130**

Appendix C

Spin-Orbit Coupling Models and Quantum Theory

Given an atom containing a single electron, one usually imagines that the spinning electron is in orbit around a fixed nucleus. It is also reasonable to consider that the spinning electron is fixed in space and that the nucleus is in orbit around the electron as shown in the figure 82.

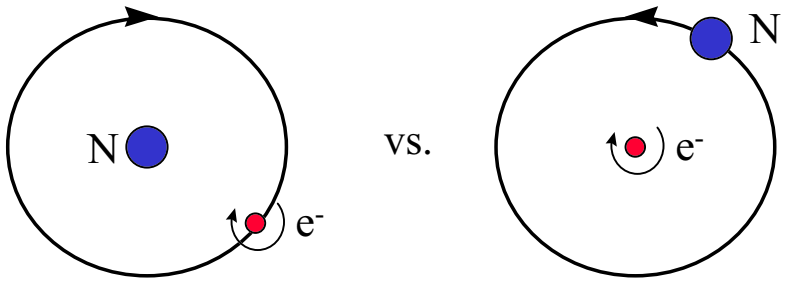

Figure 82. A one-electron atom as viewed from two legitimate perspectives. The interaction of the magnetic field produced by the nuclear orbital motion (right) and the magnetic field due to the electron spin causes spin-orbit coupling.

Assuming a frame of reference fixed on the electron, the charged nucleus moves around the electron. The electron is effectively located inside a current loop which produces a magnetic field. This relativistic magnetic field exists perpendicular to the plane of the orbit. It surrounds the spinning electron. Due to some asymmetry of charge distribution on the electron, a magnetic field is also produced along the electron spin-axis. The interaction of these two magnetic fields is described as spin-orbit (S-O) coupling.[20]

The energy of the system is determined by the relative orientations of the spin axis and the orbital angular momentum of the electron. If several relative orientations are possible, a corresponding number of states of different energy will result. It is this effect that causes the multiplet states of atoms and molecules to divide into closely spaced sets of energy levels. In atomic spectroscopy, these distinct energy levels produce *fine structure* within the atomic line spectra.[467] The effect is also partially responsible for the multiplet splitting observed in triplet states of organic molecules.

S-O coupling causes an additional term to appear in the total Hamiltonian operator as follows:

$$H' = H + H_{so}$$

where H' is the perturbed Hamiltonian, H is the initial unperturbed Hamiltonian, and H_{so} is the S-O coupling term. As a result of S-O coupling, the wave function of the lowest triplet state T_1 is not a pure spin triplet wave function $\psi(T_1)$, but a perturbed wave function $\psi'(T_1)$ as follows:

[467] S. Gasiorowicz, **Quantum Physics**, 2nd Edition, New York: John Wiley & Sons, Inc., 1996.

$$\psi'(T_1) = \psi(T_1) + \sum_n \alpha_n \psi(S_n)$$

where $\psi(S_n)$, are the pure spin wave functions of the various singlet states S_n and α_n are the S-O perturbation coefficients. This equation illustrates how the triplet state can be contaminated by singlet character.[12] The α_n coefficients are referred to as *mixing coefficients* between T_1 and S_n.

McGlynn has discussed this mixing of spin states in terms of a comparison of *pure spin states* vs. *nominal spin states*.[20] A pure spin state is one that exhibits a time-independent spin angular momentum. Transitions between pure spin states of different multiplicities are spin forbidden. However, the perturbing effects of S-O coupling are such that the spin angular momentum can no longer be considered to be time-independent. Therefore, one must rely on nominal spin states to describe a given spin state in terms of a small mixture of states of other spin multiplicities. This concept is illustrated in figure 83.

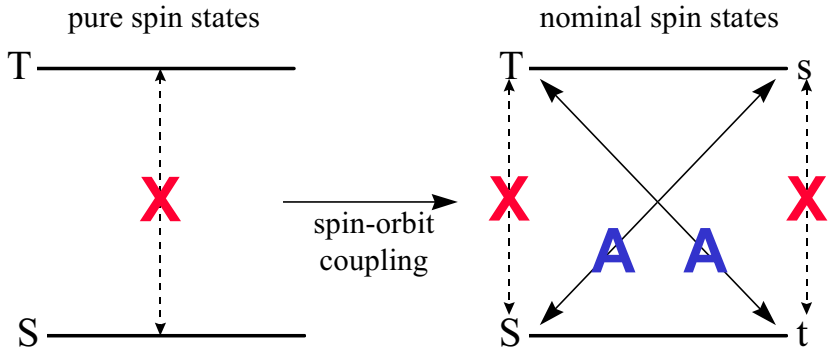

Figure 83. An illustration of the effect of spin-orbit coupling on transitions between states of different multiplicities (according to McGlynn, et al.).
X = spin forbidden transition; A = spin allowed transition; S = pure spin singlet state;
T = pure spin triplet state; t = pure spin triplet contaminant in a nominal singlet state;
s = pure spin singlet contaminant in a nominal triplet state.

Figure 83 shows that the spin allowedness of a transition between nominal singlet and triplet state is actually due to the spin allowedness of transitions between different pairs of singlet states and between different pairs of triplet states. The allowedness of the S $\leftrightarrow$ T transition is considered to be borrowed from some T $\leftrightarrow$ T transition(s) and some S $\leftrightarrow$ S transition(s).

Relying on perturbation theory, the α_n coefficients can be expressed as:

$$\alpha_n = \frac{\langle \psi(T_1) | H_{so} | \psi(S_n) \rangle}{|E(T_1) - E(S_n)|}$$

where $E(T_1)$ and $E(S_n)$ are the energies of the triplet state T_1 and singlet states S_n. A similar approach can be used to describe the perturbation of the singlet ground state by applying the mixing coefficient β_m. The wave function $\psi'(S_0)$ of the perturbed ground state S_0 is as follows:

$$\psi'(S_0) = \psi(S_0) + \sum_m \beta_m \psi(T_m)$$

where

$$\beta_m = \frac{\langle \psi(S_0)|H_{so}|\psi(T_m)\rangle}{|E(T_m)-E(S_0)|}$$

The energy terms appearing in the denominators of the mixing coefficients represent energy gaps. Since the energy gaps due to $|E(T_m)-E(S_0)|$ are larger than $|E(T_1)-E(S_n)|$, the β_m coefficients are less important than the α_n coefficients.[12]

Phosphorescence intensity is related to the radiative transition probability given by the square of the electric dipole transition moment $M(T_1,S_0)$ according to the following:

$$M(T_1,S_0) = \left\langle \psi'(T_1)\left|\sum_i e r_i\right|\psi'(S_0)\right\rangle$$

where e is the electron charge and r_i is the position vector for the i electrons (er is the electron dipole moment operator). A substitution of the expressions that correspond to $\psi'(T_1)$ and $\psi'(S_0)$ leads to the following:

$$M(T_1,S_0) = \sum_n \alpha_n M(S_n,S_0) + \sum_m \beta_m M(T_m,T_1)$$

where

$$M(S_n,S_0) = \left\langle \psi(S_n)\left|\sum_i e r_i\right|\psi(S_0)\right\rangle$$

and

$$M(T_m,T_1) = \left\langle \psi(T_m)\left|\sum_i e r_i\right|\psi(T_1)\right\rangle$$

$M(S_n,S_0)$ represents the electric dipole moment of the transition between the singlet state S_n and the ground state S_0; whereas, $M(T_m,T_1)$ represents the electric dipole moment of the transition between the triplet state T_m and the lowest triplet state T_1.[12]

These relations clearly show that the intensity of phosphorescence is stolen from the allowed transitions $S_n \leftrightarrow S_0$ and $T_m \leftrightarrow T_1$. This mechanism is the basic process of S-O coupling. The magnitude of the effect of S-O coupling decreases with increasing energy gaps of the perturbing states. Since β_m coefficients generally make a negligible contribution to the phosphorescence process, it is often only necessary to consider the α_n mixing coefficient. The polarization of the phosphorescence emission, $M(T_1 \rightarrow S_0)$ depends on the polarization of the perturbing transitions $M(S_n \leftrightarrow S_0)$ and/or $M(T_m \leftrightarrow T_1)$. Thus, the polarization of the 0,0 band of the phosphorescence can provide information regarding the mechanisms of direct S-O coupling. Unfortunately, very little work has been done in measuring phosphorescence polarization from compounds adsorbed on solid surfaces because of problems arising from scattered light.[2]

The $\langle \psi(T_1)|H_{so}|\psi(S_n)\rangle$ part of the α_n mixing coefficient is proportional to ζ, the **S-O coupling factor**. For hydrogen-like atoms,

$$\zeta_{nl} = \left[\frac{e^2\hbar^2}{2m^2c^2a_0^3}\right]\left[\frac{Z^4}{n^3(l+1)\left(l+\frac{1}{2}\right)l}\right]$$

where e is the electronic charge, $\hbar$ is $h/2\pi$ (h being Planck's constant), m is the electronic mass, c is the velocity of light, a_0 is the Bohr radius, Z is the atomic number of the atom and n and l are the principal and orbital angular momentum quantum numbers respectively of the electron of concern.[20] Note that the S-O coupling factor is directly proportional to Z^4. For hydrogen itself, Z = 1 and the influence of the atomic number on S-O coupling is very small. As atomic number increases and atoms become heavier, the influence of Z on the S-O coupling factor becomes significant. Furthermore, since the prior model is notably oversimplified, the Z dependence is postulated to be even greater for a many-electron atom. Becker has proposed that the $S \leftrightarrow T$ probability is dependent on Z^8 if a central field potential is assumed.[17]

The larger the nuclear charge, the larger the magnetic field produced by its apparent orbital motion. S-O coupling is greatest in those atoms having a large nuclear charge. Therefore, S-O coupling increases as atomic number (Z) increases. The closer the electron is to the nucleus, the larger the apparent angular momentum of the nucleus must be in order to counteract the attractive coulombic forces. Thus, the S-O coupling will be larger. S-O coupling is especially significant in atoms having filled or nearly filled outer shells (i.e. the noble gases or halogens.). Electrons that have penetrating orbits will experience a greater nuclear charge and be more strongly S-O coupled.

The probability is small that $T_1 \leftrightarrow S_0$ transitions will occur in a molecule containing only "light" atoms such as carbon and hydrogen. This probability can be increased by attaching a heavy-atom (by chemical means) to the part of the molecule in which the transition is localized. This is referred to as the *internal heavy-atom S-O coupling effect*. The internal heavy-atom can exert such a strong magnetic field on the molecule's excited electron that the unpairing of electron spin is facilitated. For example, Ermaloev and colleagues have shown in LTP studies that the naphthalene molecule exhibits a ϕ_P of 0.051 and a k_{isc} of 1×10^5.[468] In the same LTP study, a single iodine substituent (i.e. iodonaphthalene) improved ϕ_P to 0.38 and k_{isc} to approximately 3×10^9. Nevertheless, it should be noted that the spin-orbit effects in an isolated heavy-atom are typically larger in magnitude than the spin-orbit coupling that is produced by the attachment of the same heavy-atom to an aromatic system. This observation isn't unexpected since the electrons involved in the $\pi \rightarrow \pi^*$ or $n \rightarrow \pi^*$ transitions will spend only part of their time in the vicinity of the heavy-atom substituent.

A heavy-atom can also be contained in the environment immediately surrounding the phosphor. In phosphorescence spectroscopy, the *external heavy-atom S-O coupling effect* is generally more useful than the internal effect since it isn't necessary to first synthesize the analyte of interest to include a heavy-atom within its structure. An important question is whether the

---

[468] V.L. Ermaloev, I.P. Kotylar, and K.K. Switashev, *Izvest. Akad. Nauk. SSSR.*, 1960, Ser. F17, V. 24, p. 492.

external heavy-atom effect merely increases the S-O coupling already present in the aromatic or whether it introduces a new and different kind of S-O coupling. In the case of 1-halonaphthalenes, LTP experiments suggest that the external heavy-atom effect increases the S-O coupling that is already present in the phosphor.[20] For example, even though phosphorescence intensity increases significantly with increasing Z of the external heavy-atom, the shape of the absorption spectrum remains unchanged. This indicates that no excess vibronic perturbations are introduced by the external heavy-atom effect. Furthermore, the external heavy-atom effect has been discovered to be greater for those phosphors that have larger internal perturbations.[469,470] These experimental findings agree well with perturbation calculations found elsewhere.[20] Although internal and external heavy-atom effects are very similar, further investigations will be required before additional generalizations can be made.

According to McGlynn, "No significant discussion of spinorbit coupling induced by external heavy-atom-containing molecules is available. A number of interpretations are, of course, possible; however, it is difficult to say theoretically which one of these interpretations provides the dominant spinorbit coupling route.".[20] Two common theories describe the interplay of a phosphor and a heavy-atom in terms of either *charge-transfer* or *electron exchange* interactions. In both cases, theory speculates that the π electrons undergoing the transition must spend a brief amount of time in the vicinity of the heavy-atom. Even though the phosphorescence community has not yet agreed upon a favored mechanism, it's generally accepted that both routes rely on "intensity stealing" from the phosphor's surroundings. As an example, the $S_0 \rightarrow T_1$ transition of an aromatic can effectively steal intensity from some perturber transitions.[20] On the other hand, the data provided by Ermaloev and colleagues shows that an increase in transition strength is only partially responsible for RTP enhancement. A significant increase in k_{isc} is also observed. The enhancement of k_{isc} isn't unexpected since it has been shown that the primary mode of fluorescence quenching by an external heavy-atom is due to nonradiative intersystem crossing (i.e. $S_1 \rightarrow T_1$).[20] Although this process is detrimental to ϕ_F, it will contribute favorably to the magnitude of ϕ_P.

To summarize, phosphorescence intensity depends on ϕ_P which, in turn, depends on $M(T_1,S_0)$. $M(T_1,S_0)$ depends directly on the magnitude of α_n. The mixing coefficient, α_n, is proportional to ζ_P, a spin-orbit coupling factor applicable to a particular electron within a given phosphor. For a heavy-atom such as iodine, ζ_{nl} is directly proportional to the magnitude of Z^y, where Z is iodine's atomic number (i.e. 53). Therefore, in the case of a heavy-atom, the degree of S-O coupling within the atom depends primarily on the magnitude of its atomic number. Since an external heavy-atom is thought to merely enhance the S-O coupling already present in a phosphor, the proximity of the heavy-atom to the phosphor molecule is obviously a primary concern. The spin-orbit coupling factors, ζ_P and ζ_{nl}, are also of considerable importance since both are expected to directly influence the extent of external heavy-atom RTP enhancement.

---

[469] S.P. McGlynn, R. Sunseri, and N. Christodouleas,*J. Chem. Phys.*, 1962, V. 37, p. 1818.
[470] S.P. McGlynn, M.J. Reynolds, G.W. Daigre, and N.D. Christodouleas,*J. Phys. Chem.*, 1962, V. 66, p. 2499.

VITA

Vince Hamner was born November 18, 1965 at Warner-Robins A.F.B., Georgia, the son of James T. and Janet G. Hamner. At Carl Albert Senior High School, he was introduced to the study of chemistry by Mr. Floyd Cook. Prior to graduating from Buckhannon-Upshur High School in 1983, Vince was mentored in advanced science and research by Mr. Fred Newman. At West Virginia Wesleyan College, Dr. Allen Hamner encouraged the pursuit of specific interests in analytical chemistry and instrumentation. Vince received the B.S. degree in chemistry from WVWC in 1987.

Vince spent the Summer of 1987 as an Analytical Researcher working under the direction of Dr. Jim Abbott at the Procter and Gamble Company. In the Fall of 1987, he joined Dr. R.E. Dessy's Lab Automation and Instrument Design research group in the Department of Chemistry at Virginia Tech. The requirements for the M.S. degree in chemistry were satisfied in August 1990 following the completion of a research project involving fiber optic polarimetry.

During the course of his graduate academic career, Vince has been employed at Virginia Tech as a teaching assistant for analytical, general, and physical chemistry laboratories and as an academic advisor for the Liberal Arts and Sciences Department. Additionally, he has been an instructor during sessions of the A.C.S. Laboratory Automation short course under the direction of Dr. Ray Dessy.

In 1995, Vince accepted a professorship in chemistry at Muskingum College in New Concord, OH. In addition to teaching general chemistry, analytical chemistry, and instrumental methods of analysis, he has sponsored undergraduate research projects involving Solid Phase Micro-Extraction (SPME) for the analysis of environmental pollutants, WWW-based “expert systems” for use in the identification of organic unknowns, and the effect of soil pH on the microbial bioremediation of hydrocarbons. In 1997, Vince relocated to Buckhannon, WV to share a faculty position in chemistry with his wife, Josette, at West Virginia Wesleyan College. He currently resides in sunny Wilmington, North Carolina.

Vince Hamner